

Figure 8-30: Calorimeter average temperatures at left, center, and right stations (exterior) for Dilbit tests.

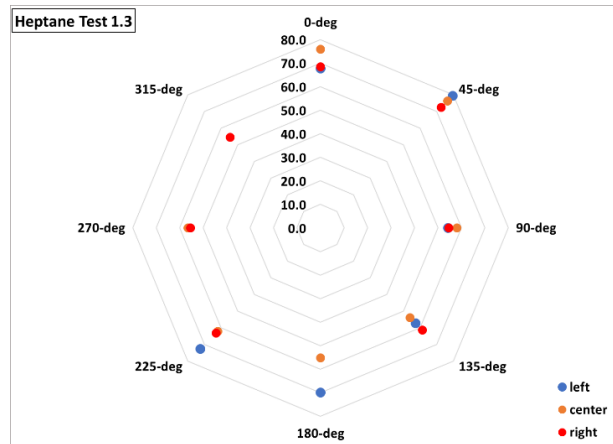
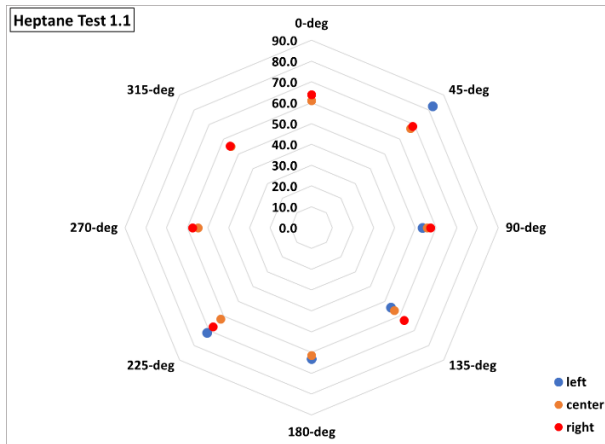


Figure 8-31: Total heat flux to calorimeter for heptane tests

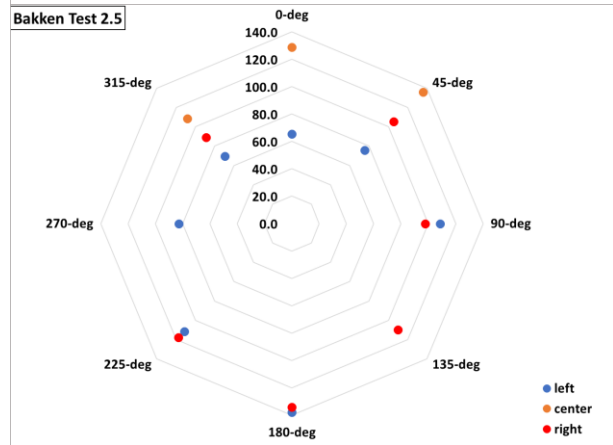
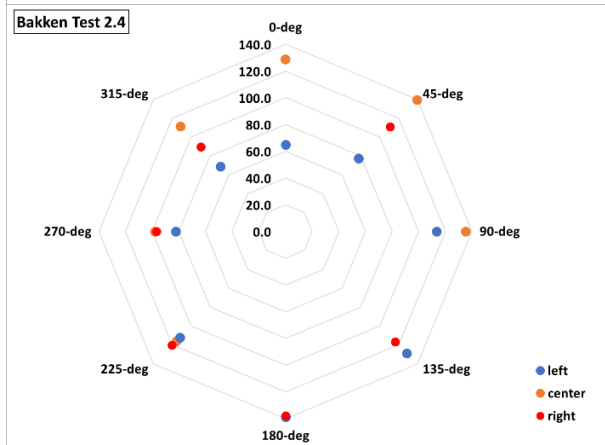
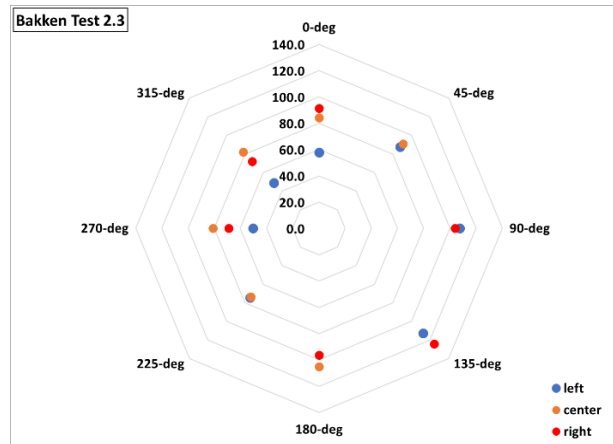
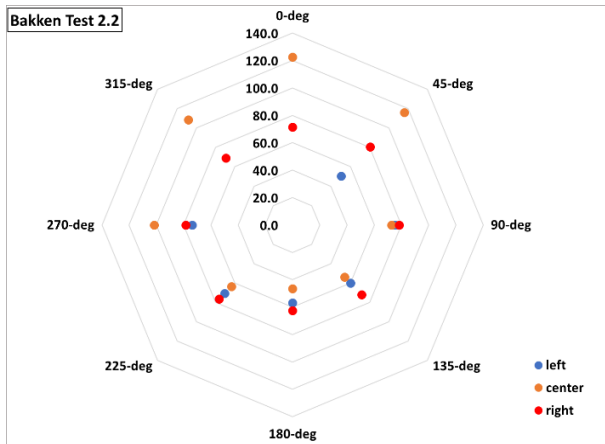


Figure 8-32: Total heat flux to calorimeter for Bakken tests

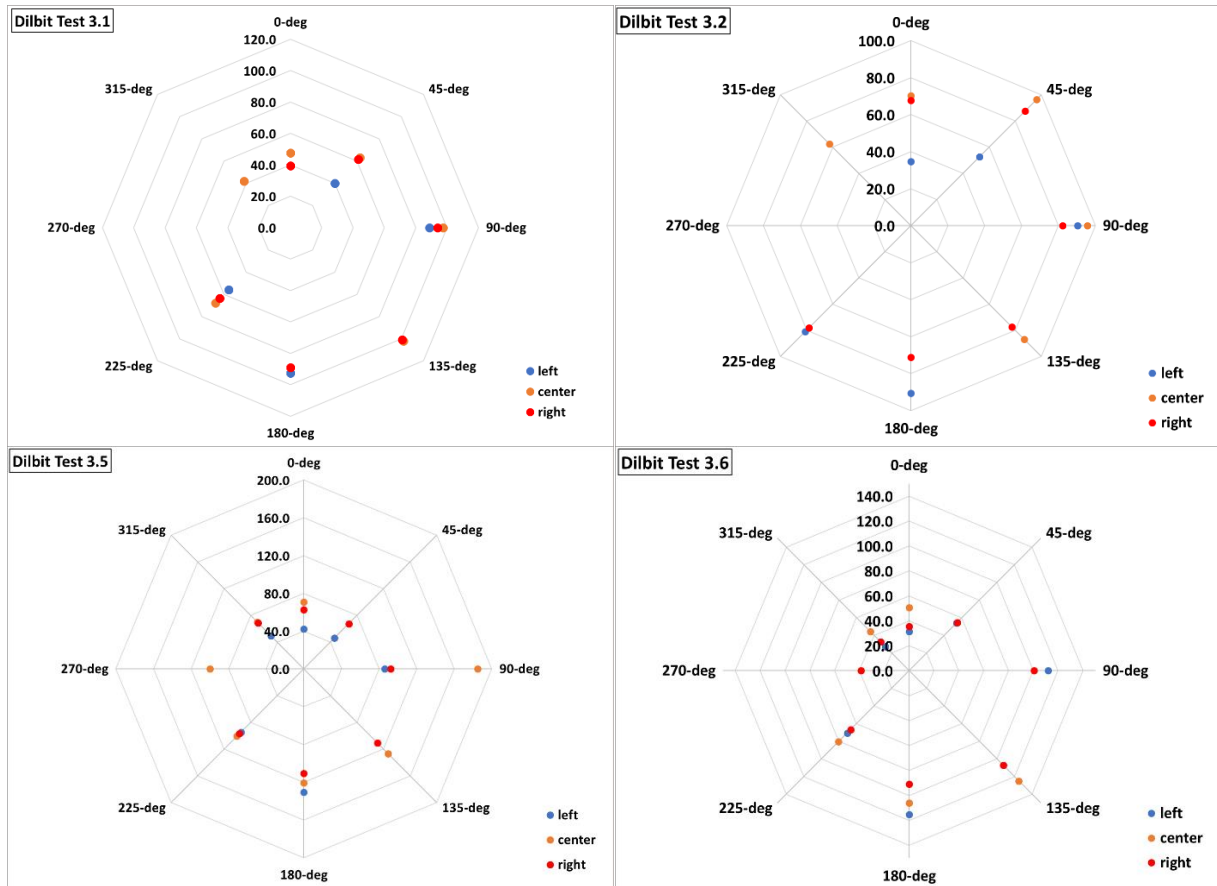


Figure 8-33: Total heat flux to calorimeter for dilbit tests

8.7. Heat release rate

Figure 8-34 shows heat release rate from CGA measurements for all test series. Dilbit test 3.4 was the only test within its series to successfully obtain CGA measurements due to difficulties with the equipment. Based on the CGA measurements the heptane tests 1.2 and 1.3 had the highest average heat release rate among the fuels which agrees with the result that the heptane has the highest burn rate among the fuels. The burn rate for Bakken Tests 2.1 and 2.6 are similar, but the heat release rate differs. Since the heat release rate for Test 2.6 agrees with the other tests it is suspected that the measurement for Test 2.1 may not be as reliable. The heat release rate measured for the dilbit indicates the highest range of variability which reflects the varying burn rate. Due to only acquiring a CGA measurement for one test it's difficult to draw firm conclusions regarding a comparison. If CGA data was acquired for the other dilbit tests, it is anticipated that it would result in the lowest heat release rate based on observation of the burn rate and flame height data among the fuels.

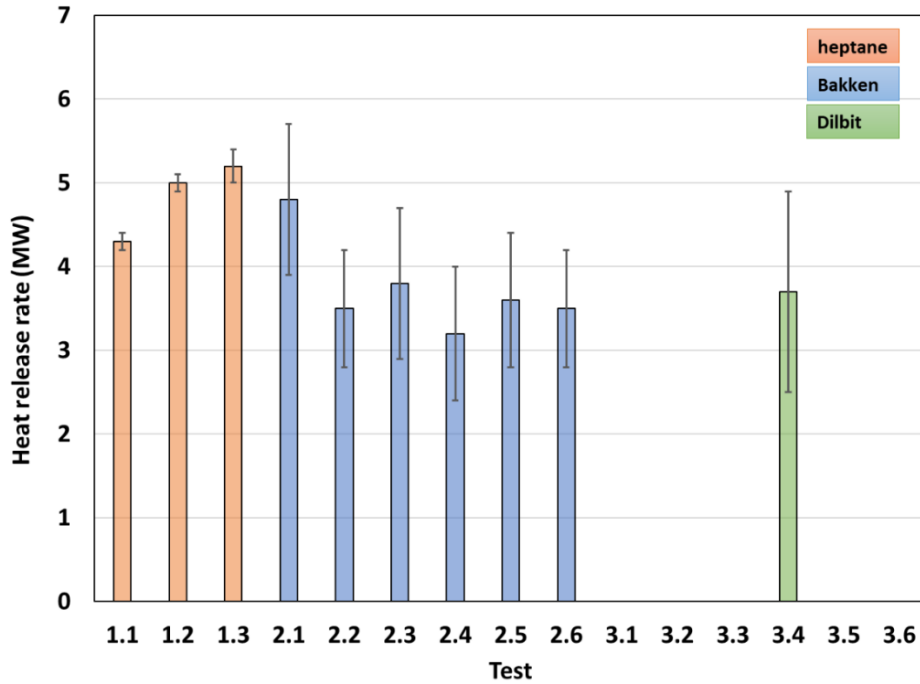


Figure 8-34: Heat release rate from CGA measurements among the test series.

8.8. Flame height

Figure 8-35 shows the average flame height among the test series. The comparison indicates that the heptane has the highest average flame height followed by the Bakken, then the dilbit. This agrees with the trend indicated by the burn rate data.

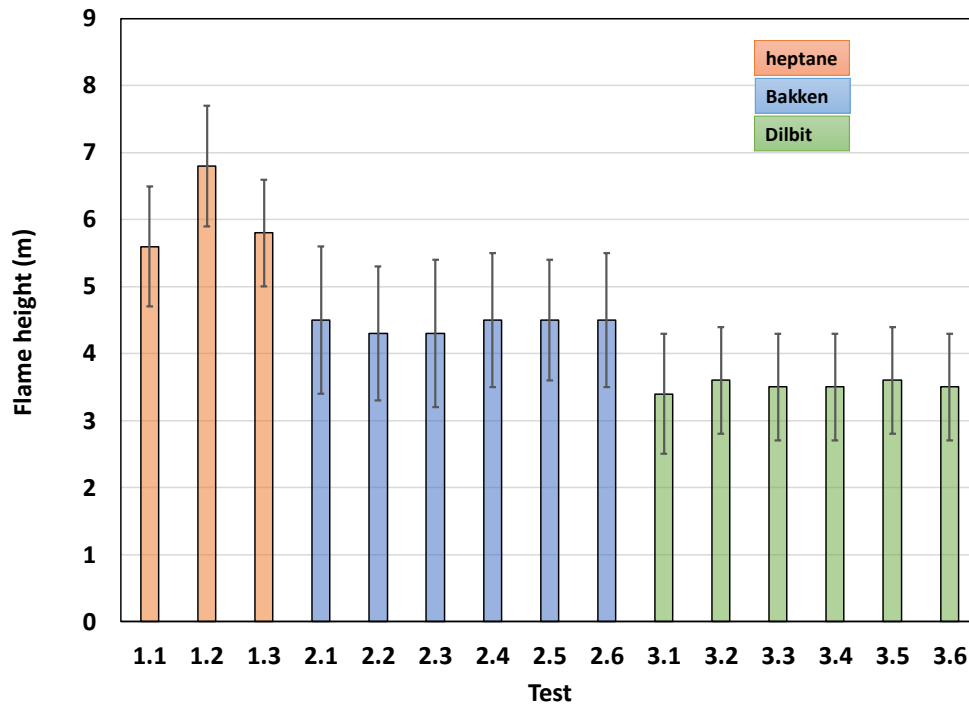


Figure 8-35: Average flame height among the test series.

This page left blank

9. CONCLUSIONS

In considering the parameter effects within a test series, the results indicate the following:

- The higher temperature fuel supply increased the burn rate by about 10% for the heptane tests, whereas it did not have a significant effect for the Bakken crude oil tests. The higher temperature fuel test for the dilbit crude oil indicated a lower average burn rate, but its range of deviation overlapped tests with lower temperatures.
- Allowing the fuel to burn down, rather than maintaining a constant fuel level, did not have a significant effect on averaged measured values from any of the instruments.
- The presence of the calorimeter had the most impact on the burn rate. For the heptane tests, the burn rate was slightly higher (~10%) in the test without the calorimeter. For the Bakken crude oil, the burn rate was higher overall (~10-15%) for tests without the calorimeter compared to tests with the calorimeter. For the dilbit crude oil, any effect was not detected though it is difficult to make a firm conclusion due to its highly variable burn rate.
- The placement of the calorimeter affected the average total heat flux from the flame to the calorimeter for the Bakken crude oil and not for the dilbit crude oil tests. The Bakken crude oil test with the calorimeter placed 0.5 m lower in the flame resulted in lower average total heat flux levels to the calorimeter (~78 kW/m² vs. ~100 kW/m²). For the dilbit crude oil there was no effect since the calorimeter was above the fuel-rich regions for both positions of 0.5 and 1 m.

In comparing the behavior among the fuels, the main conclusions are the following:

- The average burn rate for heptane is higher than Bakken and dilbit crude oils, ~0.04 kg/m²s vs. ~ 0.03 kg/m²s and ~ 0.02 kg/m²s, respectively.
- The burn rate for the dilbit crude oil was highly variable due to its mixture, comprised of a condensate (~20 vol%) and bitumen crude oil (~80 vol%).
- The average flame height for heptane is higher than the Bakken and dilbit crude oils, ~6.2 m vs. ~4.4 m and ~3.5 m, respectively.
- The average flame temperatures from the IR camera measurements are similar (~900 K) for all fuels.
- The average surface emissive power is lower for heptane than for Bakken and dilbit crude oils, ~66 kW/m² vs. ~76 kW/m² and ~71 kW/m², respectively.
- For calorimeter measurements, the Bakken crude oil resulted in the highest outer cylinder and exterior temperatures and the highest average total heat flux by about a factor of 1.5 and 1.3 higher compared to heptane and the dilbit crude oil, respectively (~95 kW/m² vs ~62.5 kW/m² and ~71.9 kW/m², respectively).

REFERENCES

- [1] D. Lord, J. Hogge and R. Allen, "Fuels Characterization for National Research Council Canada 2-m Pool Fire Test Series," Sandia National Laboratories, Albuquerque, NM, SAND2020-XXXX, 2020 (to be published).
- [2] A. Luketa, B. Blanchat, D. Lord, J. Hogge, A. Cruz-Cabrera and R. Allen, "Pool Fire and Fireball Experiments in Support of the US DOE/DOT/TC Crude Oil Characterization Research Study," Sandia National Laboratories, Albuquerque, NM, SAND2019-9189, 2019.
- [3] Beck, J.V., "Users Manual for IHCP1D, a Program for Calculating Surface Heat Fluxes," Beck Engineering Consultants Co., Okemos, Michigan, 48864, Oct. 30 1999.
- [4] Janssens, M.L., "Measuring Rate of Heat Release by Oxygen Consumption," *Fire Technology*, pp. 234-248, 1991.
- [5] "Canada Crude Quality Monitoring Program," [Online]. Available: <https://crudemonitor.ca/condensates/index.php?acr=CFT>.
- [6] Biteau, H., et al., "Calculation Methods for the Heat Release Rate of Materials of Unknown Composition," *Fire Safety Science, Proceedings of the Ninth International Symposium*, pp. 1165-1176, 2008.

APPENDIX A: EQUATIONS AND ASSUMPTIONS FOR CALCULATIONS

A.1. Heat flux calculations

The following energy balances were assumed for the DFT and calorimeter heat flux calculations.

Calorimeter:

$$q_{total} = \alpha q_{incident} + q_{convection} = q_{absorbed} + \epsilon \sigma T_{surface}^4$$

DFT:

$$q_{incident} = \frac{q_{absorbed}}{\alpha} + \sigma T_{surface}^4 + \frac{h}{\alpha} (T_{surface} - T_{\infty})$$

where $h = 30 \text{ W/m}^2\text{K}$

Figure A-1 provides the dimensions and materials used for the calculations. The absorbed flux is what the calorimeter absorbs and is material- and construction-dependent. Typically, it is reported as negative because it's considered to be an energy sink, while the total flux is positive since it is considered to be an energy source. The total heat flux is the incident flux plus the convective flux from the flame to the calorimeter. These two fluxes are combined because of uncertainty regarding the convection coefficient.

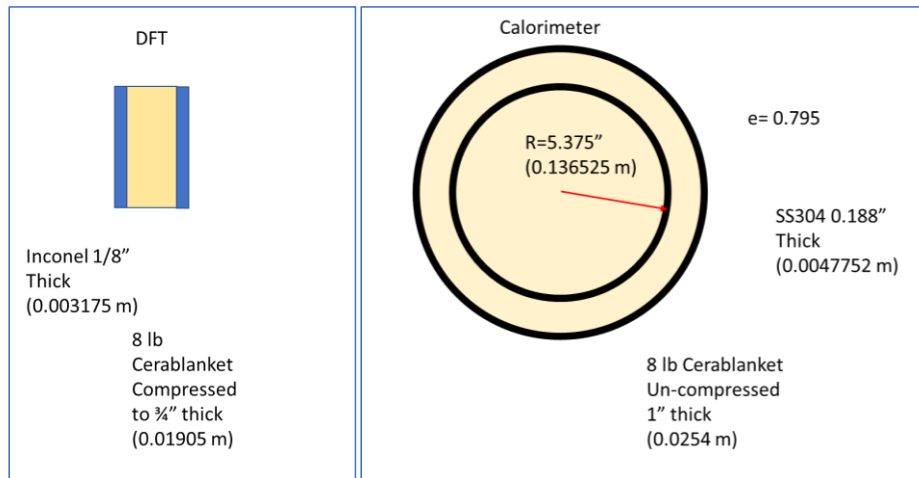


Figure A-1: DFT and Calorimeter specifications for heat flux calculations.

The thermal properties used for the calculations are the following.

Equations for density, thermal conductivity, and specific heat for SS304:

- $\rho = -0.4678 T + 7877 \text{ (kg/m}^3\text{)}$ where T is in $^{\circ}\text{C}$.
- $k = 14.898 + 0.015703 T - 1.56 * 10^{-6} T^2 \text{ (W/m-K)}$ where T is in $^{\circ}\text{C}$.
- $C_p = -5592 + 2731 \ln(T) - 417.9 \ln(T)^2 + 22.07 \ln(T)^3 \text{ (J/kg-K)}$ where T is in K .

Equations for density, thermal conductivity, and specific heat for Inconel 600:

- $\rho = -0.000035549 * T^2 - 0.36036496 * T + 8348.313$ (kg/m³) where T is in °C.
- $k = 12.93 + 0.01664 * T$ (W/m-K) where T is in °C.
- $C_p = \begin{cases} 427 + 0.328 T - 3.6 \times 10^{-4} T^2 + 1.62 \times 10^{-7} T^3, T < 600^\circ C \\ 486 + 0.328 T - 3.6 \times 10^{-4} T^2 + 1.62 \times 10^{-7} T^3, T \geq 600^\circ C \end{cases}$ (J/kg-K)
where T is in °C.

Equations for density, thermal conductivity, and specific heat for Cerablanket insulation:

- The density we are concerned with is 8 lb/ft³ (128 kg/m³). The density does change when compressed, which occurs in DFTs. So, the compression from 1 inch blanket to 3/4 inches when assembling DFTs increases the density by 1/3 to (1.33*8=) 10.67 lb/ft³ or 170.67 kg/m³
- $\ln(k) = -3.37 + 2.82 \times 10^{-3} * T - 7.77 \times 10^{-7} * T^2$ (W/m-K) where T is in °C (compressed)
- $\ln(k) = -3.54 + 3.13 \times 10^{-3} * T - 7.77 \times 10^{-7} * T^2$ (W/m-K) where T is in °C (uncompressed)
- $C_p = -0.00011 * T^2 + 0.39276 * T + 788.099$ (J/kg-K) where T is in °C

The measured emissivity used for the calculation is provided in Table A-1.

Table A-1: Measured emissivity for DFT instruments used for test series

	Heptane and Bakken tests	Dilbit tests
Location from center of pool (m)	Front plate	
2	0.895	0.818
4	0.870	0.660

A.2. Heat Release Rate

To determine the heat release rate, the procedure to reduce the data followed that from reference [4]. The equations are as follows:

$$M_e = 18 + 4(1 - X_{H_2O}^e)(X_{O_2}^e + 4X_{CO_2}^e + 2.5) \quad (1)$$

$$\frac{\dot{m}_a}{M_a} = \frac{(1 - X_{H_2O}^e)(1 - X_{O_2}^e - X_{CO_2}^e - X_{CO}^e)}{(1 - X_{H_2O}^o)(1 - X_{O_2}^o - X_{CO_2}^o)} \frac{\dot{m}_e}{M_e} \quad (2)$$

$$\varphi = \frac{X_{O_2}^o(1 - X_{CO_2}^e - X_{CO}^e) - X_{O_2}^e(1 - X_{CO_2}^o)}{(1 - X_{O_2}^e - X_{CO_2}^e - X_{CO}^e)X_{O_2}^o} X_{O_2}^e \frac{M_{O_2}}{M_e} \dot{m}_e \quad (3)$$

$$\dot{q} = \left[E\varphi - (E_{CO} - E) \frac{(1 - \varphi) X_{CO}^e}{2 X_{O_2}^e} \right] M_{O_2} \frac{\dot{m}_a}{M_a} (1 - X_{H_2O}^o) X_{O_2}^o \quad (MW) \quad (4)$$

Where,

E – energy released by complete combustion per unit mass of oxygen consumed. Average value for hydrocarbons is 13.1 MJ/kg but if fuel composition is known, then a more precise value can be used. However, the stoichiometric reactions for the crude oils are unknown, thus this average value was used along with a standard deviation of 1.86 as a best estimate. The standard deviation value was taken from reference [6].

E_{co} – Net heat release per unit mass of O_2 consumed for combustion of CO to CO_2 (≈ 17.6 MJ/kg of O_2).

X – mole fraction

a – incoming air

e – exhaust gases

\dot{m} – mass flow rate (kg/s)

o – value before combustion

To determine the theoretical heat release rate based on the burn rate and heat of combustions, the values of 44,560 kJ/kg, 48,359 kJ/kg, and 43,275 kJ/kg were used for heptane, Bakken crude oil, and dilbit crude oil, respectively. These were determined by measurements taken by Intertek for this project.

A.3. IR Camera

The following procedure was used to determine the surface emissive power from measurements taken from the MWIR camera.

The main MWIR camera is calibrated to receive photon counts with a 95% efficiency. The camera is considered linear between 450°C and 1400°C. If pixels have temperatures in each frame that are out of the temperature range, then the data is considered uncalibrated and the pixels is assigned a NaN value. The NaN pixel values will not be considered or have any effect in future calculations. To calculate temperature, an emissivity must be assumed. Most hydrocarbons will become optically thick at a pool diameter of 2 m and thus, an emissivity of one can be assumed. A slightly lower value was used for heptane since it does not soot as heavily as crude oil. A transmissivity value was also required to determine temperature. This was calculated using Hitran. Due to the uncertainty of the emissivity and transmissivity values, a sensitivity analysis was performed.

The temperature data for each pixel is then converted to surface emissive power by the following equation:

$$SEP = \sigma T^4$$

Where SEP is the surface emissive power, σ is $\frac{2\pi^5\kappa^4}{15c^2h^3}$, T is the temperature in Kelvins, κ is the Boltzmann's constant, h is Planck's constant and c is the speed of light. The SEP calculated is corrected for transmission losses. Figure A-2 shows the counts from the camera (top-left panel), temperature in Kelvins (top-center panel), and SEP in kW/m² (top-right panel) at 1030.3 seconds from start of experiment. The panels at the bottom (from left to right) show the max and mean SEP

through time, the instantaneous histogram of the SEP, instantaneous bounded dimensions of the fire, and the dimension through time.

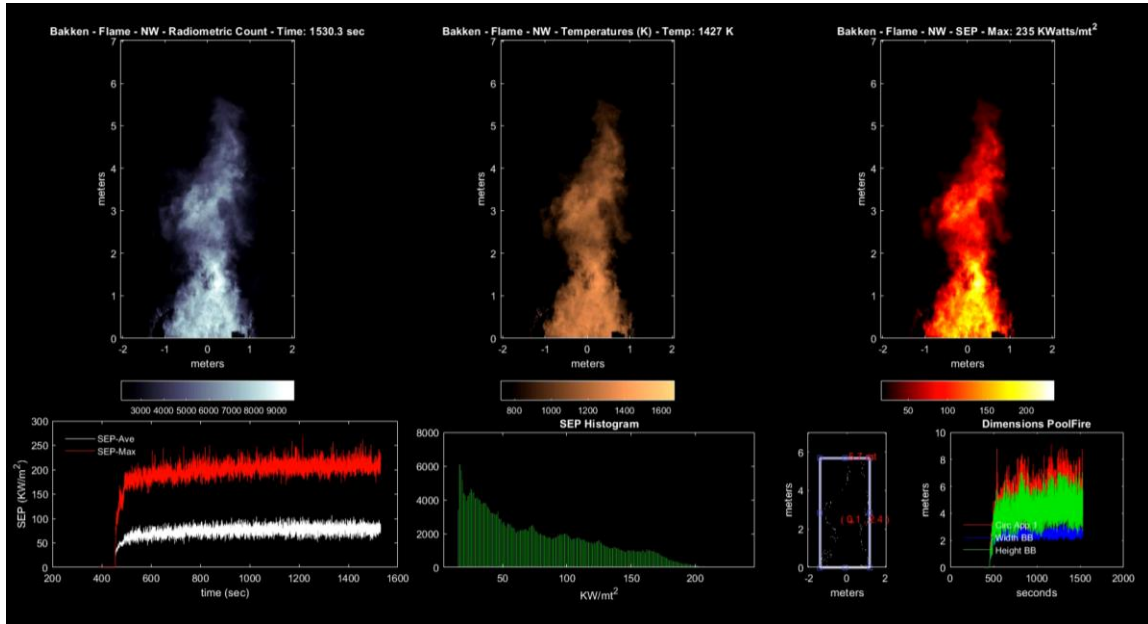


Figure A-2: Data frame with (top row) images from MWIR camera (from left to right) counts, temperature, and SEP. From left to right – bottom row: History curves for maximum and average SEP, histogram for the instantaneous SEP, Box fit for flame, and fire dimension history.

Frames taken during steady-state were averaged for temperature and SEP, see Figure A-3. Similarly, the maximum values for temperature were determined for each frame on the list and averaged.

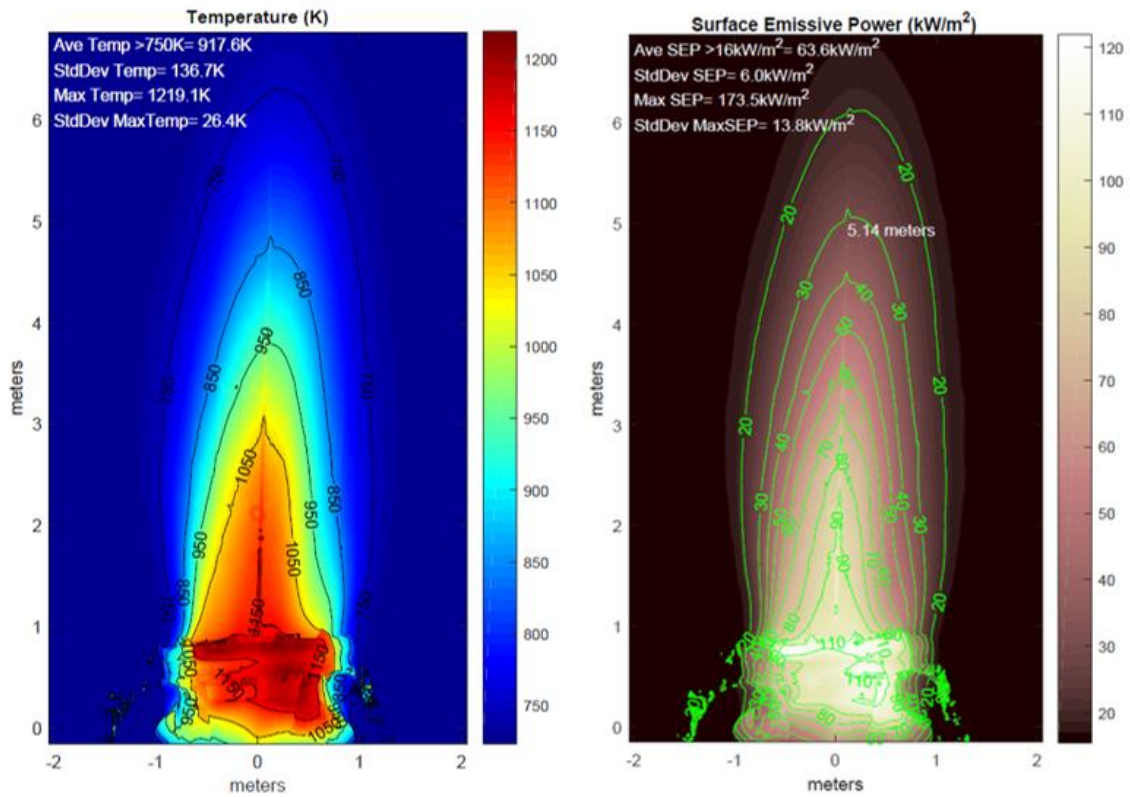


Figure A-3: Average temperature and average SEP from heptane Test 1.1. Panel (a): temperature distribution calculated with emissivity (ϵ) of 0.97 and air transmission (T_x) of 0.95. Panel (b): SEP distribution calculated with emissivity (ϵ) of 1.0 and air transmission (T_x) of 0.95.

The vertical profiles from the two averages can be seen in Figure A-4 through Figure A-16. Notice that for the figures the temperature is calibrated between 450°C and 1200°C (723.15K and 1473.15K). In each figure, the profile in the top panel is calculated with emissivity (ϵ) of 0.97 and air transmission (T_x) of 0.95. The profile in the bottom panel is calculated with ϵ of 1.0 and air T_x of 0.95.

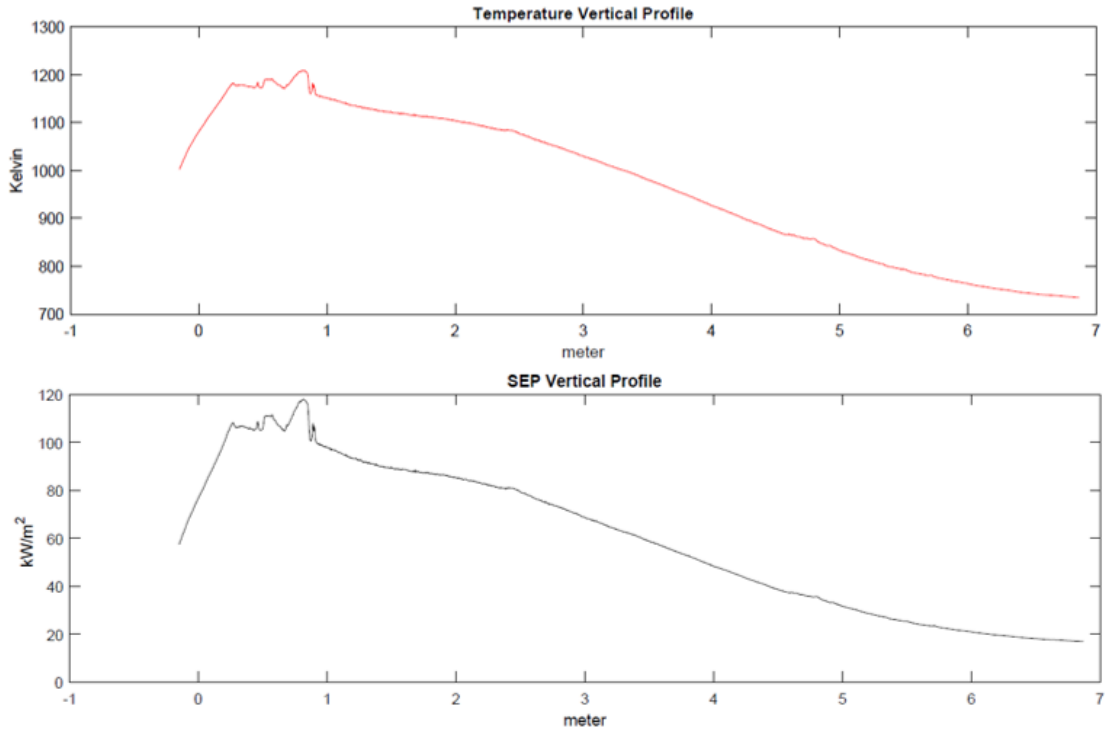


Figure A-4: Average temperature and average SEP vertical profiles for heptane Test 1.1 with calorimeter.

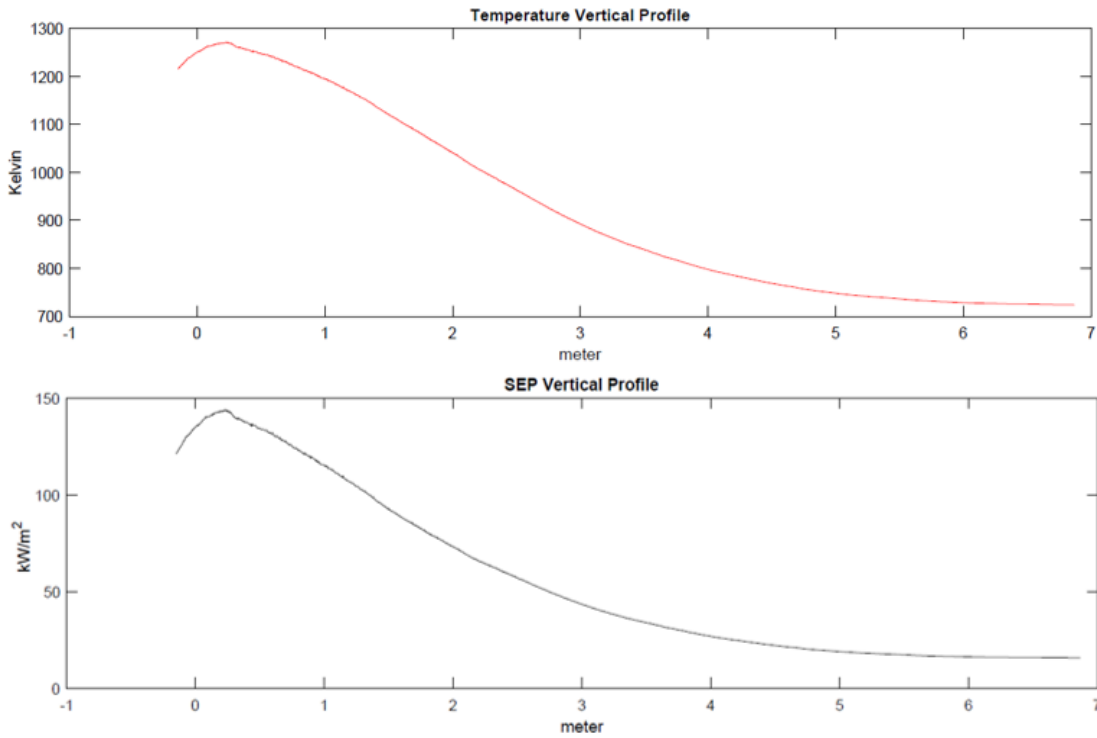


Figure A-5: Average temperature and average SEP vertical profiles for Bakken Test 2.1 without calorimeter.

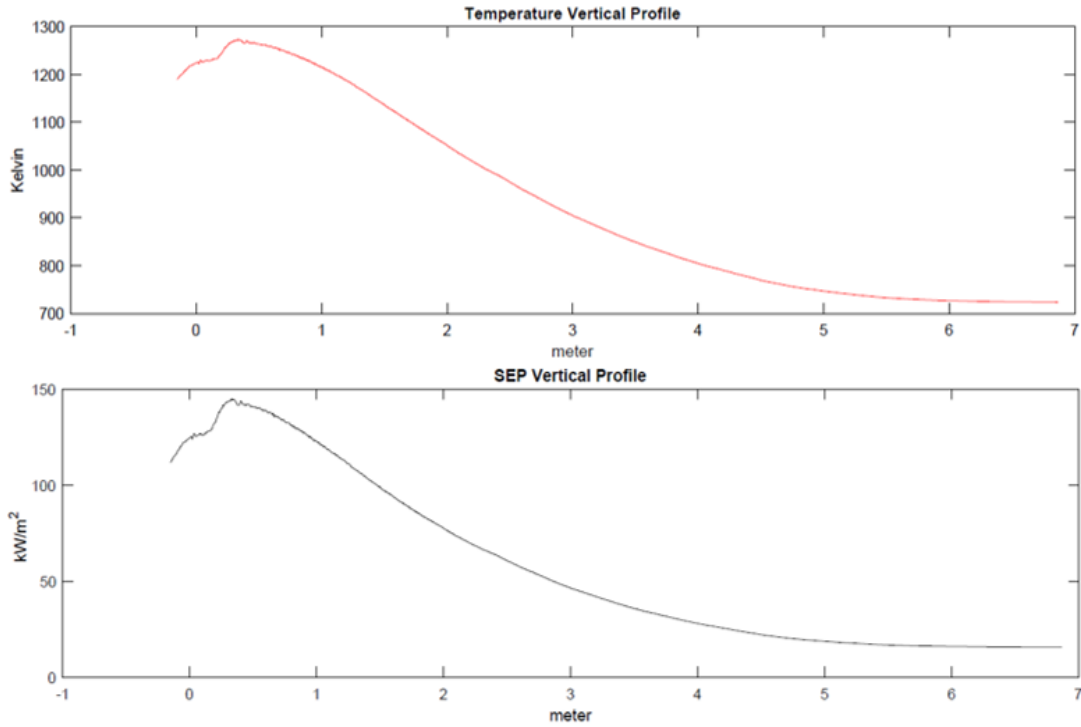


Figure A-6: Average temperature and average SEP vertical profiles for Bakken Test 2.2 with calorimeter.

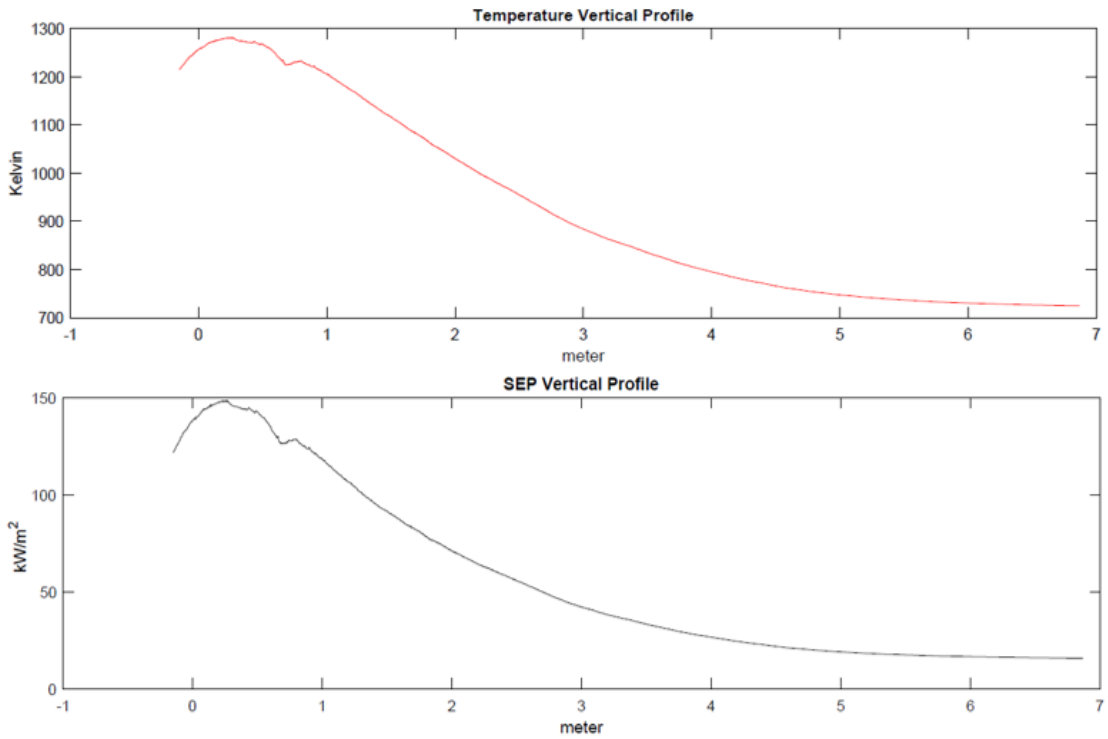


Figure A-7: Average temperature and average SEP vertical profiles for Bakken Test 2.3 with calorimeter.

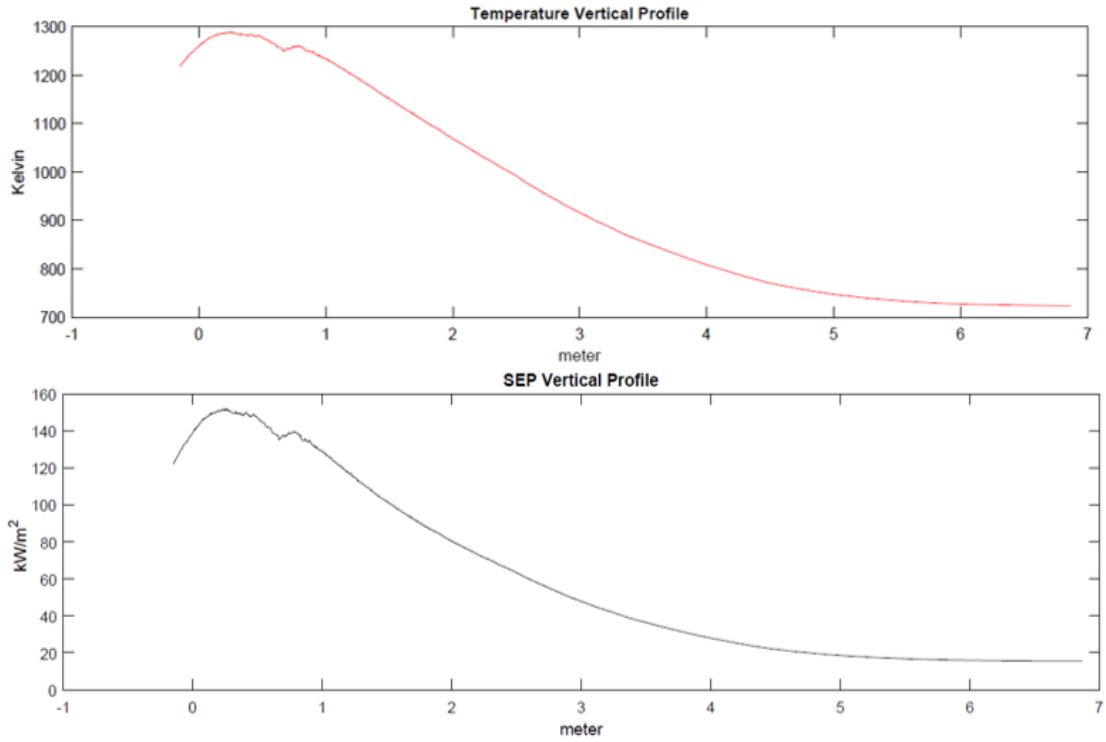


Figure A-8: Average temperature and average SEP vertical profiles for Bakken Test 2.4 with calorimeter.

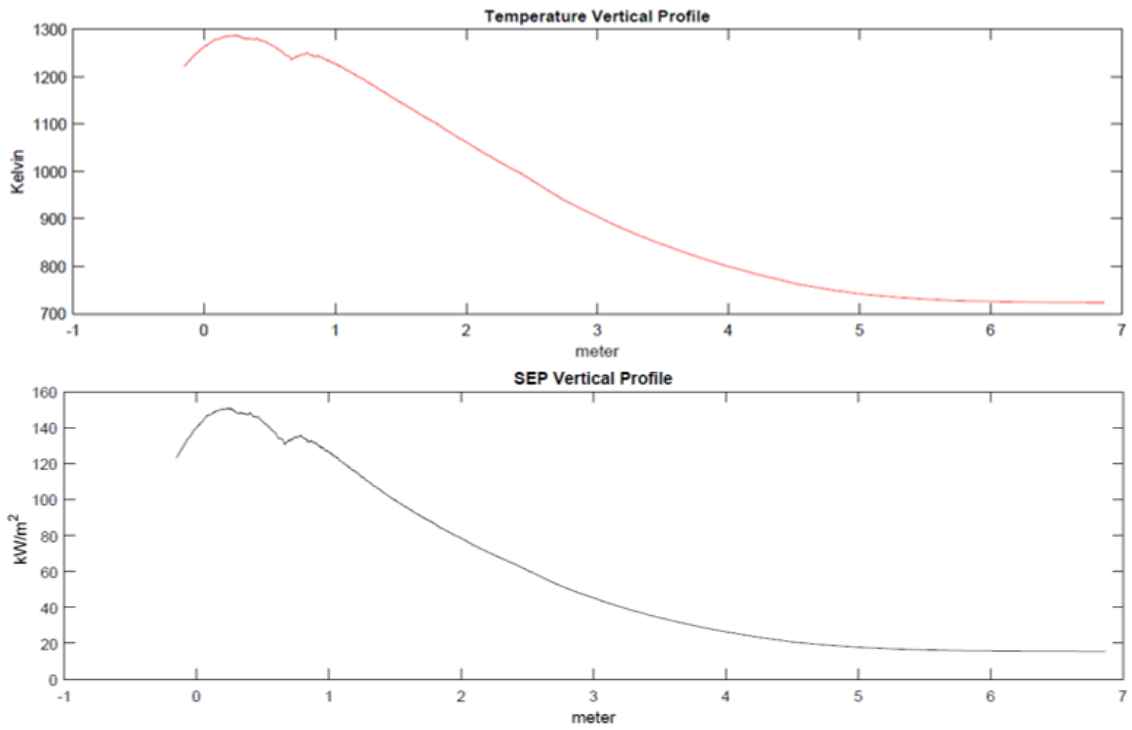


Figure A-9: Average temperature and average SEP vertical profiles for Bakken Test 2.5 with calorimeter.

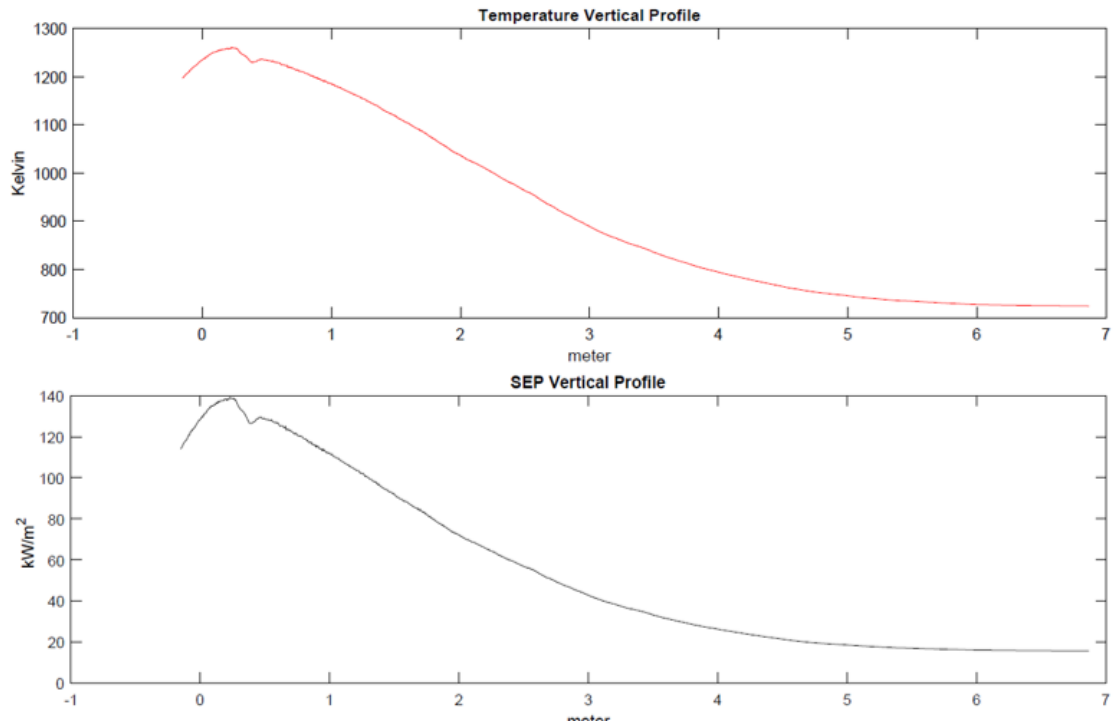


Figure A-10: Average temperature and average SEP vertical profiles for Bakken Test 2.6 without calorimeter.

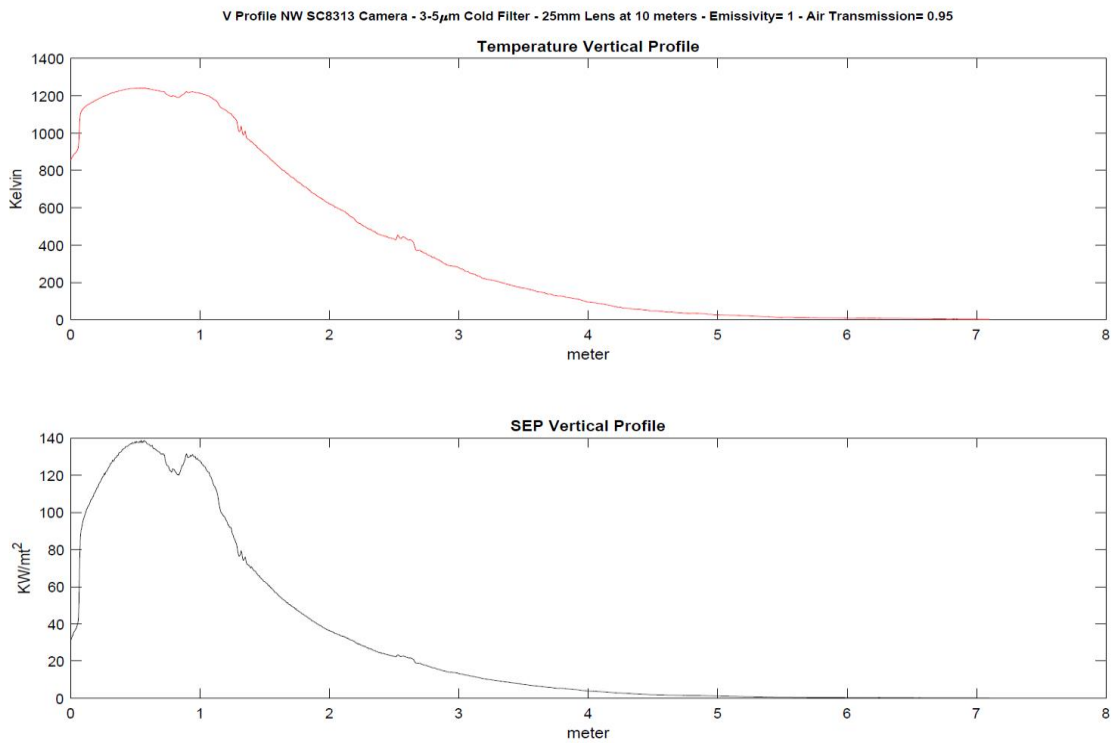


Figure A-11: Average temperature and average SEP vertical profiles for dilbit Test 3.1 with calorimeter.

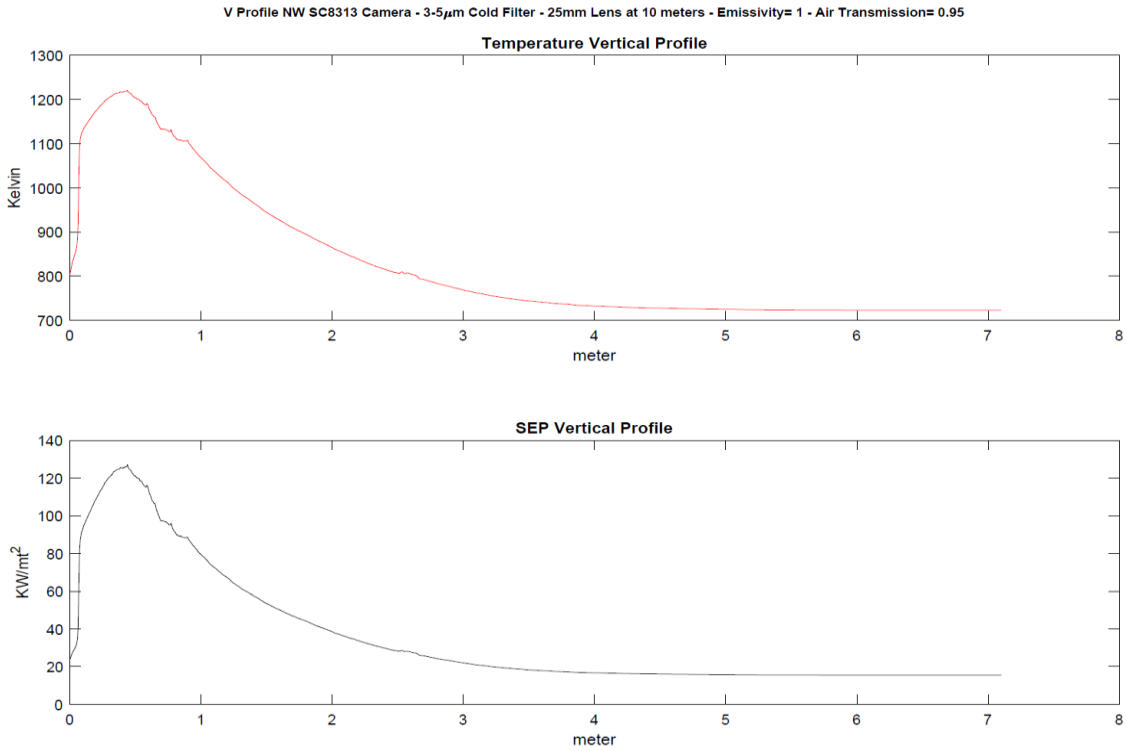


Figure A-12: Average temperature and average SEP vertical profiles for dilbit Test 3.2 with calorimeter.

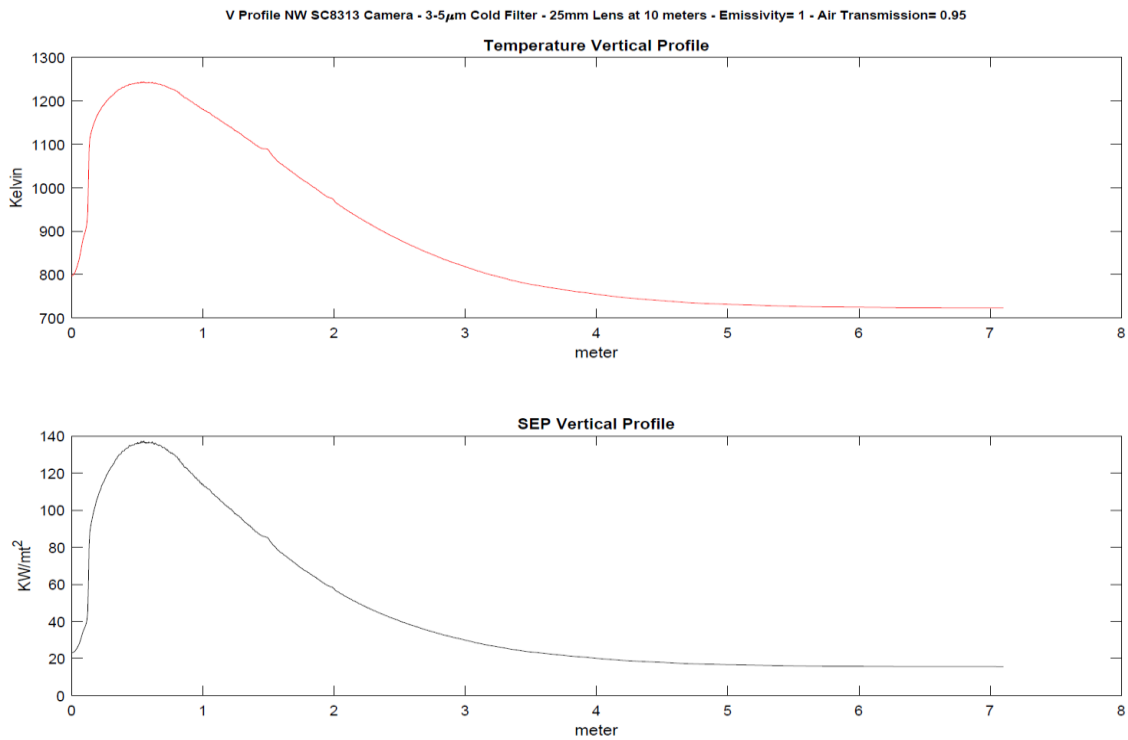


Figure A-13: Average temperature and average SEP vertical profiles for dilbit Test 3.3 without calorimeter.

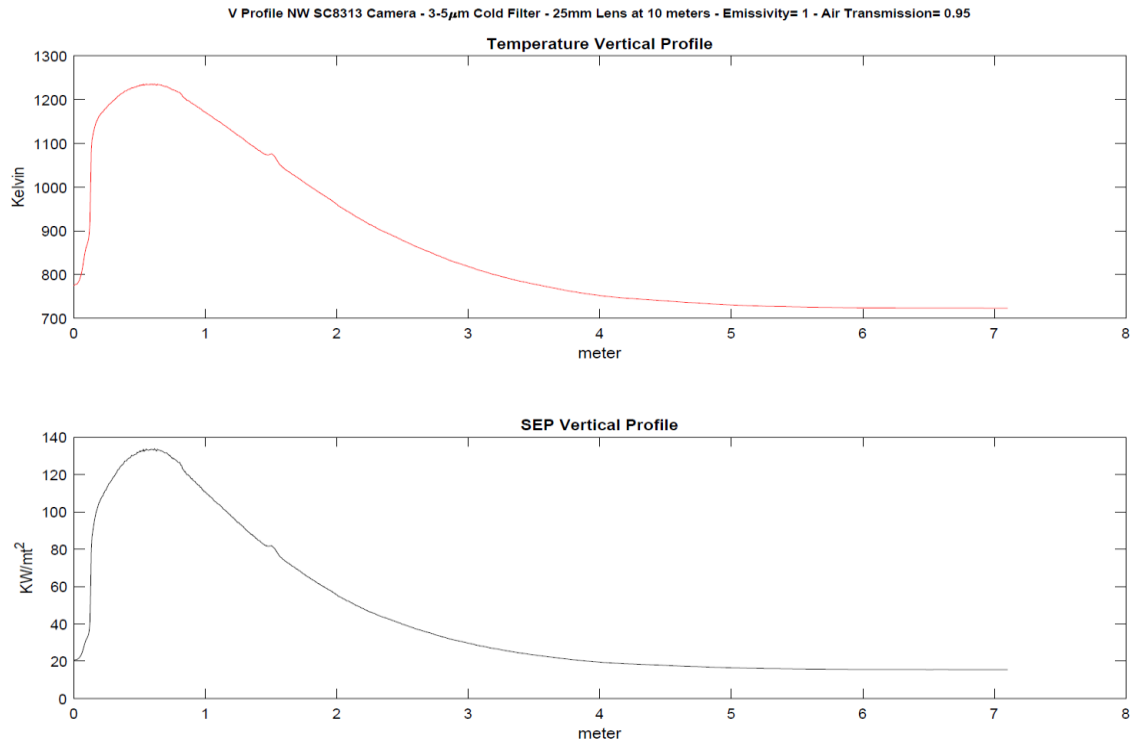


Figure A-14: Average temperature and average SEP vertical profiles for dilbit Test 3.4 without calorimeter.

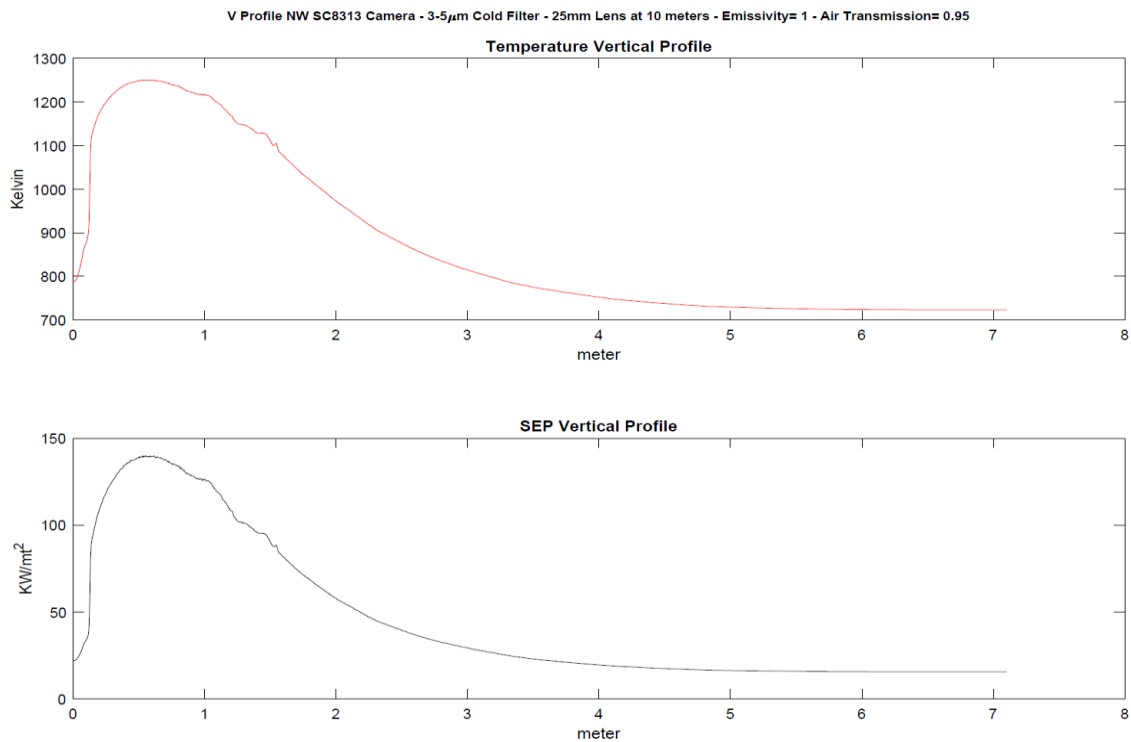


Figure A-15: Average temperature and average SEP vertical profiles for dilbit Test 3.5 with calorimeter.

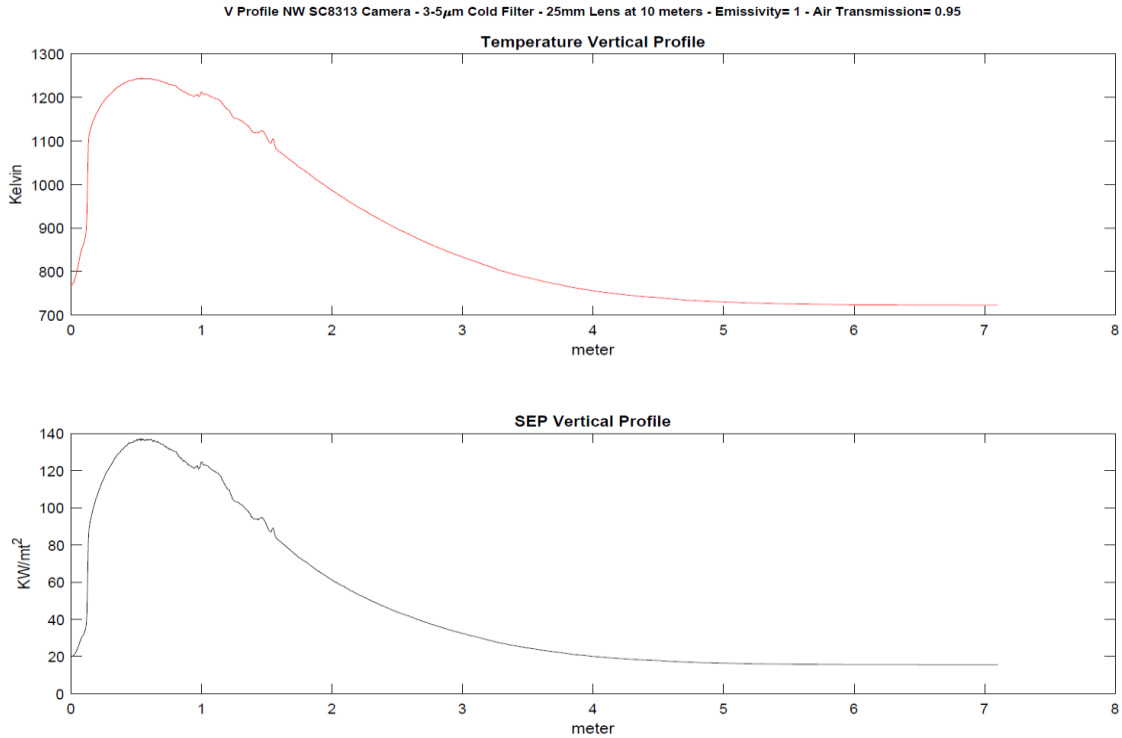


Figure A-16: Average temperature and average SEP vertical profiles for dilbit Test 3.6 with calorimeter.

The calculations of air path transmission were estimated using HiTran for a 10-meter path, with the assumption of “SubArctic Lat 60N,” during the winter time. “SubArctic Lat 60N” is one of six environmental options provided for partial pressure estimations in HiTran. While Albuquerque is located at 35-degree latitude north, its desert area location tends to behave more like the “SubArctic Lat 60N” for the level of humidity. We should notice that for the 3-5 μ m transmission band, water and CO₂ are the main gases that will affect absorption. CO₂ is ubiquitous regardless of the season and location and its effects on absorption are well defined after a couple of meters. Water absorption effects become pronounced after 5 meters, and the calculations with HiTran predict 0.94, but given the dryness during the tests in December of 2017 and January of 2018, it was selected at 0.95. Due to the uncertainty in values for emissivity and transmissivity, a sensitivity analysis was performed using various values. See Table A-2 for the sensitivity analysis for Test 1.1. Figure A-17 and Figure A-18 show a graphical depiction of the same sensitivity analysis for SEP and temperature, respectively.

Table A-2: SEP and temperature sensitivity to emissivity and transmissivity (Test 1.1)

Emissivity	Air Path Tx	Peak SEP (kW/m²)	Overall SEP (kW/m²)	Peak Temp (K)	Overall Temp (K)	Height at 30 kW/m² (m)
1.00	0.97	168.92	62.45	1200.31	911.46	5.11
1.00	0.96	171.20	63.04	1204.07	912.70	5.13
1.00	0.95	173.55	63.64	1207.89	913.93	5.14
1.00	0.94	175.96	64.28	1211.77	915.21	5.16
1.00	0.93	178.44	64.91	1215.72	916.50	5.16
1.00	0.92	180.99	65.56	1219.73	917.78	5.19
1.00	0.91	183.61	66.24	1223.81	919.10	5.20
1.00	0.90	186.30	66.92	1227.97	920.44	5.22
1.00	0.89	189.07	67.62	1232.19	921.80	5.23
0.99	0.97	171.13	63.02	1203.95	912.67	5.13
0.99	0.96	173.45	63.63	1207.73	913.88	5.14
0.99	0.95	175.84	64.24	1211.57	915.15	5.16
0.99	0.94	178.29	64.86	1215.48	916.41	5.16
0.99	0.93	180.81	65.52	1219.45	917.69	5.18
0.99	0.92	183.39	66.18	1223.49	919.00	5.19
0.99	0.91	186.06	66.87	1227.59	920.32	5.22
0.99	0.90	188.79	67.55	1231.77	921.67	5.23
0.99	0.89	191.61	68.26	1236.02	923.04	5.25
0.98	0.97	173.41	63.62	1207.65	913.85	5.14
0.98	0.96	175.77	64.22	1211.46	915.11	5.15
0.98	0.95	178.19	64.86	1215.32	916.37	5.16
0.98	0.94	180.68	65.48	1219.25	917.62	5.18
0.98	0.93	183.24	66.15	1223.24	918.92	5.19
0.98	0.92	185.86	66.81	1227.30	920.23	5.22
0.98	0.91	188.57	67.49	1231.43	921.56	5.23
0.98	0.90	191.35	68.20	1235.63	922.91	5.25
0.98	0.89	194.22	68.91	1239.90	924.29	5.27
0.97	0.97	175.74	64.21	1211.42	915.09	5.15
0.97	0.96	178.14	64.84	1215.24	916.34	5.16
0.97	0.95	180.60	65.46	1219.13	917.59	5.18
0.97	0.94	183.13	66.12	1223.07	918.87	5.19
0.97	0.93	185.73	66.77	1227.09	920.16	5.21
0.97	0.92	188.40	67.46	1231.17	921.48	5.23
0.97	0.91	191.15	68.14	1235.32	922.81	5.25
0.97	0.90	193.98	68.87	1239.55	924.16	5.27

Emissivity	Air Path Tx	Peak SEP (kW/m²)	Overall SEP (kW/m²)	Peak Temp (K)	Overall Temp (K)	Height at 30 kW/m² (m)
0.97	0.89	196.89	69.58	1243.85	925.56	5.31
0.96	0.97	178.14	64.84	1215.24	916.34	5.16
0.96	0.96	180.57	65.45	1219.08	917.58	5.18
0.96	0.95	183.08	66.10	1222.99	918.84	5.19
0.96	0.94	185.65	66.75	1226.96	920.12	5.21
0.96	0.93	188.29	67.43	1231.00	921.42	5.23
0.96	0.92	191.01	68.12	1235.11	922.74	5.25
0.96	0.91	193.80	68.81	1239.28	924.08	5.27
0.96	0.90	196.68	69.55	1243.53	925.46	5.31
0.96	0.89	199.64	70.27	1247.86	926.81	5.31
0.95	0.97	180.60	65.46	1219.13	917.59	5.18
0.95	0.96	183.08	66.10	1222.99	918.84	5.19
0.95	0.95	185.62	66.74	1226.92	920.11	5.21
0.95	0.94	188.23	67.41	1230.92	921.39	5.23
0.95	0.93	190.92	68.10	1234.98	922.70	5.25
0.95	0.92	193.68	68.78	1239.11	924.02	5.27
0.95	0.91	196.52	69.50	1243.31	925.39	5.30
0.95	0.90	199.45	70.24	1247.58	926.72	5.31
0.95	0.89	202.46	70.97	1251.93	928.09	5.34

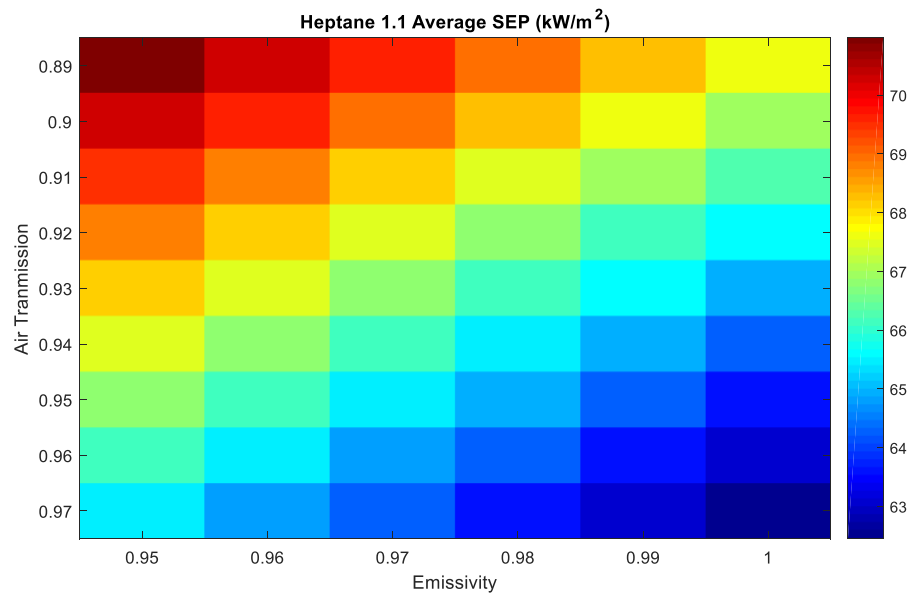
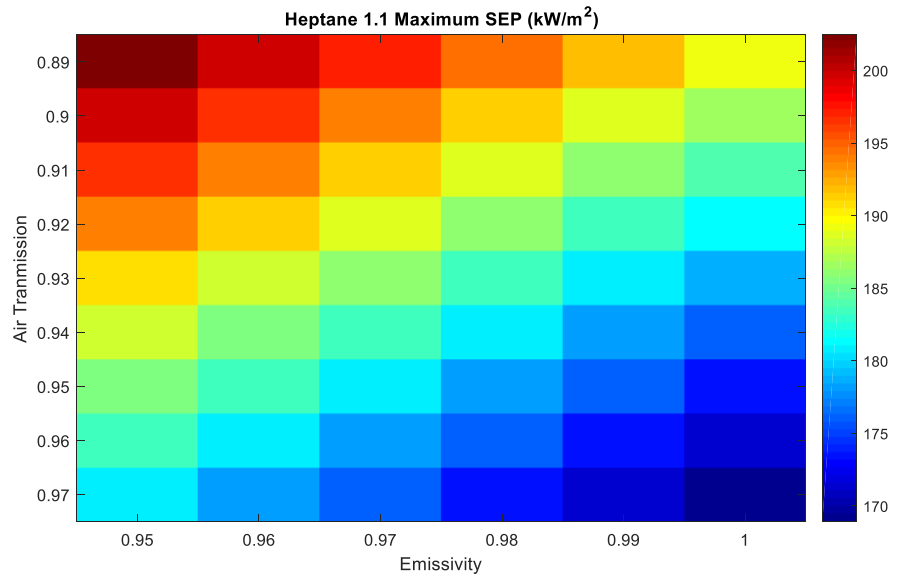


Figure A-17: Graphical depiction of the SEP sensitivity analysis from Table 2 for heptane Test 1.1.

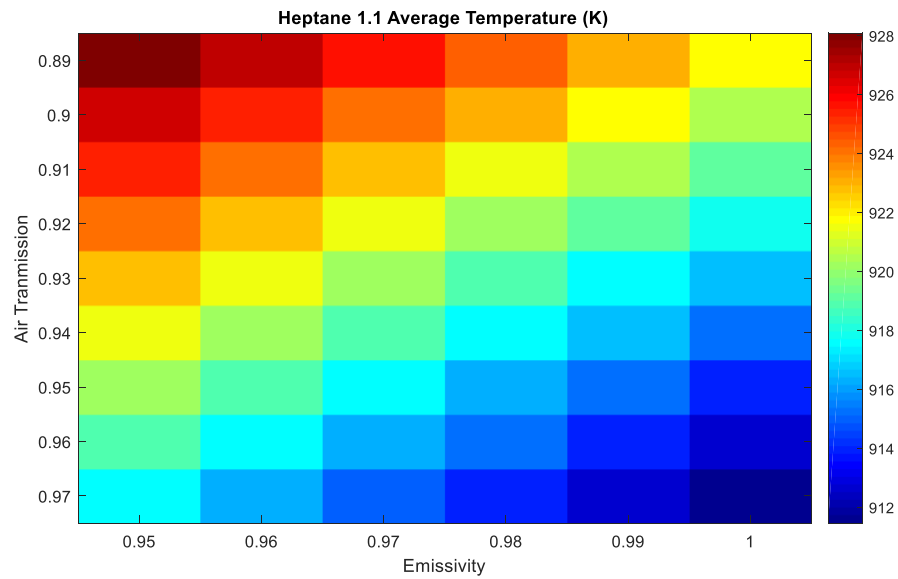
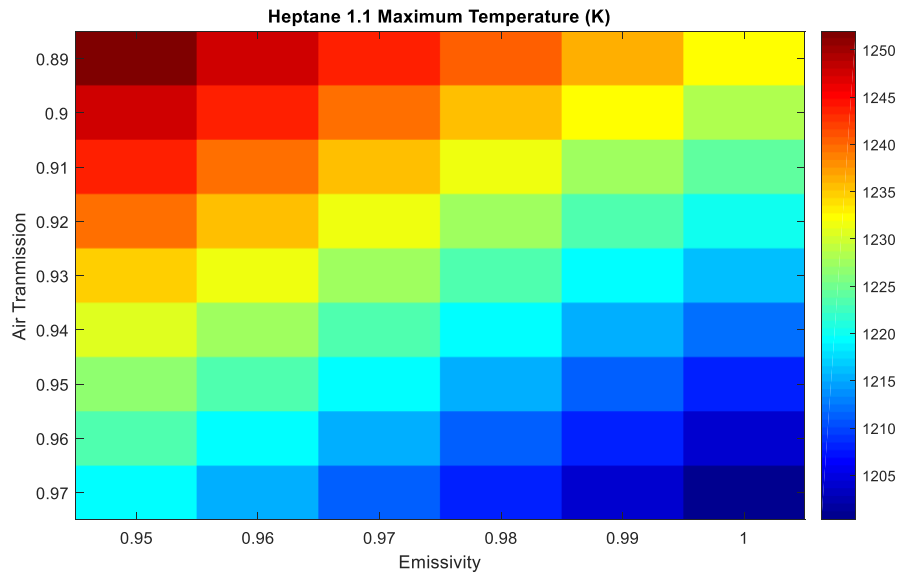


Figure A-18: Graphical depiction of the temperature sensitivity analysis from Table 2 for heptane Test 1.1.

DISTRIBUTION

Email - external

Name	Company Email Address	Company Name
Yoon Ko	Yoon.Ko@nrc-cnrc.gc.ca	National Research Council of Canada, Fire Safety, 1200 Montreal Rd, Building M-59, Ottawa, Ontario, Canada K1A 0R6

Email—Internal

Name	Org.	Sandia Email Address
Technical Library	9536	libref@sandia.gov

This page left blank

This page left blank



Sandia
National
Laboratories

Sandia National Laboratories is a multimission laboratory managed and operated by National Technology & Engineering Solutions of Sandia LLC, a wholly owned subsidiary of Honeywell International Inc. for the U.S. Department of Energy's National Nuclear Security Administration under contract DE-NA0003525.

Supplement B. Crude oil Characterization report

SANDIA REPORT

SAND2021-3389
Printed March 2021



Sandia
National
Laboratories

Fuels Characterization for National Research Council Canada 2-m Pool Fire Test Series

David L. Lord; Joseph W. Hogge; Raymond G. Allen

Prepared by
Sandia National Laboratories
Albuquerque, New Mexico
87185 and Livermore,
California 94550

Issued by Sandia National Laboratories, operated for the United States Department of Energy by National Technology & Engineering Solutions of Sandia, LLC.

NOTICE: This report was prepared as an account of work sponsored by an agency of the United States Government. Neither the United States Government, nor any agency thereof, nor any of their employees, nor any of their contractors, subcontractors, or their employees, make any warranty, express or implied, or assume any legal liability or responsibility for the accuracy, completeness, or usefulness of any information, apparatus, product, or process disclosed, or represent that its use would not infringe privately owned rights. Reference herein to any specific commercial product, process, or service by trade name, trademark, manufacturer, or otherwise, does not necessarily constitute or imply its endorsement, recommendation, or favoring by the United States Government, any agency thereof, or any of their contractors or subcontractors. The views and opinions expressed herein do not necessarily state or reflect those of the United States Government, any agency thereof, or any of their contractors.

Printed in the United States of America. This report has been reproduced directly from the best available copy.

Available to DOE and DOE contractors from

U.S. Department of Energy
Office of Scientific and Technical Information
P.O. Box 62
Oak Ridge, TN 37831

Telephone: (865) 576-8401
Facsimile: (865) 576-5728
E-Mail: reports@osti.gov
Online ordering: <http://www.osti.gov/scitech>

Available to the public from

U.S. Department of Commerce
National Technical Information Service
5301 Shawnee Rd
Alexandria, VA 22312

Telephone: (800) 553-6847
Facsimile: (703) 605-6900
E-Mail: orders@ntis.gov
Online order: <https://classic.ntis.gov/help/order-methods/>



ABSTRACT

This report provides a detailed analysis of the physical and chemical properties of three liquid hydrocarbon fuels: heptane, Bakken crude, and a diluted bitumen, that were subsequently tested in a series of 2-m pool fire experiments at Sandia National Laboratories for the National Research Council Canada. Properties such as relative density, vapor pressure ($VPCR_x$), composition, and heat of combustion were evaluated. The heptane analysis, with relative density = 0.69 (at 15°C), confirmed that the material tested was consistent with high-purity (>99%) n-heptane. The Bakken crude, with a relative density = 0.81 (at 15°C), exhibited a vapor pressure by $VPCR_{0.2}(37.8^\circ\text{C})$ in the range 120-157 kPa. The dilbit, with a relative density = 0.92 (at 15°C) exhibited a vapor pressure by $VPCR_{0.2}(37.8^\circ\text{C})$ in the range 85-98 kPa. Solids remaining in the test pans after the pool fires were also collected and weighed. No detectable solids were left after the heptane burns. In contrast, the crude oils left some brittle, black solid residue. On average, dilbit pool fires left about 40× more residue by mass than Bakken pool fires for equivalent mass of fuel feed.

ACKNOWLEDGEMENTS

This work was funded by the National Research Council Canada and Transport Canada. Additional oil properties data was made available through sharing agreements between Transport Canada and the U.S. Department of Energy.

The authors would like to thank Louis Ory from Intertek for sampling support, Amanda Prefontaine from InnoTech Alberta for consultation on sample handling and analysis methods, and the Fire Sciences team at Sandia National Laboratories for their help with fuel storage, conditioning, and sampling required to meet the objectives of this research study.

CONTENTS

1. Introduction.....	11
2. n-Heptane Fuel Properties Characterization.....	13
2.1. n-Heptane Sampling Methods.....	13
2.2. n-Heptane Analysis Methods.....	14
3. Bakken Crude Sampling and Analysis Methods.....	15
3.1. Large Oil Sample Acquisition and Tanker Operations.....	15
3.2. Subsampling Schedule.....	15
3.3. Subsampling Methods.....	16
3.3.1. Sampling Events B1, B2, and B3.....	16
3.3.2. Liquid Phase Subsampling (B4) prior to first Bakken pool fire (Test 2.3).....	17
3.3.3. Liquid Phase Subsample (B6) prior to last Bakken Pool Fire (Test 2.6).....	18
3.3.4. Solids Sampling (B5 and B7) after Bakken Pool Fires.....	19
3.4. Bakken Crude Analysis Methods.....	21
3.4.1. Analysis of Sampling Events B1, B2 and B8.....	21
3.4.2. Analysis of Sampling Events B4 and B6.....	21
3.4.2.1. VPCR _x (I) (ASTM D6377-M) Expansion Series.....	22
3.4.2.2. Pressurized Compositional Analysis.....	23
3.4.2.3. Unpressurized Physical Properties Determination.....	23
3.4.3. Equation of State (EOS) Modeling.....	23
4. Diluted Bitumen Sampling and Analysis Methods.....	25
4.1. Dilbit Sample Acquisition.....	25
4.2. Subsampling Schedule.....	25
4.3. Subsampling Methods.....	26
4.3.1. Liquid Phase Subsampling (D2) Prior to First Dilbit Pool Fire (Test 3.1).....	26
4.3.2. Liquid Phase Subsampling (D4) prior to Last Dilbit Pool Fire (Test 3.6).....	28
4.3.3. Solid phase subsampling (D3) after the first Dilbit Pool Fire (Test 3.1).....	29
4.3.4. Solids sampling (D5) after the last Dilbit Pool Fire (Test 3.6).....	31
4.4. Dilbit Crude Analysis Methods.....	31
4.4.1. Analysis of Sampling Events D1, D2, D4.....	31
5. Experimental Results.....	33
5.1. General statement on fuels comparison.....	33
5.1.1. Fuel Visual Properties.....	33
5.2. n-Heptane Analysis Results.....	34
5.3. Crude Oil Unpressurized Properties.....	35
5.3.1. Bakken Physical Properties (Sampling Event B1 – Loading Site).....	35
5.4. Fuel Compositions.....	36
5.4.1. Bakken Whole Oil Composition.....	36
5.4.2. Dilbit Whole Oil Composition.....	39
5.5. Fuel Vapor Pressures.....	42
5.5.1. Bakken VPCR _x (37.8°C; 100°F) Results.....	42
5.5.2. Bakken VPCR _x (50°C; 122°F) Results.....	43
5.5.3. Dilbit VPCR _x (37.8°C; 100°F) Results.....	44
5.5.4. Dilbit VPCR _x (122°F; 50°C) Results.....	45
5.5.5. Equation of State-Modeled VPCR _x (I).....	46
5.6. Other Selected Properties.....	50

5.6.1. Other Bakken Properties.....	50
5.6.2. Other Dilbit Properties.....	51
6. Additional Observations.....	53
6.1. Comparison of Bakken and Dilbit Properties.....	53
6.2. Diluent Composition in the Dilbit.....	53
6.3. Boiling Point Distributions of the Fuels.....	55
6.4. Density vs. VPCR.....	56
6.5. Post-Burn Solids Mass.....	60
6.5.1. Bakken Residue.....	60
6.5.2. Dilbit residue.....	61
7. Summary.....	63
8. References.....	65
Appendix A. Dilbit Tank Fill Data.....	68
Appendix B. Tabular Listing of VPCR _x Data.....	69
B.1. Bakken VPCR _x Data.....	69
B.1.1. Direct measurements taken at 37.8 °C and 50 °C.....	69
B.1.2. Summary of measurements on shared Bakken samples from Luketa, Blanchat et al. (2019).....	70
B.1.3. Values calculated from process simulator.....	70
B.2. Dilbit VPCR _x Data.....	71
B.2.1. Direct measurements taken at 37.8 and 50°C.....	71
B.2.2. Values calculated from process simulator.....	72
Appendix C. Tabular Listing of Compositional Data.....	73
C.1. <i>n</i> -Heptane Compositional Data.....	73
C.2. Bakken Compositional Data and Whole Oil Properties.....	75
C.3. Dilbit Compositional Data and Whole Oil Properties.....	77

LIST OF FIGURES

Figure 2-1. Photo of the manual drum pump (drum thief sampler) used to transfer heptane from the drums to the glass bottles.....	13
Figure 2-2. Photo of heptane source drum (green barrel) and sampling bottles (clear glass, three shown) used here.....	14
Figure 3-1. Sandia custom pressurized oil tanker (right) taking a load of crude while displacing water to vacuum truck (left).....	15
Figure 3-2. Photo of a 1-L capacity piston cylinder (in shipping case) used to collect pressurized crude oil during Sampling Event B4.....	17
Figure 3-3. Conceptual drawing of tanker recirculation loop and sampling valve.....	17
Figure 3-4. Photos taken during Sampling Event B6 (Burn Site Subsampling 3) at the Sandia thermal test complex on January 31, 2018, prior to the sixth and final 2-m pool fire. Left photo shows a 500-mL capacity floating piston cylinder during oil fill. Right photo shows a “Boston Round” glass bottle containing about 700 mL Bakken crude.....	18
Figure 3-5. Photo of transfer process from 500-mL piston cylinder to 1-L piston cylinder on laboratory benchtop. The sample transfer line was evacuated with a vacuum pump prior to sample transfer and then the sample was pushed from the 500-mL piston cylinder into the 1-L piston cylinder with an inert gas.....	19

Figure 3-6. Photos of full pan with two insets taken after the January 19, 2018 pool fire, sampling event B5. Spot samples were taken and sent to an offsite laboratory for analysis.....	20
Figure 3-7. Photo of full pan taken after the January 31, 2018 pool fire (sampling event B7). Spot samples were collected and sent to an offsite laboratory for analysis.....	21
Figure 4-1. Photo of eight of the ten modified propane cylinders sent to Sandia to supply the dilbit pool fire testing.....	25
Figure 4-2. Schematic of recirculation loop (a) (reproduced from Prefontaine (2018)) and photo of actual setup.....	27
Figure 4-3. Schematic of combined recirculation/sampling loop reproduced from Prefontaine (2018).....	27
Figure 4-4. Photo of unpressurized glass bottle during ASTM D4057 fill process with dilbit from Tank 12.....	28
Figure 4-5. Photo of pressurized piston cylinder fill process with dilbit from Tank 9. Oil feed on the far end of the cylinder moves the internal piston while displacing glycol through the outlet valve from the close end. The volume of glycol displaced is a primary indicator of sample volume captured in the cylinder.....	29
Figure 4-6. Photo of post-burn solids remaining after Test 3.1. Total mass of solids was measured at 31.48 kg.....	30
Figure 4-7. Close-up photo of sampling post-burn residue from the center of the pan for Test 3.1 on February 7.....	30
Figure 4-8. Photo of post-burn solids remaining after test 3.6. Total mass remaining was measured at 19.60 kg.....	31
Figure 5-1. Comparison of heptane (left), Bakken (center) and diluted bitumen (right) visual properties captured during bottle sampling.....	34
Figure 5-2. Dissolved gas compositions (N_2 , C_1 , CO_2) in Bakken samples taken at loading and at the Sandia burn site.....	37
Figure 5-3. Light ends compositions (C_2 - nC_5) in Bakken samples taken at loading and at the Sandia burn site.....	38
Figure 5-4. Whole oil carbon number plots for Bakken oil sampled at loading and burn sites listed by sampling event and replicate number.....	39
Figure 5-5 Dissolved gas contents for the dilbit subsamples at initial subsampling in December and at Sandia's thermal test complex.....	40
Figure 5-6 Light ends (C_2 - nC_5) measured for the dilbit subsamples.....	41
Figure 5-7 Whole oil compositions measured for the dilbit subsamples.....	42
Figure 5-8. Pressure-expansion column charts showing measured $VPCR_x(100^\circ F; 37.8^\circ C)$ for the Bakken loading samples (B1) and burn site samples (B2, B4, B6, and B8).....	43
Figure 5-9. Pressure-expansion column charts showing measured $VPCR_x(50^\circ C; 122^\circ F)$ for the Bakken burn site samples (B4 and B6).....	44
Figure 5-10. Pressure-expansion column charts showing measured $VPCR_x(37.8^\circ C; 100^\circ F)$ for the dilbit baseline samples (D1) and burn site samples (D2 and D4).....	45
Figure 5-11. Pressure-expansion column charts showing measured $VPCR_x(50^\circ C; 122^\circ F)$ for the dilbit samples.....	46
Figure 5-12. Column chart comparing measured $VPCR_x$ to EOS-modeled $VPCR_x$ for Bakken loading and burn site samples at $T = 100^\circ F; 37.8^\circ C$. Measured values are solid bars with 2σ error bars, modeled values are striped bars.....	47

Figure 5-13 Column chart comparing measured $VPCR_x$ to EOS-modeled $VPCR_x$ for Bakken burn site samples at $T = 50^\circ\text{C}; 122^\circ\text{F}$. Measured values are solid bars, modeled values are striped bars.....	47
Figure 5-14. Column chart comparing measured $VPCR_x$ to EOS-modeled $VPCR_x$ for dilbit loading and burn site samples at $T = 37.8^\circ\text{C}; 100^\circ\text{F}$. Measured values are solid bars, modeled values are striped bars.....	48
Figure 5-15 Column chart comparing measured $VPCR_x$ to EOS-modeled $VPCR_x$ for dilbit samples at $T = 50^\circ\text{C}; 122^\circ\text{F}$; Measured values are solid bars, modeled values are striped bars.....	49
Figure 6-1. C4-C14 compositions for the dilbit fuel alongside a condensate and bitumen that were likely used in the stream.....	54
Figure 6-2. Measured C4-C14 composition for dilbit fuel (circle, solid line) and a simulated dilbit composition using likely constituents (square, dashed line).....	55
Figure 6-3 Temperature vs. boiling point distribution for the fuels in the burn series.....	56
Figure 6-4: Overlay of density vs $VPCR_4(37.8^\circ\text{C})$ for oils from SPR, PHMSA, NDPC and DOE/DOT/TC COCRS with the fuels tested as part of this project.....	57
Figure 6-5: Overlay of density vs. $VPCR_{0.2}(50^\circ\text{C})$ for oils from SPR, COCRS, and TC with the fuels tested as part of this project.....	59

LIST OF TABLES

Table 1-1. High-level test matrix and sampling schedule.....	11
Table 3-1. Listing of sampling events related to overall crude oil project, with NRC/TC sampling indicated in white rows.....	16
Table 3-2. Temperature and expansion settings for ASTM D6377 $VPCR_x(T)$ measurements to be run on loading site subsamples.....	22
Table 3-3. Instrument settings for “Equilibrium Time” and “Equilibrium dP/dt ” required to confirm that the analysis run for each V/L has reached equilibrium conditions.....	22
Table 4-1. Listing of sampling events supporting the dilbit pool fire series.....	26
Table 5-1. Summary of average fuel properties observed in this study.....	33
Table 5-2. Analysis results for composite heptane sample collected from the 9 heptane drums delivered to Sandia.....	34
Table 5-3. Physical properties of Bakken samples taken at loading site (B1).....	35
Table 5-4. Average measured $VPCR_{0.2}(37.8^\circ\text{C}; 100^\circ\text{F})$ for the five Bakken sampling events.....	43
Table 5-5. Average measured $VPCR_{0.2}(37.8^\circ\text{C}; 100^\circ\text{F})$ for the three dilbit sampling events.....	45
Table 5-6. Physical properties of Bakken samples taken at loading site and Sandia burn site.....	51
Table 5-7. Physical properties of dilbit samples taken at loading site and Sandia burn site.....	52
Table 6-1. A brief comparison of Bakken crude and dilbit properties; bold values represent the larger of the two.....	53
Table 6-2: Sources and methods for $VPCR$ and Density data in.....	58
Table 6-3. Sources and methods for $VPCR_x(50^\circ\text{C})$ and density data in.....	60
Table 6-4. Residue mass (kg) and ratio to oil feed (kg/kg) for the 2-m Bakken pool fire series.....	61
Table 6-5. Summary of post-burn solids residue recovered from pan.....	62

EXECUTIVE SUMMARY

This report provides a detailed analysis of the physical and chemical properties of three liquid hydrocarbon fuels: high purity n-heptane, Bakken crude, and a diluted bitumen, that were subsequently tested in a series of 2-m pool fire experiments at Sandia National Laboratories for the National Research Council Canada. The results of the pool fire tests are described in a separate report¹. Fuel properties such as relative density, vapor pressure (VPCR_x), composition, and heat of combustion were evaluated. Sampling and analysis methods conformed to published industry standards and were selected based on prior related work, industry best practice, and sponsor request. The heptane analysis, with relative density = 0.69 (at 15°C), confirmed that the range of properties tested were consistent with high-purity (>99%) n-heptane. The Bakken crude, with a relative density = 0.81 (at 15°C), exhibited a vapor pressure by VPCR_{0.2}(37.8°C) in the range 120-157 kPa and composition with peak carbon numbers in the C7-C8 range coupled with a rapidly declining heavy end distribution, terminating in a lumped C25+ in the 5-8 mole% range. The diluted bitumen was the densest fuel tested, with a relative density = 0.92 (at 15°C) and a vapor pressure by VPCR_{0.2}(37.8°C) in the range 85-98 kPa. The composition was characterized by a peak mole% at C5-C6 representing the diluent, overlaid with a long, flat heavy end distribution between C10 and C24 and a lumped C25+ in the 28-30 mole% range. This composition was consistent with a 20-25% mixture by volume of condensate (diluent) with about 75-80 vol% bitumen. Heats of combustion for the three fuels ranged from 43-48 MJ/kg. Solids remaining in the test pans after the pool fires were also collected and weighed. No detectable solids were left after the heptane burns. In contrast, the crude oils left brittle, black solid residue. On average, dilbit pool fires left about 40× more residue by mass than Bakken pool fires for equivalent mass of fuel feed.

¹ Luketa, A., A. Cruz-Cabrera, W. Gill, S. Adee and J. Hogge (2019). "Experimental Results of 2-m Heptane, Bakken Crude Oil, and Dilbit Pool Fire Tests Performed for the National Research Council Canada." *in press*. Sandia National Laboratories, Albuquerque, NM 87185.

ACRONYMS AND DEFINITIONS

Abbreviation	Definition
ANSI	American National Standards Institute
ASTM	ASTM International (standards organization)
BKN	Bakken Crude Oil
CFT	Fort Saskatchewan Condensate
DOE	United States Department of Energy
DOT	United States Department of Transportation
FPC	Floating piston cylinder
GPA	Gas Processors Association
NIST	National Institute of Standards and Technology
NRC	National Research Council Canada
TC	Transport Canada
TDG	Transport of Dangerous Goods
TTC	Thermal Test Complex, Sandia National Laboratories
V/L	Vapor to liquid volume ratio (relevant to ASTM D6377 VPCR testing)
VPCR _x	Vapor pressure of crude oil at vapor-liquid volume ratio “x” by ASTM D6377

1. INTRODUCTION

This report summarizes findings from the sampling and analysis of fuels used for the National Research Council Canada (NRC) 2-m pool fire tests run at the Sandia National Laboratories Thermal Test Complex in Albuquerque, New Mexico, USA. The overarching purpose of the research program is to understand how physical and chemical properties of crude oils affect their combustion properties and hazard potential in the event of an accident involving fire during transportation and handling.

Subsamples of three liquid hydrocarbon fuels: *n*-heptane, Bakken crude oil from North Dakota (API gravity = 42.9, sulfur = 0.1 wt%), and a diluted bitumen (dilbit; API gravity = 21.7, sulfur = 3.6 wt%) from Canada were drawn at Sandia and analyzed at offsite laboratories to monitor selected physical and chemical properties including the composition and vapor pressure (VPCR_x) of the materials at selected times throughout the pool fire test series.

A high-level test matrix is shown below in Table 1-1. The scope of this report covers the fluids and solids sampling in columns 4 and 5. The combustion test descriptions and results related to column 3 are given in a separate report (Luketa, Cruz-Cabrera et al. 2019).

Table 1-1. High-level test matrix and sampling schedule.

1	2	3	4	5
		Pool Fire	Pre-burn	Post-burn
Pool Fire Test #	Fuel	Test Date	Fluids Sampling	Solids Sampling
Test Series 1				
1.1	Heptane	12/6/2017	12/4/2017	-
1.2	Heptane	12/7/2017	-	-
1.3	Heptane	12/8/2017	-	-
Test Series 2				
2.3	Bakken	1/19/2018	1/19/2018	1/22/2018
2.4	Bakken	1/24/2018	-	-
2.5	Bakken	1/25/2018	-	-
2.1	Bakken	1/29/2018	-	-
2.2	Bakken	1/30/2018	-	-
2.6	Bakken	1/31/2018	1/31/2018	2/1/2018
Test Series 3				
3.1	Dilbit	2/6/2019	1/28/2019	2/7/2019
3.2	Dilbit	2/14/2019	-	2/15/2019
3.3	Dilbit	2/20/2019	-	2/21/2019
3.4	Dilbit	2/25/2019	-	2/26/2019
3.5	Dilbit	2/27/2019	-	2/28/2019
3.6	Dilbit	3/4/2019	2/27/2019	3/5/2019

This page left blank

2. N-HEPTANE FUEL PROPERTIES CHARACTERIZATION

In this chapter, heptane sampling and property analyses are described. Heptane was used as combustion fuel in a series of 2-m pool fire tests that preceded the Bakken and dilbit pool fire test series. Heptane pool fire data is useful as baseline liquid fuel data for testing and troubleshooting analytical equipment and comparing with crude oils.

2.1. *n*-Heptane Sampling Methods

The heptane fuel arrived at Sandia from a commercial supplier in nine drums of nominally 50 gallons capacity each. A liquid subsample was taken from each using a drum thief sampler compliant with ASTM D4057 (ASTM 2012), Section 7.14: Tube Sampler--Drum or Barrel. See Figure 2-1 for a photo of the sampler used in this work. A single 500-700 mL sample was pulled from each drum, giving nine samples total. Each of these nine samples was placed into a separate unpressurized clear glass bottle. Figure 2-2 shows a drum and several of these sample bottles. An unpressurized sampling approach for collecting, holding, and transporting heptane samples was deemed acceptable in this work because the relatively low vapor pressure (~ 11 kPa @ 37.8 °C; (Williamham, Taylor et al. 1945)) and uniformity in composition of *n*-heptane minimize risk of loss of light ends and resultant property changes during sampling and handling at ambient conditions.



Figure 2-1. Photo of the manual drum pump (drum thief sampler) used to transfer heptane from the drums to the glass bottles.



Figure 2-2. Photo of heptane source drum (green barrel) and sampling bottles (clear glass, three shown) used here.

The samples were labeled and boxed at Sandia, then shipped offsite for analysis. Once the samples reached the lab, equal volumes from each of the nine bottles were combined to form a composite sample. All analytical test results presented here represent properties of this composite sample.

2.2. *n*-Heptane Analysis Methods

Heptane samples were analyzed for the following properties:

1. Purity by chromatographic method ASTM D6730-M (ASTM 2011b) for heptane
2. Relative Density by ASTM D4052 (ASTM 2011a)
3. Heat of Combustion by ASTM D240 (ASTM 2014)
4. Water Content by ASTM E1064 (ASTM 2016g)
5. Flash Point by ASTM D93A (ASTM 2013b)
 - a. Additional Flash Point by ASTM D3828 (ASTM 2016h) by sponsor request
6. Average Molecular Weight by cryoscope (freezing point depression)

3. BAKKEN CRUDE SAMPLING AND ANALYSIS METHODS

This chapter describes the methodology for sampling and analysis of the Bakken crude oil used in the pool fire test series described in Luketa, Cruz-Cabrera et al. (2019). Six pool fires were run with Bakken crude oil in this study. Sandia monitored and coordinated collection and analysis of the crude oil subsamples to establish basic physical and chemical properties of the fuel.

3.1. Large Oil Sample Acquisition and Tanker Operations

Crude oil was acquired from a terminal in North Dakota that handles Bakken production and placed in a custom-designed pressurized tanker truck. The 4,800-gal pressurized tanker (shown in Figure 3-1) used water displacement to isolate the fuel sample from changes in light ends and fixed gases. This main sample of 2,100 gallons of oil was further sampled at different times to characterize any loss of volatile components during the fire testing and the resulting effect on the testing process. These smaller samples were called “subsamples.” Additional detail on sample acquisition is provided in Luketa, Blanchat et al. (2019).



Figure 3-1. Sandia custom pressurized oil tanker (right) taking a load of crude while displacing water to vacuum truck (left)

3.2. Subsampling Schedule

The tanker load of Bakken crude oil was shared by several sponsoring entities including the U.S. Department of Energy (DOE), U.S. Department of Transportation (DOT), Transport Canada, (TC) and the National Research Council Canada (NRC) during the crude oil characterization research program. To reiterate, the 2,100-gallon tanker-load was considered the main oil sample, while the spot samples taken from the main oil for quality testing were considered subsamples. Overall, eight sampling events were planned, the first three and last of which were conducted under the DOE/DOT/TC project, and the 4th-7th were conducted under the NRC/TC project. The current report describes the sampling and analysis specific to the NRC/TC project, represented by events B4-

B7 in the lower half of Table 3-1. Information about the DOE/DOT/TC sampling and analysis plan (Events B1-B3 and B8, shaded) is given in Luketa, Blanchat et al. (2019).

Table 3-1. Listing of sampling events related to overall crude oil project, with NRC/TC sampling indicated in white rows.

Event #	Fuel	Event Name in Multi-Agency Project Schedule	Sponsor	Description
B1	Bakken	Loading Site Subsampling	DOE/DOT/TC	Fluid sampling taken at the crude oil loading site for oil before it entered the tanker
B2	Bakken	Burn Site Subsample 1	DOE/DOT/TC	Fluid sampling taken at the Sandia burn site after homogenization and just prior to use in the 5m pool fire
B3	Bakken	5-m Pool Fire Solids Residue	DOE/DOT/TC	Post-burn solids collected from the pool fire pan
B4	Bakken	Burn Site Subsample 2	NRC/TC	Fluid sampling taken at the Sandia burn site (Thermal Test Complex) after homogenization and just prior to use in the first 2-m pool fire (Pool Fire Test 2.3)
B5	Bakken	2-m Pool Fire Solids Residue	NRC/TC	Post-burn solids collected from the pool fire pan (Pool Fire Test 2.3)
B6	Bakken	Burn Site Subsample 3	NRC/TC	Fluid sampling taken at the Sandia burn site (Thermal Test Complex) after homogenization and just prior to use in the last 2-m pool fire (Pool Fire Test 2.6)
B7	Bakken	2-m Pool Fire Solids Residue	NRC/TC	Post-burn solids collected from the pool fire pan (Pool Fire Test 2.6)
B8	Bakken	July 2018 Subsample	DOE/DOT/TC	Fluid sampling taken at the Sandia burn site in the month of July 2018

3.3. Subsampling Methods

Enough sample volume was collected at each liquid sampling point (Sampling Events B1, B2, B4, B6, and B8) so that the relevant analytical portion of the analysis plan could be performed twice. As such, half of the samples were utilized in analysis and the other half were retained in reserve for backup analysis if needed.

3.3.1. Sampling Events B1, B2, and B3

Descriptions of subsampling events Loading Site Subsample (B1) and Burn Site Subsample 1 (B2) are given in Luketa, Blanchat et al. (2019). Pool fire solids residue from B3 was acquired and shipped to a lab that was under contract with TC.

3.3.2. Liquid Phase Subsampling (B4) prior to first Bakken pool fire (Test 2. 3)

A fluid subsample (B4) was taken from the pressurized tanker at the Sandia Thermal Test Complex (TTC) to establish properties of the material within one day of the first 2-m crude oil pool fire test.

Crude oil samples for vapor pressure and composition were collected using closed cylinder sampling methods displacing a glycol-water mixture, compliant with Gas Processors Association (GPA) standard GPA 2174 (GPA 2014). Source oil pressure was maintained between 40-45 psig to facilitate operation of the piston cylinder devices. Six 1-L capacity piston cylinders (see Figure 3-2) were filled to nominally 700 mL each, displacing a water-glycol mixture as the container was loaded with oil. In addition, six 700 mL samples for unpressurized physical property analysis were obtained by ASTM D4057 in 1-L glass bottles.



Figure 3-2. Photo of a 1-L capacity piston cylinder (in shipping case) used to collect pressurized crude oil during Sampling Event B4.

All the above-mentioned subsamples were pulled from a sampling manifold system attached to a recirculation loop on the pressurized Sandia tanker (see conceptual drawing in Figure 3-3). The tanker contents were circulated for several hours by a dedicated recirculation loop to homogenize the contents prior to subsampling and injection into the fire testing facility. The oil was circulated for enough time to allow at least 3 tanker volumes of oil to pass through the circulation pump.

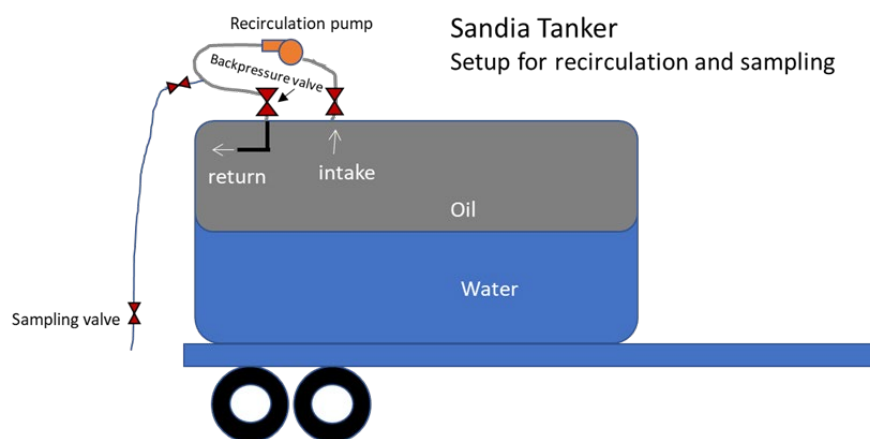


Figure 3-3. Conceptual drawing of tanker recirculation loop and sampling valve.

3.3.3. Liquid Phase Subsample (B6) prior to last Bakken Pool Fire (Test 2.6)

A fluid subsample from Sampling Event B6 (Burn Site Subsample 3) was taken from the pressurized tanker at the Sandia Thermal Test Complex (TTC) to establish properties of the material just prior to the last 2-m crude oil pool fire test (see photos in Figure 3-3).



Figure 3-4. Photos taken during Sampling Event B6 (Burn Site Subsampling 3) at the Sandia thermal test complex on January 31, 2018, prior to the sixth and final 2-m pool fire. Left photo shows a 500-mL capacity floating piston cylinder during oil fill. Right photo shows a “Boston Round” glass bottle containing about 700 mL Bakken crude.

The sampling method varied slightly from prior events because empty 1-L piston cylinders were not available at the Sandia site at the time of sampling. Instead, 500-mL piston cylinders were filled in the field using back-pressure of an inert gas to control the fill rate. The 500-mL piston cylinders were shipped to a crude oil laboratory facility in the US where the samples were transferred to 1-L piston cylinders (see Figure 3-4 for a photo and description of the setup). The 1-L piston cylinders were shipped to their final destination at another crude oil laboratory in Canada where they were analyzed. This transfer of the sample from the 500-mL piston cylinder to a 1-L piston cylinder was required since the 1-L piston cylinders were certified for transport of crude oil samples per Transport Canada regulations. Also, six 700 mL samples for unpressurized physical property analysis were obtained by ASTM D4057 in 1-L glass bottles.

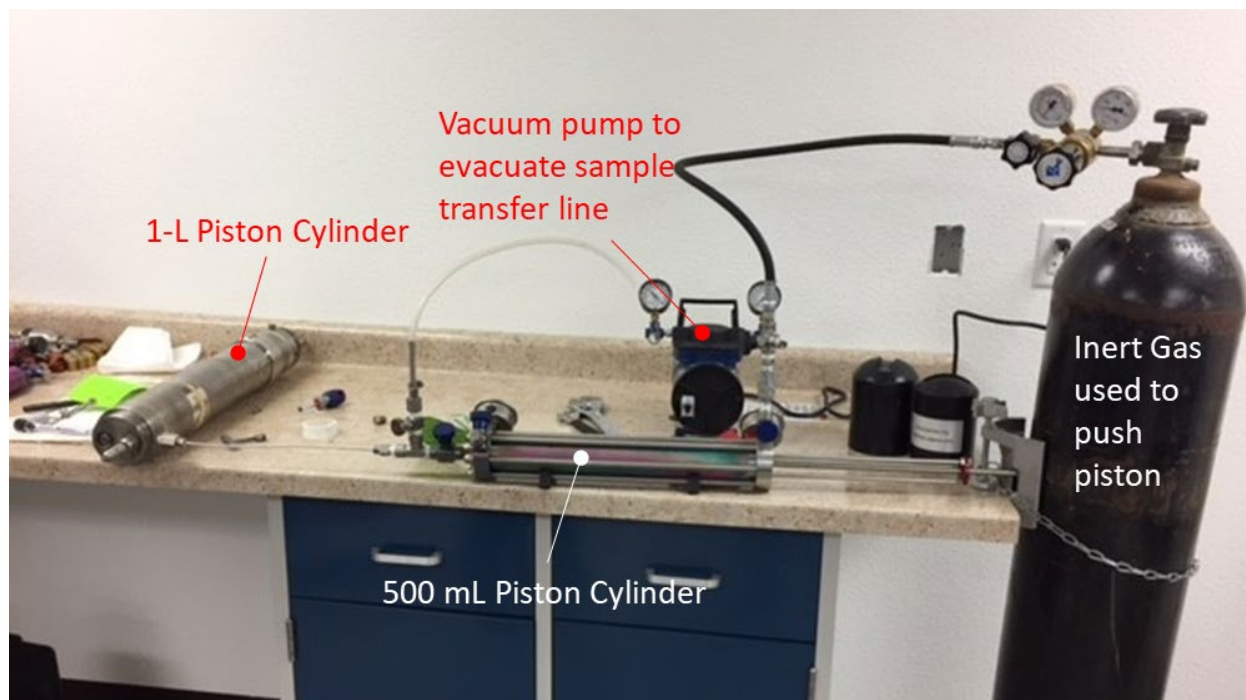


Figure 3-5. Photo of transfer process from 500-mL piston cylinder to 1-L piston cylinder on laboratory benchtop. The sample transfer line was evacuated with a vacuum pump prior to sample transfer and then the sample was pushed from the 500-mL piston cylinder into the 1-L piston cylinder with an inert gas.

3.3.4. Solid Phase Subsampling (B5 and B7) after Bakken Pool Fires

The 2-m Post Burn Solids Residue sample after pool fire test 2.3 (Sampling Event B5) and the 2-m Post Burn Solids Residue after pool fire test 2.6 (Sampling Event B7) were taken to evaluate some basic features of the residue. On-site analyses included:

- Photographs of pan
- Qualitative description of residual material (solid, slurry, viscous liquid or paste)
- Total mass of residual material

Three samples were collected and placed into plastic wide-mouth sampling jars for offsite laboratory analyses that were outside the scope of this report. The three locations for analysis represented the center of the pan, midpoint along the radius of the pan, and the outer edge against the lip of the pan. Sampling procedures were guided by ASTM D4057-12 (ASTM 2012), section 9.29.2: solid and semi-solid grab sampling.

The Bakken post-burn solids were dry and brittle. Deposition quantity and quality did not appear to depend on radius. Photos of the pan residue after the Jan 19 test (Sampling Event B5) and the Jan 31 test (Sampling Event B7), are shown in Figure 3-5 and Figure 3-6, respectively. In areas where solids deposition was thickest, a light gray dusty material appeared to sit on top of a dark black glassy solid that was cemented to the pan.



Figure 3-6. Photos of full pan with two insets taken after the January 19, 2018 pool fire, sampling event B5. Spot samples were taken and sent to an offsite laboratory for analysis.



Figure 3-7. Photo of full pan taken after the January 31, 2018 pool fire (sampling event B7). Spot samples were collected and sent to an offsite laboratory for analysis.

3.4. Bakken Crude Analysis Methods

The analysis methods used on the samples depended on the sample sources. The fluid subsamples taken at tanker loading (Event B1 in Table 3-1) were subjected to a range of physical property tests that provide a general physical description commonly used to evaluate oil quality in the midstream sector. The fluid subsamples taken at the burn site (Events B2, B4, B6, B8 in Table 3-1) were subjected to a more particular set of tests centered around volatility and combustion properties.

3.4.1. Analysis of Sampling Events B1 , B2 and B 8

Loading Site Subsampling (Sampling Event B1), Burn Site Subsample 1 (Sampling Event B2), Burn Site Subsample 4 (Sampling Event B8) and their analyses were funded and directed under the US DOE/DOT/TC project and are described in Luketa, Blanchat et al. (2019).

3.4.2. Analysis of Sampling Events B4 and B6

Sampling Events B4 and B6 were taken directly before Pool Fire Test 2.3 and 2.6, respectively. As such, detailed analyses were performed on these samples to more directly link the properties of the crude oil to the pool fires. Analysis methods for the fluids collected in Sampling Events B4 and B6 include:

- VPCR_x(T) by ASTM D6377-M (ASTM 2016b) at selected temperature and expansion points listed in Table 3-2
- Pressurized Compositional Analysis by ASTM D8003 (ASTM 2015) + ASTM D7169 (ASTM 2016a) + GOR merge
- Density by ASTM D5002 (ASTM 2013a)
- Flash Point by ASTM D56 (ASTM 2016d) and D3828 (ASTM 2016h)

- Heat of Combustion by ASTM D240 (ASTM 2014)
- Water Content by ASTM D4007 (ASTM 2016f) and D6304 (ASTM 2016c)

Subsamples for ASTM D6377 VPCR, ASTM D8003 pressurized composition, and GOR analyses were drawn from GPA 2174 pressurized cylinders due to their sensitivity to light end losses and requirement for pressurized sample injection. Flashpoint, heat of combustion, and water content samples were drawn from ASTM D4057 bottle samples. These unpressurized measurements did not show sensitivity to sampling method for similar Bakken oil in prior work (Lord, Allen et al. 2017).

3.4.2.1. VPCR_x(T) (ASTM D6377-M) Expansion Series

A vapor pressure “curve” was developed by running a series of pressure-expansion points on oil from the loading subsample. The selected temperature and expansion points are given in Table 3-2.

Table 3-2. Temperature and expansion settings for ASTM D6377 VPCR_x(T) measurements to be run on loading site subsamples.

Temperature		Expansion Ratio (x)					
(°F)	(°C)	V/L	V/L	V/L	V/L	V/L	V/L
100	37.8	0.2	0.5	1.0	1.5	2.0	4.0
122	50	0.2	0.5	1.0	1.5	2.0	4.0

Samples must be allowed to reach an effective equilibrium for each expansion point, with ASTM D6377 instrument equilibration requirements given in Table 3-3. The equilibrium requirements and sample conditioning have been modified for this project, which changes these measurements from “D6377” to “D6377-M” results, as stated in the note below Table 3-3. This analysis was run in duplicate on separate cylinders to demonstrate reproducibility.

Table 3-3. Instrument settings for “Equilibrium Time” and “Equilibrium dP/dt” required to confirm that the analysis run for each V/L has reached equilibrium conditions.

V/L	Minimum Equilibration Time (sec)	Equilibration dP/dt (kPa/min)
0.20	900	0.2
0.50	600	0.15
1.0	600	0.1
1.5	500	0.1
2.0	400	0.1
4.0	300	0.1

Note: The “M” modifier on the ASTM D6377 test method above relates specifically to the equilibrium criteria above in Table 3-3 and the temperature conditioning of the test fluid. Sandia National Laboratories requires that the test fluid be pre-conditioned to the test temperature PRIOR TO PRESSURIZED INJECTION into the sample chamber in the 6377 device, and that the sample injection tubing and pressure regulators (if required) are also maintained at the test temperature. This is done in order to prevent liquid thermal expansion effects from further pressurizing the cell before the expansion sequence starts, leading to erroneously high-pressure values for low V/L.

3.4.2.2. Pressurized Compositional Analysis

Bakken sample compositions on a “whole oil” basis were determined by combining ASTM D8003-15, ASTM D7169, and GOR flash measurements by numerical recombination. Doing so yielded whole oil descriptions with components including N_2+O_2 , CO_2 , carbon number groups including major isomers from C1-C24, and a lumped heavy portion given as C25+. Density of pressurized samples was also measured using ASTM D5002. Mole% and mass% reported in the experimental results are given by component as a percentage of the whole, original sample.

3.4.2.3. Unpressurized Physical Properties Determination

The burn site subsamples were analyzed for the following physical properties using unpressurized sampling and storage techniques. Sample collection (ASTM D4057) and handling were consistent with procedures given in each associated standard.

- Flash Point (ASTM D56 and ASTM D3828)
- Heat of Combustion (ASTM D240)
- Water Content (ASTM D4007 and ASTM D6304)

3.4.3. Equation of State (EOS) Modeling

Bakken crude oils with compositions measured by the pressurized compositional analyses described in Section 3.4.2.2 were simulated via commercially available process simulation software. This simulation used a cubic equation of state (EOS) model embedded in the process simulation software to predict properties such as vapor pressure at selected V/L and temperature based on composition. The compositional data were used to model the oil samples for several reasons:

1. A favorable comparison of modeled properties from the compositionally-based EOS with measured properties from the analytical lab provides a level of verification that the composition and properties of the whole oil are self-consistent and that the EOS model is appropriate for this particular application.
2. Producing modeled $VPCR_x$ from compositional data helps identify which compositional factors in a crude oil affect its $VPCR_x$, and in what ways.
3. Having access to a validated simulation model can enable predictions of oil properties where direct measurements are not feasible due to expense, difficulty, or safety concerns.

More information on the EOS modeling procedures used here can be found in a previous study (Lord, Allen et al. 2017).

This page left blank

4. DILUTED BITUMEN SAMPLING AND ANALYSIS METHODS

This chapter describes the methodology for sampling and analysis of the diluted bitumen (dilbit) crude oil used in the pool fire test series described in Luketa, Cruz-Cabrera et al. (2019). Six pool fires were run with dilbit crude oil in this study. Sandia monitored and coordinated collection and analysis of crude oil subsamples to establish basic physical and chemical properties of the fuel.

4.1. Dilbit Sample Acquisition

Twelve cylinders of diluted bitumen were acquired by InnoTech Alberta on November 28th and 29th, 2018 from a pipeline source in Canada. The dilbit was contained in 420-lb customized propane tanks, displacing nitrogen during fill. Approximate capacity for these cylinders was 360 L (95 gal), with a tare weight of 130 kg (290 lb). Tank ID's (1-12) were pre-assigned by InnoTech and written directly onto the tank shells. Ten tanks were then shipped to the Sandia facility in Albuquerque, NM USA in December 2018. Two tanks were retained at InnoTech. Once at Sandia, the cylinders were stored outdoors on pallets over secondary spill containment as shown in Figure 4-1.



Figure 4-1. Photo of eight of the ten modified propane cylinders sent to Sandia to supply the dilbit pool fire testing.

4.2. Subsampling Schedule

The dilbit subsampling schedule is summarized below in Table 4-1. Liter-scale loading site subsamples were acquired on November 28-29, 2018 (event D0) while the 420-lb tanks were loaded from the pipeline source. The loading subsamples were collected into floating piston cylinders and Boston Round bottles and held in retention and not analyzed. Baseline spot samples from one of the 12 tanks (tank 5) were then drawn on December 3, 2018 (D1). Additional sampling details are given in Appendix A on a sample-by-sample basis, as reported by InnoTech.

The liquid phase dilbit was sampled twice at Sandia: once (event D2) before the first pool fire and again (D4) before the last pool fire in the testing series. The solid residue that resulted from each 2-m pool fire was also sampled and weighed after each of the six pool fire tests. Two of those solid samples (event D3, D5), from the first and last fires, were packaged and sent to an offsite laboratory for analysis.

Table 4-1. Listing of sampling events supporting the dilbit pool fire series

Event #	Event Name	Description
D0	Loading Site Subsampling	Baseline fluid subsamples taken directly from pipeline source at same time as the 360L samples were collected. These samples were held in retain and not analyzed.
D1	Baseline Subsampling	Fluid sampling taken from Tank #5 to establish initial properties prior to shipping tanks to Sandia.
D2	Burn Site Subsample 1: Tank 12	Fluid sampling taken at the Sandia thermal test complex after homogenization and just prior to use in the first 2-m dilbit pool fire (Pool Fire Test 3.1).
D3	2-m Pool Fire Solids Residue	Post-burn solids collected from the pool fire pan
D4	Burn Site Subsample 2: Tank 9	Fluid sampling taken at the Sandia thermal test complex after homogenization and just prior to use in the final 2-m dilbit pool fire.
D5	2-m Pool Fire Solids Residue	Post-burn solids collected from the pool fire pan (Pool Fire Test 3.6).

4.3. Subsampling Methods

4.3.1. *Liquid Phase Subsampling (D2) Prior to First Dilbit Pool Fire (Test 3.1)*

Tank 12 was selected to supply the first pool fire test (3.1). The tank was fitted with a recirculation system that drew oil up the hanging string and out of the liquid valve, through a pneumatic diaphragm pump, and back into the vapor valve. A schematic of the recirculation loop is shown in Figure 4-2(a) next to a photo of the actual setup in Figure 4-2(b). The tank was recirculated for about 20 minutes at about 10 gallons per minute to assure that several complete volumes were recirculated prior to subsample collection.

Early efforts to mix the oil were met with problems as the centrifugal pump could not move the viscous oil. As a workaround, electrical resistance pad heaters were fixed to the outside of the dilbit tank (see orange pads in Figure 4-2(b)) to heat the oil and decrease viscosity to facilitate flow and mixing since the mixing and sampling were performed outdoors and subjected to winter temperatures near 0-5°C. Also, a pneumatic diaphragm pump was installed to replace the centrifugal pump. In the end, the heaters were never energized because the pneumatic diaphragm pump was able to move the fluid and mix without external heating.

Pressure for subsampling was generated by adding a recirculation/back pressure valve as shown in Figure 4-3, with a tee that fed a sample line fitted with a sampling valve. Pressure at the sampling valve was maintained between 20-40 psig during sampling.

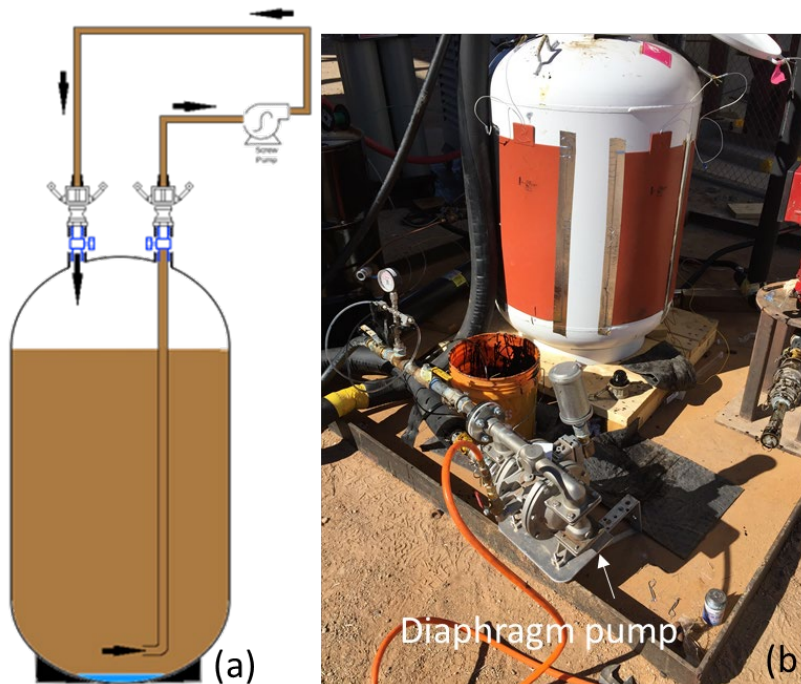


Figure 4-2. Schematic of recirculation loop (a) (reproduced from Prefontaine (2018)) and photo of actual setup.

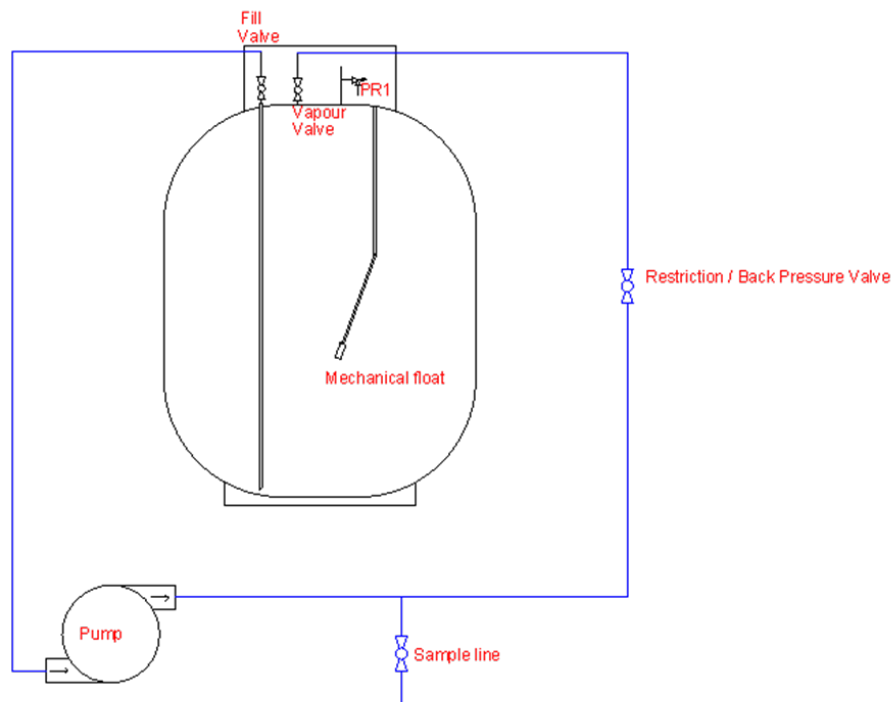


Figure 4-3. Schematic of combined recirculation/sampling loop reproduced from Prefontaine (2018).

Dilbit liquid samples for subsampling event D2 were acquired by two methods:

- GPA 2174-14 pressurized sampling using Proserv 700 mL capacity floating piston cylinders (2×700 mL)
- ASTM D4057 unpressurized sampling using Boston round bottles (4×700 mL)

The cylinders were received at Sandia already back-filled with glycol. A photo of the unpressurized ASTM D4057 bottle sampling is shown in Figure 4-4. Subsamples were acquired on 1/28/2019 between 1-2 PM local time.



Figure 4-4. Photo of unpressurized glass bottle during ASTM D4057 fill process with dilbit from Tank 12.

4.3.2. Liquid Phase Subsampling (D4) prior to Last Dilbit Pool Fire (Test 3.6)

Tank 9 was selected to supply the sixth pool fire test, which was the last in the test series. Oil pre-mixing was performed as described above in section 4.3.1.

Samples were acquired by two methods:

- GPA 2174-14 pressurized sampling using Proserv 700 mL capacity floating piston cylinders (2×700 mL)
- ASTM D4057 unpressurized sampling using Boston round bottles (4×700 mL)

A photo of the pressurized floating piston cylinder sampling is shown in Figure 4-5. The cylinders were received at Sandia already back-filled with glycol. As oil entered the inlet side of the cylinder, the piston moved to displace glycol at nominally the same volume as oil captured in the cylinder. Subsamples from Tank 9 were collected on 2/27/2019 from 11 AM to 12:20 PM local time.



Figure 4-5. Photo of pressurized piston cylinder fill process with dilbit from Tank 9. Oil feed on the far end of the cylinder moves the internal piston while displacing glycol through the outlet valve from the close end. The volume of glycol displaced is a primary indicator of sample volume captured in the cylinder.

4.3.3. Solid Phase Subsampling (D3) after the first Dilbit Pool Fire (Test 3.1)

The first 2-m dilbit pool fire, Test 3.1, was run on February 6, 2019. Post-burn solids samples were collected the next morning on February 7. The total weight of solids recovered from the pan was 69.25 lb (31.48 kg).

The solids took two general forms:

- (i) Thin, brittle, porous grey and black crust, analogous to a raised pie crust with air underneath, effectively covering the entire pan.
- (ii) A thick, glass-like, low-porosity solid that settled into low areas underneath the crust. This material did not have air underneath and had to be chipped out of the pan with a chisel.

Three spot samples of solid residue were collected from the pan. One was taken from pan center, a second from half radius, and a third at the full radius (outer perimeter). Photos of the residue in the pan on February 7 are shown in Figure 4-6 and Figure 4-7 just prior to collecting the grab samples for offsite analysis.



Figure 4-6. Photo of post-burn solids remaining after Test 3.1. Total mass of solids was measured at 31.48 kg.



Figure 4-7. Close-up photo of sampling post-burn residue from the center of the pan for Test 3.1 on February 7.

4.3.4. Solid Phase Subsampling (D5) after the last Dilbit Pool Fire (Test 3.6)

Post-burn solids samples for test 3.6 were collected on March 5, one day after completion of the last 2-m dilbit pool fire. A photo of the pan contents is shown in Figure 4-8. The residue was qualitatively similar to that described for residue left after the first dilbit pool fire in section 4.3.3. Spot samples were collected as described in section 4.3.3 and total mass of solids in the pan was measured. The spot samples were packaged and shipped offsite for analysis.



Figure 4-8. Photo of post-burn solids remaining after test 3.6. Total mass remaining was measured at 19.60 kg.

4.4. Dilbit Crude Analysis Methods

4.4.1. Analysis of Sampling Events D1, D2, D4

Dilbit samples were analyzed for selected physical properties as well as pressurized and unpressurized composition. A summary of physical properties tested on samples obtained in unpressurized “Boston Round” bottles is given in the list below.

- Initial Boiling Point by ASTM D8003 (ASTM 2015)+ ASTMD7169 (ASTM 2016a) Merge
- Flash Point, Closed Cup by ASTM D3828 (ASTM 2016h)
- Water and Sediment by ASTMD4007 (ASTM 2016f)
- Water content by Karl Fischer
- Density @15°C by ASTM D5002M (ASTM 2013a)
- Heat of Combustion by ASTM D240 (ASTM 2014)
- Sulfur by ASTM D4294 (ASTM 2016e)
- Viscosity by ASTM D445 (ASTM 2018)

- Hydrogen Sulfide and Mercaptans by UOP 163 (UOP 2010)

A summary of physical properties tested on samples obtained in pressurized floating piston cylinders (FPC) compliant with GPA 2174-14 pressurized sampling includes:

- VPCR_x(T) by ASTM D6377-M (ASTM 2016b) at selected temperature and expansion points listed in Table 3-2
- Pressurized Compositional Analysis by ASTM D8003 (ASTM 2015) + ASTM D7169 (ASTM 2016a) + GOR merge

The ASTM D6377-M VPCR methodology used for the dilbit samples was the same as for the Bakken samples described in section 3.4.2.1. Whole oil composition listed above was obtained by combining ASTM D8003-15 measurements, ASTM D7169 measurements, and GOR flash measurements by numerical recombination. Doing so yielded whole oil descriptions with components to include N₂+O₂, CO₂, carbon number groups including major isomers from C1-C24, and a lumped heavy portion given as C25+.

5. EXPERIMENTAL RESULTS

This chapter presents the analytical results for the heptane, Bakken crude, and dilbit collected and analyzed as described in Chapters 2-4. Recall these analyses were conducted in support of a series of pool fire tests run on the same fuels at the Sandia Thermal Test complex. Description and results of the pool fire testing are given in a separate report by Luketa, Cruz-Cabrera et al. (2019).

5.1. General statement on fuels comparison

A summary of basic physical properties of the three fuels tested here is given in Table 5-1. Properties such as mass density, sulfur content, VPCR, and heat of combustion provide a basic profile relevant to identification, handling, and testing. Heptane represents a refined product with a combination of density, viscosity and VPCR that facilitate easy handling at ambient conditions. Bakken represents a light, sweet crude oil with a wide boiling range and sufficient light ends content and VPCR that pressurized storage and specialized handling were imposed to retain stable properties throughout months of storage time required to complete the test series described here and elsewhere (Luketa, Blanchat et al. 2019). The dilbit, a heavy sour crude, was the most dense and viscous fluid tested here. Even so, the dilbit also contained sufficient light ends content that pressurized storage and specialized handling were imposed, similar to the Bakken. Recall from section 4.3.1 that a specialized recirculation system using a pneumatic diaphragm pump was required to overcome the viscosity and adequately mix the dilbit for sampling. Gross heats of combustion on a mass basis were similar across all three fuels.

Table 5-1. Summary of average fuel properties observed in this study

Property	Units	<i>n</i> -Heptane	Bakken	Dilbit
Density (15.56°C)	kg/m ³	687.5	805.9	923.9
API Gravity (60°F)	°	74.1	43.9	21.7
Sulfur	mass%	0.00	0.1	3.6
VPCR _{0.2} (37.8°C)	kPa	10.9 ^a	136	93
Viscosity (40°C)	mm ² /s	0.005 ^b	2.0	71.9
Heat of Combustion	MJ/kg	47.8	46.8	43.0

^a Vapor pressure for *n*-heptane calculated using process simulator. Verified using correlation from literature (Williamham, Taylor et al. 1945).

^b Viscosity for *n*-heptane calculated using correlation from literature (Sagdeev, Fomina et al. 2013). Verified via process simulator.

5.1.1. Fuel Visual Properties

Example photos of heptane (12/6/17), Bakken crude (1/31/2018) and diluted bitumen (2/27/2019) in clear glass bottles subsampled during this study are shown side-by-side in Figure 5-1. The heptane was clear, the Bakken exhibited a muddy dark green color, and the diluted bitumen was dark black. Generally speaking, crude oil color is driven by the heavy component contents, so the darker the color, the heavier the oil. Though not captured specifically in these photos, the Bakken also produced a mustard-colored foam several inches deep that formed on top of the liquid phase as it was drawn from pressurized storage into the unpressurized bottle. The foam broke up after a few minutes and settled to the stable configuration that is shown in the photo.



Figure 5-1. Comparison of heptane (left), Bakken (center) and diluted bitumen (right) visual properties captured during bottle sampling.

5.2. *n*-Heptane Analysis Results

Results received from the analysis laboratory are given in Figure 5-2. The *n*-heptane purity measured at 99.5 vol% compares well with the analysis certificate that accompanied the delivery from the supplier (see Appendix C). Other measured values such as average molecular weight, density at ambient pressure/temperature conditions, and heat of combustion compare well with reference database values obtained from the U.S. Department of Commerce National Institute of Standards and Technology (NIST). By verifying the supplier purity and comparing these properties with those of *n*-heptane from a standards database, it is reasonable to say that these samples were representative of a high-purity *n*-heptane.

Table 5-2. Analysis results for composite heptane sample collected from the 9 heptane drums delivered to Sandia.

Test	Measured		Method	NIST Reference		Comment
	Value	Unit		Value	Unit	
Chemical Formula	C ₇ H ₁₆		N/A			
Heptane Purity	99.5	Vol %	ASTM D6730			
Average Molecular Weight	102.14	g/mol	Frz Pt Depression	100.2	g/mol	
API Gravity @ 60°F	74.1	°API	ASTM D4052			
Density @ 15.56°C	0.6875	g/cm ³	ASTM D4052	0.6876	g/cm ³	T = 15.6C, P = 1 atm
Relative Density, 15.56°C/15.56°C	0.6882		ASTM D4052			
Gross Heat of Combustion	20558	BTU/lb	ASTM D240	20710	BTU/lb	
Water Content	25	mg/kg	ASTM E1064			
Corrected Flash Point	<50	°F	ASTM D93			
Flash/No Flash	Flash	°F	ASTM D3828			
Target Flash Point	-5	°F	ASTM D3828			

5.3. Crude Oil Unpressurized Properties

5.3.1. Bakken Physical Properties (Sampling Event B1 – Loading Site)

Measured physical properties for the Bakken sample taken at the loading site in North Dakota (B1) are listed in Table 5-3. The oil is considered a light, sweet crude according to the API gravity (42.9°) and total sulfur content (0.0844 wt%)(API 2011).

Table 5-3. Physical properties of Bakken samples taken at loading site (B1).

Method	Test	Result	Unit
ASTM D5002	API Gravity @ 60°F	42.9	°API
ASTM D5002	Relative Density @ 60/60°F	0.8107	
ASTM D4294	Sulfur Content	0.0844	Wt %
ASTM D445	Kinematic Viscosity 40 °C	1.996	cSt
ASTM D93A	Corrected Flash Point	<50	°F
ASTM D664A	Acid Number	< 0.10	mg KOH/g
ASTM D3230	Salt Content (as electrometric chloride)	3.8	lb/1000bbl
UOP 163	H2S	< 1	ppm Wt
UOP 163	Mercaptan Sulfur	<3	ppm Wt
ASTM D1159	Average Bromine Number	1.1	
ASTM D97	Pour Point	<-33	°C
ASTM D97	Pour Point	<-27.4	°F
ASTM D4007	Sediment And Water	<0.05	Vol %
ASTM D4928	Sample Temp - Before Mixing	24	°C
ASTM D4928	Sample Temp - After Mixing	24	°C
ASTM D4928	Water Content	0.01	Vol %
ASTM D6560	Asphaltene Content	< 0.50	Wt %
ASTM D5762	Nitrogen Content	430	ppm Wt
UOP 269	Basic Nitrogen	130.0	ppm Wt
ASTM D4530	Average Micro Method Carbon Residue	0.53	Wt %
ASTM D240	Gross Heat of Combustion	20,834	BTU/lb
ASTM D482	Average Ash	0.003	Wt %
ASTM D5708A_MOD	Iron	1.30	mg/kg
ASTM D5708A_MOD	Nickel	<0.100	mg/kg
ASTM D5708A_MOD	Sodium	7.30	mg/kg
ASTM D5708A_MOD	Vanadium	<0.100	mg/kg
UOP 46	Wax Content	< 5.0	Wt %
UOP 375	UOP Characterization Factor (K)	12.11	
ASTM D7359	Total Fluorine	<1.00	mg/kg
ASTM D7359	Total Chlorine	1.20	mg/kg
ASTM D4929B	Organic Chloride in Orig. Sample-Crude Oil	< 1.0	µg/g
ASTM D5291	Carbon Content	75.00	Wt %
ASTM D5291	Hydrogen Content	10.00	Wt %
ASTM D5291	Nitrogen Content	0.10	Wt %

5.4. Fuel Compositions

5.4.1. Bakken Whole Oil Composition

Pressurized composition from fluid samples taken at five sampling events (Events B1, B2, B4, B6, and B8) are shown graphically in Figure 5-2 and Figure 5-3. Additional compositional data for each event are shown with black outlined bars of the same color. For replicates, two-cylinder samples were taken back-to-back from the same source and analyzed. The legends for these charts organize the samples by sampling event (Event B1, B2, B4, B6, or B8) and the replicate number for that event (B1-1 or B1-2, for example). The reader should note there is an analytical process difference for the dissolved gas compositions determined under the DOE/DOT/TC-sponsored work (Events B1, B2, B8) versus the NRC/TC work (Events B4, B6). The underlying analytical method (GPA 2103-M(GPA 2003)) used in the DOE/DOT/TC work did not differentiate between O₂ and N₂, thus their contributions to the whole oil were lumped (N₂ + O₂) and are represented only as N₂ in Figure 5-2. The method used in the NRC/TC work, ASTM D8003 merge method, did differentiate and the separate components are shown in Figure 5-2.

For the dissolved gas compositions shown in Figure 5-2, there appeared to be a spike in N₂ in the first replicates of the B1, B6, and B8 samples, though the second replicates do not show the same feature. There are several possible explanations for this behavior. First, it is possible that sample handling during acquisition in the field, during the required transfer from the manual piston cylinders (MPC) to the 1-L piston cylinders (for the B6 subsamples), or during cylinder hookup to the analytical instruments in the lab introduced air into the system. Another possibility is that air could have also been introduced into the tanker during storage times (weeks to months) under periodic vacuum conditions at lower temperatures when the vapor pressure of the oil was less than the ambient pressure. The fact that paired samples (i.e., B1-1 and B1-2, or B6-1 and B6-2) pulled from the same tanker load just minutes apart showed variability similar or greater in magnitude than observed between samples separated by months suggests that the inherent sample-to-sample variability is a more likely explanation than air ingestion into the tanker.

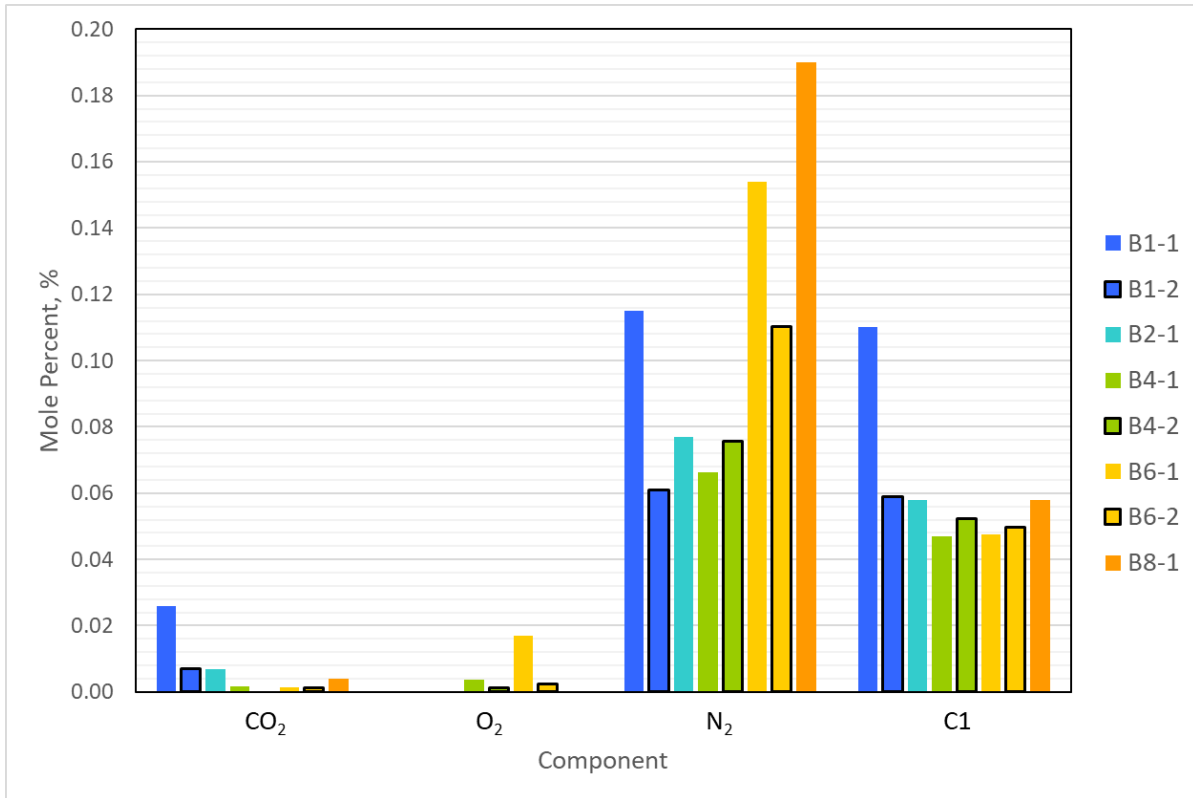


Figure 5-2. Dissolved gas compositions (N₂, C1, CO₂) in Bakken samples taken at loading and at the Sandia burn site.

The light hydrocarbons in Figure 5-3 showed little variation across all subsamples. The light end compositions held nearly constant across all the subsamples, providing evidence that the custom Sandia pressurized tanker and sampling methods did not allow escape of these components from the main sample of oil in the tanker and provided consistent fuel properties for the 2-m pool fire test series.

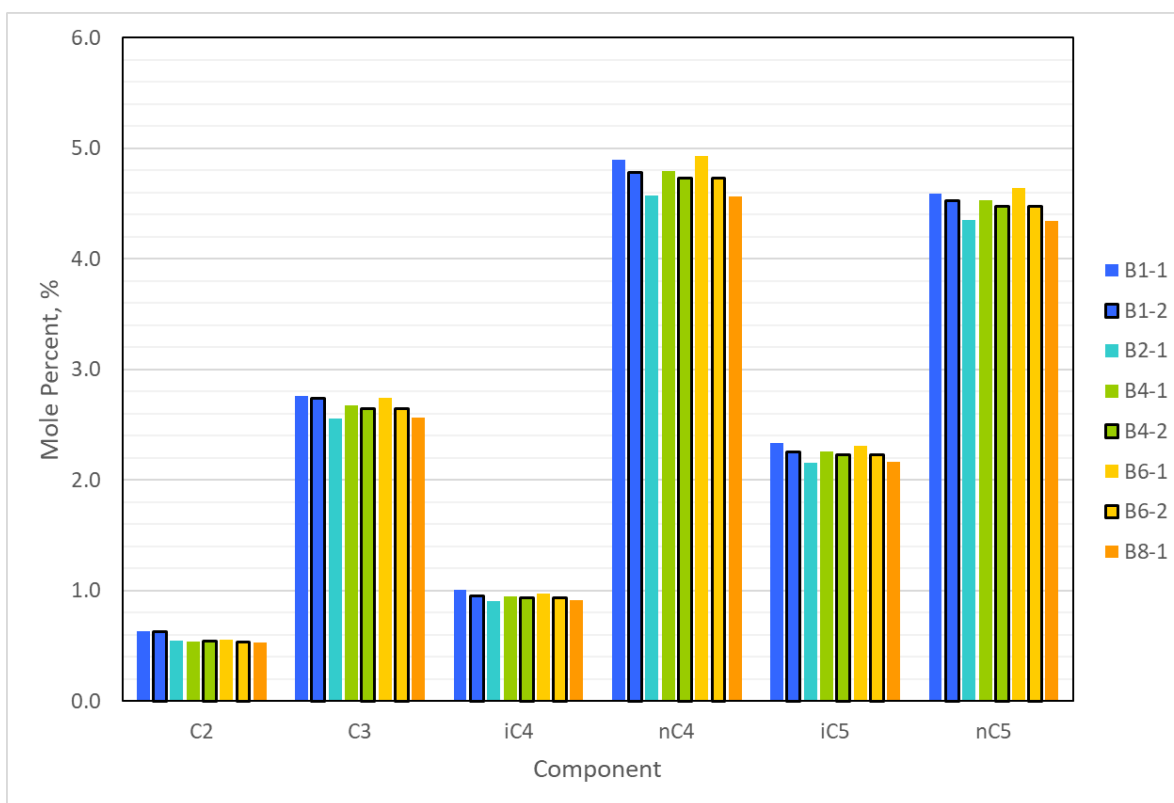


Figure 5-3. Light ends compositions (C2-nC5) in Bakken samples taken at loading and at the Sandia burn site.

Whole oil carbon number plots for the samples are given graphically as line plots in Figure 5-4, with tables of the data in Appendix C. Note dissolved gases (N_2 , CO_2 , etc.) are included in the whole oil composition (see Figure 5-2) but are not visible at the scale shown. The compositional analyses for events B1, B2, and B8 were determined by numerical merge on a suite of analytical measurements by GPA 2103-M + ASTM D2887 + ASTM D7169. Alternatively, B4 and B6 were determined by a merge of ASTM D8003 + GOR + ASTM D7169 measurements. The different compositional methods were used because these phases of the research project (B1,2,8 versus B4,6) were funded by different sponsors, and were brought together here under a sharing agreement. Details of these methods are described in a separate report (Lord, Allen et al. 2018). A close look at Figure 5-4 indicates that the four whole oil curves with higher C7-C8 peaks around 13-15 mole% were associated with the GPA 2103-M merge method (referred to in Figure 5-4 as TM1), while the four whole oil curves with lower C7-C8 peaks around 10-12 mole% were associated with the ASTM D8003 merge method (referred to in Figure 5-4 as TM2). The differences in C7-C8 are likely associated with how the middle hydrocarbons measured in the analytical procedures were binned into carbon number groups during the analytical data reduction and merge processes. As described in Lord, Allen et al. (2018), both the GPA 2103-M and ASTM D8003 merge methods were found to return whole oil compositions that were generally comparable to those from a baseline flash separator method for representative Bakken and Eagle Ford crude samples captured and analyzed in 2016-2017. While it appears there is a slight method bias, the authors do not have a basis for determining which set of whole oil curves determined via TM1 or TM2 is more accurate in this application.

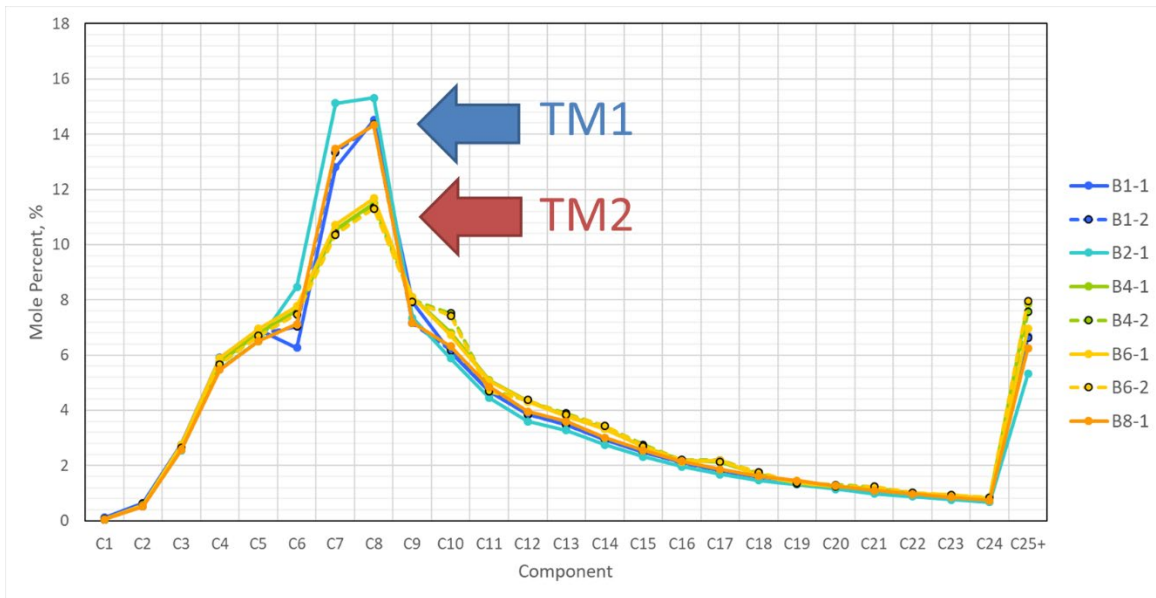


Figure 5-4. Whole oil carbon number plots for Bakken oil sampled at loading and burn sites listed by sampling event and replicate number.

5.4.2. Dilbit Whole Oil Composition

Pressurized compositions from fluid samples taken at three sampling events are shown graphically in Figure 5-5 and Figure 5-6. One replicate was taken for each of these sampling events. The legends for these charts organize the samples by sampling event and replicate, similar to what was done for the Bakken subsamples in the previous section.

The dissolved gas compositions are shown in Figure 5-5. Despite N_2 presence in the oil because of the tank loading methodology (see section 4.1), the N_2 contents seen here are the same scale as the Bakken N_2 content. At first glance, there appeared to be a spike in N_2 in the D2 sample. Similar to what was described in section 5.4.1 for the Bakken compositions, inherent sample-to-sample variability is a more likely explanation than any of the other effects.

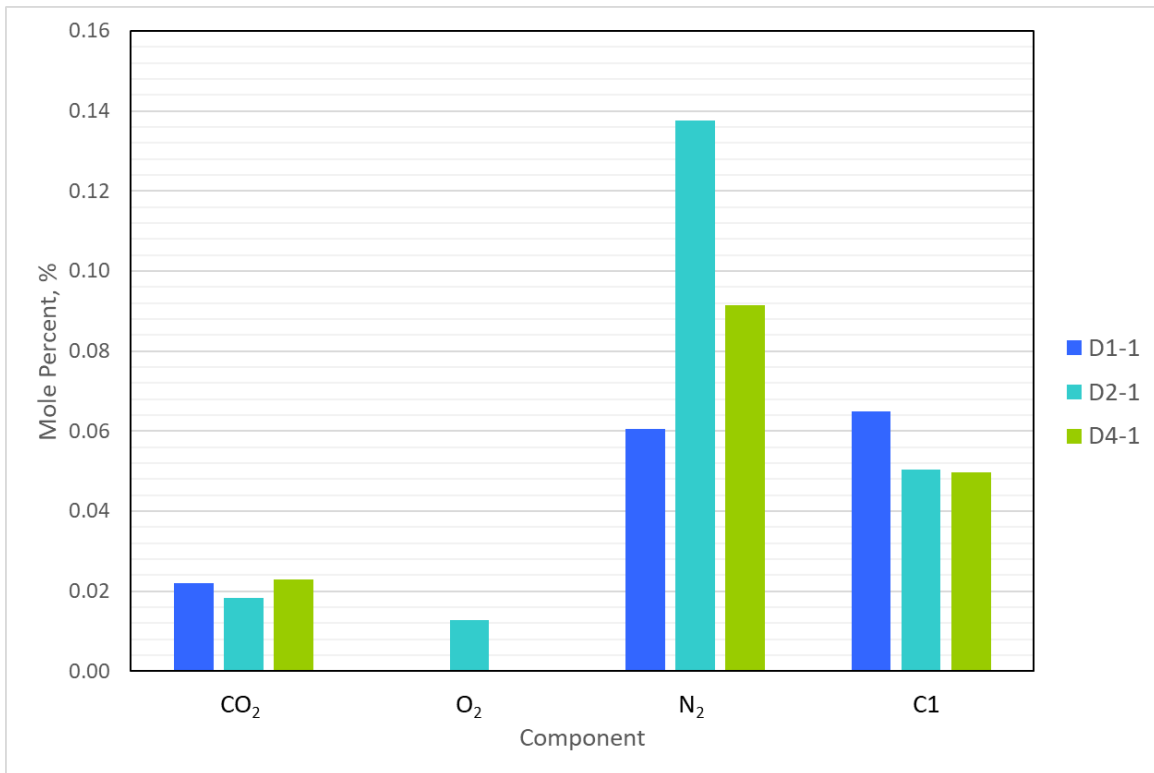


Figure 5-5 Dissolved gas contents for the dilbit subsamples at initial subsampling in December and at Sandia's thermal test complex.

The hydrocarbons in Figure 5-6 showed little variation across all subsamples. The light end compositions held nearly constant across all the subsamples, providing evidence that the propane storage tanks and subsequent sampling methods did not allow escape of these components from the oils in the tanks and provided consistent fuel properties for the 2-m pool fire test series.

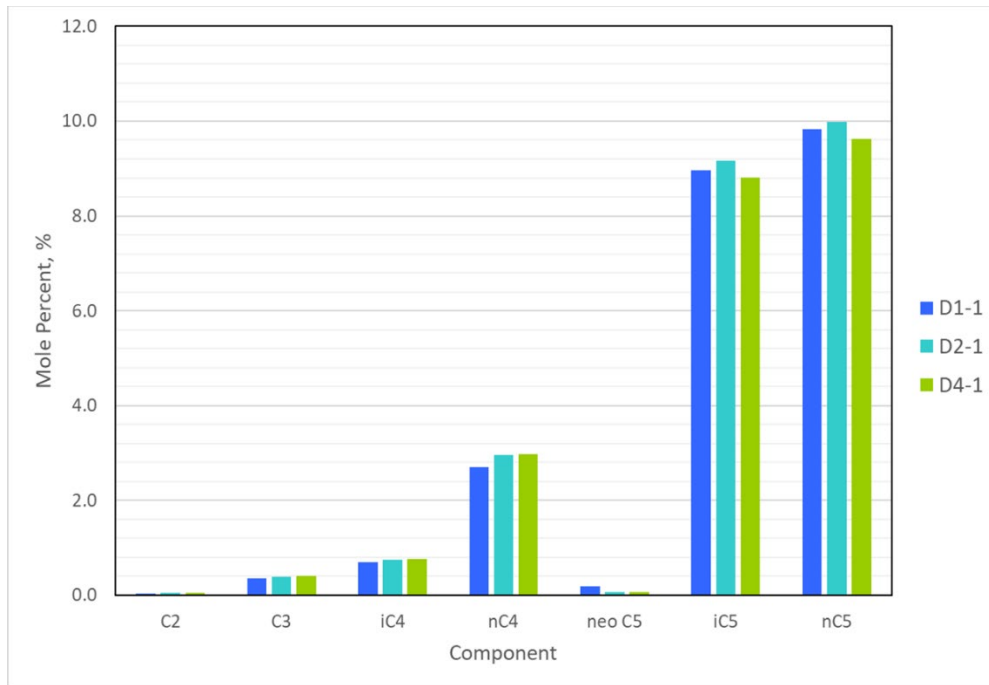


Figure 5-6 Light ends (C2-nC5) measured for the dilbit subsamples

Whole oil carbon number plots for the samples are given graphically in Figure 5-7, with tables of the data in Appendix C. In general, the whole oil compositions changed little across the three subsamples. Of note, there was a large spike at C5, a shallow local minimum around C11, and a large C25+ residual content across all three samples. This distribution is expected for diluted bitumen, which comprises a mixture of bitumen, a heavy sour oil, and a diluent, which is a condensate or mixture of light hydrocarbons, blended so that the resulting fluid meets pipeline specifications for viscosity and density. Bitumen alone would be problematic to transport via pipeline due to its inherently high viscosity. The amount and type of diluent added to the base bitumen material depends upon the price and availability of diluent and specifications for transport of the combined material. The diluent in this case is associated with the peak in mole% around C5, and the base bitumen material is associated with the heavier materials from about C10 up. While normal for dilbit, this carbon number distribution is distinct from other crudes tested in this research study that exhibit a peak in the C7 to C8 range along with a rapidly descending “tail” above C10 (recall Figure 5-4 above or see Luketa, Blanchat et al. (2019)). Additional discussion of the diluent and base bitumen compositions that comprise the dilbit samples is presented in section 6.2.

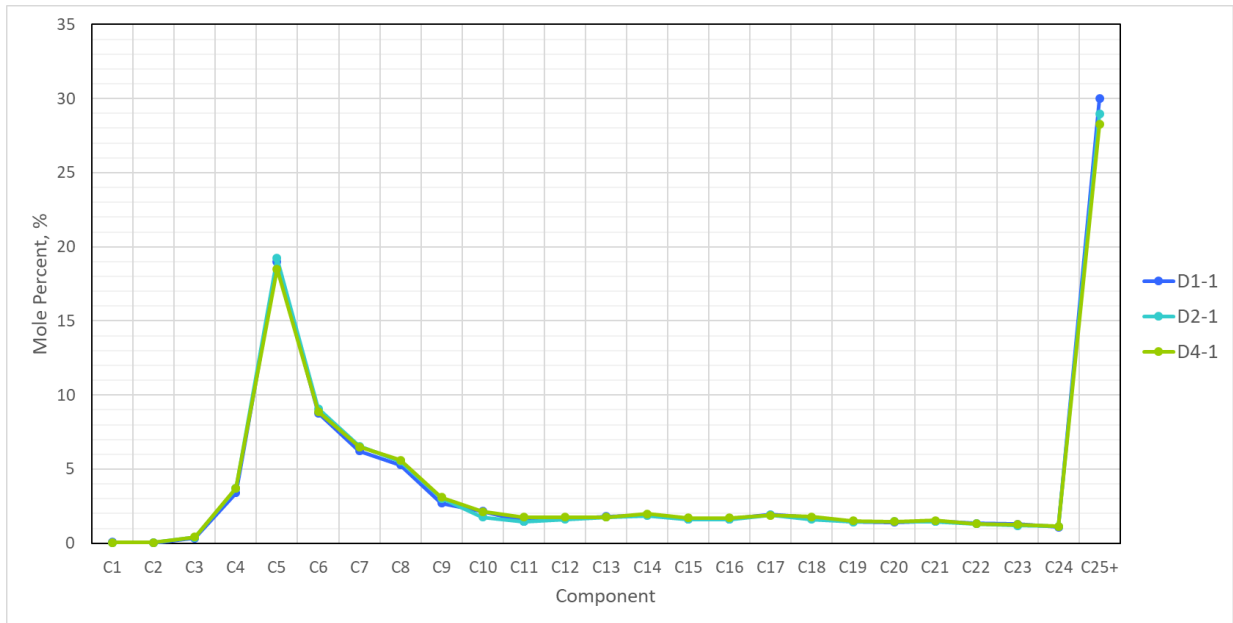


Figure 5-7 Whole oil compositions measured for the dilbit subsamples

5.5. Fuel Vapor Pressures

5.5.1. Bakken $VPCR_x(37.8\text{ C}; 100\text{ F})$ Results

$VPCR_x(37.8\text{ C}; 100\text{ F})$ results for the Bakken loading and burn site samples are summarized in Figure 5-8. Duplicate samples were collected and measured for all of the sampling events, so the error bars in the figure represent 2 times the standard deviation among those replicates. Pressure units are given in kPa on the left axis and psia on the right axis.

Of particular interest for this study are the $VPCR_x$ for events B4 and B6, which represent the properties just prior to the first and last pool fires in the series run in January 2018. Events B1, B2, and B8 provide some context for what was measured from tanker samples obtained in August 2017, October 2017, and July 2018, respectively.

Starting at the right end of the chart with $V/L = 4$, $VPCR_4(37.8\text{ C}; 100\text{ F})$ was nominally 75 kPa (11 psia) for samples from events B4 and B6. Moving to lower V/L , the vapor pressure $VPCR_x$ increases to 135-150 kPa (20-22 psia) for events B4 and B6 at $V/L = 0.2$. $VPCR_x$ data were not gathered at $V/L = 1$ and $V/L = 2$ for events B1, B2, and B8 because they were outside the scope of work under US DOE/DOE/TC.

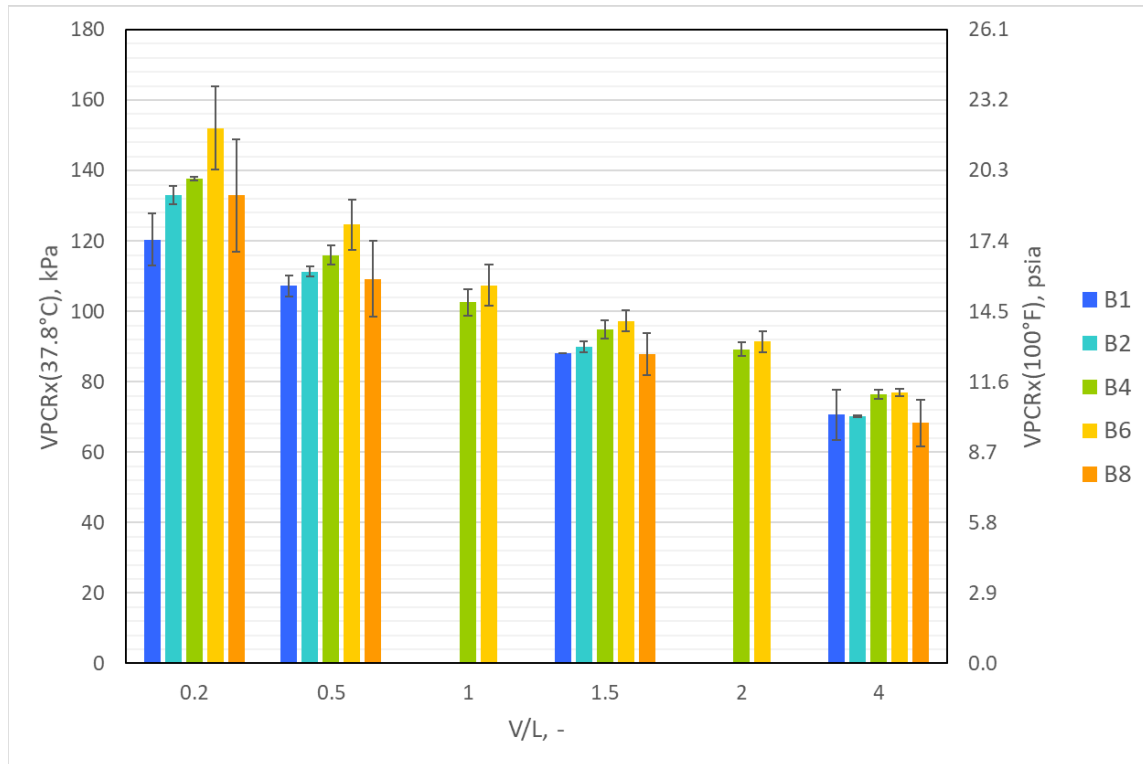


Figure 5-8. Pressure-expansion column charts showing measured VPCR_x(100°F; 37.8°C) for the Bakken loading samples (B1) and burn site samples (B2, B4, B6, and B8).

A prior Sandia study (Lord, Allen et al. 2017) indicated that the VPCR_{0.2}(37.8°C; 100°F) point is a reasonable indicator of bubble point pressure at that temperature, which can be a useful reference property. For the oils tested here, the average VPCR_{0.2}(37.8°C; 100°F) for each sampling event is given in Table 5-4. These data indicate that the bubble point pressures of the Bakken oil at T = 100°F; 37.8°C appear to range from 120-152 kPa (17.5-22.0 psia) depending on the sampling event.

Table 5-4. Average measured VPCR_{0.2}(37.8°C; 100°F) for the five Bakken sampling events.

Event	Description	VPCR _{0.2} (37.8°C; 100°F)
B1	Loading	120 kPa (17.5 psia)
B2	Burn 1	133 kPa (19.3 psia)
B4	Burn 2	138 kPa (20.0 psia)
B6	Burn 3	152 kPa (22.0 psia)
B8	July 2018	133 kPa (19.3 psia)

All of the VPCR points collected on the Bakken oil in this work, including V/L < 0.2, are reported in Appendix B.

5.5.2. Bakken VPCR_x(50°C; 122°F) Results

VPCR_x at 50°C or 122°F are reported as they are relevant to Transport of Dangerous Goods (TDG) regulations. VPCR_x(50°C; 122°F) results for the Bakken burn site samples are summarized in Figure 5-9. Only one sample at this temperature was measured for sampling events B4 and B6. Pressure units are given in kPa on the left axis and psia on the right axis.

Starting at the right end of the chart with $V/L = 4$, $VPCR_4(50^\circ\text{C}; 122^\circ\text{F})$ was nominally 97 kPa (14 psia) for samples from events B4 and B6. Moving to lower V/L , the vapor pressure $VPCR_x$ increases to 165-175 kPa (24-25 psia) for events B4 and B6 at $V/L = 0.2$.

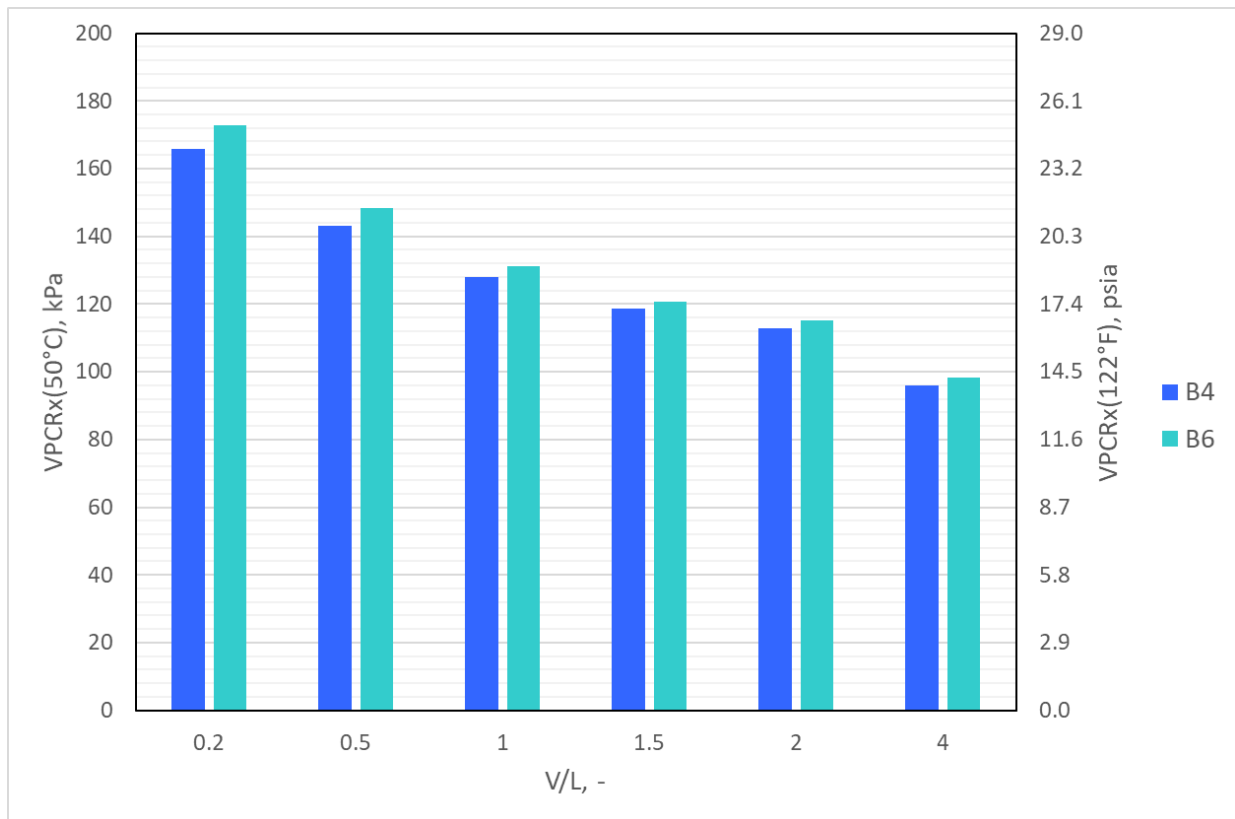


Figure 5-9. Pressure-expansion column charts showing measured $VPCR_x(50^\circ\text{C}; 122^\circ\text{F})$ for the Bakken burn site samples (B4 and B6).

5.5.3. Dilbit $VPCR_x(37.8^\circ\text{C}; 100^\circ\text{F})$ Results

$VPCR_x(37.8^\circ\text{C}; 100^\circ\text{F})$ results for the dilbit loading and burn site samples are summarized in Figure 5-10. Pressure units are given in kPa on the left axis and psia on the right axis. Of particular interest for this study are the $VPCR_x$ for D2 and D4, which represent the properties just prior to the first and last pool fires in the series run in Luketa, Blanchat et al. (2019). Starting at the right end of the chart with $V/L = 4$, $VPCR_4(37.8^\circ\text{C}; 100^\circ\text{F})$ was nominally 55 kPa (8 psia) all three samples. Moving to lower V/L , the vapor pressure $VPCR_x$ increases to 85-98 kPa (12-14 psia) at $V/L = 0.2$.

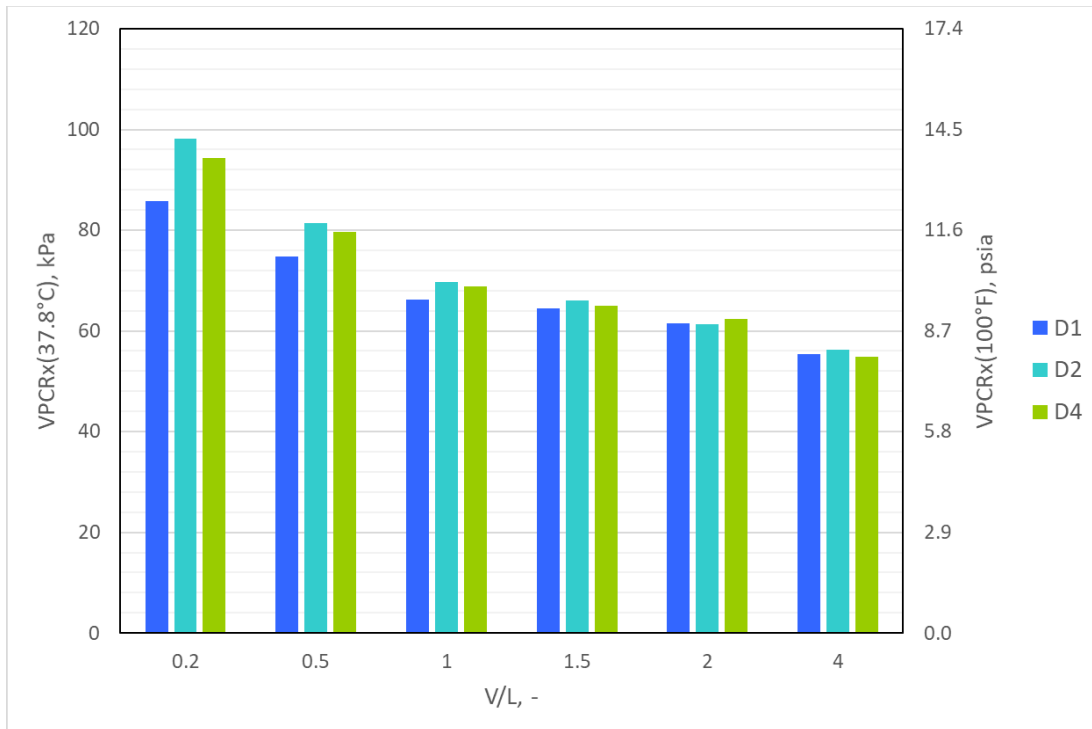


Figure 5-10. Pressure-expansion column charts showing measured VPCR_x(37.8°C; 100°F) for the dilbit baseline samples (D1) and burn site samples (D2 and D4).

As stated previously, VPCR_{0.2}(37.8°C; 100°F) is a reasonable indicator of bubble point pressure at 37.8°C (100°F). For the oils tested here, the average VPCR_{0.2}(37.8°C; 100°F) for each sampling event is given in Table 5-5. These data indicate that the bubble point pressures of the dilbit at T=37.8°C; 100°F appear to range from 85.7-98.1 kPa (12.4-14.2 psia).

Table 5-5. Average measured VPCR_{0.2}(37.8°C; 100°F) for the three dilbit sampling events.

Event	Description	VPCR _{0.2} (100°F; 37.8°C)
D1	Loading	85.7 kPa (12.4 psia)
D2	Burn Site 1	98.1 kPa (14.2 psia)
D4	Burn Site 2	94.4 kPa (13.7 psia)

5.5.4. Dilbit VPCR_x(122°F; 50°C) Results

VPCR_x(122°F; 50°C) results for the dilbit burn site samples are summarized in Figure 5-11. Starting at the right end of the chart with V/L = 4, VPCR₄(122°F; 50°C) was nominally 80 kPa (11.5 psia) for the three samples. Moving to lower V/L, the vapor pressure VPCR_x increases to 115-135 kPa (17-20 psia) at V/L = 0.2.

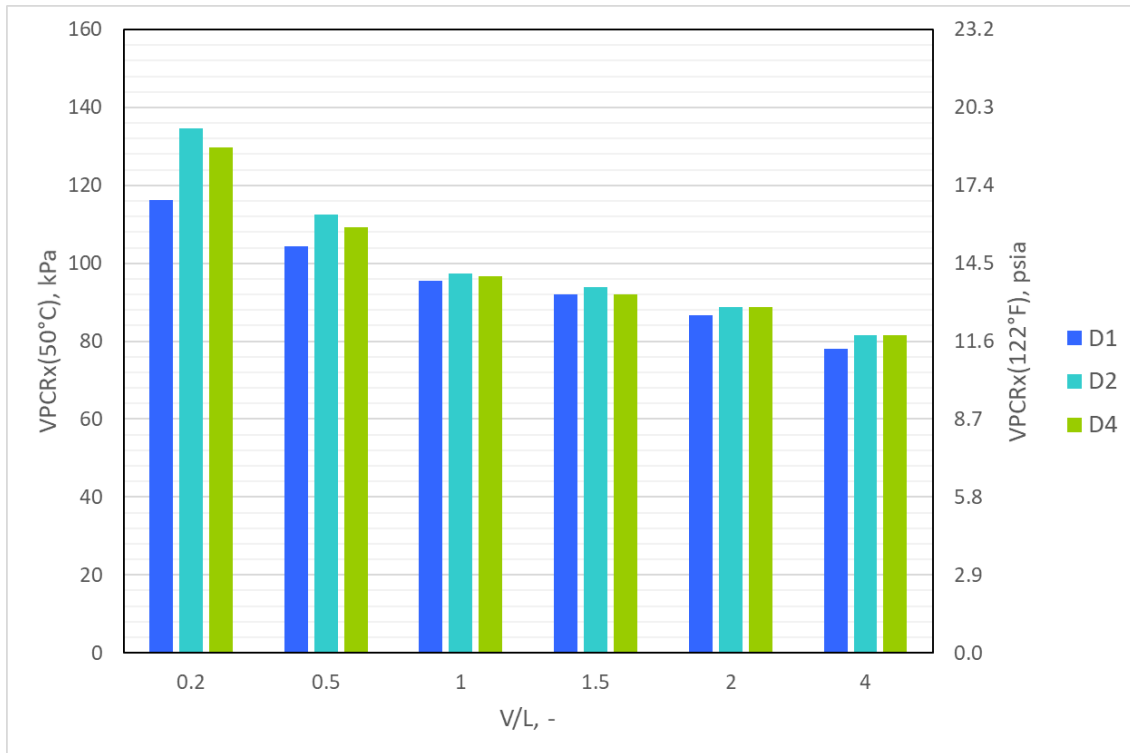


Figure 5-11. Pressure-expansion column charts showing measured $VPCR_x(50^\circ\text{C}; 122^\circ\text{F})$ for the dilbit samples.

5.5.5. Equation of State -Modeled $VPCR_x(T)$

The compositional data were used as received from the analytical laboratories and passed through an equation of state (EOS) model to simulate $VPCR_x$ at 37.8°C (100°F) and 50°C (122°F). These results are shown in Figure 5-12 through Figure 5-15. The average of measured $VPCR_x$ replicates (given by solid bars) for each sampling event are given with EOS-modeled $VPCR_x$ from $V/L = 0.2$ to 4 (shown as striped bars). Error bars shown for the EOS-modeled $VPCR_x$ represent twice the standard deviation between simulations using different measured compositions from the same sampling event. Since only one composition was measured for each of the B2 and B8 sampling events, no error bars are shown. The magnitude of deviation between the measured $VPCR_x$ values and the EOS modeled $VPCR_x$ values are consistent with sample to sample variations observed between cylinders in prior work by the authors (Lord, Allen et al. 2017).

Bakken results are given in Figure 5-12 and Figure 5-13. In particular, the first compositional replicates for Bakken subsamples B1 and B6 showed high N_2 levels (see Figure 5-2). These correlated to larger EOS-modeled $VPCR_x(100^\circ\text{F}; 37.8^\circ\text{C})$ in Figure 5-12, especially at low V/L .

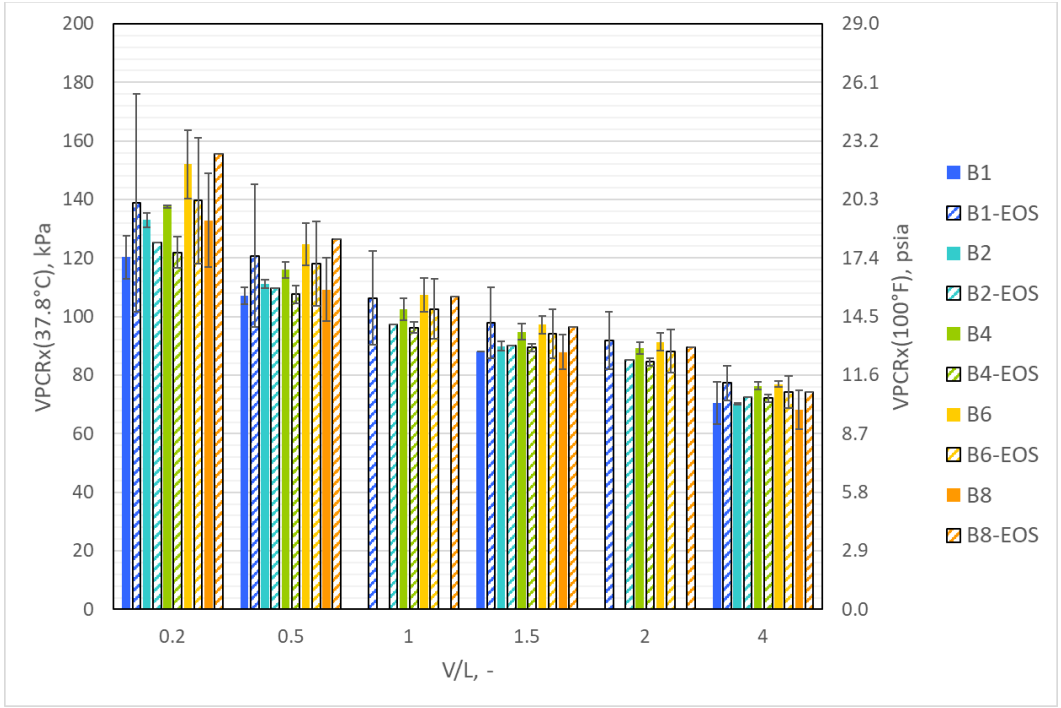


Figure 5-12. Column chart comparing measured VPCR_x to EOS-modeled VPCR_x for Bakken loading and burn site samples at T = 100°F; 37.8°C. Measured values are solid bars with 2σ error bars, modeled values are striped bars.

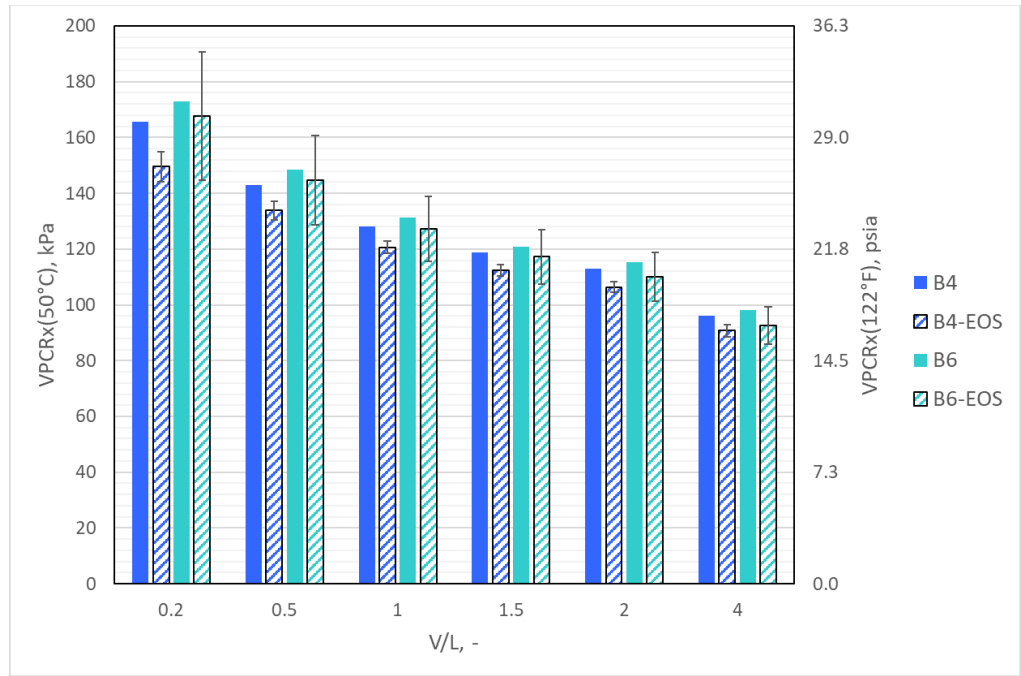


Figure 5-13 Column chart comparing measured VPCR_x to EOS-modeled VPCR_x for Bakken burn site samples at T = 50°C; 122°F. Measured values are solid bars, modeled values are striped bars.

Dilbit $VPCR_x$ results are given in Figure 5-14 and Figure 5-15. No error bars are shown for the measured or EOS-modeled $VPCR_x$ since no additional replicates were analyzed in either case. The reasonable agreement between measured and modeled $VPCR_x$ indicates that the compositions and vapor pressures measured for these oils are self-consistent, and that the EOS model performance for $VPCR_x$ in this pressure and temperature range is reasonably accurate. A close review of the higher temperature 50°C case reveals a bias, however: the EOS-modeled $VPCR_x$ values are all around 10-15% lower than the measured values. This same bias is not seen in the $T = 37.8^\circ\text{C}$ case. The authors pose several possible explanations for this temperature sensitivity in EOS performance. A primary factor is likely associated with the diluent composition, dominated by C5 and C6 components, many of which exhibit pure component boiling points in the range from 37.8 to 50°C. The EOS-simulated heating appears to volatilize less material, indicated by lower simulated $VPCR_x$, than the actual heating. There is a practical necessity to lump the continuum of different components that actually appear in a crude into bins, in this case by carbon number, for facilitating laboratory reporting and subsequent modeling. It is possible that this simplification was more compatible with EOS performance and $VPCR$ calculations at $T = 37.8^\circ\text{C}$ than at 50°C. Another possibility is that some of the EOS empirical tuning parameters, namely binary interaction coefficients (BICs), that were likely optimized by the EOS software vendor for a wide range of oils, were not optimized for dilbit. The dilbit is an extreme case of co-existence of large concentrations of light and heavy end carbon molecules that may require some attention to tuning BICs for those component pairs.

The general finding from the EOS modeling effort is that the measured $VPCR_x$ for each sample correlates well with the underlying composition, providing confidence that the property measurements and compositional measurements are sufficiently accurate and self-consistent for the purpose of this work.

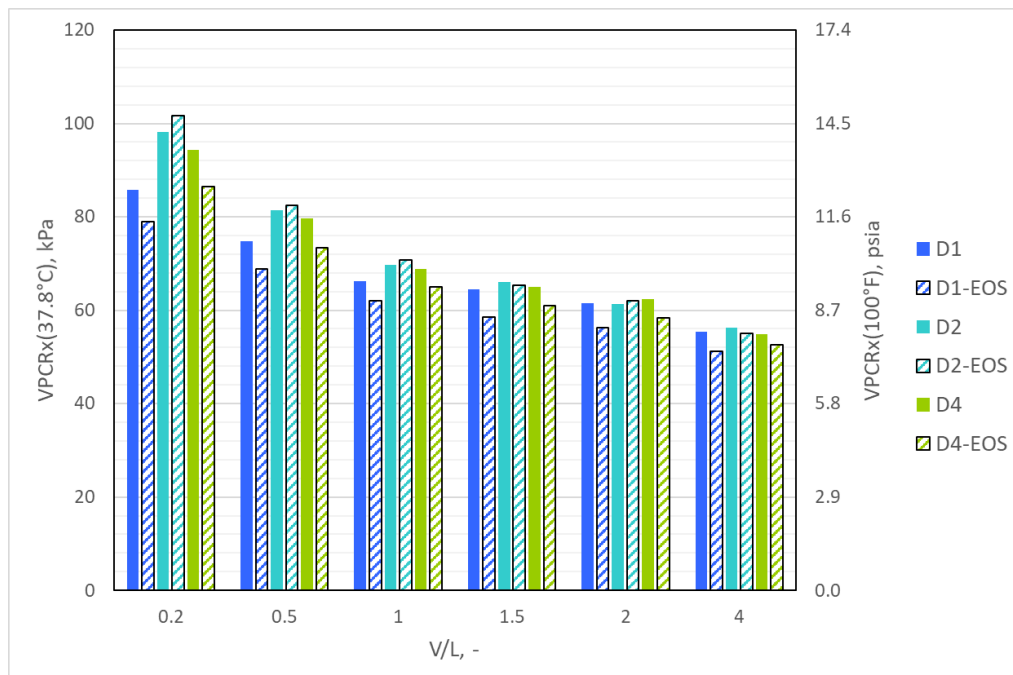


Figure 5-14. Column chart comparing measured $VPCR_x$ to EOS-modeled $VPCR_x$ for dilbit loading and burn site samples at $T = 37.8^\circ\text{C}$; 100°F . Measured values are solid bars, modeled values are striped bars.

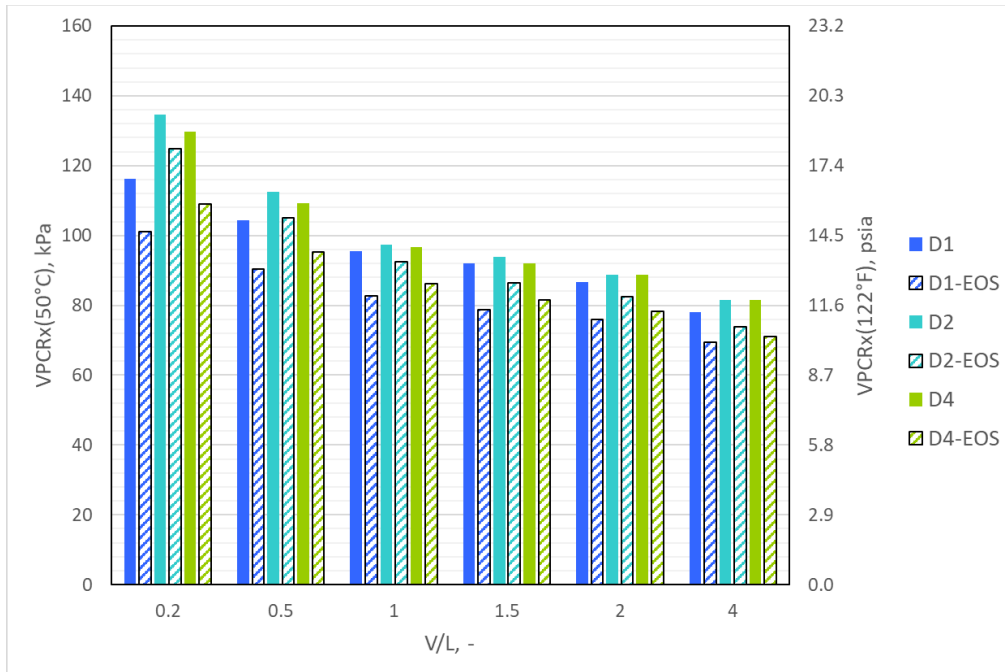


Figure 5-15 Column chart comparing measured VPCR_x to EOS-modeled VPCR_x for dilbit samples at T = 50°C; 122°F;. Measured values are solid bars, modeled values are striped bars.

5.6. Other Selected Properties

5.6.1. Other Bakken Properties

Physical properties from fluid samples taken for the Bakken crude at the four different sampling events are shown in Table 5-6. The $VPCR_{0.2}$ (37.8°C; 100°F) data are reproduced from section 5.5.1. Heat of combustion for samples B4 and B6 are around 46.0 MJ/kg, which is typical of a hydrocarbon liquid fuel (Luketa, Blanchat et al. 2019). Note that subsamples B1, B2, and B8 underwent different methods for determining density, water content and flash point than events B4 and B6, as listed in the table below. The density was measured with a digital density analyzer (ASTM D5002), within 0.3% through time. For water content, ASTM D4377 referenced potentiometric Karl Fischer titration (range: 0.02-2 % water), while ASTM D6304 was for coulometric Karl Fischer titration (range: 0.001-2.500 % water). The water contents were low for subsamples B1, B2, B4, and B8. The water content for subsample B6 was an order of magnitude larger than the others and hints at the possibility of small amounts of entrained water, as explained in Section F.3.2.5 of the corresponding DOE/DOE/TC project report (Luketa, Blanchat et al. 2019). ASTM D93A, D56A, and D3828 all used closed cup testers to determine flash points, though ASTM D93A and D56A required a slow, constant heating rate, and ASTM D3828 specified isothermal testing at discrete temperatures. Measured flash points were at the lower limits of resolution (< 10°C; < 50°F and < -30°C; < -22°F) for the methods used. ASTM D3828 covers tests within a range of -30°C to 300°C, while the ASTM D56A test results only applied down to 10°C; 50°F. The Bakken crude flashed at the lower temperature limit of the laboratory setup (1°C; 34°F) using ASTM D93A and D56A, but the test methods indicated that the analyst should begin checking when the sample is 10°C (18°F) below the expected flash point, so < 10°C (< 50°F) was reported, though the actual observed flash point was $\leq 1^\circ\text{C}$ ($\leq 34^\circ\text{F}$). The viscosity for subsample B1 was similar to that measured for other light oils, which is higher than condensate streams, but smaller than many blends commonly seen in pipelines (Enbridge Pipelines and Enbridge Energy Partners 2018). The initial boiling points were measured for B4 and B6 using ASTM D8003 + ASTM D7169 merge.

Table 5-6. Physical properties of Bakken samples taken at loading site and Sandia burn site.

Property	Unit	Method	B1	B2	B4	B6	B8
Description			Loading	Burn Site 1	Burn Site 2	Burn Site 3	July 2018
Sampling Date			8/17/2017	10/2/2017	1/18/2018	1/31/2018	7/18/2018
VPCR _{0.2} (37.8°C; 100°F)	kPa	ASTM D6377-M	120	133	138	152	133
Density (15.6°C; 60°F)	kg/m ³	ASTM D5002-M	812.3	811.3	809.6	810.0	812.4
Sulfur	wt%	ASTM D4294	0.0844	--	--	--	--
Heat of Comb.	MJ/kg	ASTM D240	48.5	49.3	46.0	46.0	44.1
Water Content	wt%	ASTM D4377	0.012	0.016	--	--	0.009
Water Content	wt%	ASTM D6304	--	--	0.01	0.16	--
Flash Point	°C; °F	ASTM D93A	< 10; < 50	--	--	--	--
Flash Point	°C; °F	ASTM D56A	--	< 10; < 50	--	--	< 10; < 50
Flash Point	°C; °F	ASTM D3828	--	--	< -30; < -22	< -30; < -22	--
Viscosity (40°C; 104°F)	mm ² /s	ASTM D445	1.996	--	--	--	--
Initial Boiling Point	°C; °F	ASTM D8003 + D7169 merge	--	--	-42.2; -44.0	-42.2; -44.0	--

5.6.2. Other Dilbit Properties

Physical properties from fluid samples taken for the dilbit at three different sampling events are shown in Table 5-7. Subsample D1 was taken from tank 5, subsample D2 from tank 12, and subsample D4 from tank 9. This is different from the Bakken subsamples, which were taken from the same tanker at several points through time. Thus, the dilbit data shown in the table do not represent a change in properties of one material through time, but rather, a glimpse into the properties of three separate samples from three different tanks on three different dates. Most of the properties listed showed little variation among the tanks, which is expected because the tanks were filled from the same pipeline source over the course of two days. The VPCR_{0.2}(37.8°C; 100°F) data were reproduced from section 5.5.3, and show a 1.8 psia variation, which is typical at V/L = 0.2. Heats of combustion for the samples were around 43.0 MJ/kg, which is typical of a hydrocarbon liquid fuel. The water contents for the dilbit were high relative to approximations of the water solubility, which were calculated from density and elemental hydrogen content to be somewhere around 0.1 wt% (Amani, Gray et al. 2014). Water is ever-present in the production and processing of dilbit, so it is actively removed to help meet the pipeline specification of < 0.5 wt% basic sediment and water. The water contents measured here are consistent with the pipeline specifications, yet may indicate free-phase water in the samples. The dilbit flashed at the lowest temperature for the ASTM D3828 setup, thus they are listed as < -30°C; < -22°F. There was about 10% variation in the measured viscosity, which is high relative to variation that would have been expected had the same sample been measured, as shown in the test method (ASTM 2018). Additionally, these viscosities measured high relative to historical records of comparable dilbits, which list viscosity at 40°C between 50-55 mm²/s (Enbridge Pipelines and Enbridge Energy Partners 2012; Enbridge Pipelines and Enbridge Energy Partners 2018). The initial boiling points were measured using ASTM D8003 + ASTM D7169 merge.

Table 5-7. Physical properties of dilbit samples taken at loading site and Sandia burn site.

Property	Unit	Method	D1	D2	D4
Description			Loading	Burn Site 1	Burn Site 2
Sampling Date			12/3/2018	1/28/2019	2/27/2019
Sample Tank			5	12	9
VPCR_{0.2} (37.8°C; 100°F)	kPa	ASTM D6377-M	85.7	98.1	94.4
Density (15°C; 59°F)	kg/m ³	ASTM D5002-M	923.5	924.2	923.9
Sulfur	wt%	ASTM D4294	3.68	3.65	3.42
Hydrogen Sulfide	ppm	UOP 163	6	0	2
Mercaptans	ppm	UOP 163	114	100	120
Heat of Comb.	MJ/kg	ASTM D240	42.8	43.1	43.2
Water Content	wt%	ASTM D4007	0.450	0.200	0.275
Flash Point	°C; °F	ASTM D3828	< -30; < -22	< -30; < -22	< -30; < -22
Viscosity (40°C; 104°F)	mm ² /s	ASTM D445	76.41	70.26	68.99
Initial Boiling Point	°C; °F	ASTM D8003 + ASTM D7169 merge	-0.6; 30.9	-0.6; 30.9	-0.6; 30.9

6. ADDITIONAL OBSERVATIONS

6.1. Comparison of Bakken and Dilbit Properties

Table 6-1 gives a concise comparison of the two crudes tested as part of this project. Oil properties averaged over all sampling events are listed, with the higher of the two in bold. The Bakken crude showed higher vapor pressure than the dilbit, though the dilbit had a higher < C6 content than the Bakken. This may seem counterintuitive at first glance, but further analysis reveals that the dilbit contained > 5.5 wt% C5, while the Bakken crude was around 3 wt% C5. This means that the majority of the material in the dilbit below C6 had relatively low volatility, leading to a lower vapor pressure than the Bakken, which had greater C1-C4 contents. The heats of combustion for the Bakken samples were slightly higher than the heats of combustions for the dilbit samples, though they were both relatively close and within the region expected for hydrocarbons. Since the flash points for both materials were below the lower limit of the test methods, several methods were employed to predict the flash points of each material. These predictions were based on VPCR₄, the temperature at which 10 vol% of the material vaporizes, and the normal boiling point (Alqaheem and Riazi 2017). Each method predicted the Bakken crude to have a lower flash point than the dilbit, though both were calculated to be below the lowest temperature for ASTM D3828 (-30°C; -22°F). The dilbit was approximately 35 times more viscous than the Bakken crude at 40°C, which is expected since the dilbit is a mixture of an extremely viscous base bitumen material that is diluted with light condensate hydrocarbons to meet pipeline specifications.

Table 6-1. A brief comparison of Bakken crude and dilbit properties; bold values represent the larger of the two.

Property	Units	Bakken	Dilbit
VPCR _{0.2} (37.8°C; 100°F)	kPa	136	92.7
Density (15°C; 60°F)	kg/m ³	805.9	923.9
Sulfur Content	wt%	0.08	3.58
< C6 Content	wt%	6.0	6.7
Heat of Comb.	MJ/kg	46.8	43.0
Water Content	wt%	0.06	0.3
Flash Point	°C; °F	< -30; < -22	< -30; < -22
Viscosity (40°C)	mm ² /s	2.0	71.9
Initial Boiling Point	°C; °F	-42.2; -44.0	-0.6; 30.9

6.2. Diluent Composition in the Dilbit

Observations from the pool fire testing described in Luketa, Cruz-Cabrera et al. (2019) indicated that the dilbit exhibited distinct behavior from the Bakken crude in several key combustion parameters, calling for a closer look at the compositional makeup of the dilbit to possibly understand why this occurred.

One important question pertaining to the burns was the compositional breakdown of the diluent, the bitumen, and the diluent-to-bitumen ratio in the dilbit. The carbon number plot in Figure 6-1 shows the average dilbit composition across the loading and burn samples. Also included in the plot are distributions of a condensate from 12/7/2018 (converted from a vol% distribution found at

<https://crudemonitor.ca/condensates>), and a bitumen (neatbit), from 2018 samples (converted from a boiling point distribution taken as part of the Bitumen Assay Program by the government of Alberta). Neatbit is defined in Birn, Osuna et al. (2014) as “..a nearly pure bitumen product containing about 1-2% diluent.” The dilbit supplier noted that the dilbit was likely blended from these two streams. The condensate shows a clear peak at C5, with gradually decreasing composition as carbon number increases. The bitumen contained very little material up to C8, with gradually increasing compositions at C9 and above.

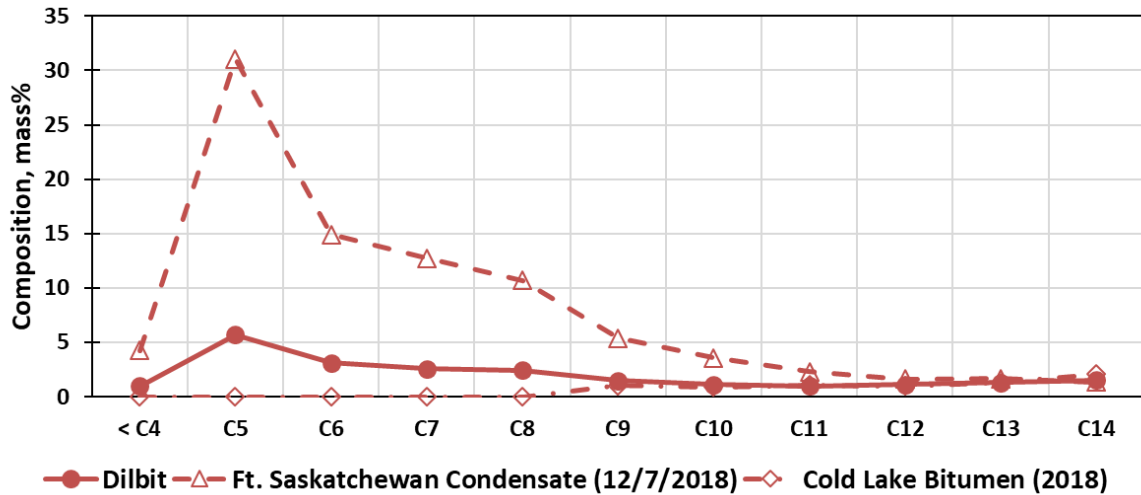


Figure 6-1. C4-C14 compositions for the dilbit fuel alongside a condensate and bitumen that were likely used in the stream.

The condensate and neatbit compositional data were combined using a commercially available process simulator and compared to the loading dilbit sample in Figure 6-2. A mixture of 20-25 vol% condensate and 75-80 vol% bitumen matched the dilbit composition well. According to Sandia contacts in industry, this type of mixture can be found in the supply chain. The composition of such a mixture (22 vol% condensate, 78 vol% bitumen) was plotted below with the dilbit. The calculated mixture showed a local minimum around C12, which is consistent with the minimum observed in the dilbit compositional data. Thus, the diluent in the dilbit caused the spike at C5, while the overlapping diluent and bitumen distributions caused the minimum at C11.

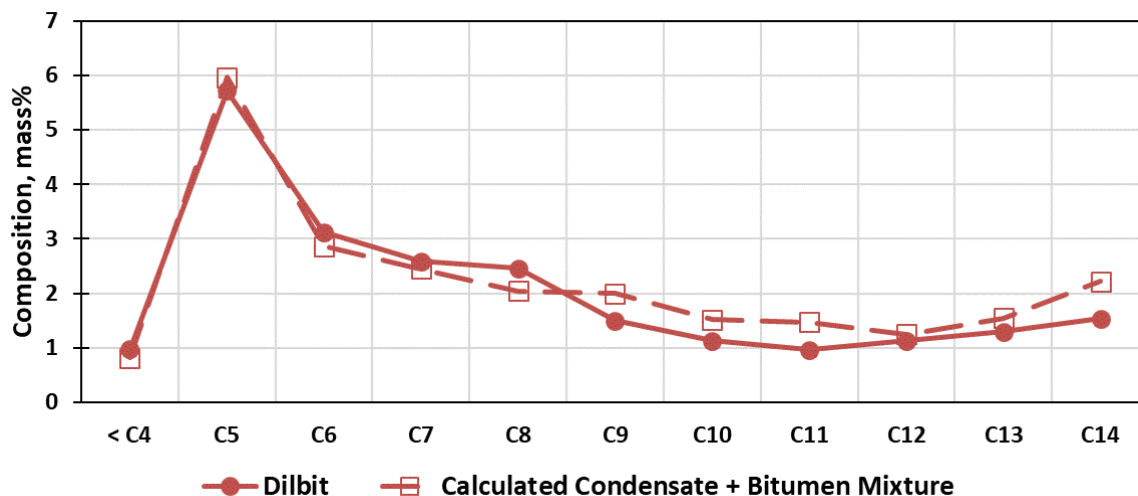


Figure 6-2. Measured C4-C14 composition for dilbit fuel (circle, solid line) and a simulated dilbit composition using likely constituents (square, dashed line).

6.3. Boiling Point Distributions of the Fuels

As mentioned in the parallel Sandia report on burn characteristics (Luketa, Cruz-Cabrera et al. 2019), the dilbit fuel showed transient burn behavior consistent across all the burns that was not seen in the Bakken burns. In Figure 6-3, composition is represented by assigning each component a boiling point and simulating the distillation of the material with increasing temperature using a commercially available process simulator equipped with an Equation of State. Carbon numbers associated with each temperature regime are marked in the plot for reference. Several interesting characteristics can be gleaned from the figure. First, since the *n*-heptane was > 99 mass% pure, nearly all the material would boil off at one temperature. Thus, the *n*-heptane curve is shown as a vertical line near the temperature regime assigned to C7. The Bakken and dilbit oils contained multiple components that would boil at different temperatures, thus resulting in more gradual distributions. Below ~ 95 °C, the Bakken and dilbit boiling point distributions were similar, reaching ~ 12 mass% boiled at 95 °C. Above 95 °C, the Bakken distributions climb smoothly before leveling off around 500 °C – echoing a smoothly decreasing carbon number distribution. The dilbit curves show three basic regimes: steeply increasing mass% with temperature up to 100 °C (slope = 0.13 mass%/°C), a less steep region between 100-250 °C (slope = 0.06 mass%/°C), and steeply increasing mass% with temperature above 250 °C (slope = 0.14 mass%/°C). This behavior indicates a dip in the carbon number distribution between C7 and C12 relative to the overall distribution, which was verified in the previous section.

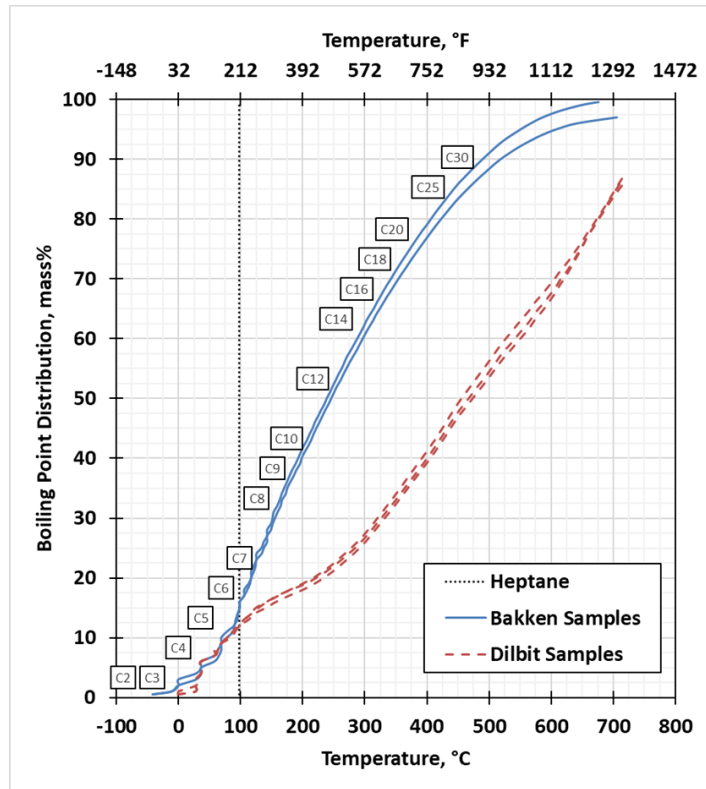


Figure 6-3 Temperature vs. boiling point distribution for the fuels in the burn series

6.4. Density vs. VPCR

Some perspective on where these oil properties fall relative to other oils in the North American supply chain may be gained from reviewing a plot of $VPCR_4(37.8^\circ\text{F})$ versus density (60°F), shown in Figure 6-4. A brief summary of the data sources and the measurement methods are given in Table 6-2. In the figure, ASTM D6377-measured $VPCR_x$ values (closed symbols) are shown where available.

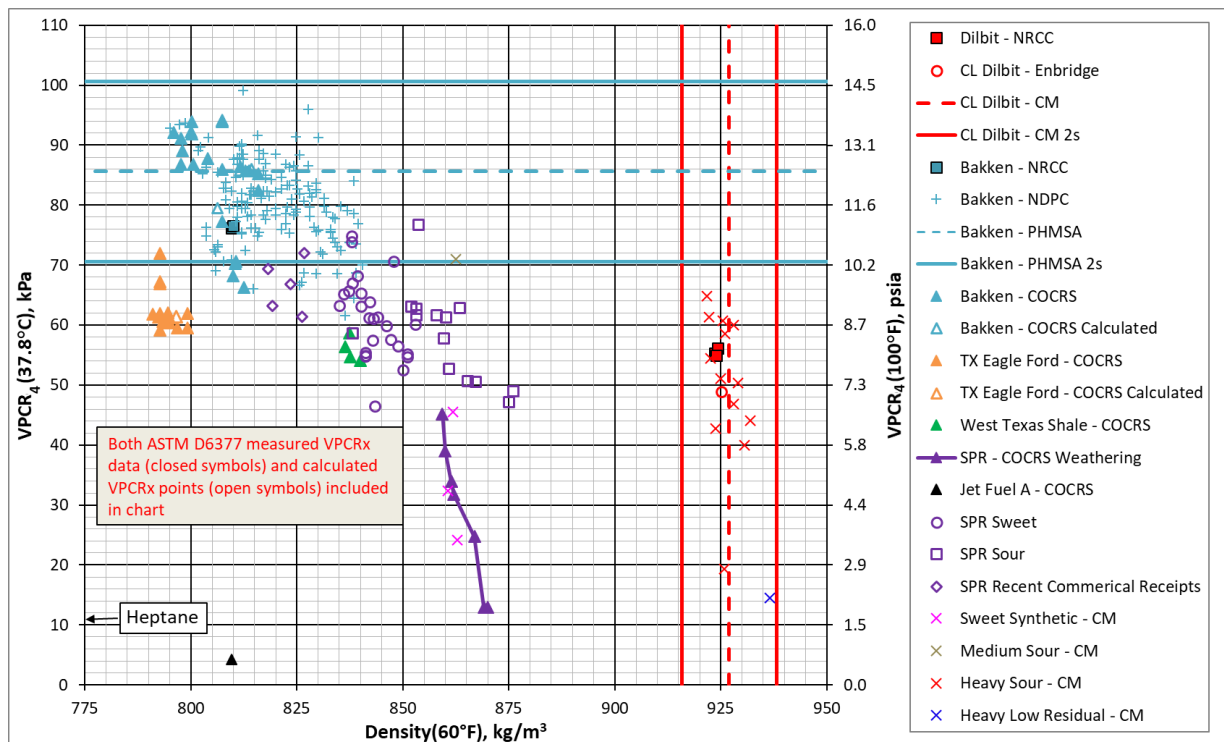


Figure 6-4: Overlay of density vs VPCR₄(37.8°C) for oils from SPR, PHMSA, NDPC and DOE/DOT/TC COCRS with the fuels tested as part of this project.

For systems where only compositional data were available, calculated VPCR_x points (open symbols) are shown based on equation of state calculations. Note that PHMSA did not list individual density values, so the mean VPCR₄ and 2 standard deviation (2σ) lines from that body of data were computed and added to the figure. Likewise, CrudeMonitor tracked the density, but not VPCR_x, of a representative dilbit (Cold Lake dilbit, abbreviated CL) through time. Thus, the mean density and 2 standard deviation (2σ) lines from that body of data over the past ten years were computed and added to the figure.

As densities increase in the figure, smaller VPCR₄ values were observed for incrementally lighter oils, with three notable exceptions: dilbit, the heavy sour streams from CrudeMonitor, and jet fuel. Dilbit was a combination of diluent (very light constituents) and bitumen (very heavy constituents) blended to achieve low enough viscosity to meet pipeline specifications. The diluent comprises light components which drive vapor pressure, while the bitumen comprises heavy ends which drive the density. Thus, the dilbit occupies an interesting place on the plot. The heavy sour streams from CrudeMonitor were stated to exhibit seasonality, which includes strategic blending of light and heavy constituents depending on ambient conditions. This effect is captured by the wide band on the CL dilbit density. Jet fuel was a specific cut of C9-C13 hydrocarbons with no light ends and no heavy ends that is specifically engineered for jet engine performance. Thus, fluids blended or engineered to optimize other properties (flashpoint, viscosity, vapor pressure, etc.) occupy different zones on the density vs. VPCR₄ plot than crudes that are only lightly-conditioned.

The fuels from this study occupy interesting spots in the parameter space compared to other historical data. The Bakken-NRC oil exhibited around the same VPCR and density as the NDPC, PHMSA, and COCRS Bakken oils – VPCR₄ ranged from about 70-100 kPa (10-14 psia) with a mean value around 86 kPa (12.5 psia). The dilbit-NRC oil sits close to other dilbit determinations: within the historical density band for CL dilbit from CrudeMonitor, and just 7 kPa (1 psia) above the CL dilbit measurement from Enbridge. The dilbit-NRC oil sits in the middle of a cluster of data from the “Heavy Sour” group on the CrudeMonitor website, which consists of several dilbits. Heptane density ($\rho = 688 \text{ kg/m}^3$) was below the lower limit shown on this chart, though its VPCR₄ was around 12 kPa (1.6 psia).

Table 6-2: Sources and methods for VPCR and Density data in Figure 6-4.

Plot Label	Source	VPCR _x Method	Density Method
Dilbit – NRC	This Report	ASTM D6377	ASTM D5002
CL Dilbit – Enbridge	(Enbridge Pipelines and Enbridge Energy Partners 2018)	VPCR ₄ at 37.8°C	Not Listed
CL Dilbit – CM	(Crudemonitor 2019)	N/A	Not Listed
Bakken – NRC	This Report	ASTM D6377	ASTM D5002
Bakken – NDPC	(Auers, Couture et al. 2014)	ASTM D6377	ASTM D5002
Bakken – PHMSA	(Auers, Couture et al. 2014; PHMSA 2014)	ASTM D6377	N/A
Bakken - COCRS	(PHMSA 2014; Lord, Allen et al. 2018; Luketa, Blanchat et al. 2019)	ASTM D6377	ASTM D5002
Bakken – COCRS Calculated	(Lord, Allen et al. 2018; Luketa, Blanchat et al. 2019)	Calculated	ASTM D5002
TX Eagle Ford – COCRS	(Lord, Allen et al. 2018; Luketa, Blanchat et al. 2019)	ASTM D6377	ASTM D5002
TX Eagle Ford – COCRS Calculated	(Lord, Allen et al. 2018; Luketa, Blanchat et al. 2019)	Calculated	ASTM D5002
West Texas Shale - COCRS	(Lord, Allen et al. 2018; Luketa, Blanchat et al. 2019)	ASTM D6377	ASTM D5002
SPR – COCRS Weathering	(Luketa, Blanchat et al. 2019)	ASTM D6377	ASTM D5002
Jet Fuel A – COCRS	(Luketa, Blanchat et al. 2019)	ASTM D6377	ASTM D5002
SPR Sweet	SPR Database	Calculated	ASTM D5002
SPR Sour	SPR Database	Calculated	ASTM D5002
SPR Recent Commercial Receipts	SPR Database	Calculated	ASTM D5002
Sweet Synthetic – CM	(Crudemonitor 2019)	VPCR ₄ at 37.8°C	Not Listed

Plot Label	Source	VPCR _x Method	Density Method
Medium Sour – CM	(Crudemonitor 2019)	VPCR ₄ at 37.8°C	Not Listed
Heavy Sour – CM	(Crudemonitor 2019)	VPCR ₄ at 37.8°C	Not Listed
Heavy Low Residual – CM	(Crudemonitor 2019)	VPCR ₄ at 37.8°C	Not Listed

Figure 6-5 shows density at 60°F versus VPCR_{0.2}(50°C; 122°F), with a brief summary of the data sources and measurement methods in Table 6-3. The vapor pressure at 50°C is important in regulation of transportation of dangerous goods as a delineation point between a material that is defined as a liquid or a gas (TC 2019). Also, in practical hydrocarbon transportation scenarios, the actual vapor-to-liquid volumes are much less than 4:1 due to economic drivers, with 1% (0.01:1) referenced in ANSI/API (2014). Previous work has shown that uncertainties in ASTM D6377M measurements of VPCR increase as V/L decreases, and V/L = 0.2 was identified as a practical minimum for crude oil with the available technology that correlated well with an independent measure of bubble point pressure (Lord, Allen et al. 2018). Thus, V/L = 0.2 was selected as the smallest V/L for display here. In the plot, there is more variation in the VPCR_{0.2}(50°C; 122°F) values than the VPCR₄(37.8°C; 100°F) data on the previous plot. Data from this study are listed (squares) with those performed in a previous TC study (Prefontaine 2015) and the COCRS (Luketa, Blanchat et al. 2019). The dilbit data from this report fell in the same VPCR_{0.2}(50°C; 122°F) and density region as the dilbits measured in the TC study. The Bakken VPCR_{0.2}(50°C; 122°F) data from this report compared well to the calculated Bakken data from the COCRS. In general, the Bakken VPCR_{0.2}(50°C; 122°F) and density points sat between the light oils and condensates from the TC study.

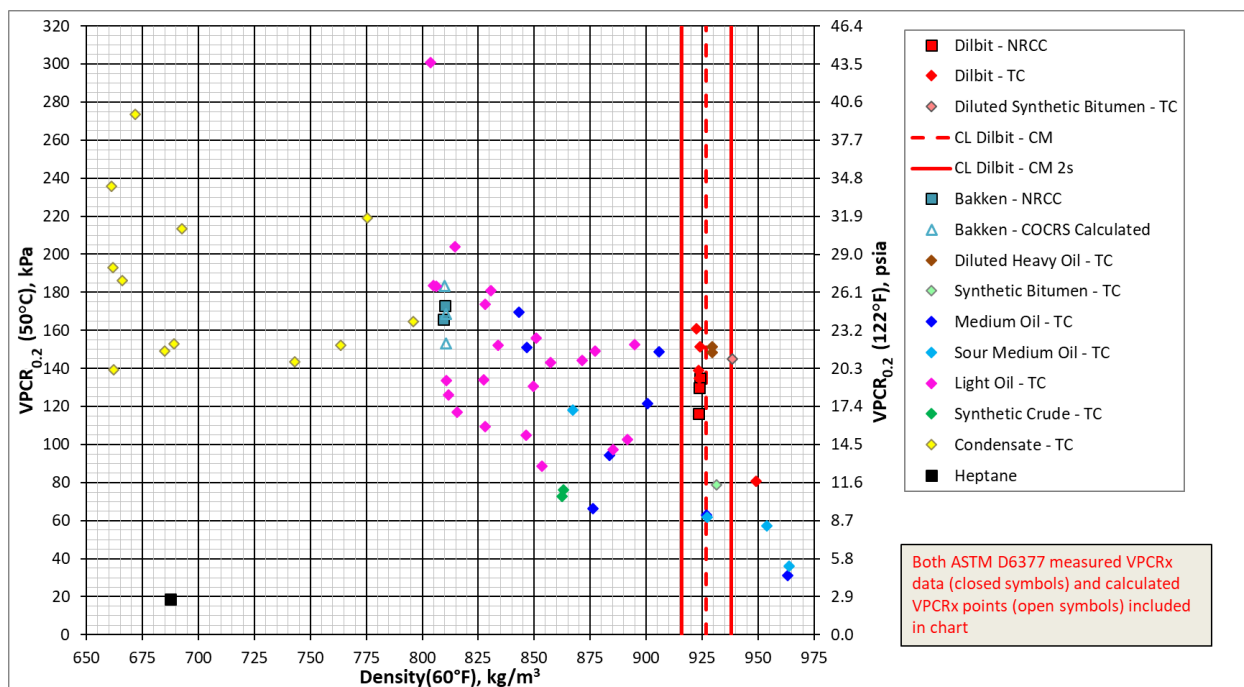


Figure 6-5: Overlay of density vs. VPCR_{0.2}(50°C) for oils from SPR, COCRS, and TC with the fuels tested as part of this project

Table 6-3. Sources and methods for VPCR_x(50°C) and density data in Figure 6-5.

Plot Label	Source	VPCR _x Method	Density Method
Dilbit – NRC	This Report	ASTM D6377	ASTM D5002
Dilbit – TC	(Prefontaine 2015)	ASTM D6377	ASTM D5002
Diluted Synthetic Bitumen – TC	(Prefontaine 2015)	ASTM D6377	ASTM D5002
CL Dilbit – CM	(Crudemonitor 2019)	N/A	Not Listed
Bakken – NRC	This Report	ASTM D6377	ASTM D5002
Bakken – COCRS Calculated	(Luketa, Blanchat et al. 2019)	Calculated	ASTM D5002
Diluted Heavy Oil – TC	(Prefontaine 2015)	ASTM D6377	ASTM D5002
Synthetic Bitumen – TC	(Prefontaine 2015)	ASTM D6377	ASTM D5002
Medium Oil – TC	(Prefontaine 2015)	ASTM D6377	ASTM D5002
Sour Medium Oil – TC	(Prefontaine 2015)	ASTM D6377	ASTM D5002
Light Oil – TC	(Prefontaine 2015)	ASTM D6377	ASTM D5002
Synthetic Crude – TC	(Prefontaine 2015)	ASTM D6377	ASTM D5002
Condensate – TC	(Prefontaine 2015)	ASTM D6377	ASTM D5002
Heptane	Various	Calculated ^a	Supplier Value ^b

^a Vapor pressure for *n*-heptane calculated using process simulator. Verified using correlation from literature (Williamham, Taylor et al. 1945).

^b Density for heptane given in the Certificate of Analysis in Appendix C.

6.5. Post-Burn Solids Mass

6.5.1. Bakken Residue

Post-burn solids from the first and last Bakken pool fires were collected and quantified in Table 6-4. Oil feed (kg) was determined by measuring fuel tank weight before and after each test, and residue (kg) was measured from residue remaining in the pan. The residue ratio (mass residual/mass oil feed) is given for both tests and measured at 0.003 to 0.004. Mean residue ratio for the Bakken pool fire series was 0.003 with standard deviation 0.001.

Table 6-4. Residue mass (kg) and ratio to oil feed (kg/kg) for the 2-m Bakken pool fire series.

Pool Fire Test ID		2.3	2.6
Pool Fire Test Date		1/19/2018	1/31/2018
Sampling Event #		B3	B7
Sampling Description		Post-test residue grab sample + residue mass	Post-test residue grab sample + residue mass
Fuel Supply Temperature	(°C)	20 ± 5	20 ± 5
Fuel Feed Method		Constant Level	Non-continuous fuel feed, allow to burn down
Oil Feed	(kg)	253	203
Residue	(kg)	0.7	0.8
Ratio (Residue/Feed)	(kg/kg)	0.003	0.004

6.5.2. Dilbit residue

Table 6-5 contains a summary of solids remaining after the six tests in the dilbit pool fire series. Tests are listed chronologically. The residue ratio (mass residual/mass oil feed) is given for each test, and ranged from 0.089 to 0.179 depending on test conditions. Mean residue ratio across the six dilbit tests was 0.129, with standard deviation at 0.03. The constant-level fuel feed method with fuel supply temperature at 20 ± 5°C exhibited the most repeatable results for residue ratio, with all four tests in the range 0.117 to 0.139. Allowing the fuel to simply burn down with no fresh feed created the highest residue ratio at 0.179. Test 3.6 where the fuel was heated to 60 ± 5°C left the lowest residue ratio of 0.089. All of the dilbit residue ratios were much higher than observed for the Bakken 2-m pool fire test series summarized in Table 6-4, where ratios measured 0.003-0.004. As such, dilbit left, on average, about 40 times more residue by mass than Bakken in the 2-m pool fire configuration.

Table 6-5. Summary of post-burn solids residue recovered from pan

Pool Fire Test ID		3.1	3.2	3.3	3.4	3.5	3.6
Pool Fire Test Date		2/6/2019	2/14/2019	2/20/2019	2/25/2019	2/27/2019	3/4/2019
Sampling Event		D3	-	-	-	-	D5
Sampling Description		Post-test residue grab sample + residue mass	Residue mass only	Residue mass only	Residue mass only	Residue mass only	Post-test residue grab sample + residue mass
Fuel Supply Temperature	(°C)	20 ± 5	20 ± 5	20 ± 5	20 ± 5	20 ± 5	60 ± 5
Fuel Feed Method		Constant Level	Constant Level	Constant Level	Non-continuous fuel feed, allow to burn down	Constant Level	Constant Level
Oil Feed Mass	(kg)	268	256	243	221	243	230
Residue Mass	(kg)	31.5	28.4	32.9	39.7	29.3	19.6
Ratio (Residue/Feed)	(kg/kg)	0.12	0.11	0.14	0.18	0.12	0.09

7. SUMMARY

This report documents the sampling methods and analysis results of fuel characterization associated with 2-m pool fire testing of high-purity n-heptane, Bakken crude, and a diluted bitumen at Sandia National Laboratories for the National Research Council Canada.

Sampling and analysis methods were selected to be consistent with published industry standards and best practices. Basic physical and chemical properties were evaluated. Where available, measured values obtained here were compared to reference values, properties of similar oils, and equation of state model output.

High-level findings were as follows:

- 1) Heptane sample properties were consistent with high-purity (>99%) n-heptane and checked against the manufacturer statement of purity and NIST reference standard values
- 2) Bakken samples represented a light (43.9 °API), sweet (sulfur = 0.084 mass%) crude
 - a) Bakken $VPCR_{0.2}(37.8^{\circ}\text{C})$ ranged from 120 kPa-152 kPa depending on sampling time and analysis laboratory
 - b) While some variations in sample-to-sample Bakken $VPCR_x$ and composition were noted, these correlated strongly with laboratory and analytical methods, suggesting that method bias in sampling & analysis was more likely the cause than property changes of the base crude sample with time during sample storage
 - c) Calculated $VPCR_x$ (37.8°C and 50°C) using whole oil composition passed through an EOS model compared well with measured $VPCR_x$ by ASTM D6377-M
- 3) The diluted bitumen represented a heavy (21.7 °API), sour (sulfur = 3.6 mass%) crude
 - a) Dilbit $VPCR_{0.2}(37.8^{\circ}\text{C})$ ranged from 86 kPa-94 kPa
 - b) A compositional analysis was consistent with a mixture of 20-25 vol% condensate (comprising C4-C8) and 75-80 vol% bitumen
 - c) Dilbit properties were stable with time across grab samples
 - d) Calculated $VPCR_x$ (37.8°C and 50°C) using whole oil composition passed through an EOS model generally compared well with measured $VPCR_x$ by ASTM D6377-M. Some method bias appeared in the T = 50°C comparison where EOS-modeled $VPCR_x$ values were all around 10-15% lower than the measured values, but compared better at T = 37.8°C.

This page intentionally blank

8. REFERENCES

- Alqaheem, S. S. and M. R. Riazi (2017). "Flash Points of Hydrocarbons and Petroleum Products: Prediction and Evaluation of Methods." *Energy & Fuels* **31**(4): 3578-3584.
- Amani, M. J., M. R. Gray and J. M. Shaw (2014). "On correlating water solubility in ill-defined hydrocarbons." *Fuel* **134**: 644-658.
- ANSI/API 2014 (Sep-2014) "Classifying and Loading of Crude Oil into Rail Tank Cars." **Recommended Practice 3000**. American Petroleum Institute, Washington, DC.
- API (2011). "Crude Oil Category Assessment Document." High Production Volume Testing Group. American Petroleum Institute, Washington, DC 14-Jan-2011.
- ASTM 2012 "Standard Practice for Manual Sampling of Petroleum and Petroleum Products." **ASTM D4057-12**. ASTM International, West Conshohocken, PA 19428-2959.
- ASTM 2016a "Standard Test Method for Boiling Point Distribution of Samples with Residues Such as Crude Oils and Atmospheric and Vacuum Residues by High Temperature Gas Chromatography." **ASTM D7169-16**. ASTM International, West Conshohocken, PA 19429-2959.
- ASTM 2013a "Standard Test Method for Density and Relative Density of Crude Oils by Digital Density Analyzer." **ASTM D5002-13**. ASTM International, West Conshohocken, PA 19428-2959.
- ASTM 2011a "Standard Test Method for Density, Relative Density, and API Gravity of Liquids by Digital Density Meter." **ASTM D4052-11**. ASTM International, West Conshohocken, PA 19428-2959.
- ASTM 2011b "Standard Test Method for Determination of Individual Components in Spark Ignition Engine Fuels by 100-Metre Capillary (with Precolumn) High-Resolution Gas Chromatography." **ASTM D6730-01 (Reapproved 2011)**. ASTM International, West Conshohocken, PA 19428-2959.
- ASTM 2015 "Standard Test Method for Determination of Light Hydrocarbons and Cut Point Intervals in Live Crudes and Condensates by Gas Chromatography." **ASTM D8003-15**. ASTM International, West Conshohocken, PA 19428-2959.
- ASTM 2016b "Standard Test Method for Determination of Vapor Pressure of Crude Oil: VPCRx(Expansion Method)." **ASTM D6377-16**. ASTM International, West Conshohocken, PA 19428-2959.
- ASTM 2016c "Standard Test Method for Determination of Water in Petroleum Products, Lubricating Oils, and Additives by Coulometric Karl Fischer Titration." **ASTM D6304-11 (Reapproved 2016)**. ASTM International, West Conshohocken, PA 19428-2959.
- ASTM 2016d "Standard Test Method for Flash Point by Tag Closed Cup Tester." **ASTM D56-16a**. ASTM International, West Conshohocken, PA 19429-2959.
- ASTM 2014 "Standard Test Method for Heat of Combustion of Liquid Hydrocarbon Fuels by Bomb Calorimeter." **ASTM D240-14**. ASTM International, West Conshohocken, PA 19428-2959.
- ASTM 2018 "Standard Test Method for Kinematic Viscosity of Transparent and Opaque Liquids (and Calculation of Dynamic Viscosity)." **ASTM D445-19**. ASTM International, West Conshohocken, PA 19428-2959.
- ASTM 2016e "Standard Test Method for Sulfur in Petroleum and Petroleum products by Energy Dispersive X-Ray Fluorescence Spectrometry." **ASTM D4294-16**. ASTM International, West Conshohocken, PA 19428-2959.

ASTM 2016f "Standard Test Method for Water and Sediment in Crude Oil by the Centrifuge Methods (Laboratory Procedure)." **ASTM D4007-11 (Reapproved 2016)**. ASTM International, West Conshohocken, PA 19428-2959.

ASTM 2016g "Standard Test Method for Water in Organic Liquids by Coulometric Karl Fischer Titration." **ASTM E1064-16**. ASTM International, West Conshohocken, PA 19428-2959.

ASTM 2013b "Standard Test Methods for Flash Point by Pensky-Martens Closed Cup Tester." **ASTM D93-13**. ASTM International, West Conshohocken, PA 19429-2959.

ASTM 2016h "Standard Test Methods for Flash Point by Small Scale Closed Cup Tester." **ASTM D3828-16a**. ASTM International, West Conshohocken, PA 19428-2959.

Auers, J. R., R. M. Couture and D. L. Sutton (2014). "The North Dakota Petroleum Council Study on Bakken Crude Properties." Bakken Crude Characterization Task Force. North Dakota Petroleum Council, Bismarck, ND 58501. 4-Aug-2014.

Birn, K., J. Osuna, C. Velasquez, J. Meyer, S. Owens and M. Cairns (2014). "Crude by Rail: The new logistics of tight oil and oil sands growth." IHS Energy. https://ihsmarket.com/pdf/IHS-Oil-Sands-Dialogue-Crude-by-rail-dec-2014_210390110913052132.pdf

Crudemonitor. (2019). from <https://crudemonitor.ca/>.

Enbridge Pipelines, I. and L. Enbridge Energy Partners (2012). 2012 Crude Characteristics. https://www.enbridge.com/~media/Enb/Documents/Shippers/Crude_Characteristics_Booklet.pdf?la=en.

Enbridge Pipelines, I. and L. Enbridge Energy Partners (2018). 2018 Crude Characteristics. https://www.enbridge.com/~media/Enb/Documents/Shippers/Crude_Characteristics_Booklet.pdf?la=en.

GPA 2014 "Obtaining Liquid Hydrocarbons Samples for Analysis by Gas Chromatography." **GPA 2174-14**. Gas Processors Association, Tulsa, OK 74145.

GPA 2003 "Tentative Method for the Analysis of Natural Gas Condensate Mixtures Containing Nitrogen and Carbon Dioxide by Gas Chromatography." **GPA Standard 2103-03**. Gas Processors Association, Tulsa, OK 74145.

Lord, D., R. Allen and D. Rudeen (2017). "DOE/DOT Crude Oil Characterization Research Study, Task 2 Test Report on Evaluating Crude Oil Sampling and Analysis Methods." **SAND2017-12482**. Sandia National Laboratories, Albuquerque, NM 87185. Nov-2017.

Lord, D., R. Allen, D. Rudeen, C. Wocken and T. Aulich (2018). "DOE/DOT Crude Oil Characterization Research Study, Task 2 Test Report on Evaluating Crude Oil Sampling and Analysis Methods, Revision 1 - Winter Sampling." **SAND2018-5909**. Sandia National Laboratories, Albuquerque, NM 87185. Jun-2018.

Luketa, A., T. K. Blanchat, D. L. Lord, A. Cruz-Cabrera, J. Hogge and R. Allen (2019). "Pool Fire and Fireball Experiments in Support of the US DOE/DOT/TC Crude Oil Characterization Research Study." **SAND 2019-9189**. Sandia National Laboratories, Albuquerque, NM USA 87185. August.

Luketa, A., A. Cruz-Cabrera, W. Gill, S. Adee and J. Hogge (2019). "Experimental Results of 2-m Heptane, Bakken Crude Oil, and Dilbit Pool Fire Tests Performed for the National Research Council Canada." *in press*. Sandia National Laboratories, Albuquerque, NM 87185.

PHMSA (2014). "Operation Safe Delivery Update." U.S. Department of Transportation, Washington, D.C. Jul-2014.

Prefontaine, A. (2015). "Final Report: Crude Oil Sampling and Analysis." Transport Dangerous Goods Directorate. Transport Canada. 10-Aug-2015. <https://www.tc.gc.ca/eng/tdg/safety-menu-1242.html>

Prefontaine, A. (2018). "Sample Plan: Collecting Samples from Modified 420 lb. Propane Tanks." *Proprietary*. InnoTech Alberta, Edmonton, AB, Canada. 07-Dec-2018.

- Sagdeev, D. I., M. G. Fomina, G. K. Mukhamedzyanov and I. M. Abdulagatov (2013). "Experimental Study of the Density and Viscosity of n -Heptane at Temperatures from 298 K to 470 K and Pressure upto 245 MPa." International Journal of Thermophysics **34**(1): 1-33.
- TC (2019). "Transportation of Dangerous Goods Regulations, Part 1." Government of Canada. **Transport Canada**. from <https://www.tc.gc.ca/eng/tdg/clear-part1-475.html#sec14>.
- UOP 2010 "Hydrogen Sulfide and Mercaptan Sulfur in Liquid Hydrocarbons by Potentiometric Titration." **UOP 163**. ASTM International, West Conshohocken, PA 19428-2959.
- Williamham, C. B., W. J. Taylor, J. M. Pignocco and F. D. Rossini (1945). "Vapor Pressures and Boiling Points of Some Paraffin, Alkylcyclopentane, Alkylcyclohexane, and Alkylbenzene Hydrocarbons." J. Res. Nat. Bur. Stand. (U.S.) **35**(3): 219-244.

APPENDIX A. DILBIT TANK FILL DATA

Sample Reference	Means of Containment	Sample Date	Sample Point	Start Time	End Time	Ambient Temperature (°C)	Barometric Pressure (hPa)	Sample Source Fluid Pressure (psi)	Sample Source Fluid Temperature (°C)	Volume Collected (L)	Comments
Day 1 Baseline samples											Baseline samples were collected directly from the source (pipeline) on each sampling day. These samples are being held at InnoTech Alberta in case further analysis is required.
FPC S/N 831453, CL7 Dilbit, Day 1 Baseline	Floating Piston Cylinder	28/Nov/18	Terminal	8:26	10:43	0	921	143	9.8	0.56	
Bottle #1 Day 1	1 L Boston Round Bottle	28/Nov/18	Terminal	8:26	10:43	0	921	143	9.8	1	
Bottle #1 Day 2	1 L Boston Round Bottle	28/Nov/18	Terminal							1	
Day 2 Baseline samples											
FPC S/N 830748, CL7 Dilbit, Day 2 Baseline	Floating Piston Cylinder	29/Nov/18	Terminal	8:05	10:46	-5	925	140	2.3	0.56	
Bottle #1 Day 1	1 L Boston Round Bottle	29/Nov/18	Terminal	8:05	10:46	-5	925	140	2.3	1	
Bottle #1 Day 2	1 L Boston Round Bottle	29/Nov/18	Terminal	8:05	10:46	-5	925	140	2.3	1	
Tank 5, CL7 dilbit	420 lb propane tank	28/Nov/18	Terminal	8:26	10:43	0	921	143	9.8	360	
Tank 6, CL7 Dibit	420 lb propane tank	28/Nov/18	Terminal	8:26	10:43	0	921	143	9.8	360	
Tank 1, CL7 Dibit	420 lb propane tank	28/Nov/18	Terminal	11:45	14:06	4.5	923	130	10.4	360	
Tank 2, CL7 Dibit	420 lb propane tank	28/Nov/18	Terminal	11:45	14:06	4.5	923	130	10.4	360	
Tank 12, CL7 Dibit	420 lb propane tank	28/Nov/18	Terminal	15:00	17:30	7.9	922	132	10.4	360	
Tank 8, CL7 Dibit	420 lb propane tank	28/Nov/18	Terminal	15:00	17:30	7.9	922	132	10.4	360	
Tank 11, CL7 Dibit	420 lb propane tank	29/Nov/18	Terminal	8:05	10:46	-5	925	140	2.3	360	
Tank 3, CL7 Dibit	420 lb propane tank	29/Nov/18	Terminal	8:05	10:46	-5	925	140	2.3	360	
Tank 10, CL7 Dibit	420 lb propane tank	29/Nov/18	Terminal	11:27	13:43	-1	931	140	5.2	360	
Tank 7, CL7 Dibit	420 lb propane tank	29/Nov/18	Terminal	11:27	13:43	-1	931	140	5.2	360	
Tank 4, CL7 Dibit	420 lb propane tank	29/Nov/18	Terminal	14:23	16:51	3	929.3	140	5.2	360	
Tank 9, CL7 Dibit	420 lb propane tank	29/Nov/18	Terminal	14:23	16:51	3	929.3	140	5.2	360	

APPENDIX B. TABULAR LISTING OF VPCR x DATA

B.1. Bakken VPCR_x Data

B.1.1. Direct measurements taken at 37.8 °C and 50 °C

Direct measurements																	
Label	B4-100-FPC-1- a-M	B4-100-FPC-1- b-M	B4-100-FPC-2- a-M	B4-100-FPC-2- b-M	B4-100-FPC-3- a-M	B4-100-FPC-3- b-M	B4-122-FPC-1- a-M	B4-122-FPC-1- b-M	B6-100-FPC-1- a-M	B6-100-FPC-1- b-M	B6-100-FPC-2- a-M	B6-100-FPC-2- b-M	B6-100-FPC-2- c-M	B6-100-FPC-2- d-M	B6-122-FPC-1- a-M	B6-122-FPC-1- b-M	
Event Abbreviation	B4	B4	B4	B4	B4	B4	B4	B4	B6	B6	B6	B6	B6	B6	B6	B6	
Sampling Date	1/18/2018	1/18/2018	1/18/2018	1/18/2018	1/18/2018	1/18/2018	1/18/2018	1/18/2018	1/31/2018	1/31/2018	1/31/2018	1/31/2018	1/31/2018	1/31/2018	1/31/2018	1/31/2018	
Temperature	100	100	100	100	100	100	122	122	100	100	100	100	100	100	122	122	
Sample Container	FPC	FPC	FPC	FPC	FPC	FPC	FPC	FPC	FPC	FPC	FPC	FPC	FPC	FPC	FPC	FPC	
Cylinder Replicate	1	1	2	2	3	3	1	1	1	1	2	2	2	2	1	1	
Repeatability Replicate	a	b	a	b	a	b	a	b	a	b	a	b	c	d	a	b	
Sampling Temperature (F)																	
Sampling Pressure (psig)																	
Measured/SimUlated	M	M	M	M	M	M	M	M	M	M	M	M	M	M	M	M	
VPCR _x (at these V/L)	0.0																
	0.05																
	0.1																
	0.2	20.00	19.99	19.97	19.97	19.93	19.93	24.03	24.03	22.66	22.64	21.86	21.84	21.03	21.03	25.09	25.06
	0.5	16.62	16.62	17.01	17.03	16.80	16.84	20.73	20.74	18.42	18.46	17.87	17.85	17.54	17.54	21.51	21.52
	1.0	14.68	14.69	15.19	15.19	14.74	14.74	18.57	18.55	15.88	15.87	15.56	15.56	14.98	14.99	19.03	19.03
	1.5	13.63	13.63	13.98	13.98	13.67	13.66	17.22	17.23	14.26	14.26	14.17	14.17	13.75	13.72	17.41	17.61
2.0	12.84	12.84	13.10	13.11	12.88	12.89	16.36	16.38	13.42	13.40	13.27	13.29	12.93	12.92	16.71	16.72	
4.0	11.04	11.05	11.17	11.18	10.99	10.99	13.92	13.94	11.21	11.20	11.21	11.21	11.01	11.01	14.26	14.24	

B.1.2. Summary of measurements on shared Bakken samples from Luketa, Blanchat et al. (2019)

Label	B1-100-FPC-1	B1-100-FPC-2	B2-100-FPC-1	B2-100-FPC-1	B2-100-FPC-2	B6-100-MPC-	B6-100-MPC-	B6-100-MPC-	B6-100-MPC-	B8-100-MPC-	B8-100-MPC-	B8-100-MPC-	B8-100-MPC-	
	M	M	a-M	b-M	M	1-a-M	1-b-M	2-a-M	2-b-M	1-a-M	1-b-M	2-a-M	2-b-M	
Event Abbreviation	B1	B1	B2	B2	B2	B6	B6	B6	B6	B8	B8	B8	B8	
Sampling Date	8/17/2017	8/17/2017	10/2/2017	10/2/2017	10/2/2017	7/18/2018	7/18/2018	7/18/2018	7/18/2018	10/4/2018	10/4/2018	10/4/2018	10/4/2018	
Temperature	100	100	100	100	100	100	100	100	100	100	100	100	100	
Sample Container	FPC	FPC	FPC	FPC	FPC	MPC	MPC	MPC	MPC	MPC	MPC	MPC	MPC	
Cylinder Replicate	1	2	1	1	2	1	1	2	2	1	1	2	2	
Repeatability Replicate			a	b		a	b	a	b	a	b	a	b	
Sampling Temperature (F)	75		70	70	70									
Sampling Pressure (psig)	148		45	45	45									
Measured/Simulated	M	M	M	M	M	M	M	M	M	M	M	M	M	
VPCR _x (at these V/L)	0.0													
	0.05	18.53	18.10	27.71	28.00	26.61	22.64	23.56	20.75	21.49				
	0.1		17.40	19.78	19.95	21.50	22.33	22.32	19.66	19.82	19.18	18.99	19.02	19.01
	0.2	17.83	17.07	19.18	19.15	19.42	20.11	20.08	18.60	18.31	18.15	18.10	17.79	18.05
	0.5	15.70	15.40	16.09	16.04	16.21	16.23	16.56	15.22	15.37	15.25	15.25	15.30	15.40
	1.0													
	1.5		12.79	13.16	13.08	12.96	13.06	13.03	12.53	12.34	12.40	12.37	12.25	12.40
	2.0													
4.0	9.87	10.61	10.18	10.23	10.18	10.10	10.38	9.54	9.58	9.58	9.68	9.58	9.65	

B.1.3. Values calculated from process simulator

Values calculated from process simulator																	
Label	B1-100-FPC-1	B1-100-FPC-2	B1-122-FPC-1	B1-122-FPC-2	B2-100-FPC-2	B2-122-FPC-2	B4-100-FPC-1	B4-122-FPC-1	B4-100-FPC-2	B4-122-FPC-2	B6-100-FPC-1	B6-122-FPC-1	B6-100-FPC-2	B6-122-FPC-2	B8-100-WD-4	B8-122-WD-4	
	U	U	U	U	U	U	U	U	U	U	U	U	U	U	U	U	
Event Abbreviation	B1	B1	U	B1	B2	B2	B4	B4	B4	B4	B6	B6	B6	B6	B8	B8	
Sampling Date	8/17/2017	8/17/2017	8/17/2017	8/17/2017	10/2/2017	10/2/2017	1/18/2018	1/18/2018	1/18/2018	1/18/2018	1/31/2018	1/31/2018	1/31/2018	1/31/2018	7/18/2018	7/18/2018	
Temperature	100	100	122	122	100	122	100	122	100	122	100	122	100	122	100	122	
Sample Container	FPC	FPC	FPC	FPC	FPC	FPC	FPC	FPC	FPC	FPC	FPC	FPC	FPC	FPC	WD	WD	
Cylinder Replicate	1	2	1	2	2	2	1	1	2	2	1	1	2	2	4	4	
Repeatability Replicate																	
Sampling Temperature (F)																	
Sampling Pressure (psig)																	
Measured/Simulated	U	U	U	U	U	U	U	U	U	U	U	U	U	U	U	U	
VPCR _x (at these V/L)	0.0	192.16	148.17	223.40	178.28	152.31	181.00	143.14	171.49	150.17	178.54	198.51	222.42	167.18	195.51	212.71	240.93
	0.05	177.41	140.04	208.41	169.99	142.45	170.97	139.42	162.88	140.46	168.77	175.78	205.04	153.95	182.19	190.99	219.30
	0.1	166.79	134.11	197.44	163.80	135.21	163.57	134.66	156.54	133.45	161.57	163.53	192.63	144.59	172.61	175.82	203.96
	0.2	152.10	125.76	182.13	154.93	125.35	153.15	120.04	147.57	123.79	151.46	147.20	175.82	131.99	159.50	155.69	183.36
	0.5	129.35	112.11	157.52	139.73	109.63	136.09	106.53	132.65	108.64	134.99	123.21	150.33	113.05	139.10	126.59	152.83
	1.0	111.99	100.67	137.96	126.28	97.39	122.00	95.51	119.85	96.83	121.43	106.24	131.39	99.04	123.18	106.80	131.05
	1.5	102.18	93.63	126.51	117.67	90.19	113.41	88.95	111.76	89.92	113.15	97.06	120.69	91.14	113.81	96.46	119.25
	2.0	95.41	88.43	118.37	111.19	85.06	107.12	84.03	105.71	84.96	107.07	90.79	113.17	85.60	107.06	89.57	111.20
4.0	79.36	75.22	98.66	94.42	72.40	91.23	71.71	90.03	72.65	91.54	76.06	94.97	72.18	90.28	74.12	92.43	

B.2. Dilbit VPCRx Data

B.2.1. Direct measurements taken at 37.8 and 50°C

Direct measurements													
Label	D1-100-FPC-1- a-M	D1-100-FPC-1- b-M	D1-122-FPC-1- a-M	D1-122-FPC-1- b-M	D2-100-FPC-1- a-M	D2-100-FPC-1- b-M	D2-122-FPC-1- a-M	D2-122-FPC-1- b-M	D4-100-FPC-1- a-M	D4-100-FPC-1- b-M	D4-122-FPC-1- a-M	D4-122-FPC-1- b-M	
Event Abbreviation	D1	D1	D1	D1	D2	D2	D2	D2	D4	D4	D4	D4	
Sampling Date	11/28/2018	11/28/2018	11/28/2018	11/28/2018	12/3/2018	12/3/2018	12/3/2018	12/3/2018	1/28/2019	1/28/2019	1/28/2019	1/28/2019	
Temperature	100	100	122	122	100	100	122	122	100	100	122	122	
Sample Container	FPC	FPC	FPC	FPC	FPC	FPC	FPC	FPC	FPC	FPC	FPC	FPC	
Cylinder Replicate	1	1	1	1	1	1	1	1	1	1	1	1	
Repeatability Replicate	a	b	a	b	a	b	a	b	a	b	a	b	
Sampling Temperature (F)													
Sampling Pressure (psig)													
Measured/SimUlated	M	M	M	M	M	M	M	M	M	M	M	M	
0.0													
0.05	117.10	116.60	141.20	141.20	143.60	143.70	194.30	194.40					
0.1	91.20	90.70	123.30	123.30	115.70	115.40	145.40	145.40					
0.2	85.80	85.60	116.30	116.30	98.10	98.10	134.50	134.70	94.40	94.30	129.80	129.60	
0.5	74.70	74.70	104.40	104.40	81.50	81.40	112.60	112.40	79.70	79.50	109.30	109.20	
1.0	67.90	64.70	95.50	95.70	69.80	69.50	97.20	97.30	68.90	68.90	96.60	96.60	
1.5	64.40	64.50	92.10	92.00	66.00	66.00	93.90	93.90	64.90	65.00	92.20	91.80	
2.0	61.50	61.60	86.40	86.80	61.10	61.50	88.40	89.30	62.40	62.30	88.70	88.70	
4.0	55.30	55.30	78.10	78.20	56.20	56.20	81.60	81.60	54.90	54.90	81.40	81.50	

VPCRx (at these V/L)

B.2.2. Values calculated from process simulator

Values calculated from process simulator							
Label	D1-100-FPC-1--	D1-122-FPC-1--	D2-100-FPC-1--	D2-122-FPC-1--	D4-100-FPC-1--	D4-122-FPC-1--	
	U	U	U	U	U	U	
Event Abbreviation	D1	D1	D2	D2	D4	D4	
Sampling Date	11/28/2018	11/28/2018	12/3/2018	12/3/2018	1/28/2019	1/28/2019	
Temperature	100	122	100	122	100	122	
Sample Container	FPC	FPC	FPC	FPC	FPC	FPC	
Cylinder Replicate	1	1	1	1	1	1	
Repeatability Replicate							
Sampling Temperature (F)							
Sampling Pressure (psig)							
Measured/SimUlated	U	U	U	U	U	U	
VPCR_x (at these V/L)	0.0	99.58	122.23	144.15	167.76	114.44	137.35
	0.05	91.55	114.10	127.25	150.86	103.36	126.24
	0.1	86.06	108.47	115.95	139.46	95.90	118.68
	0.2	78.92	101.07	101.66	124.90	86.39	108.90
	0.5	68.78	90.29	82.51	105.01	73.34	95.20
	1.0	62.00	82.77	70.79	92.45	65.02	86.10
	1.5	58.56	78.75	65.32	86.35	60.95	81.43
	2.0	56.31	76.00	61.96	82.45	58.35	78.31
4.0	51.22	69.33	55.01	73.83	52.65	70.98	

APPENDIX C. TABULAR LISTING OF COMPOSITIONAL DATA

C.1. *n*-Heptane Compositional Data

n-Heptane manufacturer certificate of analysis

parchem
fine & specialty chemicals

Certificate of Analysis

N-HEPTANE, HIGH PURITY
 Lot/Batch #: C17H29DRM-000HP99
 Customer PO #: 00001
 Parchem Order #: 33008

Test	Limit	Result
Assay (as <i>n</i> -Heptane)	≥ 99.0%	99.45%
Assay (as C7 Hydrocarbons)	≥ 99.5%	99.98%
Assay (Total Hydrocarbons)	≥ 99.9%	99.98%
Specific Gravity (15.56°C)	0.680 – 0.695	0.689
Titration Acid	≤ 0.0003 meq/g	< 0.003 meq/g
Residue after Evaporation	≤ 10 ppm	0 ppm
Sulfur Compounds (as S)	≤ 0.005%	0.000%
Water	≤ 0.03%	< 0.01%

QA Review: KJ Shue

QA Approval: BS

ISO 9001 | DCAT | SOCMA | LinkedIn | Facebook | Twitter

parchem - fine & specialty chemicals | 415 Huguenot Street, New Rochelle, NY 10801 | Tel: 914-654-9800 | www.parchem.com | dok@parchem.com
 Form#: 2343 Date: 1.20.11 Revision: 10 Revision Date: 12.2.2016

n-Heptane analytical laboratory report of analysis

Sample ID:	2018-NOLA-000177-010	Date Taken:	8-Jan-18
Sample Designated As:	HEPTANE	Date Submitted:	8-Jan-18
Vessel/Location:	TTC SANDIA HEPTANE	Date Tested:	11-Jan-18
Representing:	TTC SANDIA HEPTANE Equal Composite		

Method	Test	Result	Unit
ASTM D4052	API Gravity @ 60°F	74.1	°API
ASTM D4052	Density @ 15.56°C	0.6875	g/cm³
ASTM D4052	Relative Density, 15.56°C/15.56°C	0.6882	
ASTM D6730	Ignition Fuels by 100-m GC	See Attached Report	
ASTM D6730	Heptane Purity	99.5	Vol %
* ASTM D240	Gross Heat of Combustion	20558	BTU/lb
ASTM E1064	Water Content	25	mg/kg
ASTM D93	Procedure Used	A	
* ASTM D93	Corrected Flash Point	<50	°F
* ASTM D3828	Procedure Used	A	
* ASTM D3828	Flash/No Flash	Flash	
* ASTM D3828	Target Flash Point	-5	°F
LWI_ELDF_007_001	Average Molecular Weight	102.14	g/mol

* Outside Scope of Method * Outside Laboratory

C.2. Bakken Compositional Data and Whole Oil Properties

		Bakken							
Label		B1-FPC-1	B1-FPC-2	B2-FPC-3	B4-1	B4-2	B6-1	B6-2	B8-WD-4
Event Abbreviation		B1	B1	B2	B4	B4	B6	B6	B8
Sampling Date		8/17/2017	8/17/2017	10/2/2017	1/18/2018	1/18/2018	1/31/2018	1/31/2018	7/18/2018
Sample Container		FPC	FPC	FPC					WD
Event Replicate		1	2	3	1	2	1	2	4
Composition (mol%)	CO2	0.0260	0.0070	0.0070	0.0018	0.0000	0.0015	0.0012	0.0040
	CO				0.0000	0.0000	0.0000	0.0000	
	H2S				0.0000	0.0000	0.0000	0.0000	
	He				0.0000	0.0000	0.0000	0.0000	
	H2				0.0002	0.0000	0.0000	0.0000	
	O2				0.0038	0.0013	0.0169	0.0025	
	N2	0.1150	0.0610	0.0770	0.0662	0.0756	0.1540	0.1101	0.1900
	C1	0.1100	0.0590	0.0580	0.0469	0.0524	0.0475	0.0496	0.0580
	C2	0.6350	0.6300	0.5470	0.5441	0.5460	0.5569	0.5398	0.5300
	C3	2.7560	2.7370	2.5570	2.6734	2.6442	2.7427	2.6453	2.5660
	iC4	1.0110	0.9560	0.9080	0.9522	0.9366	0.9733	0.9350	0.9120
	nC4	4.8920	4.7840	4.5760	4.7931	4.7295	4.9279	4.7297	4.5660
	neo C5				0.0097	0.0000	0.0000	0.0000	
	iC5	2.3390	2.2520	2.1600	2.2594	2.2321	2.3082	2.2295	2.1680
	nC5	4.5910	4.5260	4.3500	4.5298	4.4741	4.6407	4.4715	4.3390
	C6	5.83	6.54	7.83	7.17	7.08	7.31	7.06	6.65
	Benzene	0.43	0.50	0.64	0.45	0.43	0.46	0.42	0.47
	C7	12.80	13.35	15.12	10.54	10.41	10.72	10.36	13.47
	C8	14.51	14.35	15.31	11.50	11.36	11.68	11.30	14.33
	C9	7.91	7.16	7.35	8.09	8.01	8.10	7.94	7.17
	C10	6.10	6.17	5.88	6.81	7.51	6.72	7.43	6.31
	C11	4.69	4.74	4.46	5.09	4.75	5.05	4.68	4.85
	C12	3.85	3.86	3.60	4.35	4.34	4.32	4.37	3.96
	C13	3.47	3.48	3.28	3.81	3.90	3.79	3.84	3.60
	C14	2.94	2.95	2.76	3.34	3.42	3.33	3.45	3.02
	C15	2.49	2.50	2.32	2.69	2.76	2.68	2.70	2.55
	C16	2.12	2.10	1.96	2.20	2.19	2.13	2.21	2.16
	C17	1.81	1.81	1.68	2.13	2.19	2.20	2.14	1.86
	C18	1.59	1.58	1.47	1.69	1.75	1.64	1.76	1.62
	C19	1.43	1.43	1.31	1.36	1.36	1.38	1.37	1.46
	C20	1.24	1.23	1.15	1.24	1.30	1.26	1.25	1.26
	C21	1.08	1.08	0.99	1.17	1.23	1.14	1.24	1.10
	C22	0.97	0.96	0.88	1.01	1.01	0.98	1.02	0.98
C23	0.84	0.83	0.76	0.87	0.92	0.94	0.93	0.85	
C24	0.74	0.73	0.67	0.84	0.83	0.81	0.84	0.74	
C25	0.66	0.66	0.61	0.785	0.757	0.697	0.796	0.625	
C26	0.61	0.59	0.54						
C27	0.54	0.54	0.50						
C28	0.49	0.48	0.43						
C29	0.44	0.44	0.38						
C30+	3.96	3.93	2.86						

	Bakken							
Label	B1-FPC-1	B1-FPC-2	B2-FPC-3	B4--1	B4--2	B6--1	B6--2	B8-WD-4
Event Abbreviation	B1	B1	B2	B4	B4	B6	B6	B8
Sampling Date	8/17/2017	8/17/2017	10/2/2017	1/18/2018	1/18/2018	1/31/2018	1/31/2018	7/18/2018
Sample Container	FPC	FPC	FPC					WD
Event Replicate	1	2	3	1	2	1	2	4
IBP, °C (ASTM D86)				32.90	32.90	27.30	27.30	
Flash Pt-closed cup, °C (ASTM D3828)				<-30	<-30	<-30	<-30	
Sediment, % (ASTM D4007)				0.03	0.03	0.03	0.03	
Water, % (ASTM D4007)				0.00	0.00	0.12	0.12	
Water+Sediment, % (ASTM D4007)				0.03	0.03	0.15	0.15	
Water, mass% (Karl Fischer)				0.01	0.01	0.16	0.16	
Density @ 15 °C, kg/m^3 (ASTM D5002)				809.60	809.60	810.00	810.00	
Heat of Combustion, MJ/kg (ASTM D240)				46.02	46.02	45.97	45.97	
Sulfur, mass% (ASTM D4294)								
Viscosity, cSt (ASTM D445)								
H2S, ppm (UOP 163)								
Mercaptans, ppm (UOP 163)								
Specific Gravity at 60°F	0.80	0.80	0.80					0.80
API Gravity at 60°F	44.54	44.84	45.18					44.67
Molecular Weight	160.55	156.56	153.83					156.30
Pounds per Gallon (in Vacuum)	6.70	6.69	6.68					6.70
Pounds per Gallon (in Air)	6.69	6.68	6.67					6.69
Cu. Ft. Vapor per Gallon @ 14.696 psia	15.84	16.22	16.47					16.26
Specific Gravity at 60°F	0.94	0.94	0.95					0.95
API Gravity at 60°F	18.66	18.50	17.30					18.17
Molecular Weight	548.66	550.07	537.56					544.56
Pounds per Gallon (in Vacuum)	7.86	7.87	7.93					7.88
Pounds per Gallon (in Air)	7.85	7.86	7.92					7.87
Cu. Ft. Vapor per Gallon @ 14.696 psia	5.43	5.43	5.60					5.49
Shrinkage Factor	0.99	0.99	0.99					0.99
Flash Factor, Cu.Ft./STBbl.	2.11	7.10	15.27					5.74
Simulated Flash Factor (69F)	2.30	0.50						
Color Visual	Straw	Straw	Straw					Dark Amber
API Gravity @ 60° F	42.52	42.55	42.76					42.51
< C6 mass%	6.17	6.17	5.99	5.91	5.84	6.22	5.80	5.91

C.3. Dilbit Compositional Data and Whole Oil Properties

		Dilbit		
Label		D1-FPC-1	D2-FPC-1	D4-FPC-1
Event Abbreviation		D1	D2	D4
Sampling Date		12/3/2018	1/28/2019	2/27/2019
Sample Container		FPC	FPC	FPC
Event Replicate		1	1	1
Composition (mol%)	CO2	0.0220	0.0183	0.0230
	CO	0.0000	0.0000	
	H2S	0.0000	0.0000	
	He	0.0000	0.0000	
	H2	0.0000	0.0000	
	O2	0.0000	0.0127	
	N2	0.0606	0.1375	0.0915
	C1	0.0649	0.0504	0.0498
	C2	0.0382	0.0417	0.0430
	C3	0.3601	0.3962	0.4125
	iC4	0.7012	0.7416	0.7538
	nC4	2.6936	2.9511	2.9819
	neo C5	0.1803	0.0689	0.0646
	iC5	8.9704	9.1680	8.8073
	nC5	9.8367	9.9882	9.6282
	C6	8.34	8.60	8.40
	Benzene	0.45	0.47	0.47
	C7	6.23	6.55	6.51
	C8	5.29	5.53	5.62
	C9	2.70	3.04	3.11
	C10	2.16	1.76	2.15
	C11	1.49	1.45	1.77
	C12	1.66	1.62	1.76
	C13	1.80	1.76	1.75
	C14	1.92	1.88	1.99
	C15	1.65	1.61	1.72
	C16	1.64	1.60	1.70
	C17	1.95	1.90	1.89
	C18	1.74	1.61	1.79
	C19	1.48	1.45	1.53
C20	1.41	1.47	1.46	
C21	1.50	1.47	1.54	
C22	1.35	1.32	1.32	
C23	1.30	1.20	1.26	
C24	1.10	1.15	1.14	
C25	30.00	28.98	28.25	
C26				
C27				
C28				
C29				
C30+				

Label	Dilbit		
	D1-FPC-1	D2-FPC-1	D4-FPC-1
Event Abbreviation	D1	D2	D4
Sampling Date	12/3/2018	1/28/2019	2/27/2019
Sample Container	FPC	FPC	FPC
Event Replicate	1	1	1
IBP, °C (ASTM D86)	33.30	33.60	34.00
Flash Pt-closed cup, °C (ASTM D3828)	<-30.0	<-30.0	<-30.0
Sediment, % (ASTM D4007)	0.05	<0.025	0.03
Water, % (ASTM D4007)	0.45	0.20	0.28
Water+Sediment, % (ASTM D4007)	0.50	0.20	0.30
Water, mass% (Karl Fischer)	0.75	0.51	0.56
Density @ 15 °C, kg/m ³ (ASTM D5002)	923.50	924.20	923.90
Heat of Combustion, MJ/kg (ASTM D240)	42.84	43.28	43.41
Sulfur, mass% (ASTM D4294)	3.68	3.65	3.42
Viscosity, cSt (ASTM D445)	76.41	70.26	68.99
H2S, ppm (UOP 163)	6.30	0.50	2.00
Mercaptans, ppm (UOP 163)	113.60	99.60	120.00
Specific Gravity at 60°F			
API Gravity at 60°F			
Molecular Weight			
Pounds per Gallon (in Vacuum)			
Pounds per Gallon (in Air)			
Cu. Ft. Vapor per Gallon @ 14.696 psia			
Specific Gravity at 60°F			
API Gravity at 60°F			
Molecular Weight			
Pounds per Gallon (in Vacuum)			
Pounds per Gallon (in Air)			
Cu. Ft. Vapor per Gallon @ 14.696 psia			
Shrinkage Factor			
Flash Factor, Cu.Ft./STBbl.			
Simulated Flash Factor (69F)			
Color Visual			
API Gravity @ 60° F			
< C6 mass%	6.54	6.85	6.67

DISTRIBUTION

Email—External (encrypt for OUO)

Name	Company Email Address	Company Name
Yoon Ko	Yoon.Ko@nrc-cnrc.gc.ca	National Research Council Canada
Celia Lam	Celia.Lam@nrc-cnrc.gc.ca	National Research Council Canada

Email—Internal

Name	Org.	Sandia Email Address
Anay Luketa	01532	aluketa@sandia.gov
Technical Library	01177	libref@sandia.gov

This page left blank

This page left blank



**Sandia
National
Laboratories**

Sandia National Laboratories is a multimission laboratory managed and operated by National Technology & Engineering Solutions of Sandia LLC, a wholly owned subsidiary of Honeywell International Inc. for the U.S. Department of Energy's National Nuclear Security Administration under contract DE-NA0003525.

Supplement C. Preliminary test report

Experimental Testing at 1/10th Scale on Railcar Engulfed in Crude Oil Fire

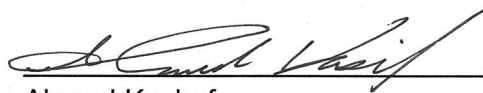
Progress Report for FY 2015/16

Author:



Cecilia Lam, Research Officer

Approved:



Ahmed Kashef
Program Leader, Fire Laboratory Transition
NRC Construction

Report No: A1-007572.1
Report Date: 31 March 2016
Contract No: A1-010647 (formerly A1-007572, see note below)
Agreement date: 3 September 2015 (original agreement)
8 January 2016 (Amendment No. 1)
Program: Fire Laboratory Transition

v+39 pages

NOTE: Contract A1-007572 was transferred to Contract A1-010647 due to the decommissioning of the NRC full-scale fire test facility being used for this project. The remaining experimental testing for this project was subsequently moved to Sandia National Laboratories, USA under the new contract. As a result, this report (A1-007572.1) has been integrated into a larger report (A1-010647-01) and should not be considered separate from the rest of report A1-010647-01.

This report may not be reproduced in whole or in part without the written consent of the National Research Council Canada and the Client.

Table of Contents

Table of Contents.....	i
List of Figures	iii
Executive Summary	v
1. Introduction	1
2. Experimental Setup.....	1
2.1 Test Facility.....	1
2.2 Fuel Pan	2
2.3 Fuel Pan Instrumentation	2
2.3.1 Load Cells	2
2.3.2 Thermocouple Rake	2
2.3.3 Liquid Level Sight Tube	3
2.4 Fuel Feed System.....	4
2.5 Pipe Calorimeter	5
2.6 Other Instrumentation	8
2.6.1 Heat Flux Meters	8
2.6.2 Heat Release Rate Measurement.....	8
2.6.3 Fourier Transform Infrared Spectroscopy	8
2.6.4 Video	9
2.6.5 Data Acquisition System.....	9
3. Crude Oil Sampling.....	9
3.1 Sample Collection	9
3.2 Post-Delivery Sampling.....	9
4. Test Protocol.....	10
5. Results.....	10
5.1 Preliminary Test #1 (Diesel)	10
5.1.1 Test-Specific Protocol.....	10
5.1.2 Load Cells Under Pan.....	11
5.1.3 Thermocouple Rake in Pan	12
5.1.4 Liquid Level Sight Tube	13
5.1.5 Heat Flux from Fire	13
5.1.6 Heat Release Rate	13
5.1.7 FTIR	14

5.2 Preliminary Test #2 (Diesel)	14
5.2.1 Test-Specific Protocol.....	14
5.2.2 Load Cells Under Pan.....	14
5.2.3 Thermocouple Rake in Pan	15
5.2.4 Liquid Level Sight Tube	16
5.2.5 Heat Flux from Fire.....	17
5.2.6 Heat Release Rate	17
5.2.7 FTIR	18
5.3 Reference Test (Heptane).....	18
5.3.1 Test-Specific Protocol.....	18
5.3.2 Load Cells Under Pan.....	19
5.3.3 Thermocouple Rake in Pan	20
5.3.4 Liquid Level Sight Tube	22
5.3.5 Heat Flux from Fire.....	22
5.3.6 Heat Release Rate	22
5.3.7 FTIR	23
5.3.8 Flame Temperatures Near Calorimeter.....	23
5.3.9 Total Incident Heat Flux to Calorimeter.....	28
5.3.10 Net Heat Flux to Calorimeter	33
5.3.11 Calorimeter Surface Temperatures.....	36
6. Summary and Recommendations	38
References	38
Supplement A – Fuel Pan Engineering Drawings.....	A-1
Supplement B – Crude Oil Feed System.....	B-1
Supplement C – Calorimeter Engineering Drawings	C-1
Supplement D – Statement of Work by Omnicon Consultants Inc.....	D-1
Supplement E – Summary of Results of Crude Oil Sample Homogeneity Testing.....	E-1

List of Figures

Figure 1. Thermocouple rake for measuring temperatures in the fuel and substrate.	3
Figure 2. Typical recorded image of liquid level sight tube.	4
Figure 3. Thermocouple locations in each measurement plane in the calorimeter (not to scale).	6
Figure 4. Modification to bottom portion of exterior support ribs (not to scale).	7
Figure 5. Location of calorimeter in fuel pan (not to scale).	8
Figure 6. Measured weight of fuel pan in Preliminary Test #1.	11
Figure 7. Temperatures measured in the fuel pan in Preliminary Test #1. Legend gives height of thermocouples above pan bottom.	12
Figure 8. Liquid level sight tube readings for Preliminary Test #1.	13
Figure 9. Measured weight of fuel pan in Preliminary Test #2.	15
Figure 10. Temperatures measured in the fuel pan in Preliminary Test #2. Legend gives height of thermocouples above pan bottom.	16
Figure 11. Liquid level sight tube readings for Preliminary Test #2.	17
Figure 12. Heat release rate for Preliminary Test #2.	18
Figure 13. Measured weight of fuel pan in Reference Test.	19
Figure 14. Temperatures measured in the fuel pan in Reference Test. Legend gives height of thermocouples above pan bottom.	21
Figure 15. Time when fuel surface passed thermocouples in fuel layer.	22
Figure 16. Heat release rate for Reference Test.	23
Figure 17. Temperatures measured 51 mm (2") away from outer surface of calorimeter, along west measurement plane.	24
Figure 18. Temperatures measured 51 mm (2") away from outer surface of calorimeter, along centre measurement plane.	24
Figure 19. Temperatures measured 51 mm (2") away from outer surface of calorimeter, along east measurement plane.	25
Figure 20. Time-averaged temperatures at 51 mm (2") distance from outer surface of calorimeter, along west measurement plane.	26
Figure 21. Time-averaged temperatures at 51 mm (2") distance from outer surface of calorimeter, along centre measurement plane.	27
Figure 22. Time-averaged temperatures at 51 mm (2") distance from outer surface of calorimeter, along east measurement plane.	28
Figure 23. Total incident heat flux to calorimeter, along west measurement plane.	29
Figure 24. Total incident heat flux to calorimeter, along centre measurement plane.	30
Figure 25. Total incident heat flux to calorimeter, along east measurement plane.	30
Figure 26. Time-averaged total incident heat flux to calorimeter, along west measurement plane.	31
Figure 27. Time-averaged total incident heat flux to calorimeter, along centre measurement plane.	32
Figure 28. Time-averaged total incident heat flux to calorimeter, along east measurement plane.	33
Figure 29. Net heat flux to calorimeter, along west measurement plane.	34
Figure 30. Net heat flux to calorimeter, along centre measurement plane.	35

Figure 31. Net heat flux to calorimeter, along east measurement plane.35
Figure 32. Outer surface temperatures of calorimeter, along west measurement plane.36
Figure 33. Outer surface temperatures of calorimeter, along centre measurement plane.....37
Figure 34. Outer surface temperatures of calorimeter, along east measurement plane.....37

Executive Summary

The current work stems from a literature review, conducted by NRC in 2015, on the behaviour of crude oil, condensates and ethanol in rail tank cars exposed to pool fires established by these fuels. A recommendation resulting from the literature review was to improve understanding of the fire-related parameters affecting heating of the tank car by conducting initially 1/10th scale experiments simulating a tank car engulfed in a crude oil pool fire. Larger scale experiments could be conducted later, if desired. These experiments would focus on the fire environment external to the tank car and would not involve any lading behaviour. A key parameter of interest in the experiments would be the presence of light-end hydrocarbon components in the crude oil and their effects on the fire behaviour. This report describes all work completed prior to March 31, 2016 for the 1/10th scale experiments.

In preparation for testing, crude oil from a rail loading facility in Alberta was sampled into customized, air-tight barrels using a water displacement method. This method allowed the oil to be transferred without being exposed to atmospheric air, thus permitting capture and retention of all light-end components. The same method, but in reverse, would be used to pump the oil out of the barrel and into the fuel pan while the oil in the pan was burning. As a result, the light-end components would contribute directly to the fire, simulating an accident scenario involving a leaking rail tank car continuously feeding fuel into the fire.

All fires were established over a 1.2 m by 2.4 m (4' x 8') fuel pan. A pipe calorimeter of 0.33 m (13-1/8") outer diameter and 1.8 m (6') length was used to simulate the tank car inside the fire. The calorimeter was instrumented so that the temperature at and the heat flux to its outer surface could be assessed. Additional measurement parameters included the fuel burning rate, temperatures in the fuel and substrate layers, flame temperatures near the calorimeter, and heat release rate.

Two preliminary tests using diesel and one reference test using heptane were conducted in FY2015/16. In all tests, the fuel was floated on top of water inside the pan. The preliminary tests were intended to verify operation of the fuel feed system and optimize the test protocol, while the reference test generated baseline data for comparison to crude oil.

Based on these three tests, it is recommended that several improvements be made to the fuel feed system before proceeding with the crude oil tests. A suitable pressure vessel should be installed as a run tank, instead of using the crude oil drum. With the vessel designed to withstand higher pressures than the drum, higher flow rates could be achieved, increasing the length of the steady burning period during each test. An additional recommendation is to automate control of the fuel feed system in order to improve control of the fuel layer thickness inside the pan.

1. Introduction

In 2015, NRC conducted a literature review for Transport Canada [1] on the behaviour of crude oil, condensates and ethanol in rail tank cars exposed to pool fires established by these fuels. Based on this review, a research plan was recommended to improve current understanding of the behaviour of both the fire and lading. The research plan included a progression of experimental testing, starting at the small scale and gradually building up to larger scales. As an initial step, a series of 1/10th scale tests was proposed to allow examination of a variety of pertinent parameters, before selecting the most critical ones and proceeding to larger scale testing. The 1/10th scale tests would be divided into two phases: one involving no lading to allow focus on the fire environment external to the tank car, and the other focussing on the lading behaviour. The current report describes the work completed prior to March 31, 2016 that was related to the 1/10th scale tests without lading.

The objective of the present experiments was to simulate a tank car engulfed in a crude oil pool fire and to examine the fire-related parameters affecting the level of heat flux incident on the outer surface of the tank car. A key parameter of interest was the presence of light-end hydrocarbon components in the crude oil and their effects on the fire behaviour. Thus, much effort was put into properly sampling and handling the crude oil so that the light-end components could be retained in the oil until burnt.

It should be noted that Sandia National Laboratories of Albuquerque, NM is conducting a related series of experiments on crude oil, allowing for potential comparison of the results from both laboratories. However, the Sandia research is focussed on the properties of crude oils produced in the US. The research conducted by NRC will cover a representative range of crude oils transported by rail in Canada, and will focus on the interaction between the fire and engulfed tank car.

2. Experimental Setup

2.1 Test Facility

The fire tests described in this report were conducted in the Burn Hall at the NRC full-scale fire test facility in Mississippi Mills, Ontario. The test bay was situated under a 6 m x 6 m (20' x 20') exhaust hood connected to a duct and exhaust fan system that collected the smoke and hot gases produced by the fire. The test bay was surrounded on three sides (north, east and west) by a concrete block wall approximately 3 m (10') high.

Due to the flow patterns inside the Burn Hall, fires in this test bay have traditionally exhibited a tendency to tilt slightly towards the north wall. To mitigate this effect in the present experiments, wind screens were positioned south of the test bay (where no concrete block wall was present) to try to reduce the fire-generated air flow that would push the flames towards the north wall. The wind screens were constructed from 1.2 m x 2.4 m (4' x 8') steel sheets perforated with 6 mm (¼") holes, spaced 10 mm (3/8") apart, to give an opening equivalent to 42% of the total

area. Ten of these steel sheets were individually mounted on wooden frames and situated to partially block the air flow from the south side of the test bay in order to reduce the tilt of the fire.

2.2 Fuel Pan

The fuel pan was a 1.2 m x 2.4 m (4' x 8') steel pan, with a height of 0.20 m (8"). Supplement A contains engineering drawings for the fuel pan. A pipe nipple (1" NPT) passed through the centre of the pan base and formed part of the fuel feed system (Section 2.4). Two pipe nipples passed through one side wall – one of these (2" NPT) served as a drainage port and the other (¼" NPT) was used in the system for monitoring the level of the fuel surface (Section 2.3.3).

The pan was attached to legs with adjustable height. Attached to the base of the legs were 'feet' that rested on load cells to measure the weight of the pan and its contents. These 'feet' were designed such that only vertical downward forces could be transmitted to the load cell. The load cells are described further in Section 2.3.1.

The pan was surrounded by a cement board floor, level with the base of the pan. This was intended to be similar to the setup at Sandia National Laboratories and would permit better comparison between the experiments performed by the two labs.

2.3 Fuel Pan Instrumentation

2.3.1 Load Cells

The fuel pan rested on four Honeywell Model 41 load cells, each with 227 kg (500 lb) capacity. The load cells measured the change in weight of the pan and its contents over time, providing an independent measure of how much fuel was supplied to the pan and of the rate of burning when fuel was not being supplied to the pan.

2.3.2 Thermocouple Rake

A thermocouple rake (Figure 1) was located inside the fuel pan to measure temperatures in the fuel layer and the substrate below the fuel layer. It consisted of 19 Type K (chromel-alumel) thermocouples spaced 6 mm (¼") apart in the vertical direction and spanning heights of 76 to 191 mm (3" to 7.5") above the base of the fuel pan. The thermocouples were held in place by Swagelok fittings welded to a vertical stainless steel plate of 6 mm (¼") thickness. Due to the size of the fittings, the thermocouples could not be positioned along a single vertical line but instead spanned a horizontal distance of approximately 45 mm (1¾"). The thermocouples protruded out from the vertical plate by approximately 64 mm (2.5"). Each thermocouple was enclosed in a stainless steel sheath with an outer diameter of 3 mm (1/8") to permit submersion in liquids.



Figure 1. Thermocouple rake for measuring temperatures in the fuel and substrate.

2.3.3 Liquid Level Sight Tube

The ¼" port in the side wall of the fuel pan (Section 2.2) was connected to a 0.6 m (2') long stainless steel flexible hose, which was then connected to approximately 2 m (6.5') of clear plastic tubing. The open end of the plastic tubing was shielded from the fire by a concrete block wall located along one side of the test bay. This portion of the tubing was mounted vertically to a wooden board, beside a ruler, and its image recorded by a nearby video camera, as shown in Figure 2.

Prior to each test, the ¼" port was capped off inside the pan and the tubing was filled with either water or antifreeze (depending on the ambient temperature). Once the pan was filled with enough water such that the ¼" port was fully submerged, the cap was removed. Because the liquid in the tubing was connected directly to the liquid in the pan, this method offered a remote and visual way of monitoring the level of the liquid inside the pan through equivalence of hydrostatic pressure in the pan and at the open end of the tubing. The recorded video images could also be used to estimate the fuel burning rate when fuel was not being supplied to the pan. When calculating the fuel burning rate, differences in density (ρ) between the fuel and the liquid in the sight tube would need to be accounted for, via Equation 1 (where Δh refers to the rate of change in height of the liquid).

$$\Delta h_{fuel} = \frac{\rho_{sight\ tube} \Delta h_{sight\ tube}}{\rho_{fuel}} \quad (1)$$

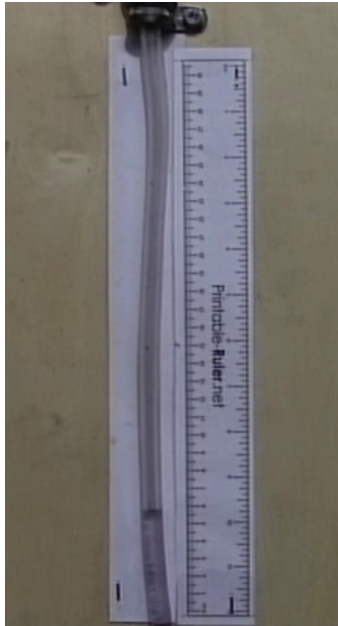


Figure 2. Typical recorded image of liquid level sight tube.

2.4 Fuel Feed System

As described in Section 3.1 and Supplement D, the crude oil was supplied in barrels with ball valves screwed into both bungs in the lid of the barrel. These valves protected the crude oil inside the barrel from being exposed to the ambient surroundings. A water displacement method was used to transfer the crude oil from the barrel to the fuel pan at a controlled flow rate. This method involved pumping water into the barrel through one valve to displace the crude oil and force it to exit the barrel through the other valve at an equivalent volumetric flow rate. The same method, but in reverse, was used to transfer the crude oil sample into the barrel (Section 3.1). The water displacement technique permitted retention of all light-end hydrocarbon components in the crude oil because the oil was transferred in single phase and was not exposed to atmospheric pressure until it reached the fuel pan.

Supplement B contains an overall sketch of the crude oil feed system. Water was supplied from the Burn Hall at approximately 690-830 kPa (100-120 psi). It was sent through a pressure regulator, which limited the maximum pressure that could be placed on the fuel feed system. The water then passed through either of two lines: a 19 mm ($\frac{3}{4}$ ") diameter line for higher flow rates or a 13 mm ($\frac{1}{2}$ ") diameter line for lower flow rates. Each line contained a ball valve for controlling flow into the line, a globe or needle valve to allow adjustment of the flow rate, a flow meter to measure and record the flow rate, and a check valve to prevent backflow through the meter. From there, the water was sent to either the crude oil barrel or a bypass. A flow totalizer before the barrel inlet measured how much water was sent to the barrel.

The purpose of the bypass was to divert some of the water away from the crude oil barrel in order to lower the pressure in the barrel. A needle valve in the bypass line allowed the pressure

to be controlled by changing how much water was diverted away from the barrel. As an emergency precaution, an additional bypass containing initially a manually-actuated ball valve, but subsequently replaced by an automatic pop-up safety relief valve, was inserted close to the barrel inlet to allow all of the water to be diverted away from the barrel if the barrel suddenly experienced overpressure.

The crude oil exited the barrel at the same volumetric flow rate as the water entering the barrel. As indicated in Section 3.2, a floating piston cylinder (FPC) was used to collect a sample of crude oil from the barrel immediately prior to testing. For this, the oil was directed away from the fuel pan (by closing a ball valve) and sent to the inlet of a three-way valve. The three-way valve was connected to a vacuum pump on one side and the FPC on the other. The vacuum pump was used to purge air from the line up to the inlet of the FPC. A set of ball and needle valves at each end of the FPC was used to control flow into and out of the FPC. A drain was available before the needle valve at the FPC inlet to allow venting of approximately three times the volume of the sampling line prior to filling the FPC with a fresh sample of oil. As the FPC was filled with oil, an equivalent volume of the water/glycol mixture that was used to precharge the FPC was discharged from the outlet. The protocol for collecting the crude oil sample is described in greater detail in Supplement B.

After sampling, the crude oil from the barrel was directed towards the fuel pan. On its way there, the oil passed through a sight glass so that the system operator could visually confirm when all the crude oil was emptied out of the barrel. A flow meter was also installed to verify the flow rate of the oil.

At the fuel pan, the oil passed through a pipe nipple in the base of the pan (Section 2.2) before entering a dispersion head inside the pan. The dispersion head consisted of two 0.9 m (3') long pipe nipples connected by a tee and capped at the open ends. Each pipe nipple had 8 holes (4 in front, 4 in the back) of 10 mm (3/8") diameter spaced equally along its length. The oil entered the dispersion head through the tee and exited through the 10 mm holes into the fuel pan. The dispersion head was positioned such that the holes were located above the substrate existing below the fuel layer in the pan. This would ensure that the fuel sat on top of the substrate and prevent formation of any emulsion when the substrate was water.

2.5 Pipe Calorimeter

The design of the pipe calorimeter was based on a cylinder of 0.33 m (13-1/8") outer diameter and 1.8 m (6') length, approximately 1/10th the size of a rail tank car. Supplement C contains engineering drawings for the calorimeter. The cylinder was constructed from two half-pipes that were rolled to size from 4.8 mm (3/16") thick stainless steel plate. The half-pipes had flanges running along their length that were bolted together to form a cylinder. These flanges contained a slot for insertion of a high-temperature silica rope seal to prevent any direct entry of hot gases into the cylinder. Support ribs were attached to the outer circumference of the cylinder in four equally-spaced locations to permit the cylinder to sit on a flat surface without rolling. Pegs of 13 mm (1/2") diameter and 51 mm (2") length also protruded from the outer surface of the cylinder at various locations to serve as attachment points for thermocouples (described later).

The thermal mass of these external features was kept as low as possible in order to minimize their effects on the instrumentation inside the calorimeter.

A smaller stainless steel pipe, of 0.27 m (10¾") outer diameter and 1.8 m (6') length, was located concentrically inside the cylinder. This pipe was sized so that there was a 25 mm (1") space between its outer surface and the larger cylinder. It was held in place by three spacer rings that just fit inside the larger cylinder. The thermal mass of these rings was kept small in order to minimize conduction between the two cylinders. The space between the cylinders was filled with a layer of 25 mm (1") thick, 128 kg/m³ (8 lb/ft³) density, Fibrefrax Durablanket S insulation. A roll of this ceramic fibre blanket insulation was also inserted inside the smaller cylinder to minimize convective effects within the calorimeter.

Three cross-sectional measurement planes were spaced equally (0.46 m or 18" apart) along the length of the calorimeter, halfway between the exterior support ribs. As shown in Figure 3, each measurement plane contained eight measurement stations spaced uniformly (every 45°) around the circumference of the calorimeter. Each measurement station contained three thermocouples aligned along the same radius. One thermocouple was located outside the calorimeter, attached to the peg described earlier, such that it was offset from the outer surface of the calorimeter by 51 mm (2"). This thermocouple measured flame temperature. The peg was offset from the measurement plane by 51 mm (2") in order to minimize its effects on the thermocouple measurements. The other two thermocouples were located inside the calorimeter, attached to the inner surface of the larger cylinder and to the outer surface of the smaller cylinder. The temperatures measured by these thermocouples were subsequently input into a one-dimensional inverse heat conduction analysis [2] to determine the temperature at and the heat flux to the fire-exposed surface of the calorimeter.

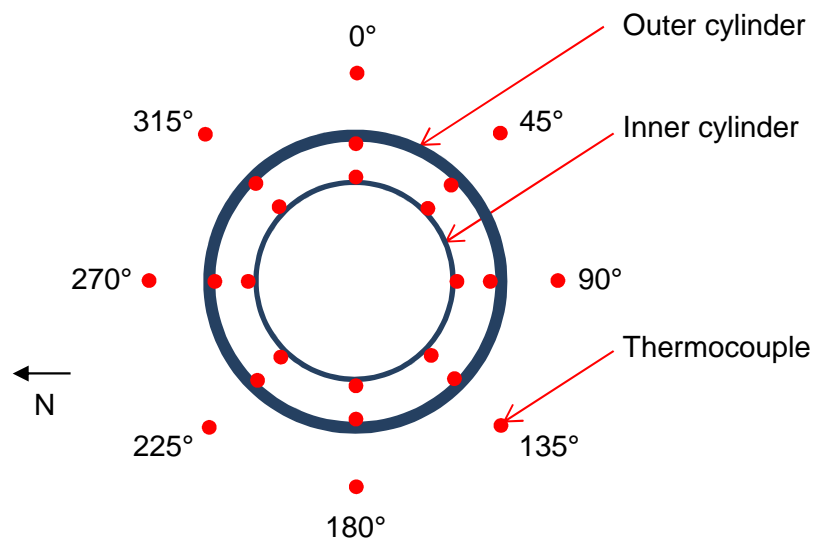


Figure 3. Thermocouple locations in each measurement plane in the calorimeter (not to scale).

The ends of the calorimeter were covered with stainless steel end caps to prevent flames from entering the calorimeter. At the centre of each end cap was a 0.1 m (4") diameter hole for thermocouple wires to pass through. Each bundle of thermocouple wires was wrapped in ceramic fibre blanket insulation to protect the wires from direct exposure to the fire.

The entire outer surface of the calorimeter was painted with Pyromark 2500 flat black paint in order to achieve a diffuse, gray surface. After drying, the painted pieces were cured as per the manufacturer instructions (480°F for 2 hours, followed by an increase to 1000°F over a 1 hour period) to maximize resistance to thermal shock.

A minor modification was made to the calorimeter design shown in Supplement C. A portion of the exterior support ribs along the bottom of the calorimeter was cut out, as shown in Figure 4. This was so that the ribs would fit over top of the dispersion head of the fuel feed system when the calorimeter was placed just above the fuel surface. In addition, in all tests, the calorimeter was centred longitudinally in the fuel pan, but shifted by 25 mm (1") off the long axis of the pan (to the north side, as shown in Figure 5). This would prevent interference between the pegs protruding from the bottom of the calorimeter and the dispersion head when the calorimeter was just above the fuel surface, yet allow comparison of results between tests in which the calorimeter elevation was varied.

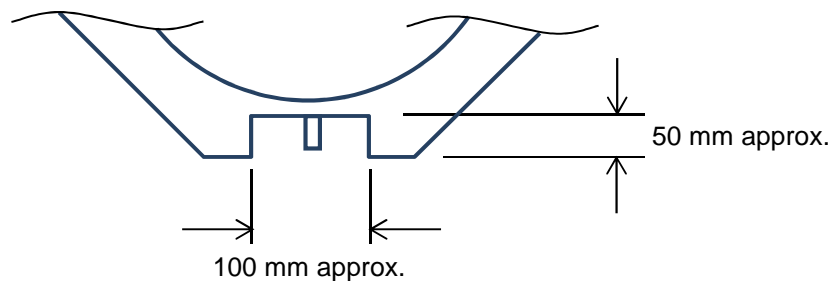


Figure 4. Modification to bottom portion of exterior support ribs (not to scale).

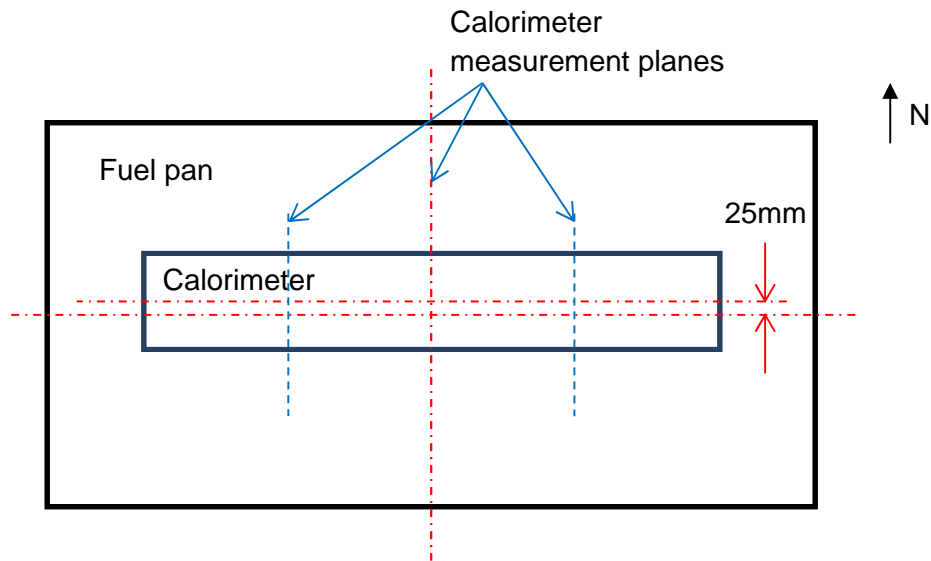


Figure 5. Location of calorimeter in fuel pan (not to scale).

2.6 Other Instrumentation

2.6.1 Heat Flux Meters

Two Gardon gauges [3] were used to measure radiative heat flux from the fire. One gauge was 4.3 m south of the fuel pan centre, while the other was 3.5 m west of the pan centre. Both gauges were elevated approximately 1.2 m above the base of the fuel pan.

2.6.2 Heat Release Rate Measurement

Smoke and gases produced by the fire were collected using the exhaust hood system located above the test bay. The hood system was connected through a duct system to an exhaust fan system. A measuring station in the duct system contained a thermocouple to measure the gas temperature and a bi-directional probe (pitot tube) to measure the pressure difference produced by the flow in the duct. These measurements were used to estimate the equivalent volumetric flow rate at standard atmospheric conditions.

Meanwhile, gas samples were taken from the centre of the duct and sent to a combustion gas analyzer that used non-dispersive infrared to measure CO and CO₂ concentrations and an electrochemical cell to measure O₂ concentrations. These concentrations, along with the estimated volumetric flow rate of the exhaust gases, were used to determine the heat release rate of the fire using the oxygen depletion method [4].

2.6.3 Fourier Transform Infrared Spectroscopy

A gas sampling probe was placed in the northwest region of the fuel pan, approximately 50 mm above the rim of the pan and in the same plane as the west wall of the pan. The probe was connected to a 10 m long, unheated sampling line and the gas sample passed through a 50°C trap before being heated to 150°C and introduced into a Fourier Transform Infrared (FTIR) spectrometer/continuous gas analyzer (MKS 2030). This setup was to allow the heavy-end hydrocarbon components to be excluded and only light-end components to be sent to the spectrometer. Although it could not be used to accurately measure concentrations of individual

hydrocarbons, it could provide relative indications of whether the types of hydrocarbons being burned changed throughout a test.

2.6.4 Video

In addition to the video camera on the liquid level sight tube (Section 2.3.3), video cameras were used to live-stream and record the instrumentation in the fuel feed system (2 pressure gauges, 3 flow meters and 1 totalizer). Three additional cameras were used to record the fire, from the southwest, south and southeast sides.

2.6.5 Data Acquisition System

All instrumentation cables were connected to a data logger with a sampling frequency of 1 Hz.

3. Crude Oil Sampling

3.1 Sample Collection

Omnicon Consultants Inc. of Edmonton, Alberta was subcontracted to advise on sourcing and selecting an appropriate crude oil for fire testing, as well as to coordinate the collection of the crude oil samples and their transportation to the NRC test facility in approved means of containment. A key criterion for the crude oil sampling method was that the properties of the crude oil at the source conditions should not change during sampling, handling and transportation. All light-end components (including methane, ethane, propane and butane) present in the crude oil at the sample point should be captured and retained in the same concentrations throughout sampling, handling and transportation. Thus, the samples had to be taken under pressure and transferred in single-phase condition to the sample container. To meet this criterion within reasonable budget and schedule, Omnicon Consultants customized an off-the-shelf barrel that was already approved for transporting crude oil to allow for single-phase transfer of the oil into and out of the barrel without exposure to atmospheric pressure via a water/glycol displacement method. Details of the sample container and sample collection method are provided in Supplement D.

Ten barrels of a full-range distribution crude oil, with limited bias on either the light or heavy end components and representative of typical crude oil production being transported by rail in Canada, were collected and delivered to NRC. Initial properties of the crude oil were measured using sub-samples taken at the midpoint of sample transfer into each of the 10 barrels. Testing on the 10 sub-samples was conducted for composition (ASTM D8003), simulated distillation (ASTM D7169), vapour pressure (ASTM D6377), density (ASTM D5002) and H₂S content (UOP 163). The test results are summarized in Supplement E. The results demonstrate that the 10 barrels of crude oil were reasonably homogeneous when the samples were collected.

3.2 Post-Delivery Sampling

Upon arrival at NRC, the crude oil barrels were placed in a temporary storage area that was maintained at approximately 12°C. Shortly afterwards (within 24 h of arrival), crude oil was found to have seeped through the threads of the larger (2") bung in the lid of the barrel. It was

not noticed at the time of arrival whether there was already evidence of oil seepage. This seepage may have occurred as a result of thermal expansion of the crude oil when the barrels were placed in the storage area at NRC, since the samples were collected at -5°C (Supplement E) and the storage area was at 12°C. Although unconfirmed, exposure of the barrels to temperatures higher than -5°C may have also occurred during transportation, resulting in thermal expansion of the oil and seepage through the bung threads.

To minimize experimental uncertainty, a sample of the crude oil from each barrel will be taken using a floating piston cylinder (as described in Section 2.4) immediately prior to testing for further compositional analysis. The results will then be compared to the initial property data from the samples taken at the time of collection (Section 3.1 and Supplement E) to determine whether the composition of the oil in the barrels has been affected.

4. Test Protocol

The following general protocol was followed during the tests discussed in Section 5. Test-specific deviations from the general protocol are detailed in the individual subsections pertaining to each test.

First, the fuel pan was filled with water to a depth of 121 mm (4.75") through a hose connected to the building water supply. Fuel was then fed into the pan using the system described in Section 2.4. The fuel was ignited by means of a propane torch. Fuel continued to be fed into the pan at a rate higher than the burning rate until the desired fuel thickness was reached. At this point, the fuel feed rate was reduced to the expected burning rate in order to maintain an approximately constant fuel thickness. Once the drum of fuel was completely filled with water (and thus empty of fuel), all flow to the pan was stopped and the fire was allowed to burn itself out.

5. Results

5.1 Preliminary Test #1 (Diesel)

5.1.1 Test-Specific Protocol

The primary objective of the preliminary tests was to test the fuel feed system and the sampling protocol for the floating piston cylinder. As such, there was no calorimeter in the fuel pan, and diesel was burned on top of a 124 mm (4 7/8") thick water substrate. Although the initial temperatures of the fuel and substrate were not strictly controlled, they were measured to be approximately 8°C and 10°C for the diesel and water, respectively.

Ignition via propane torch was attempted at the southeast corner of the fuel pan once diesel started exiting the dispersion head (at approximately 19 L/min). However, it was quickly determined that an accelerant was needed, so approximately 1 L of methyl hydrate was poured into the pan to facilitate ignition. A second attempt at ignition occurred approximately 2 min later and was successful. The fire took approximately 1 min to spread over the entire pan area. The fuel flow rate was raised to 40 L/min in order to allow the fuel layer to grow, but this caused the

crude oil drum to overpressure, so the fuel flow rate was immediately decreased and the test aborted 3.5 min after ignition. The fuel that was already in the pan was allowed to mostly burn out. Boiling of the water substrate (boilover) was observed starting 9.3 min after ignition, and the fire was suppressed 10.6 min after ignition.

5.1.2 Load Cells Under Pan

Figure 6 shows the total weight of the fuel pan measured by the load cells during the test. With each of the two ignition attempts, the weight increased as fuel started flowing into the pan. Once the fuel was ignited, it continued to flow into the pan until 3.5 min (210 s), when it was allowed to burn out. The slight decrease and then increase in slope that occurred prior to stoppage of the fuel flow corresponded to the fuel feed system operators varying the flow rate to verify changes in the crude oil drum pressure.

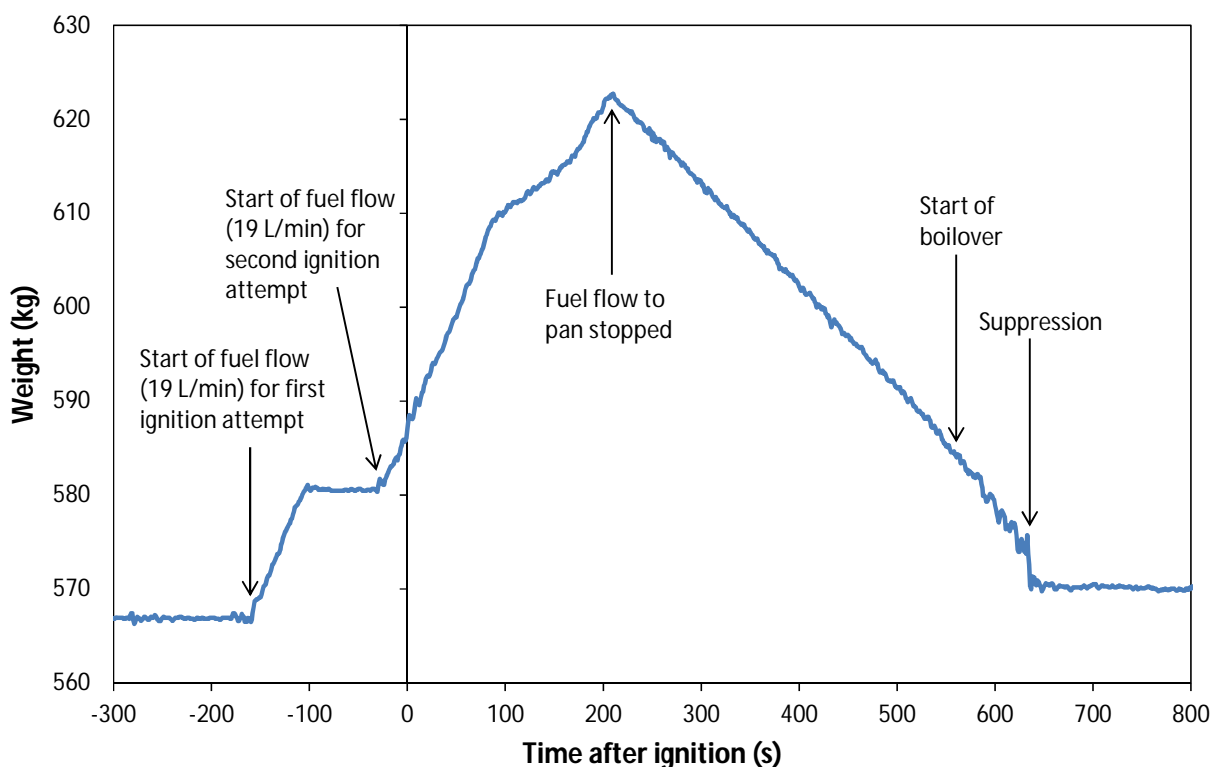


Figure 6. Measured weight of fuel pan in Preliminary Test #1.

The fuel regression rate during the period between stoppage of the fuel flow and the start of boilover was estimated to be $0.036 \text{ kg/m}^2\text{s}$, or 2.7 mm/min , assuming a fuel density of 800 kg/m^3 . This is in reasonable agreement with values found in the literature, which range from 2.4 to 3.4 mm/min for slightly smaller diesel fires of 1.3 - 1.5 m diameter [5-7], to 3.5 mm/min for slightly larger diesel fires of 2.6 m diameter [7].

During boilover, the load cell measurements fluctuated noticeably, as water and fuel were ejected from the pan. As to be expected, the average slope of the graph during this period was higher than that during the period before boilover.

5.1.3 Thermocouple Rake in Pan

Figure 7 contains a plot of the temperatures measured by the thermocouple rake located near the southwest corner of the pan. Temperatures indicative of flame presence were measured at 152 mm elevation and above once the fire reached the thermocouple rake approximately 1 min after ignition. The thermocouple at 146 mm elevation was initially in the fire, but became submerged in the fuel layer as more diesel entered the pan.

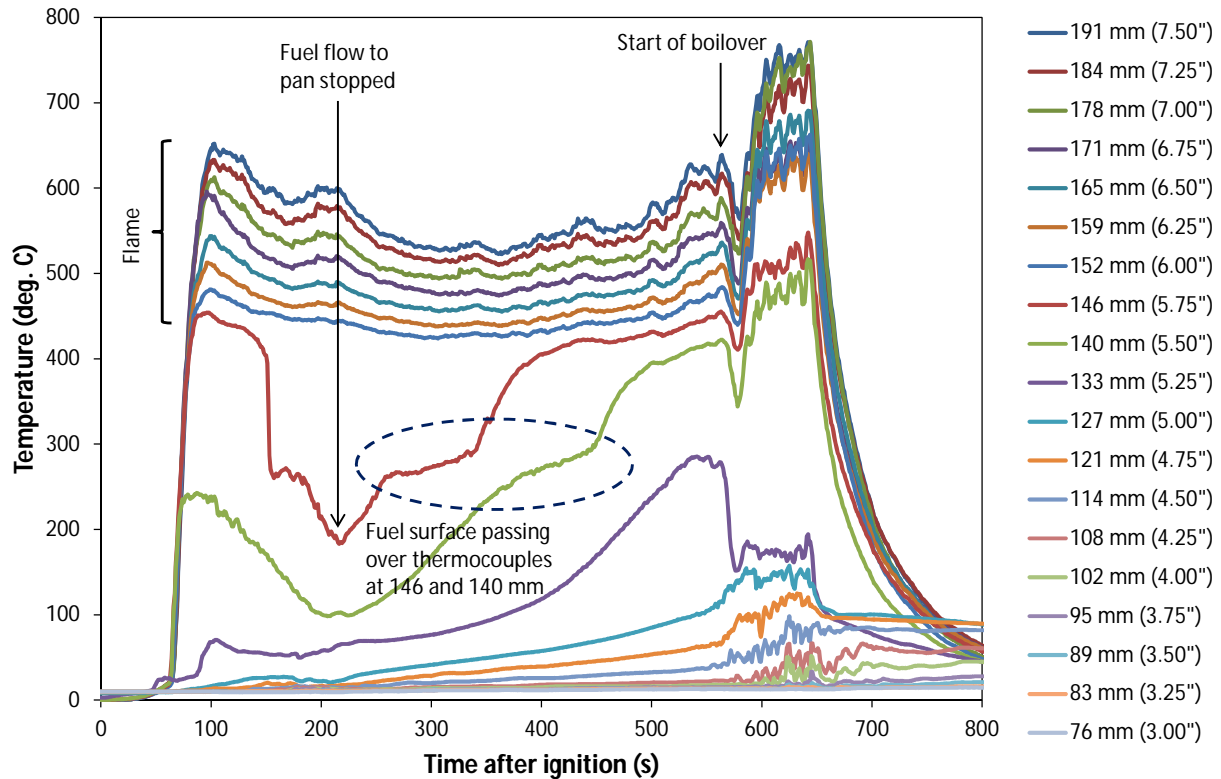


Figure 7. Temperatures measured in the fuel pan in Preliminary Test #1. Legend gives height of thermocouples above pan bottom.

Fuel regression rate could be estimated during the limited period from the time the fuel flow to the pan was stopped to the time when boilover started. As indicated by the oval drawn in Figure 7, the passage of the fuel surface over the thermocouples at 146 mm and then 140 mm elevation could be identified from the temperature time curves. As the fuel surface approached each of these thermocouples, the measured temperature gradually increased and then levelled off somewhat, before increasing again as the thermocouple exited the liquid and entered the fuel vapour/flame zone. (For a pure fuel, the temperature levels off at the boiling point, but since diesel is a mixture of compounds with different boiling points, the reaching of the boiling temperatures in Figure 7 is not as steady.) For the purposes of estimating fuel regression rate, the instant at which the fuel surface was considered to pass each thermocouple was taken to be the data point immediately before the sudden increase in temperature indicating that the thermocouple was inside the fuel vapour/flame zone. The time taken for the fuel surface to pass

from the 146 mm to the 140 mm thermocouple, divided by their separation distance, then gives the regression rate, 3.6 mm/min.

The regression rate estimated using the thermocouple data was 33% higher than that estimated using the load cell data. The accuracy of the thermocouple method was limited by the relatively large size of the thermocouples (3 mm O.D.) and their coarse spacing (6 mm apart). Smaller, more closely spaced thermocouples would be expected to give higher accuracy and better time resolution.

5.1.4 Liquid Level Sight Tube

Readings of liquid level were taken from the video of the liquid level sight tube, during the period between stoppage of the fuel flow to the pan and the start of boilover. The values are plotted in Figure 8, with a trendline fitted to the data. The slope of the trendline can be used to obtain an estimate of the fuel regression rate through Equation 1, giving a result of 3.3 mm/min. This is within 22% of the regression rate estimated from the load cell data.

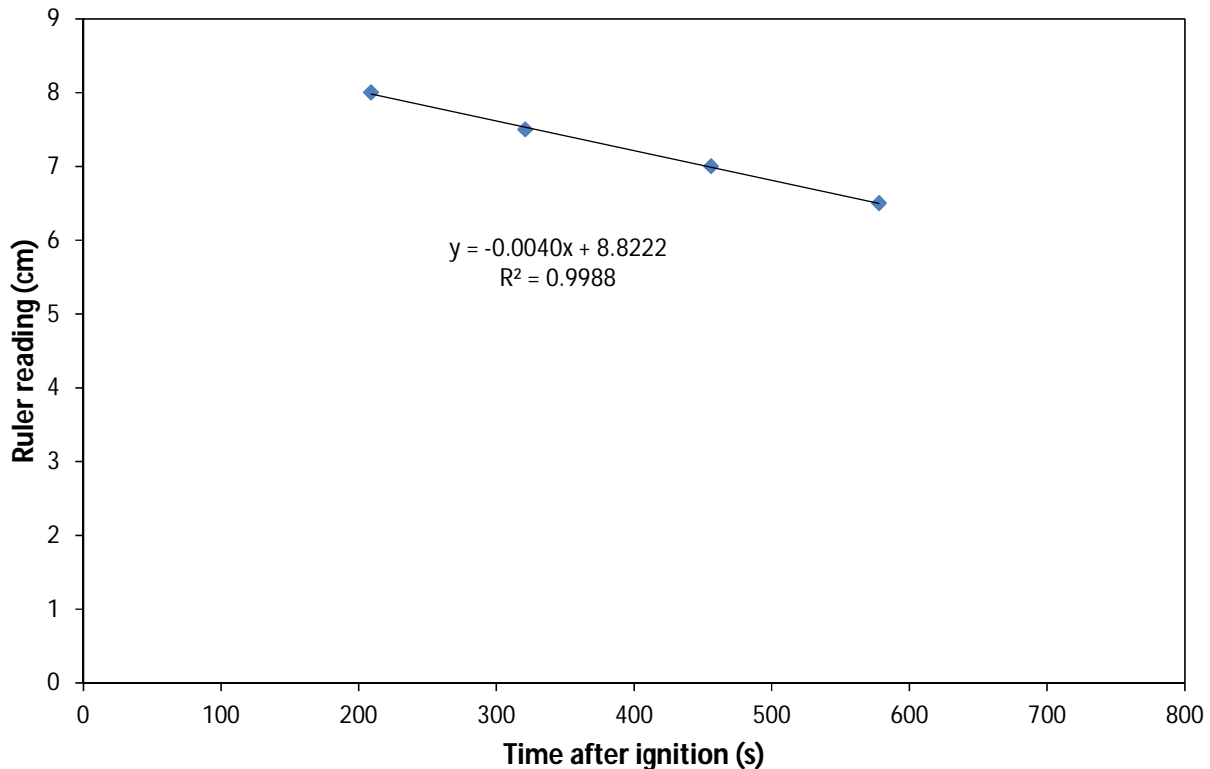


Figure 8. Liquid level sight tube readings for Preliminary Test #1.

5.1.5 Heat Flux from Fire

No heat flux data were available for this test.

5.1.6 Heat Release Rate

No heat release data were available for this test.

5.1.7 FTIR

No useful FTIR data were obtained in this test because the detector response saturated within 3-5 minutes after ignition.

5.2 Preliminary Test #2 (Diesel)

5.2.1 Test-Specific Protocol

Similar to Preliminary Test #1, this test involved burning diesel on top of a 121 mm (4.75") thick water substrate, with no calorimeter in the fuel pan. Although not strictly controlled, the initial temperatures of the diesel and water were approximately 4°C and 11°C, respectively. Ignition via propane torch was attempted at the southeast corner of the fuel pan once diesel started to exit the dispersion head (at approximately 12 L/min). Two attempts were required, with 1-2 L of heptane added to the pan to facilitate ignition. Once ignited, the fire took approximately 1 min to spread over the entire pan area. The fuel flow rate was maintained at approximately 12 L/min for about 4 min to allow the fuel layer to grow, then decreased to approximately 5 L/min and stopped 9.7 min after ignition. The remaining fuel was then allowed to burn out. Boilover was observed starting 8.7 min after ignition and the fire went out 12.6 min after ignition.

5.2.2 Load Cells Under Pan

Figure 9 shows the total weight of the fuel pan measured by the load cells during the test. Prior to ignition, the weight increased as fuel started flowing into the pan. Once the fuel was ignited, it continued to flow into the pan at approximately 12 L/min, resulting in a continued increase in the measured weight. At 250 s, the fuel flow rate was reduced to approximately 5 L/min. Since this was lower than the fuel burning rate (estimated to be 8 L/min from Section 5.1.2), the weight then started to decrease. At 524 s, when boilover began, the weight started to decrease more quickly due to both water and fuel being ejected from the pan. After the fuel flow to the pan was stopped, the rate of decrease became even greater until the fire was nearly out.

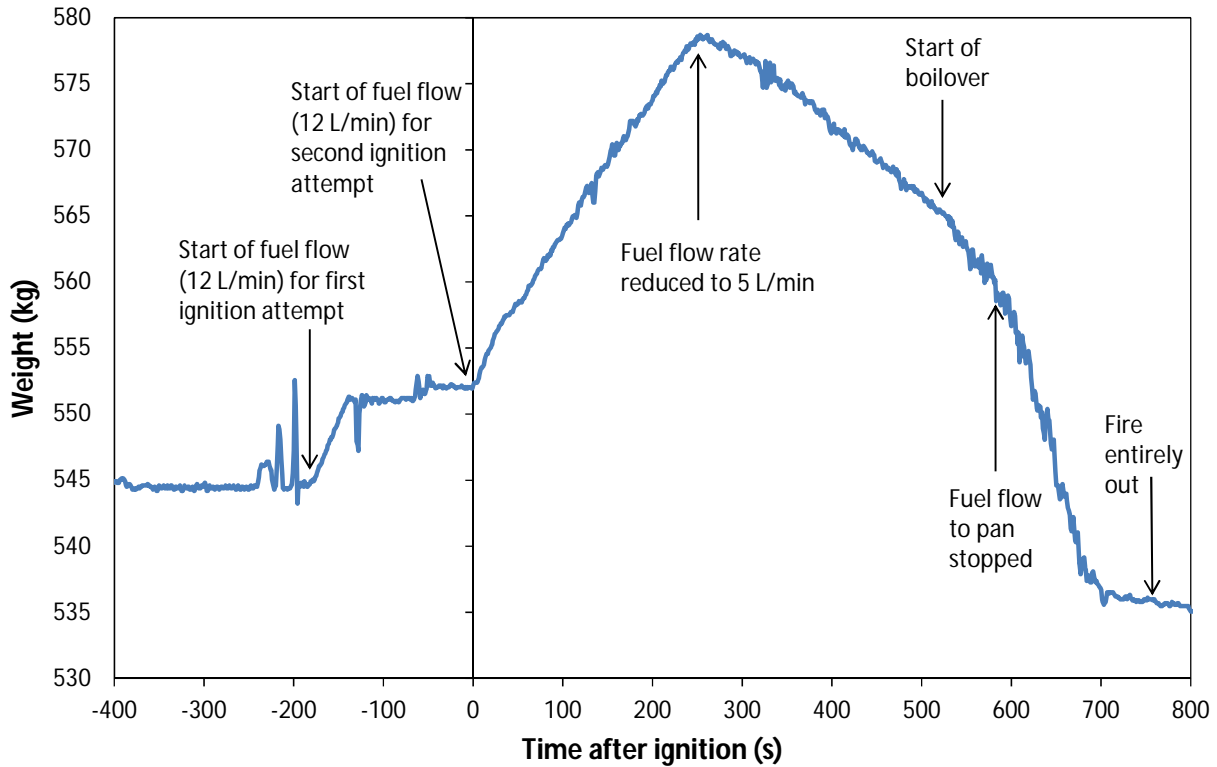


Figure 9. Measured weight of fuel pan in Preliminary Test #2.

5.2.3 Thermocouple Rake in Pan

Figure 10 contains a plot of the temperatures measured by the thermocouple rake located near the southwest corner of the pan. Temperatures indicative of flame presence were measured at 140 mm elevation and above once the fire reached the thermocouple rake approximately 1 min after ignition. The thermocouples at 127 and 133 mm elevation were initially in the fire, but entered the fuel layer (starting at 120 s for the 127 mm thermocouple and 235 s for the 133 mm thermocouple) as more diesel entered the pan. At 250 s, when the fuel flow rate was reduced to 5 L/min, the 133 mm thermocouple was already near the fuel surface, so the measured temperatures remained in the boiling range until the fuel surface receded enough for the thermocouple to fully exit the fuel layer. Since this was the only thermocouple to exit the fuel, no estimate of regression rate could be made from the thermocouple data for this test.

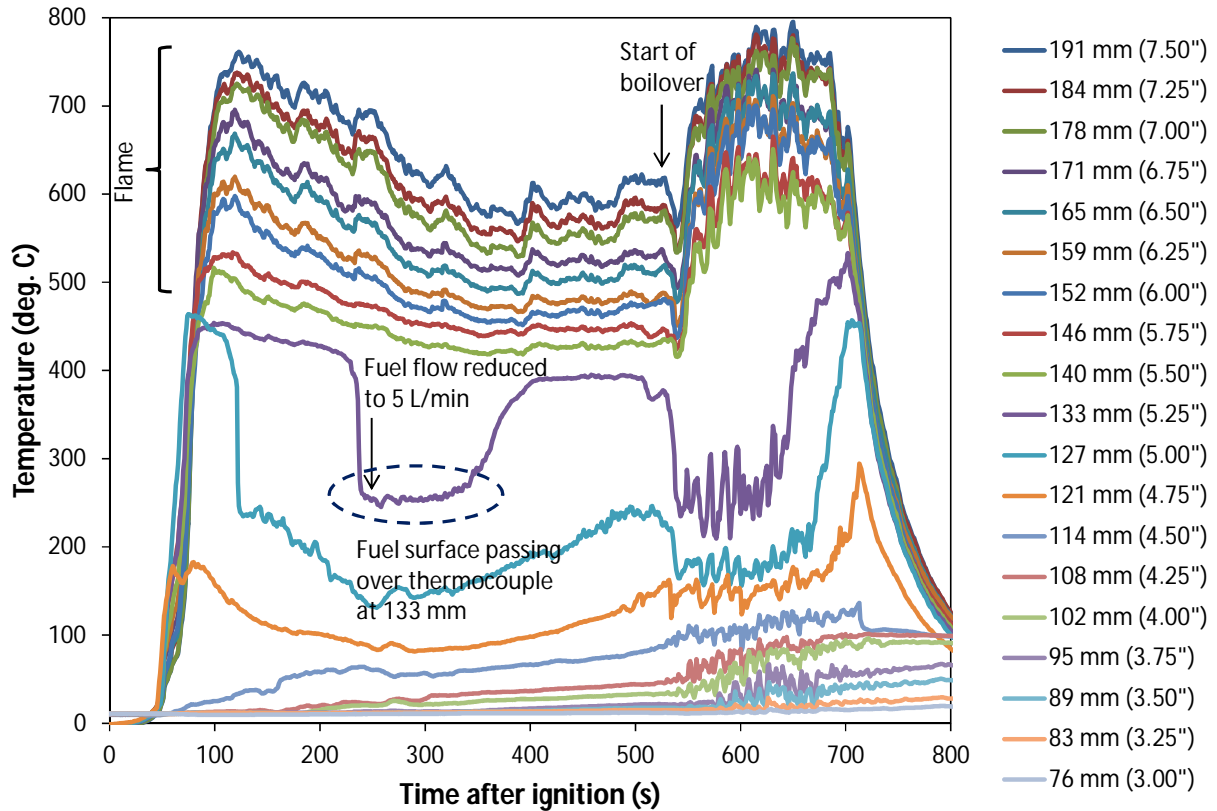


Figure 10. Temperatures measured in the fuel pan in Preliminary Test #2. Legend gives height of thermocouples above pan bottom.

5.2.4 Liquid Level Sight Tube

Readings of liquid level were taken from the video of the liquid level sight tube, during the period of steady decrease from 250 s to the start of boilover. Based on Figure 11 and correcting for differences in density via Equation 1, the rate of fuel level decrease was estimated to be 1.5 mm/min. This value may be compared to that derived from the load cell data of Figure 9. Assuming a fuel density of 800 kg/m^3 , the load cell data corresponded to a fuel level decrease of 1.4 mm/min after the flow rate to the pan was reduced. Despite the limited resolution available in the video data, the results from both methods are within 7%, a very reasonable agreement.

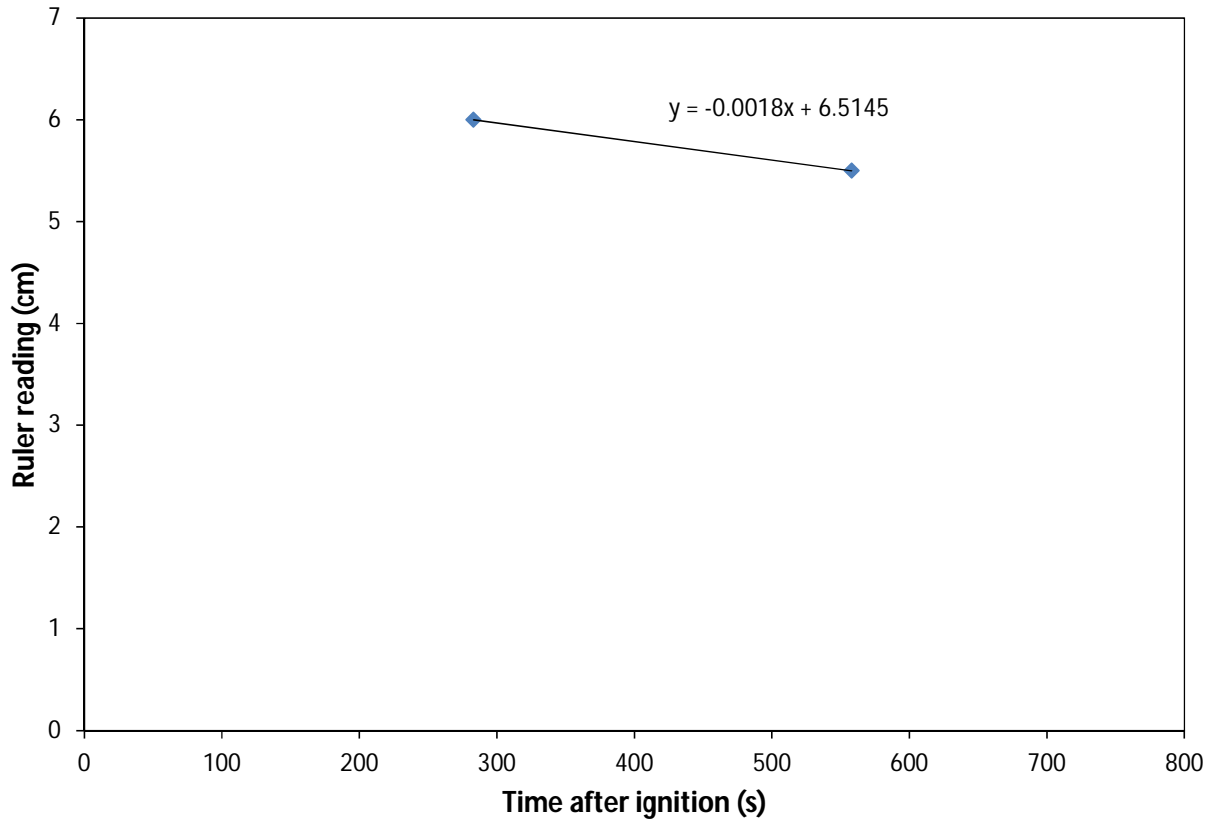


Figure 11. Liquid level sight tube readings for Preliminary Test #2.

5.2.5 Heat Flux from Fire

No heat flux data were available for this test.

5.2.6 Heat Release Rate

The heat release rate data are shown in Figure 12. The average heat release rate during the period prior to boilover was 3.6 MW, with a maximum of 4.6 MW.

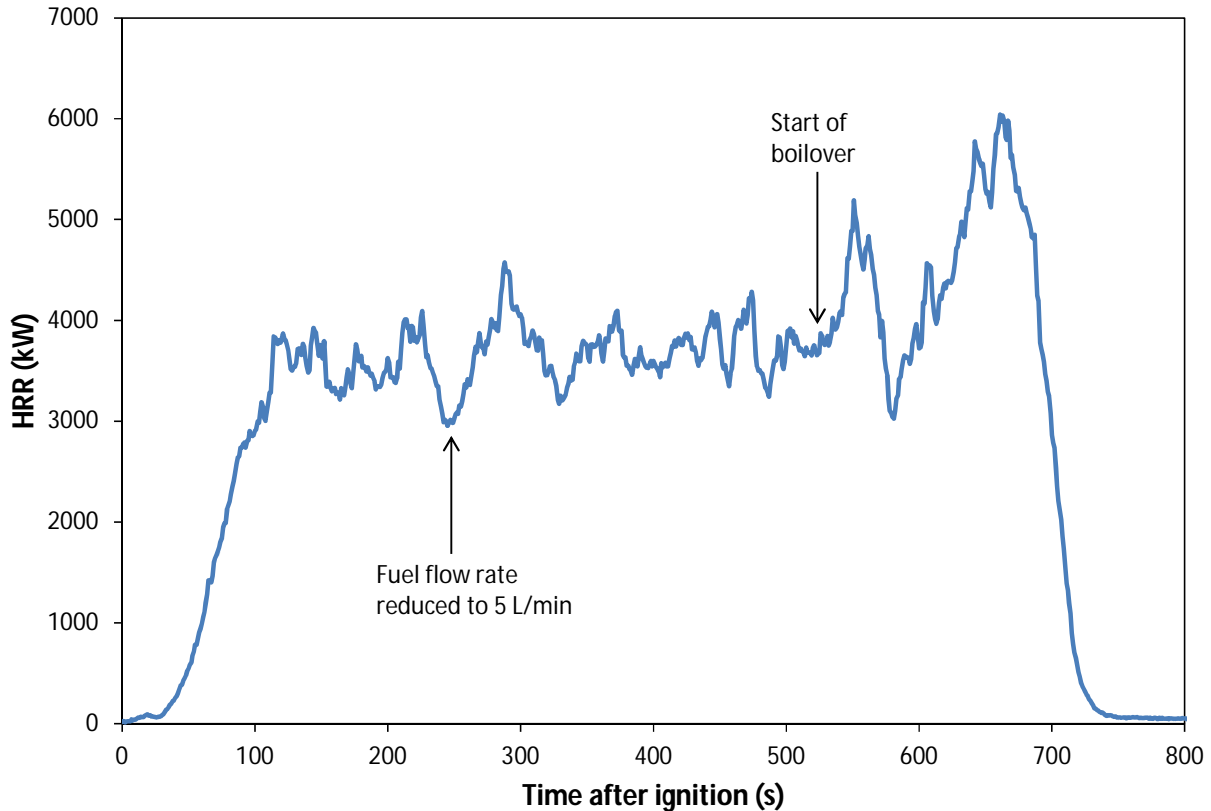


Figure 12. Heat release rate for Preliminary Test #2.

5.2.7 FTIR

No useful FTIR data were obtained in this test because the detector response saturated within 3-5 minutes after ignition.

5.3 Reference Test (Heptane)

5.3.1 Test-Specific Protocol

The objective of this test was to burn heptane, a well-characterized fuel, in order to provide baseline data against which the crude oil test results could be compared. The calorimeter was placed in the fuel pan such that the bottom of the cylinder was 0.27 m (10.5") above the base of the pan. This allowed the calorimeter to sit above the fuel surface at 1/10th the typical height of a rail tank car above the ground. Prior to ignition, the pan was filled with fuel to the desired initial thickness in order to minimize the potential for boilover. Given the expected high burning rate of heptane, the fuel feed system would not have been able to supply fuel to the pan at a sufficient rate to allow the fuel layer to grow. Thus, prior to ignition, a 0.39 m (1.5") thick layer of heptane was floated on top of a 0.12 m (4.75") thick water substrate, with the bottom of the calorimeter (cylindrical portion) situated 0.11 m (4.25") above the fuel surface. The initial temperatures of the heptane and water were 5°C and 7°C, respectively.

Ignition via propane torch occurred without any need for accelerant. The fire took approximately 1 s to spread over the entire pan area. Heptane was supplied to the pan at a rate of approximately 14 L/min until 6.3 min, when no more fuel was available. The fuel remaining in the pan was then allowed to burn out. The fire was observed to tilt by about 25° toward the west end of the calorimeter throughout much of the test, possibly due to overall flow patterns existing in the Burn Hall at the time. No boilover was observed during the test, and the fire went out 7.9 min after ignition.

5.3.2 Load Cells Under Pan

Figure 13 shows the total weight of the fuel pan measured by the load cells during the test. Prior to ignition, the weight increased as fuel started flowing into the pan. The dome shape of the weight-time curve between 0 and 378 s reflects transient changes in the burning rate, which increased with time as the fire grew to reach steady state and eventually overcame (at around 220 s) the 14 L/min rate of fuel supply to the pan. After 378 s, when the fuel flow was stopped, the weight steadily decreased until near the end of the test.

The fuel regression rate after 378 s was estimated to be 0.079 kg/m²s, or 6.9 mm/min using a fuel density of 680 kg/m³. This is higher than values found in the literature for 2 m diameter heptane fires with no engulfed large object, which range from 4.6-5.6 mm/min [8,9]. The higher burning rate of the present fire likely resulted from additional heat feedback to the fuel surface from the hot calorimeter.

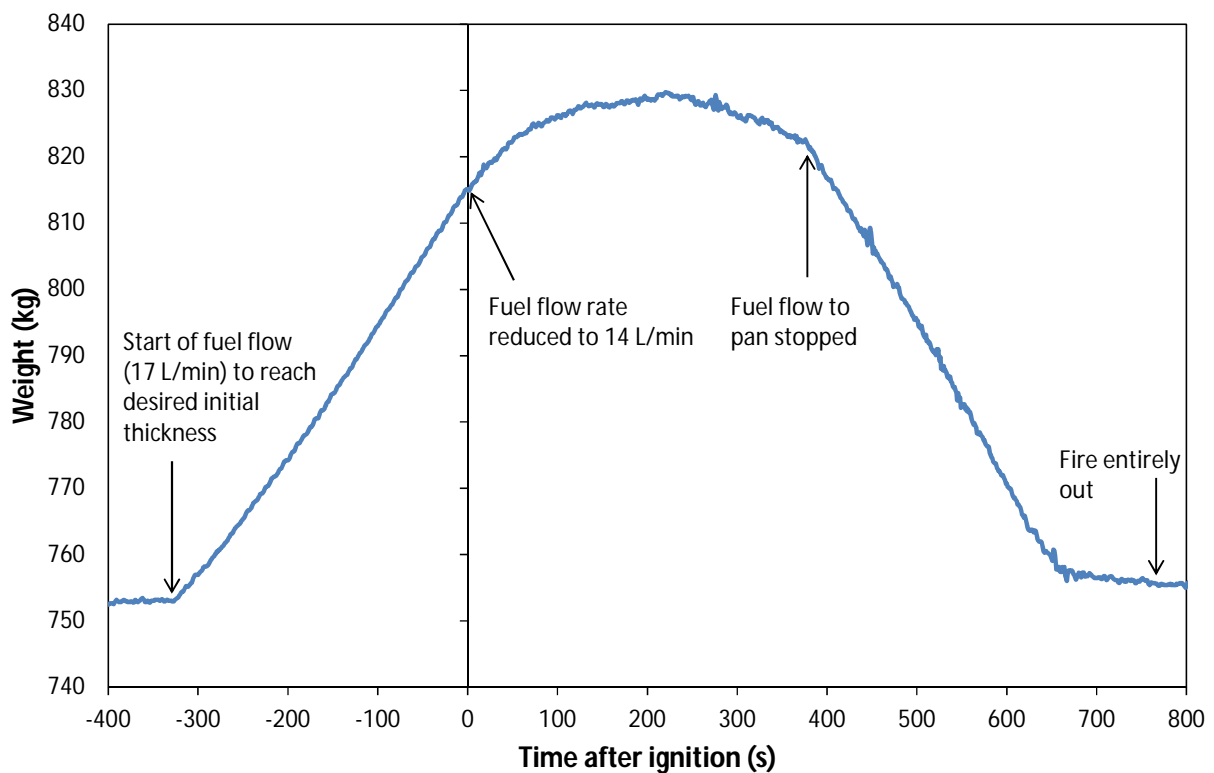


Figure 13. Measured weight of fuel pan in Reference Test.

5.3.3 Thermocouple Rake in Pan

Figure 14 contains a plot of the temperatures measured by the thermocouple rake located near the southwest corner of the pan. Temperatures indicative of flame presence were measured at 159 mm elevation and above throughout the test. The sudden temperature increase at approximately 240 s coincided with the fire starting to tilt toward the west side of the pan (as observed in the videos), resulting in better engulfment of the thermocouple rake in the fire. At the same time, the thermally massive calorimeter came into quasi-equilibrium with the fire, as discussed later in Section 5.3.10.

The thermocouple at 152 mm elevation was initially in the fire, but entered the fuel layer starting at 180 s, as fuel entered the pan more quickly than it was being burned during the early stages of the fire. As the burning rate gradually increased, this thermocouple remained near the fuel surface, so the measured temperatures stayed near the boiling point until the fuel surface receded enough for the thermocouple to fully exit the fuel layer.

Using a method similar to that described in Section 5.1.3, fuel regression rate could be estimated by examining the temperature time curves for the thermocouples between 121 and 152 mm, indicated by the oval drawn in Figure 14. The instant at which the fuel surface passed each thermocouple was identified using two methods: (1) immediately before the sudden increase in temperature indicating that the thermocouple was inside the fuel vapour/flame zone, and (2) the time when the boiling point of 98.4°C [10] was reached. As seen in Figure 15, both methods yielded approximately 7.6 mm/min as the fuel regression rate. (The thermocouple at 152 mm was not included in Figure 15 because it clearly did not fit well with the other values on the graph.) This regression rate was within 10% of that estimated using the load cell data, in reasonable agreement.

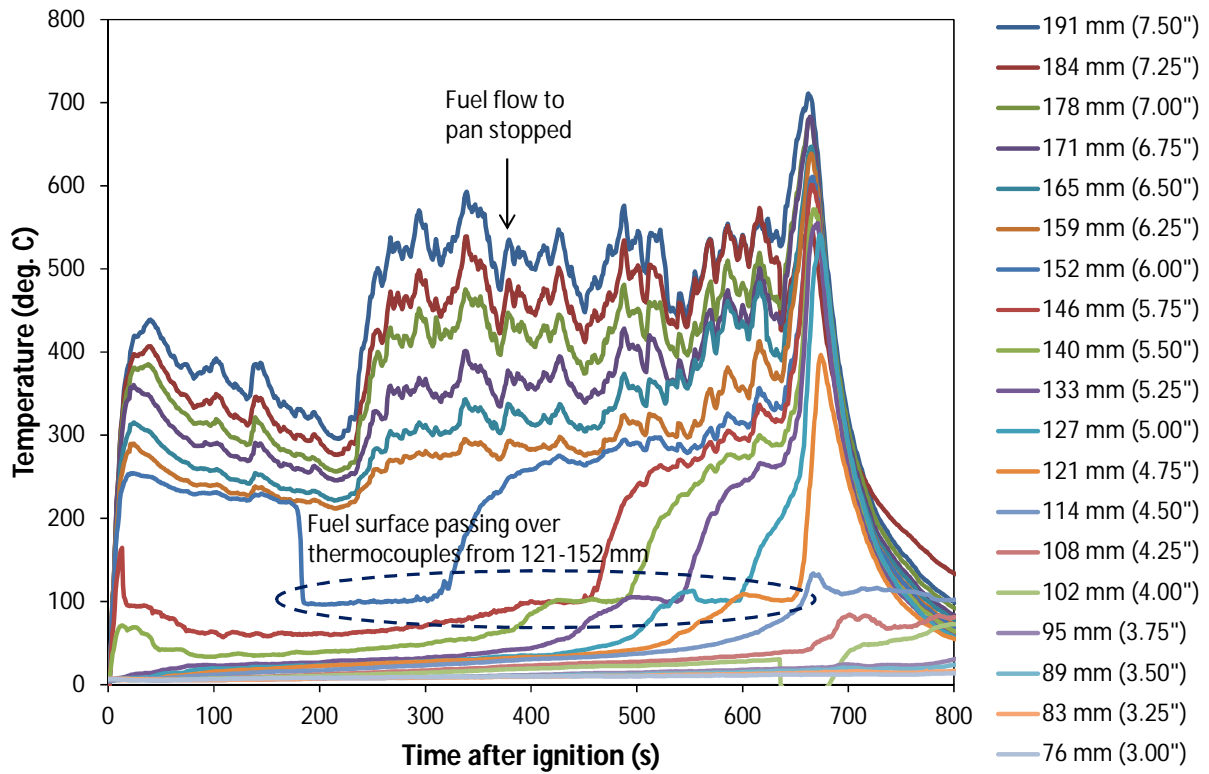


Figure 14. Temperatures measured in the fuel pan in Reference Test. Legend gives height of thermocouples above pan bottom.

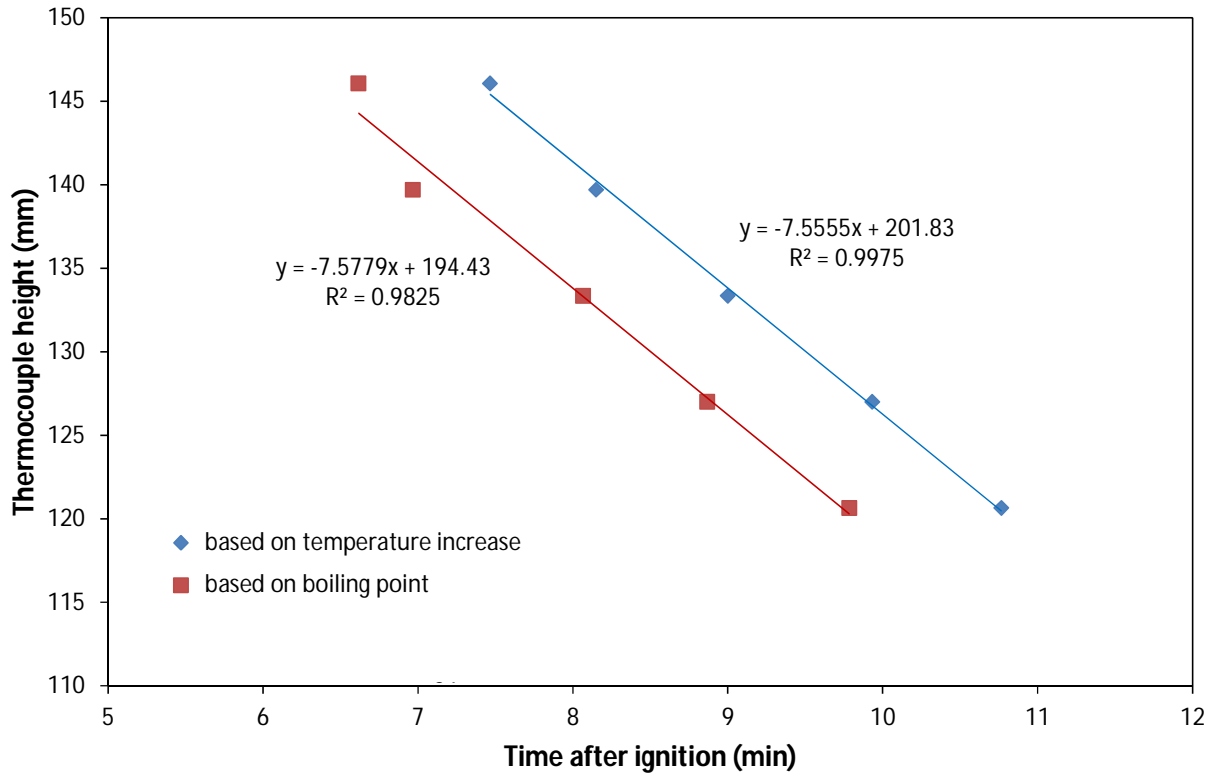


Figure 15. Time when fuel surface passed thermocouples in fuel layer.

5.3.4 Liquid Level Sight Tube

No useful data were obtained from the liquid level sight tube because it was plugged during the first half of the test.

5.3.5 Heat Flux from Fire

No heat flux data were available for this test.

5.3.6 Heat Release Rate

The heat release rate data are shown in Figure 16. The heat release rate gradually increased until approximately 300 s, when it levelled off somewhat between 8 and 10 MW. After 450 s, it increased slightly, fluctuating between roughly 9 and 11 MW for the remainder of the test. The peak heat release rate reached was 11.5 MW. These values are somewhat higher than those reported in the literature for 2 m diameter heptane fires with no engulfed large object, 6.9-7.8 MW [8], in accordance with the higher burning rate discussed in Section 5.3.2.

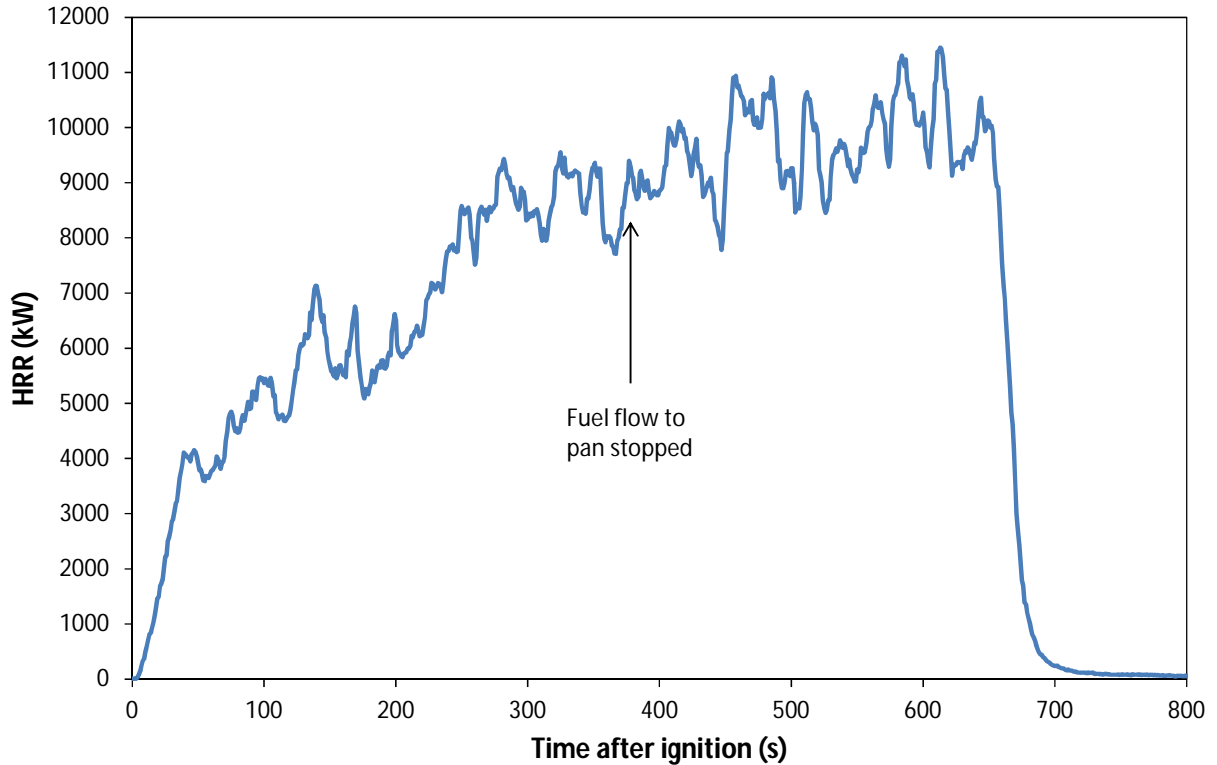


Figure 16. Heat release rate for Reference Test.

5.3.7 FTIR

No FTIR data were obtained in this test.

5.3.8 Flame Temperatures Near Calorimeter

Figure 17 to Figure 19 show the temperatures measured at a distance of 51 mm (2") from the outside surface of the calorimeter. (See Figure 3 for the thermocouple positions.) In general, the temperatures below the calorimeter (180°, 225°) were lower than those above the calorimeter (0°, 45°, 315°) because the bottom of the calorimeter was facing the oxygen-starved, fuel-rich vapour zone that exists just above the fuel surface in large pool fires. In Figure 19, which shows the east measurement plane, the temperatures at 180° and 225° suddenly increased at 240 s, while those at 0° and 45° simultaneously decreased. This corresponded to the fire tilting towards the west end of the calorimeter, as observed in the videos.

Figure 20 to Figure 22 contain time-averaged profiles of the flame temperatures for the periods 100-200 s, 300-400 s and 500-600 s. As expected based on the temperature-time plots (Figure 17 to Figure 19), the profiles corresponding to the 100-200 s time period differed from those corresponding to the 300-400 s and 500-600 s time periods because of the change in tilt of the fire after 240 s. Nevertheless, these profiles clearly show that the gases below the calorimeter were cooler than those above it when the calorimeter was fully engulfed by the fire.

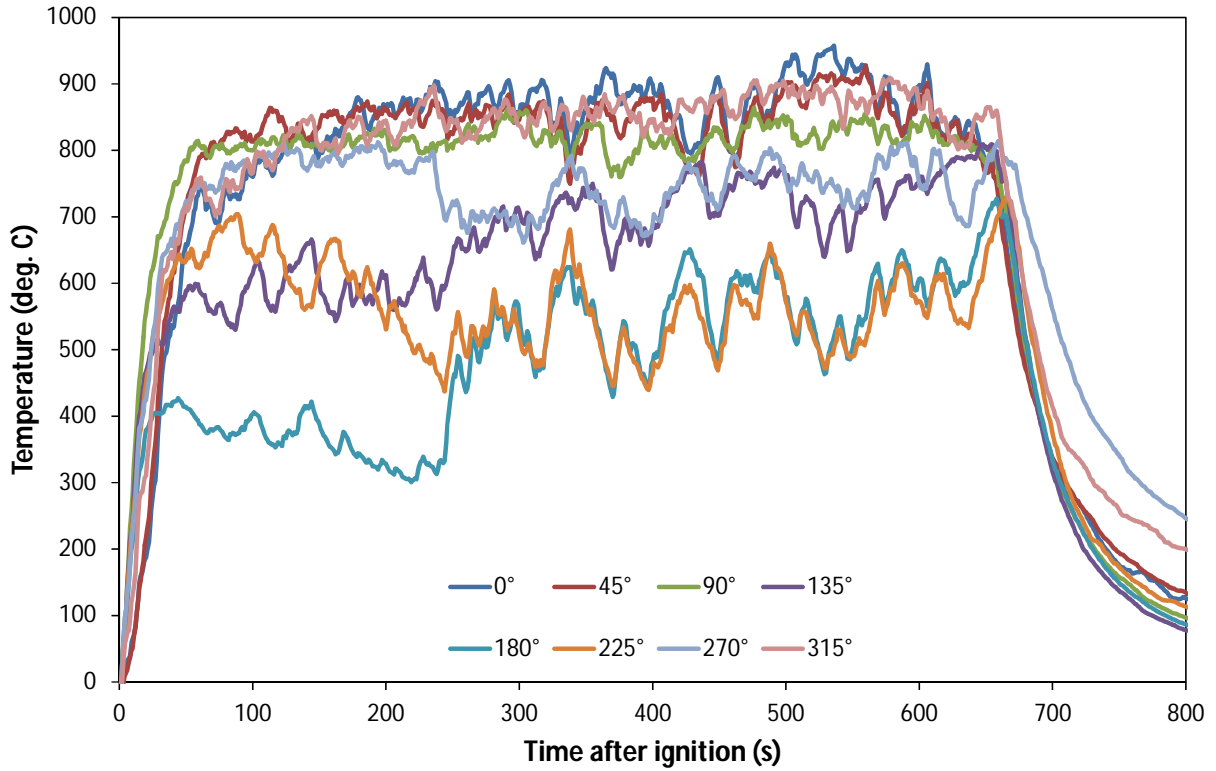


Figure 17. Temperatures measured 51 mm (2") away from outer surface of calorimeter, along west measurement plane.

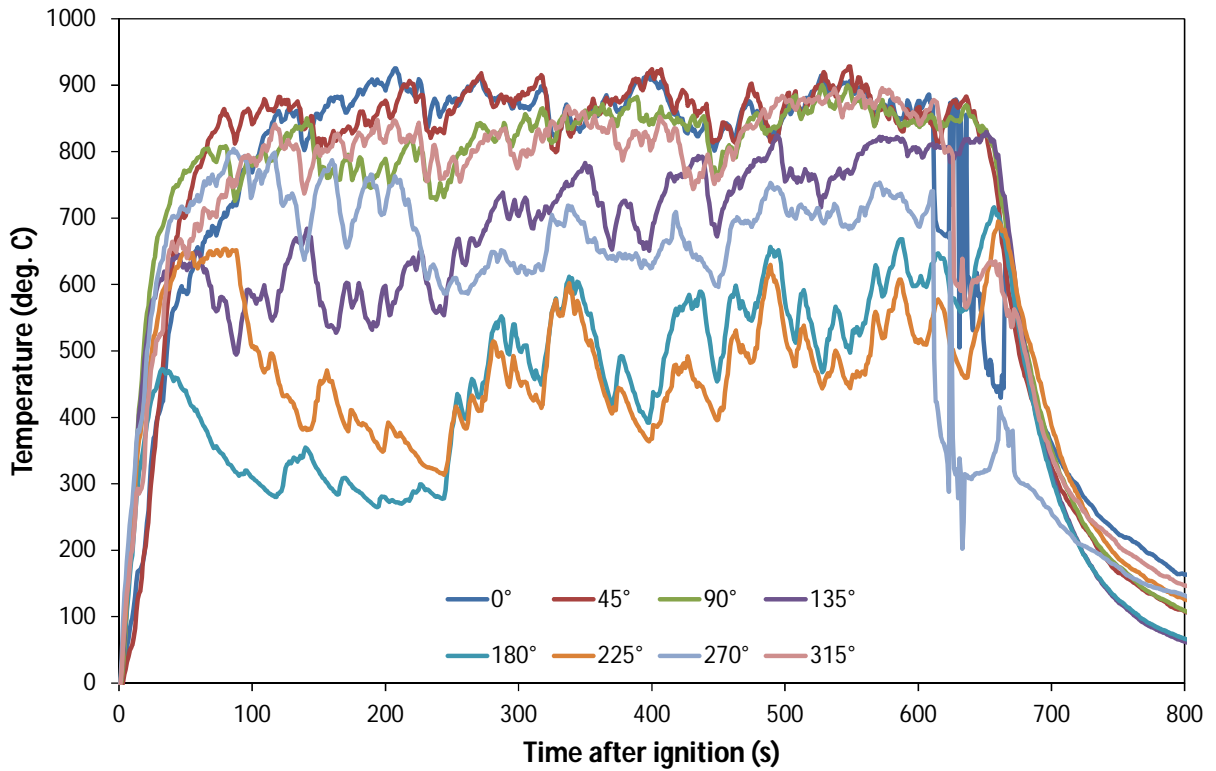


Figure 18. Temperatures measured 51 mm (2") away from outer surface of calorimeter, along centre measurement plane.

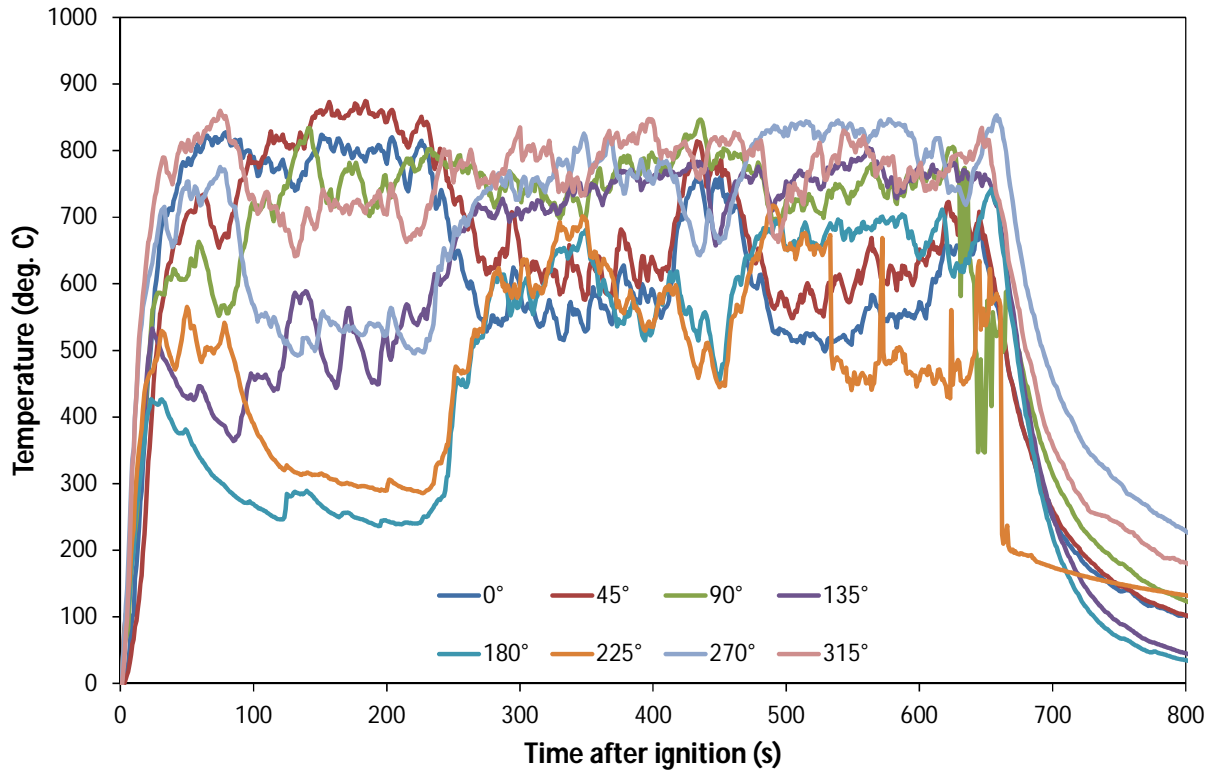


Figure 19. Temperatures measured 51 mm (2") away from outer surface of calorimeter, along east measurement plane.

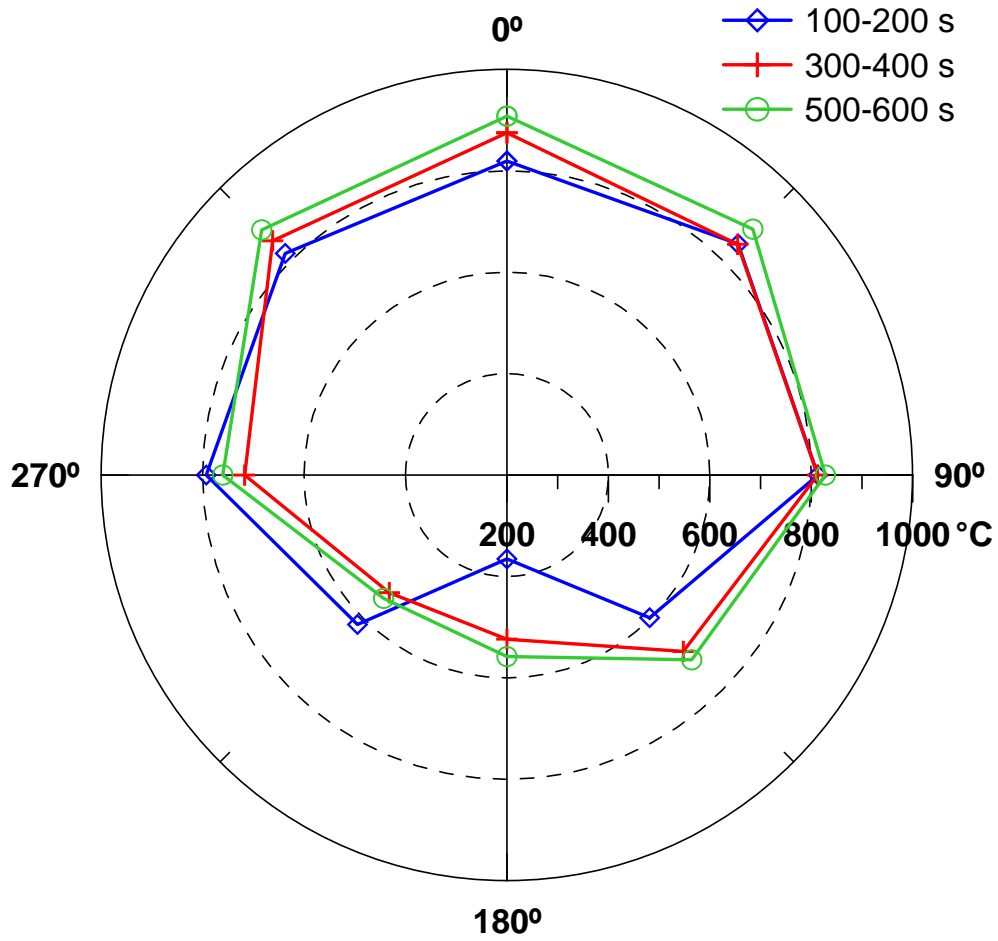


Figure 20. Time-averaged temperatures at 51 mm (2") distance from outer surface of calorimeter, along west measurement plane.

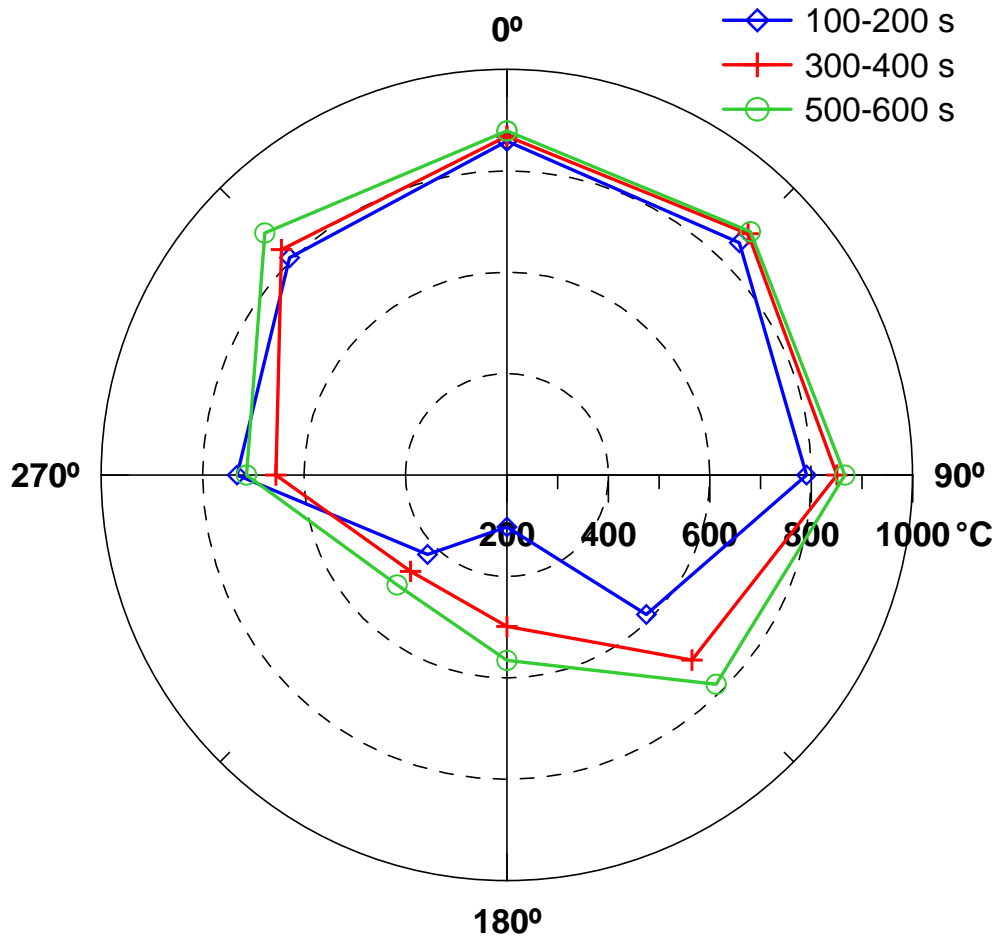


Figure 21. Time-averaged temperatures at 51 mm (2") distance from outer surface of calorimeter, along centre measurement plane.

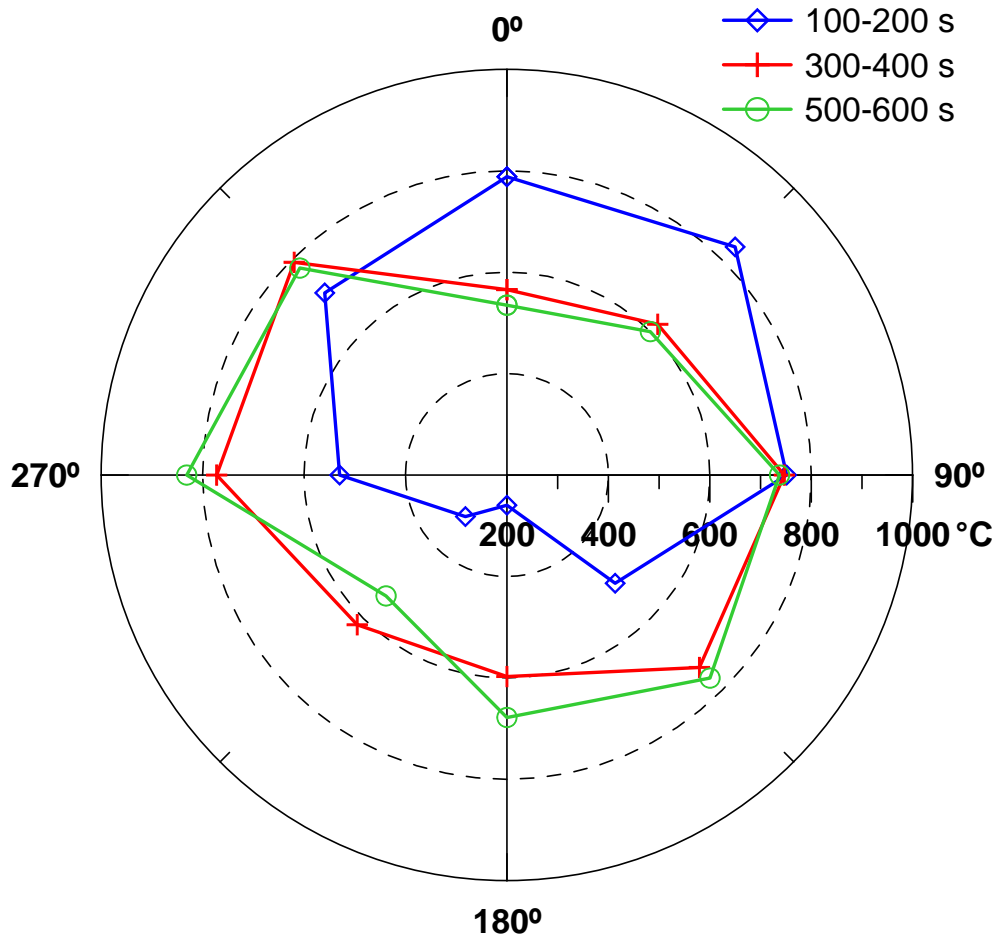


Figure 22. Time-averaged temperatures at 51 mm (2") distance from outer surface of calorimeter, along east measurement plane.

5.3.9 Total Incident Heat Flux to Calorimeter

Figure 23 to Figure 25 show the total incident heat flux from the fire to the calorimeter along the three measurement planes. (See Figure 3 for a depiction of the angular positions.) In general, the top of the calorimeter (0°, 45°, 315°) received the highest levels of heat flux, while the bottom (180°, 225°) received the lowest levels, consistent with the measured flame temperatures (Section 5.3.8). It should be noted that some of the thermocouple wires were insufficiently protected from the fire during the test, affecting the quality of the collected data. Therefore, only the unaffected data have been shown in the Figures.

In Figure 25 for the east plane, a shift in heat flux levels was apparent shortly after 200 s, with the heat flux decreasing significantly along the top of the calorimeter (0°, 45°) while increasing to a lesser extent along the bottom (135°, 180°, 225°). This was consistent with the observation from the videos that the fire tilted towards the west side of the calorimeter at that time.

The time-averaged plots shown in Figure 26 to Figure 28 provide a clearer visual presentation of the heat flux profile around the calorimeter. The profiles remained similar in shape throughout

the test, except along the east measurement plane (Figure 28), where they changed significantly when the fire began to tilt away from the east end at 240 s.

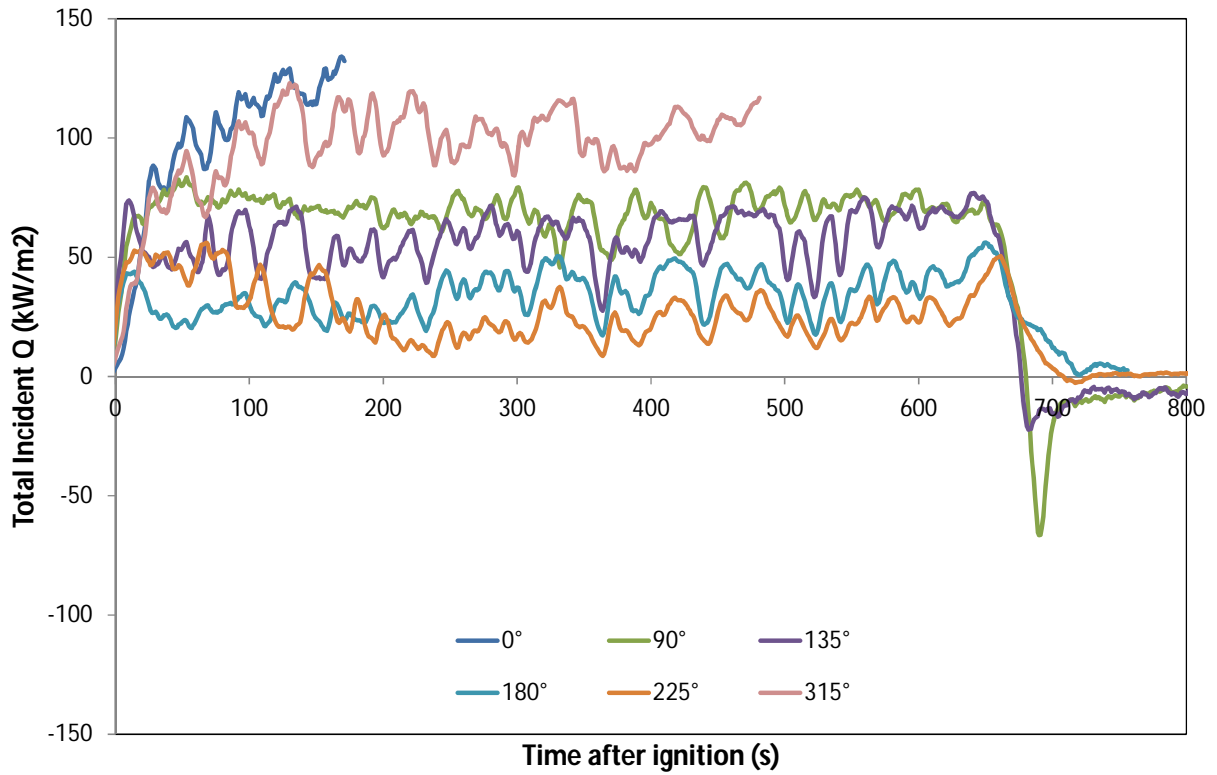


Figure 23. Total incident heat flux to calorimeter, along west measurement plane.

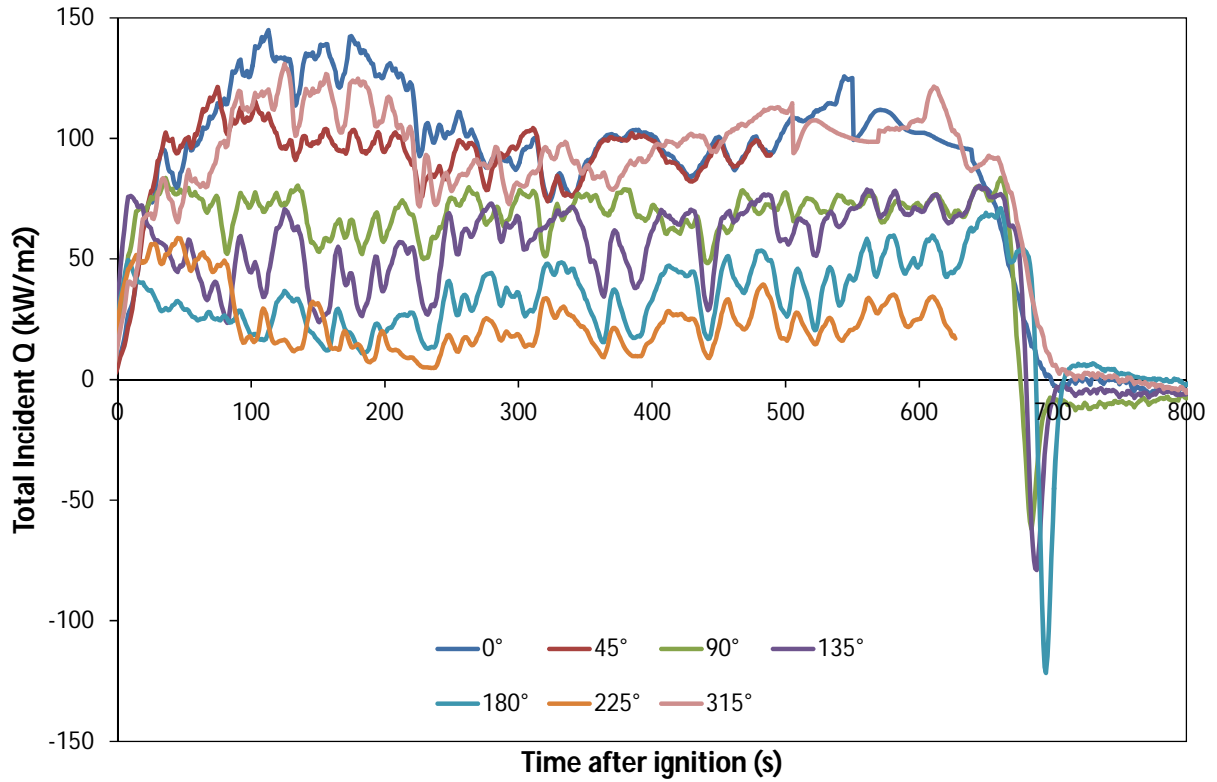


Figure 24. Total incident heat flux to calorimeter, along centre measurement plane.

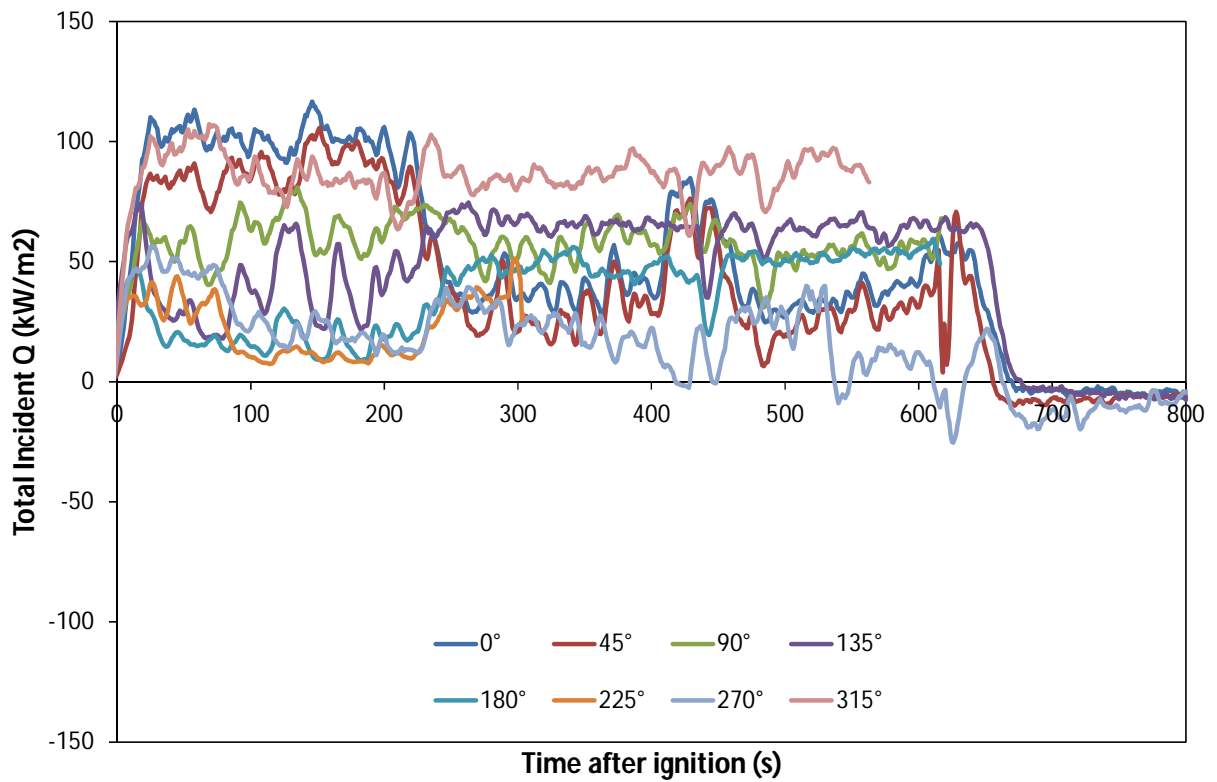


Figure 25. Total incident heat flux to calorimeter, along east measurement plane.

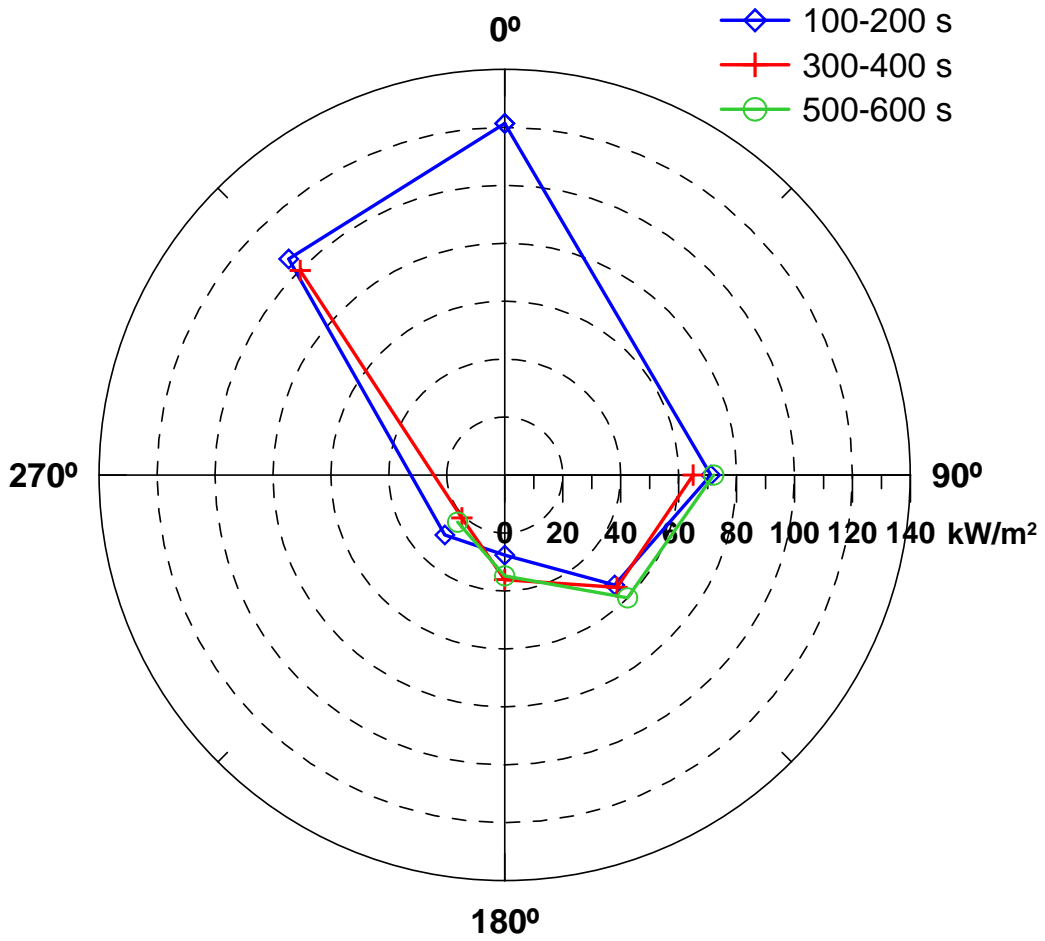


Figure 26. Time-averaged total incident heat flux to calorimeter, along west measurement plane.

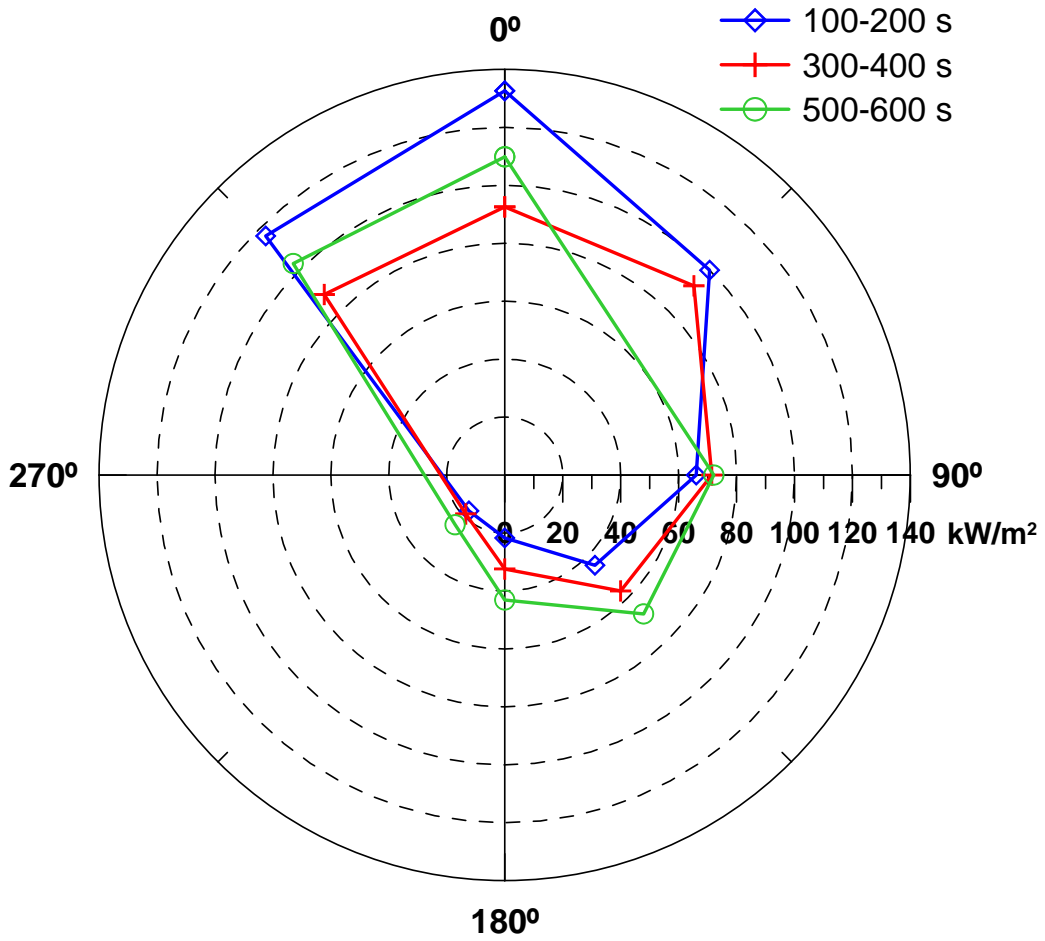


Figure 27. Time-averaged total incident heat flux to calorimeter, along centre measurement plane.

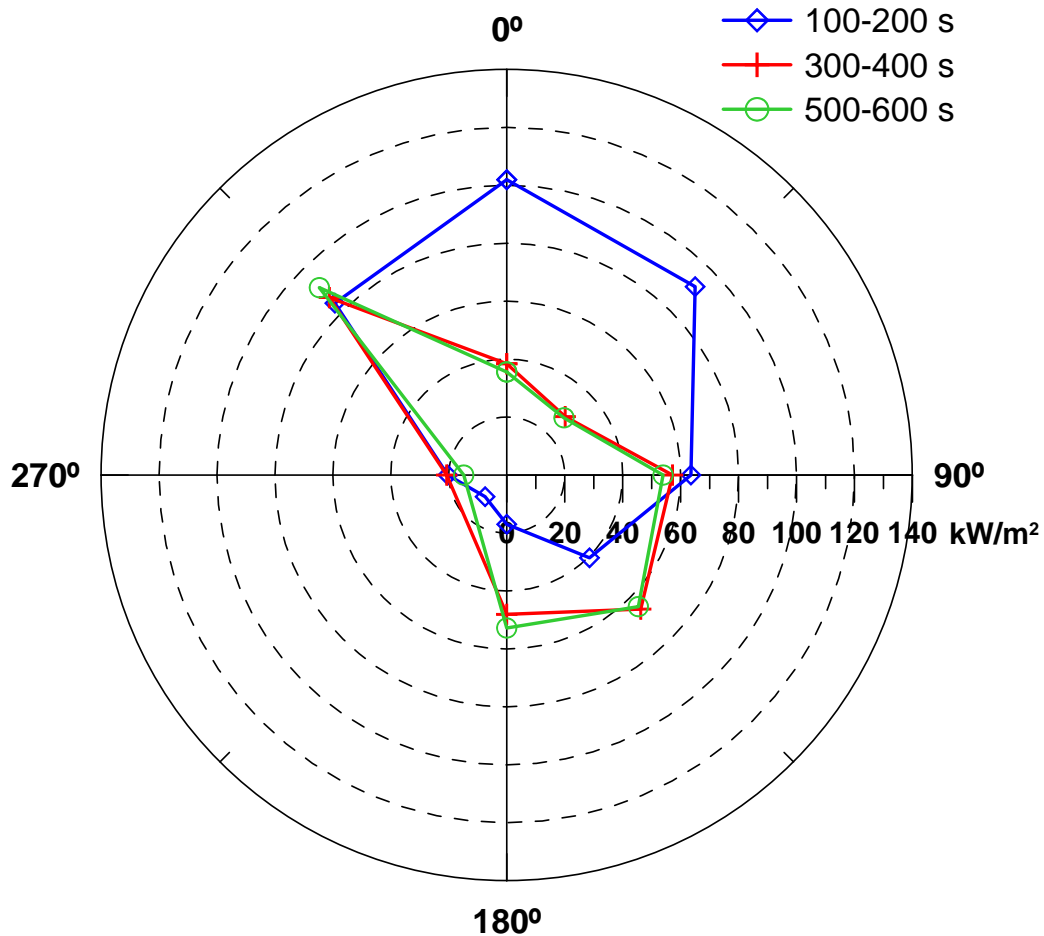


Figure 28. Time-averaged total incident heat flux to calorimeter, along east measurement plane.

5.3.10 Net Heat Flux to Calorimeter

Figure 29 to Figure 31 plot the net heat flux along the surface of the calorimeter in the three measurement planes. The net (or hot-wall) heat flux is the flux absorbed by the calorimeter and, unlike the total incident (or cold-wall) heat flux, does not account for growth in radiation heat loss from the increasingly hot surface to the environment [11].

As evident in the Figures, at the beginning of the test, the net flux increased rapidly to its maximum levels, typically within 130 s or less. The top of the calorimeter (0°, 45°, 315°) generally experienced the highest levels of net heat flux, while the bottom (180°, 225°) experienced the lowest levels, consistent with the trends in flame temperature (Section 5.3.8) and total incident heat flux (Section 5.3.9). The maximum net flux in each measurement plane occurred at 0° and ranged from 93 to 111 kW/m². The net heat flux at all measurement locations then started to decrease as the calorimeter approached thermal equilibrium with the surrounding flames. By approximately 250 s, the net flux decreased below 50 kW/m² and remained there until the end of the test, when it became negative, indicating that the calorimeter was now losing instead of gaining heat.

In the east measurement plane (Figure 31), the heat flux levels at 0° and 45° decreased significantly shortly after 200 s, while those at 180°, 225° and 270° increased slightly. This was consistent with the observation from the videos that the fire tilted towards the west side of the calorimeter at that time.

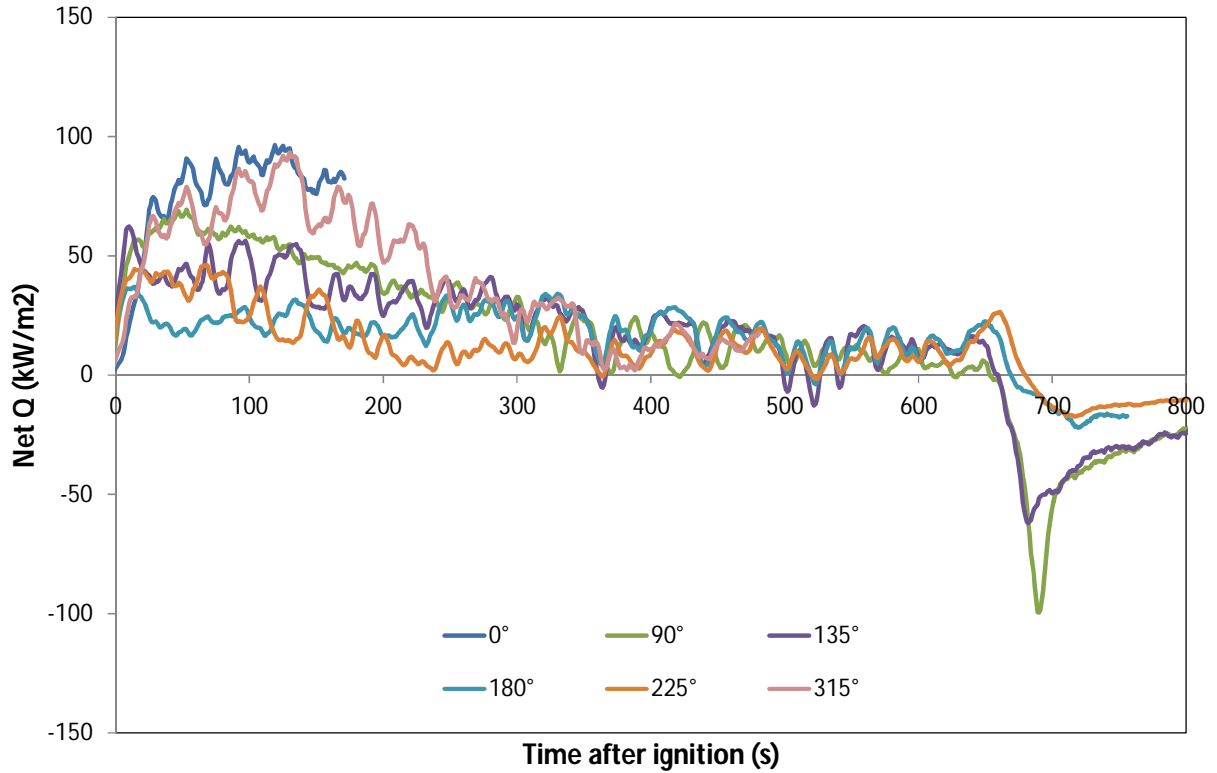


Figure 29. Net heat flux to calorimeter, along west measurement plane.

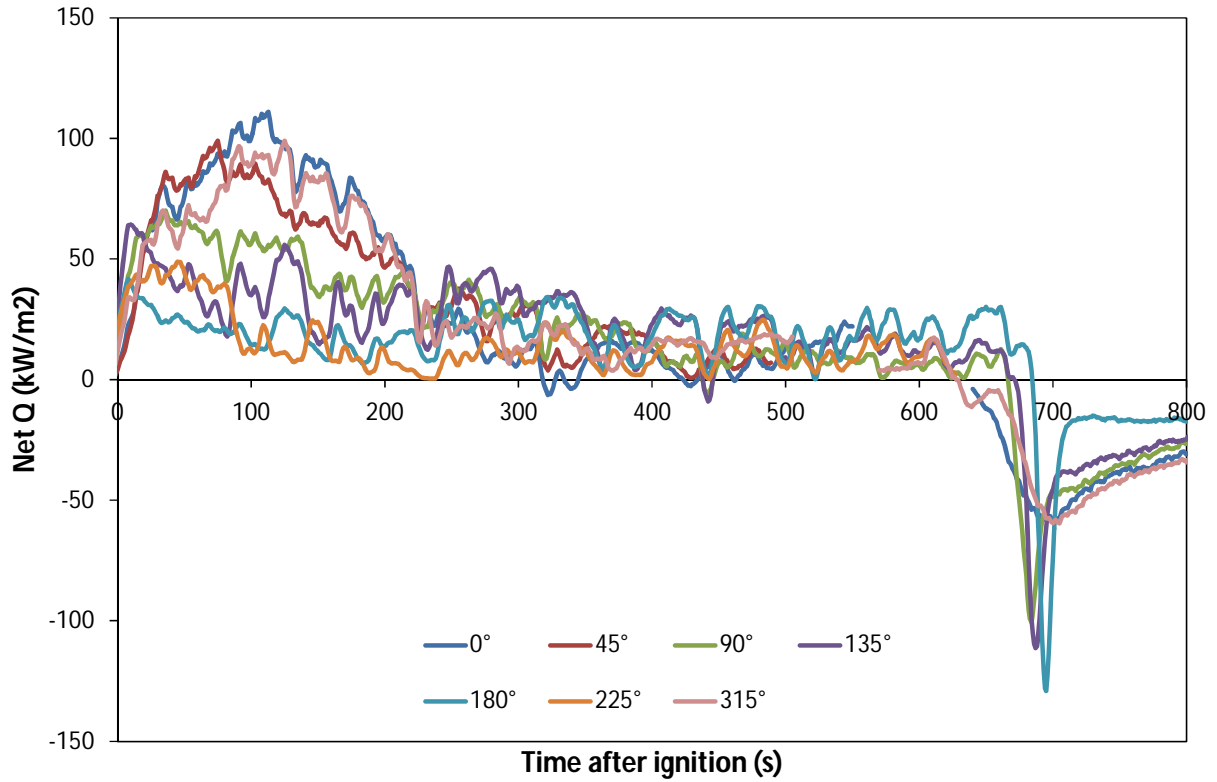


Figure 30. Net heat flux to calorimeter, along centre measurement plane.

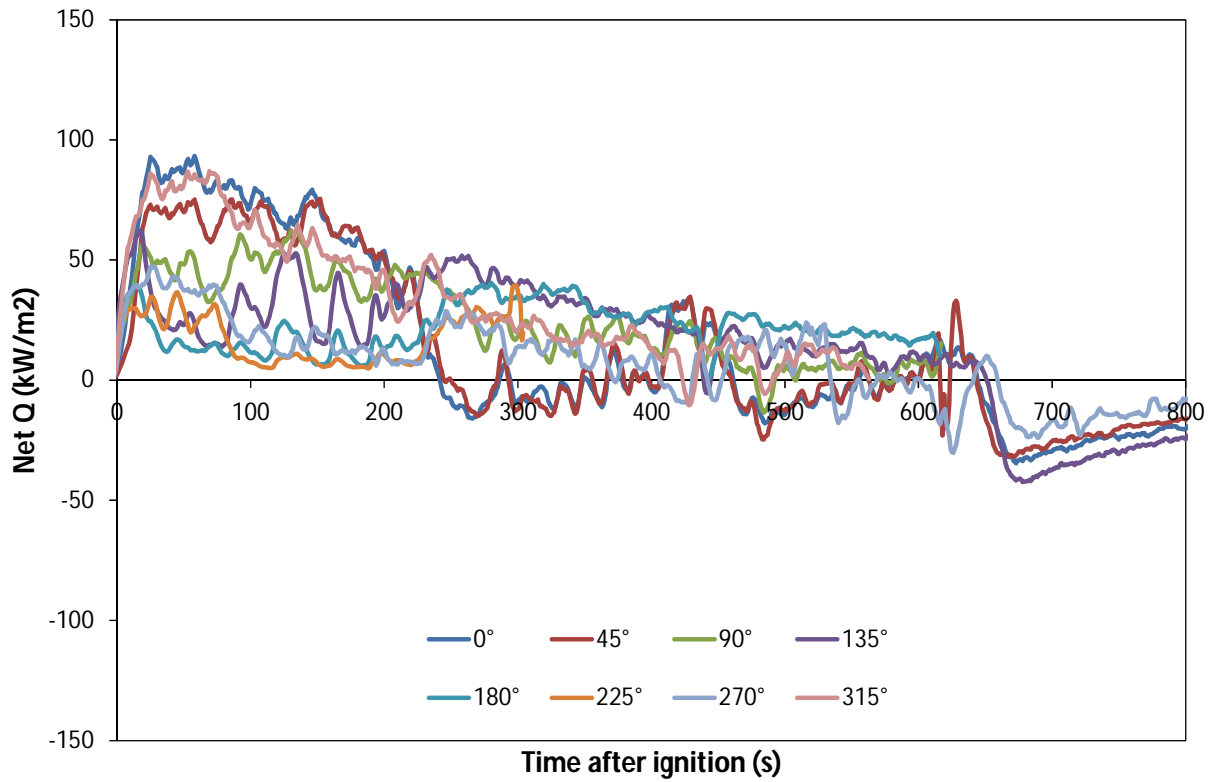


Figure 31. Net heat flux to calorimeter, along east measurement plane.

5.3.11 Calorimeter Surface Temperatures

Figure 32 to Figure 34 show the temperature along the outer surface of the calorimeter in the three measurement planes. In line with the trends shown by the flame temperature and heat flux data (Sections 5.3.8-5.3.10), the top of the calorimeter (0° , 45° , 315°) was generally hottest, while the bottom (180° , 225°) was coolest. In the east measurement plane (Figure 34), the surface temperatures at 0° and 45° increased over the first 240 s, then levelled off between 600°C and 700°C until the end of the test. This was due to the fire tilting towards the west end of the calorimeter after 240 s.

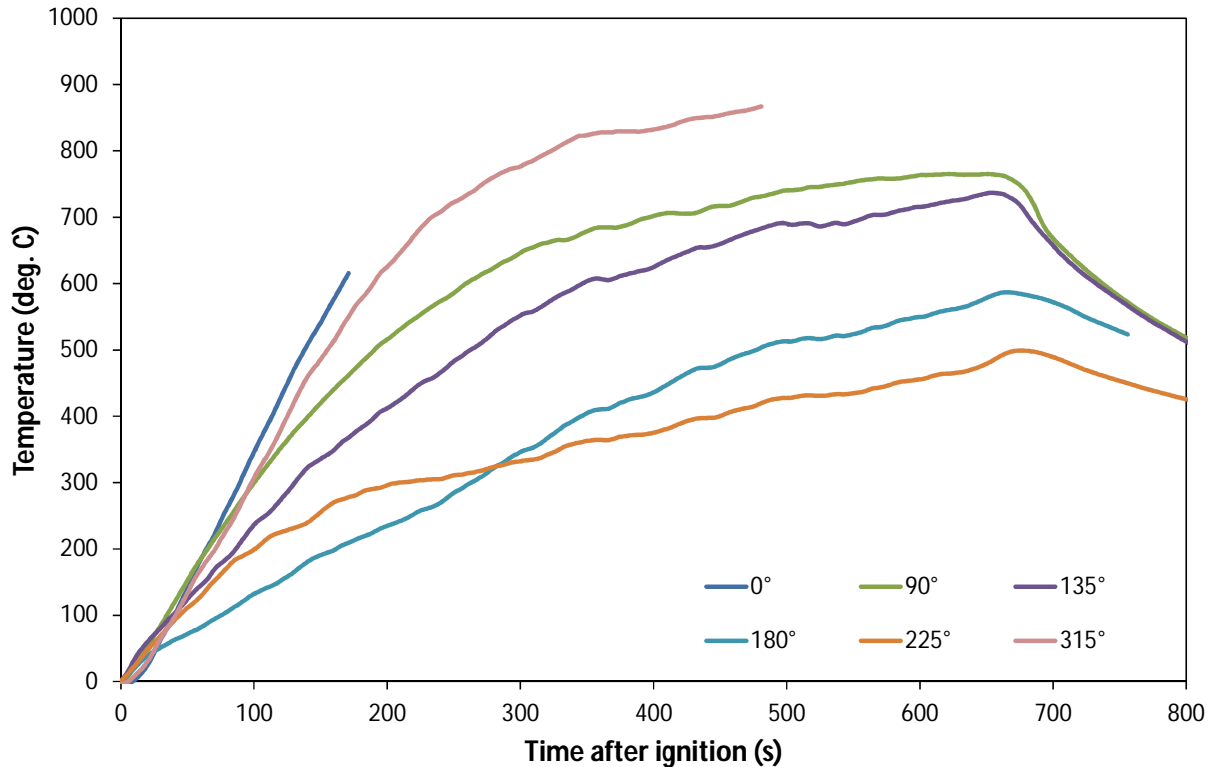


Figure 32. Outer surface temperatures of calorimeter, along west measurement plane.

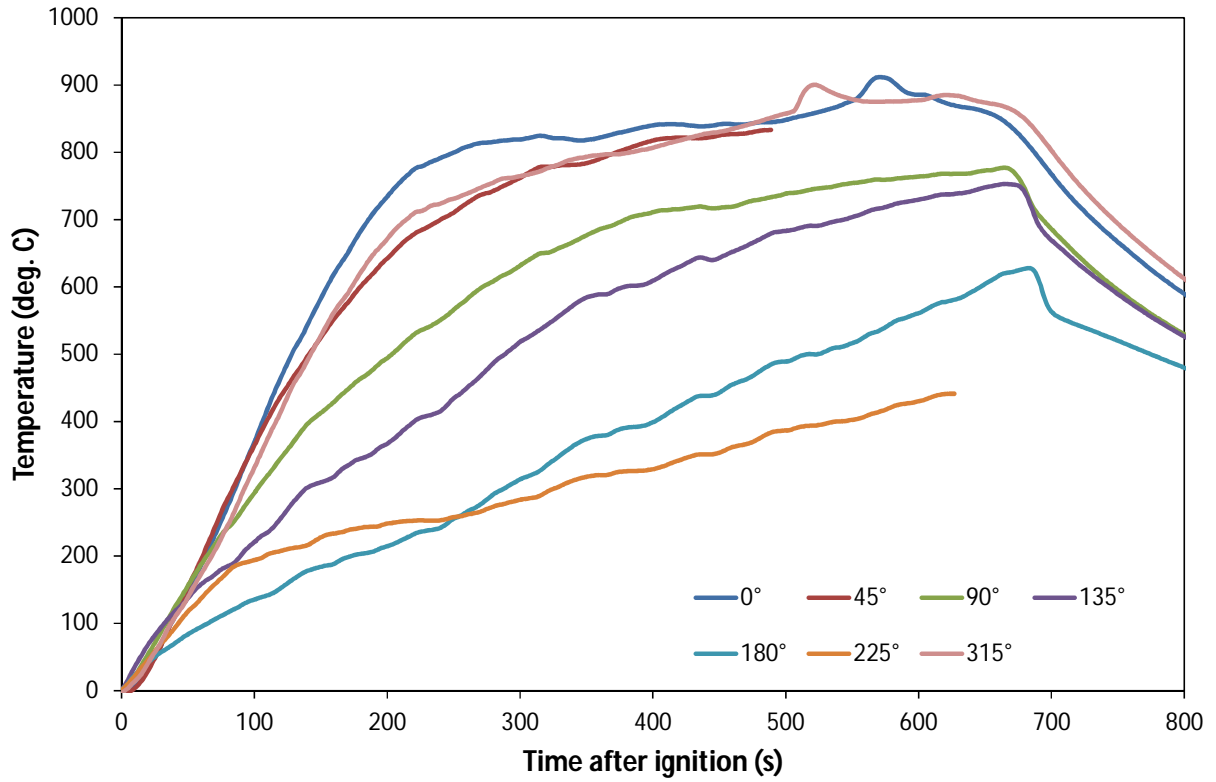


Figure 33. Outer surface temperatures of calorimeter, along centre measurement plane.

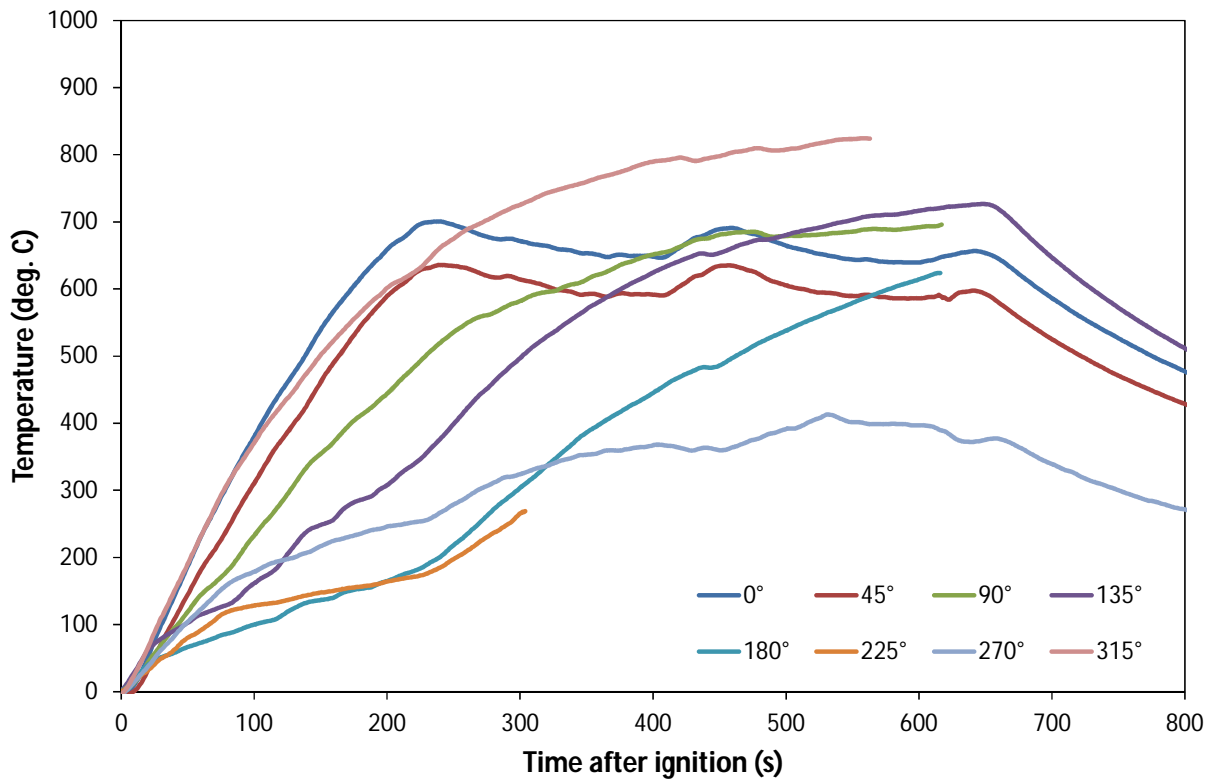


Figure 34. Outer surface temperatures of calorimeter, along east measurement plane.

6. Summary and Recommendations

This report describes the experimental setup for simulating a tank car engulfed in a crude oil pool fire at 1/10th scale. Measurements are focussed on the fire environment external to the tank car and the levels of heat flux incident on the tank car. Crude oil sampling and handling methods are designed to retain all light-end hydrocarbon components in the oil. Three tests were conducted to verify operation of the fuel feed system, optimize the test protocol and generate baseline data using heptane, a well-characterized fuel.

Based on these tests, it is recommended that certain improvements be made to the fuel feed system before proceeding with further testing. A suitable pressure vessel should be installed as a run tank, instead of using the fuel drum. Prior to testing, this vessel would be filled with crude oil using the water displacement method, and the same method would be used in reverse during testing to pump the oil into the pan. By designing this vessel to withstand higher working pressures than the crude oil drum, higher flow rates could be achieved, resulting in a longer period of steady burning during each test since the pan would be filled to the desired fuel thickness earlier. An additional recommendation is to automate control of the fuel feed system so that the fuel layer thickness inside the pan could be controlled more precisely, and no operator would need to be physically present inside the Burn Hall during testing.

References

1. Lam, C., Edwards, D. and Lougheed, G. 2015. *Rail tank cars exposed to fire – literature review of crude oil, condensate and ethanol behaviour*. Report A1-005795-01.1, National Research Council Canada, Ottawa, ON.
2. Beck, J.V. 1999. *User's manual for IHCP1D*. 7th edition, Beck Engineering Consultants Company, Okemos, MI.
3. Gardon, R. 1960. A transducer for the measurement of heat-flow rate, *Journal of Heat Transfer*, 82:396-398.
4. Janssens, M. and Parker, W. 1992. Oxygen consumption calorimetry, in *Heat Release in Fires*, edited by Babrauskas, V. and Grayson, S.J., Elsevier Science Publishing Co. Ltd, NY, NY.
5. Ferrero, F., Muñoz, M., Kozanoglu, B., Casal, J. and Arnaldos, J. 2006. Experimental study of thin-layer boilover in large-scale pool fires, *Journal of Hazardous Materials*, A137:1293-1302.
6. Chatris, J.M., Quintela, J., Folch, J., Planas, E., Arnaldos, J. and Casal, J. 2001. Experimental study of burning rate in hydrocarbon pool fires, *Combustion and Flame*, 126:1373-1383.
7. Blinov, V.I. and Khudyakov, G.N. 1961. *Diffusion burning of liquids*. Technical report, Izdatel'stvo Akademii Nauk SSSR, Moscow. T-1490a-c, English Translation: U.S. Army Engineer Research and Development Laboratories, Information Resources Branch, Translation Analysis Section, Fort Belvoir, VA.
8. Blanchat, T.K. and Suo-Anttila, J. 2011. *Hydrocarbon characterization experiments in fully turbulent fires – results and data analysis*. Technical Report SAND2010-6377, Sandia National Laboratories, Albuquerque, NM.
9. Koseki, H. and Yumoto, T. 1988. Air entrainment and thermal radiation from heptane pool fires. *Fire Technology*, 24:33-47.
10. National Institute of Standards and Technology, NIST Chemistry WebBook, <http://webbook.nist.gov/chemistry/>, accessed March 2016.

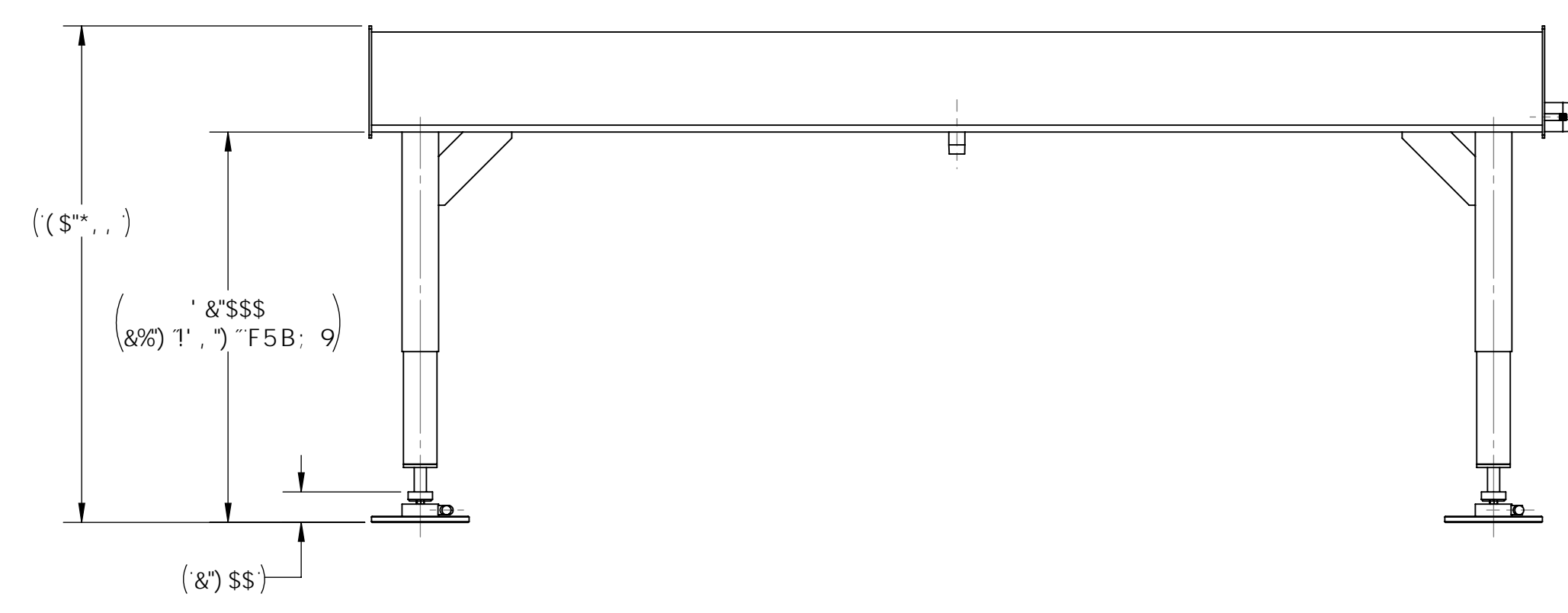
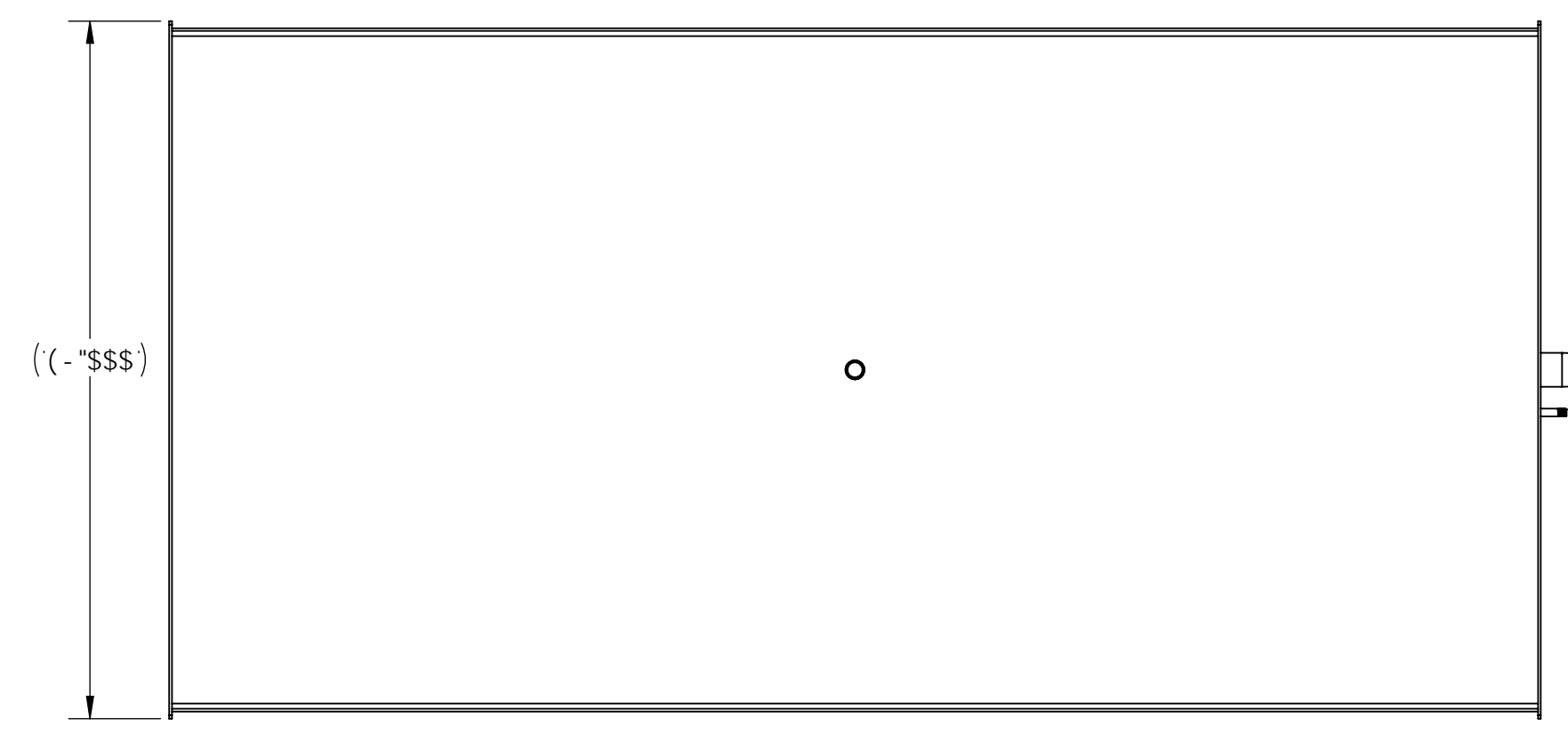
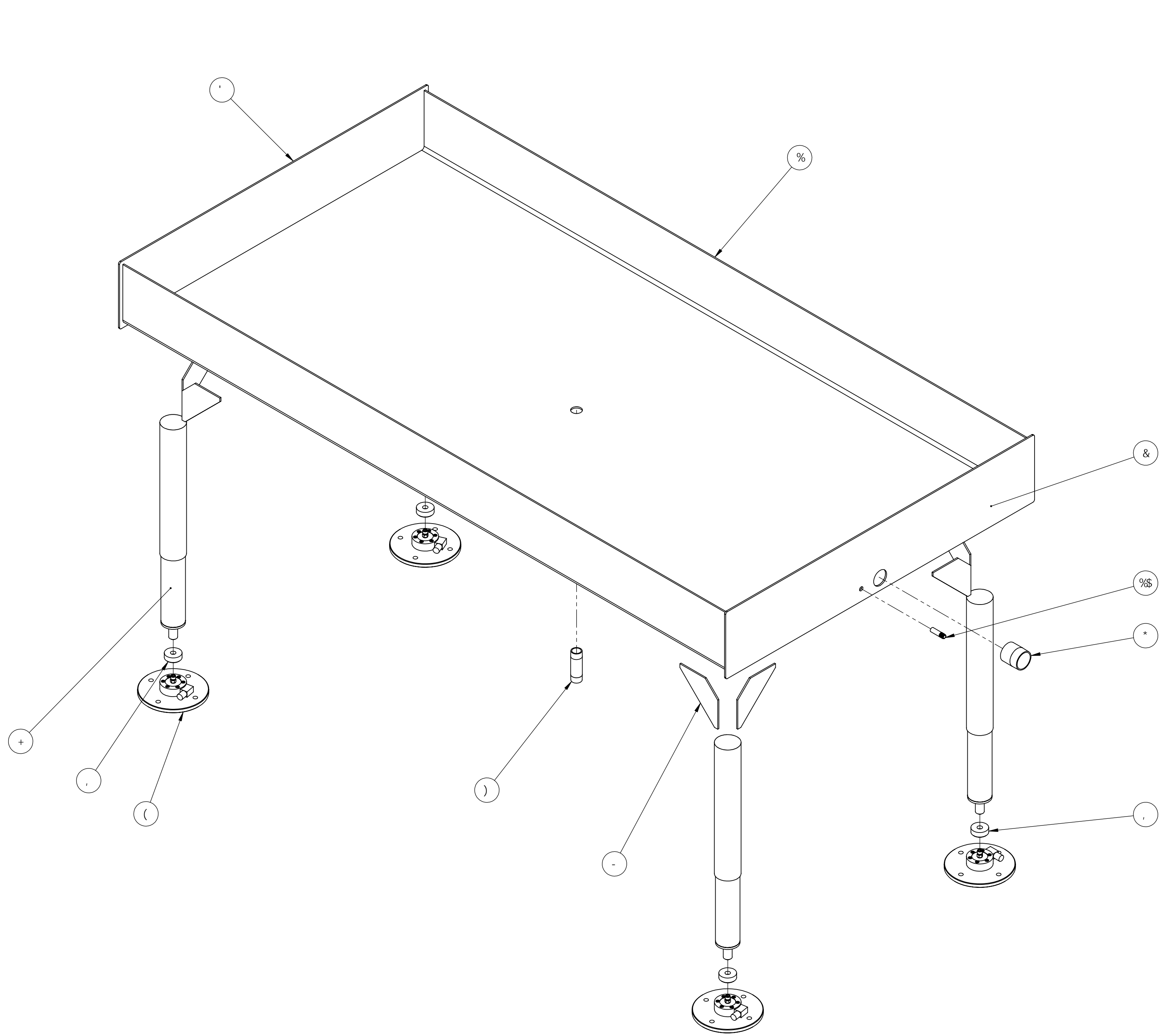
11. Keltner, N. R., Nicolette, V. F., Brown, N. N., and Bainbridge, B. L. 1990. Test unit effects on heat transfer in large fires. *Journal of Hazardous Materials*, 25:33-47.

Supplement A – Fuel Pan Engineering Drawings

7B ABC F6478 7E4J A
 AS CAP 89E8E8 7HE 7B 78F7 A
 F328E C 477 8E8E7 8B C 8 78F A 89948
 F 4 A478E 8B8E8F 8E8E8F 4H 8E8AH 7B 88A88C8A
 8E88A 477 7E4J A F 8B C 8 78F A 89948
 8E8E8A8E 8B8F 78F 78F A 4H 8E8AH 7B 88A88C8A

F0J 6GB < 8CFMF < 8CF F E 1 989CFVJ 6C8G
 NC B9 F9J 89G7 F DHC B B5H 6M05F

BCHG



#DA	8F5K -B: BC"	89G7 F-DHC B	E HM
%	%8 - , !&\$!\$D	D5B A 5-B D85H	%
&	%8 - , !&\$!\$ D	D5B 9B 8 D85H! 8F5-B	%
'	%8 - , !&\$!\$&D	D5B 9B 8 D85H	%
(%8 - , !&\$!\$&	@ C 5 B 7 9@D5 8 5G9A 6@M	(
)	((*% ? (**	% B DHD89 B-DD@)
*	++' ?% -	& B DHD89 B-DD@	%
+	7 C A A "	: @ C F >5 7 ?	(
-	%8 - , !&\$!\$) D	@ C 5 B 7 9@D5 8 5G9A 6@M	(
-	%8 - , !&\$!\$) D	>5 7 ? : 1 G9H	.
%8	++' ?%&&	%#("D89 B-DD@: 998	%

GB78E 4A88F GB7UE 4A88F
 HAT8FF BG BEJ 4B 8B87
 FAHP A 744GBA 68AGE 4E8
 477 7A88F 8A8 F 4A8 8F
 7A88F 8A8 8A 8A88F
 1K 1K 1K
 1K 1K 1K
 477 9E88E 8A8 F 888
 7A88F 8A8
 4A 1K 1K 1K
 1K 1K 1K
 8B88E 8F 8A8A 88E 8B 4
 4F88E 8E 88F 88F
 8E8A 477 F 4C 8E 8F
 6 8A8E8A8E 8B8E8F
 8E8E8E 8B8E8A8E
 1K 1K 1K

89G7 F-DHC B
 D5B A 5-B D85H
 D5B 9B 8 D85H! 8F5-B
 D5B 9B 8 D85H
 @ C 5 B 7 9@D5 8 5G9A 6@M
 % B DHD89 B-DD@
 & B DHD89 B-DD@
 : @ C F >5 7 ?
 @ C 5 B 7 9@D5 8 5G9A 6@M
 >5 7 ? : 1 G9H
 %#("D89 B-DD@: 998

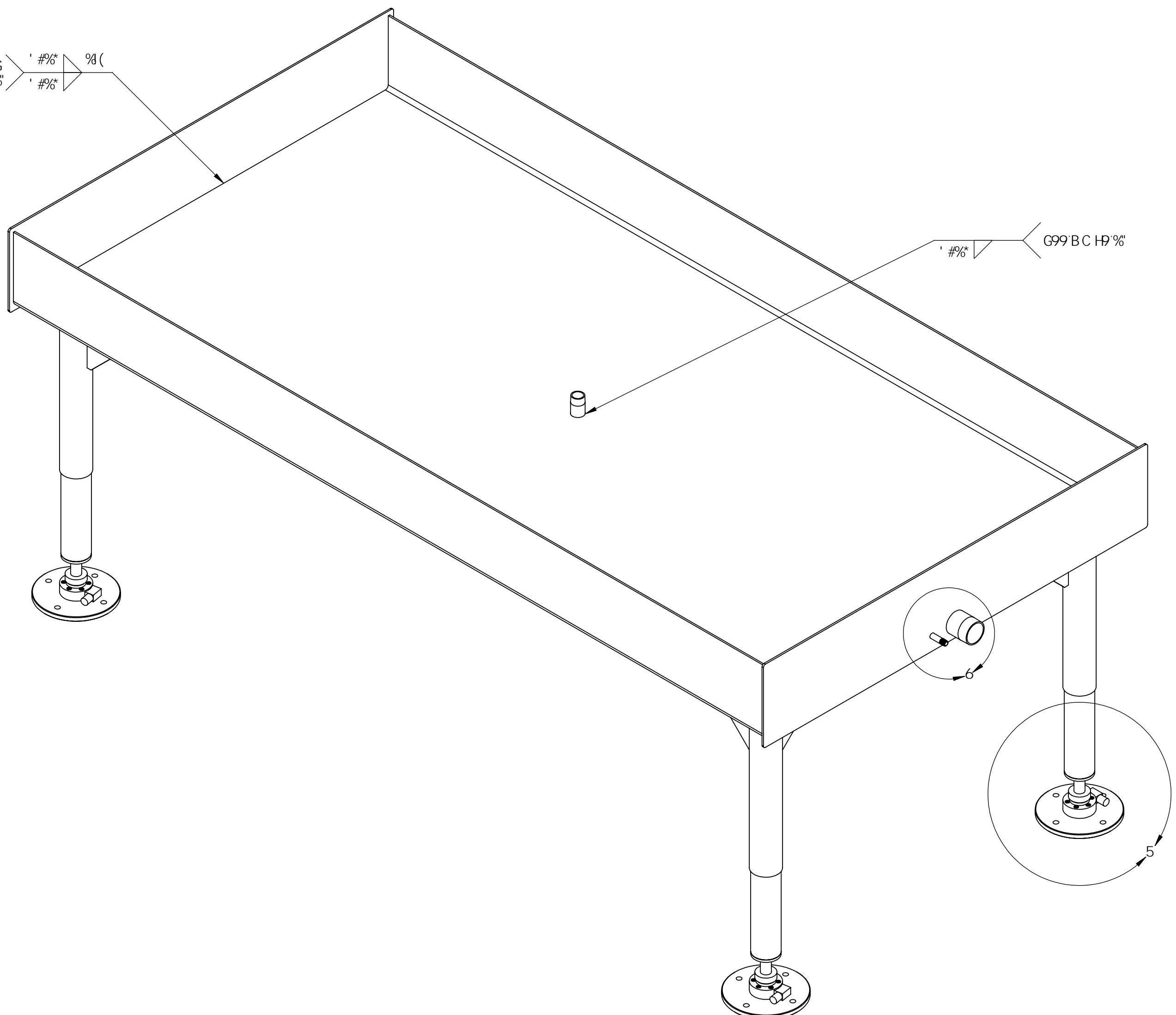
NRC-CRRC
 7Xf Za TaW9TLe WTgba Fxei Vxf
 Fxei WX WX 6baVXcgba Xg WX 9TLe WTgba
 Y 88% 1BU8Ebu FYgUNNA 7 ci bW
 : 1 9@D5B 5G9A 6@M
 %8 - , !7 5 @ C F A 9H F 5B 8 : 1 9@D5 B

8
 !

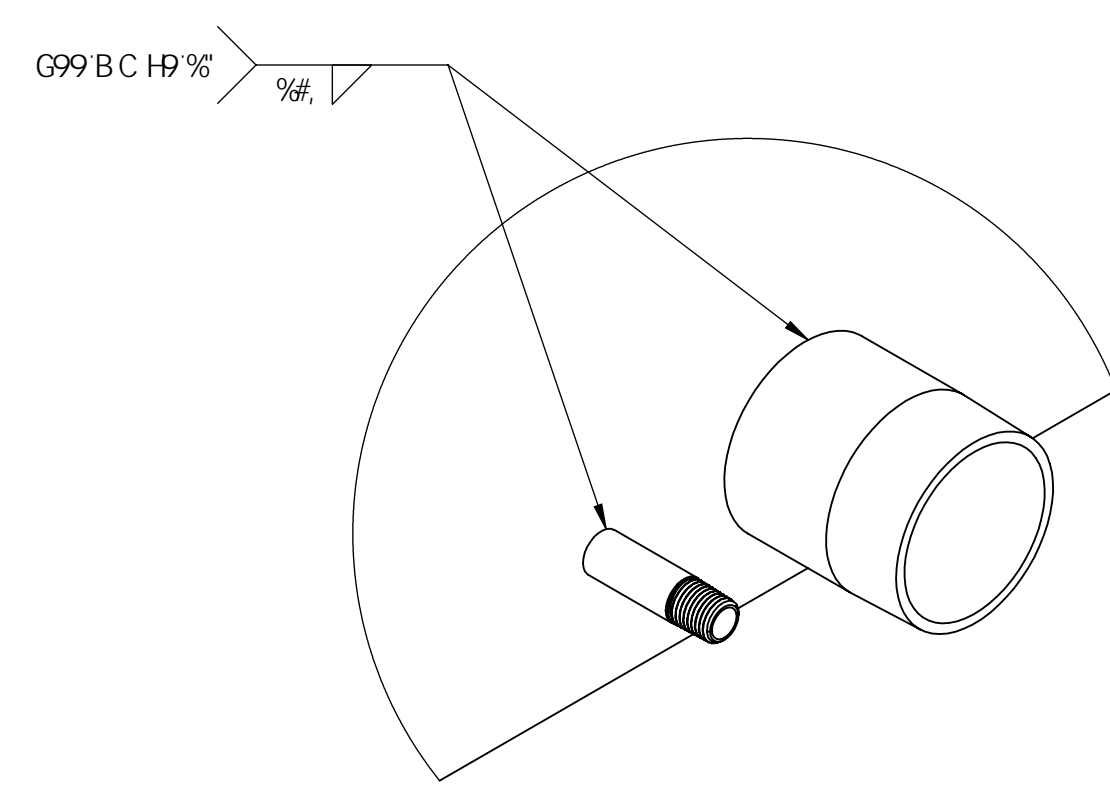
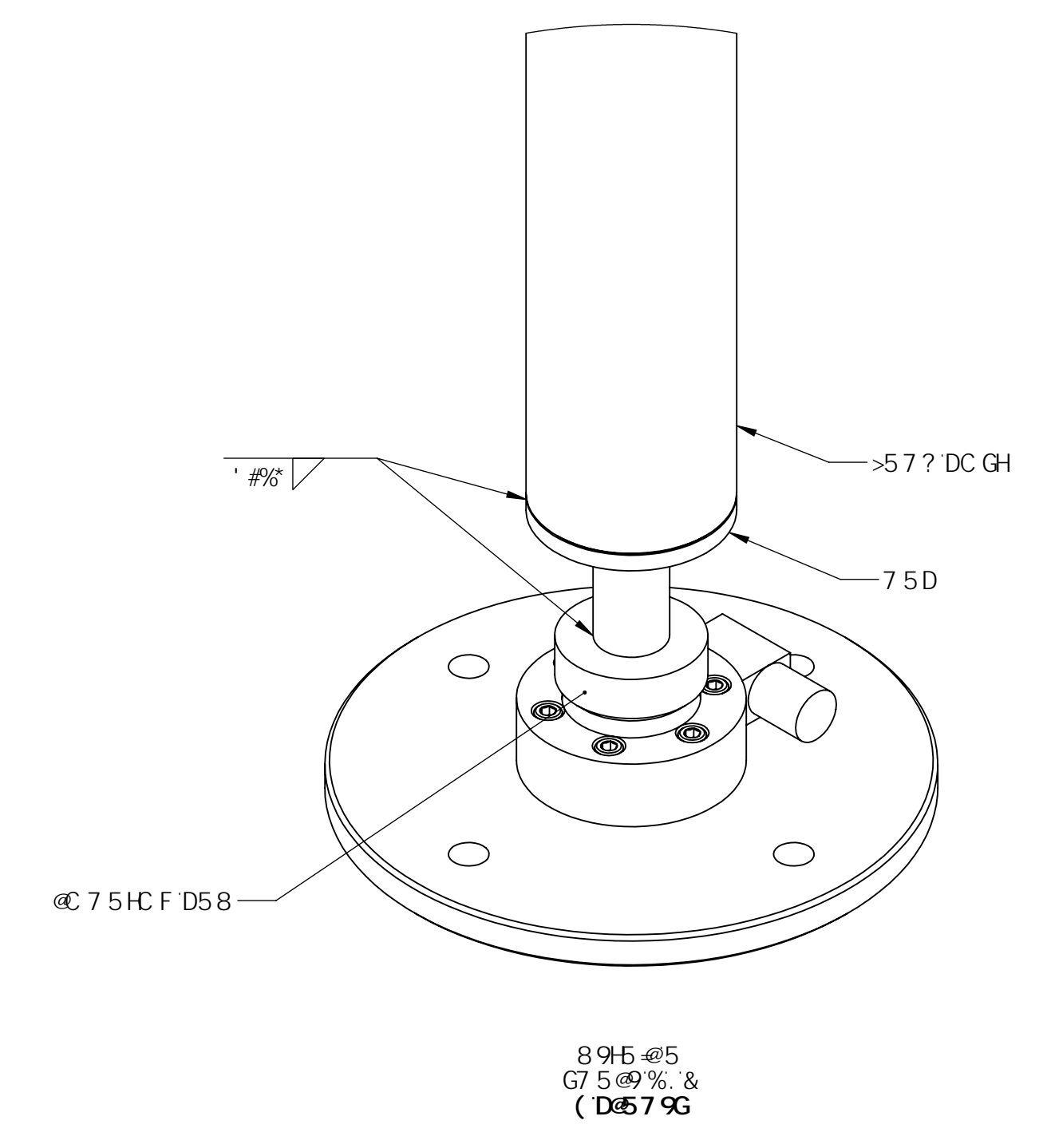
7B ABC F6478 7E4J A
 AB CAP 989888 7HE 7B 78FF A
 F328EC 477 8E8EF 6B G 8 78FF A 8994G
 F: A478E 6B88F 8E88F 4H 8E8AH 7B 68A88C8A
 E8G8A 477 7E4J A F 6B G 8 78FF A 8994G
 E8G8A8E 6B8F 78F 78FF A 4H 8E8AH 7B 68A88C8A

BCHG
 %K 9885F9K 5HF H < H

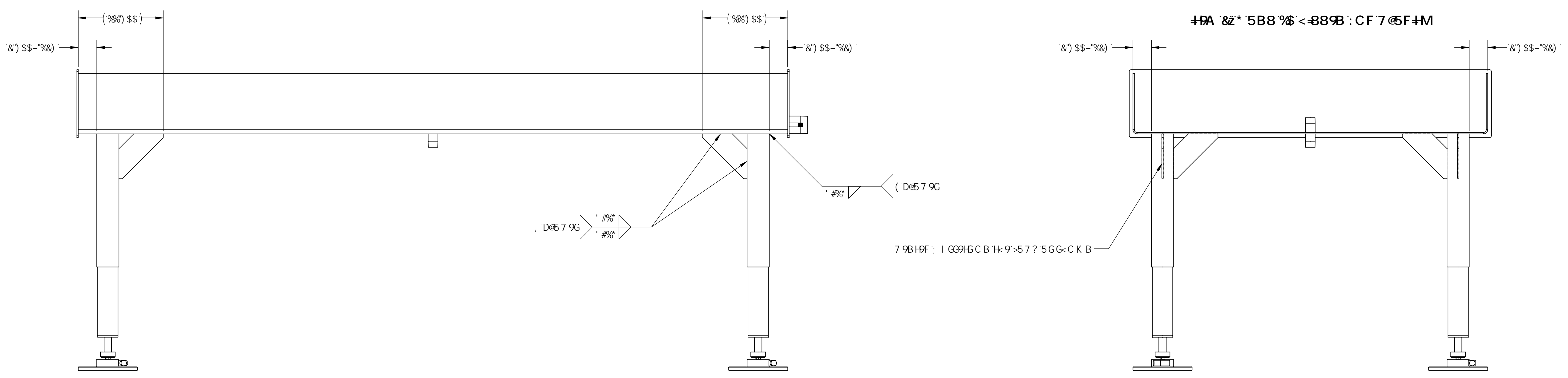
6C H: 9B 8G
 G99 BC H9 %



K 98 9L 6H; 75DH > 57? DC GH
 5B8 K 98 H F 95898 FC 8 HC @ 75HCF D58 H 9A , L



8 9H @ 6
 G7 5 @ 9 % . &

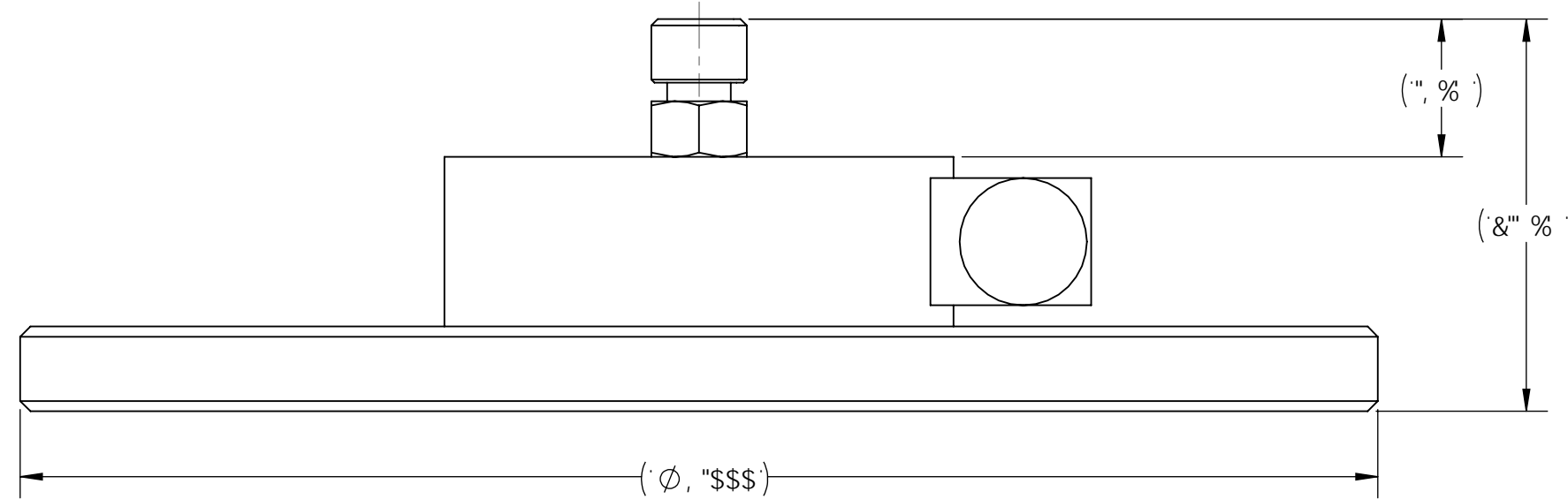
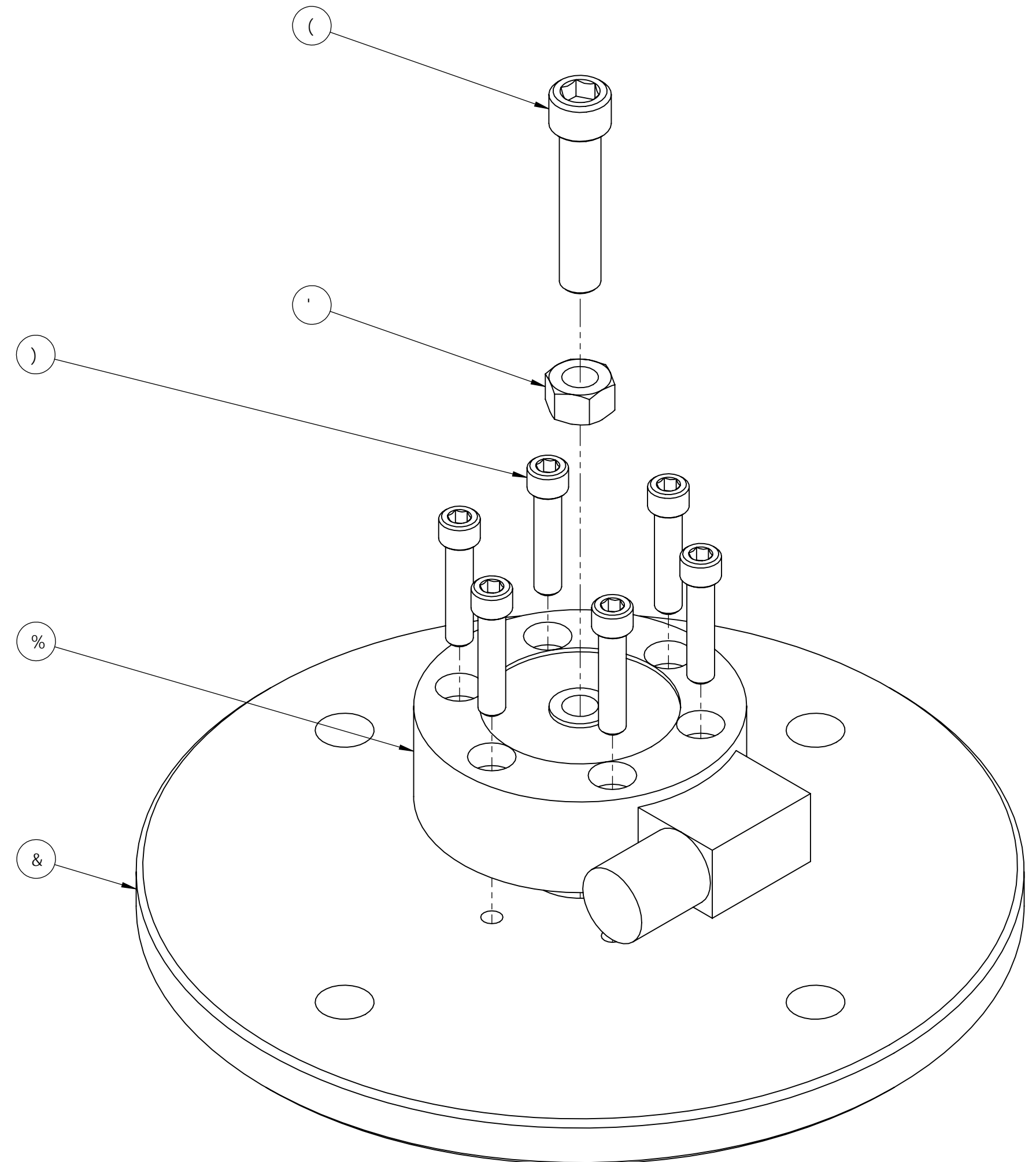
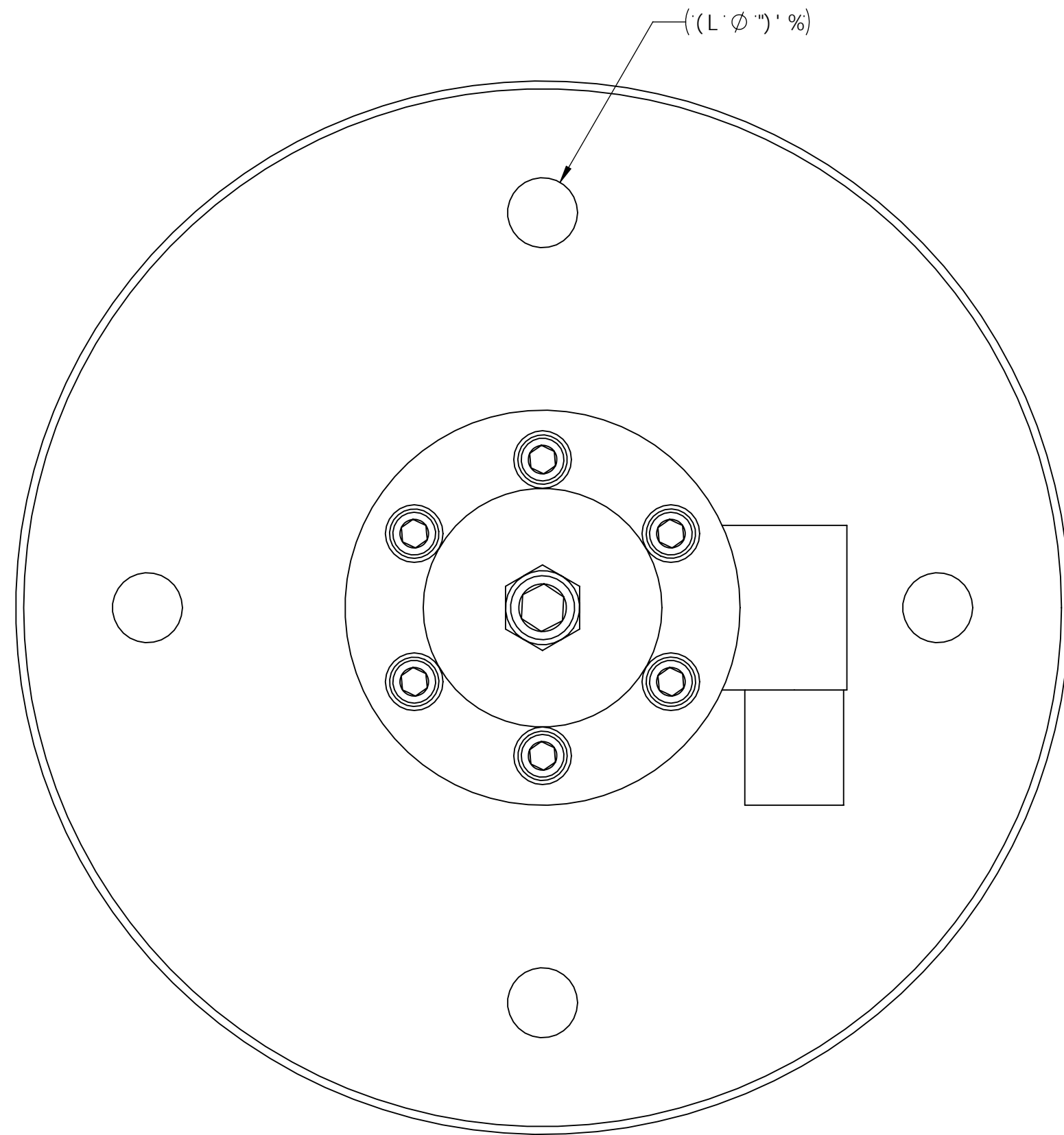


		NRC-CHRC 7Xf Vza TaW9TLe WTg'ba F'XeI Vxf F'XeI Vx W' 6ba Vxg'ba Xg W' 9TLe WTg'ba Y 68% 1BUH:bu FYg'UNA 7 ci bWg : I 9@D5 B 5G9A 6@M	
F4C 6B78	598	F0E8FF 1 68A1	
T8F1 48A88C8J	> 789A 9F G 0 88877 U E 9		
7E4J A1 78FF A 4U	> 789A 9F G 400 400	> 789A 9F G 74GB	& + 858683R
4FG 67 68A	88781 A488 8888 78 887878	880 887878	7E478 68 8778
7 CBGH	%8C - I: I 9@D5 B 5G9A 6@M	& C: 48 9 &	%
887 68E	4FF88781 887878 4FF887878	7E4J A: 4878787878	880 - 16815%
			8 !

7B ABG F647B 7E4J A:
 A8 C4F @8FHE8E FHE 7B 78FF A
 EBCBEG 477 BEEBEF GB G: 8 7BF < A B99-6B
 F < A478E GBHGBF BEEBHEF 4H 5HE84H 7B 6BA68CG-BA
 EBGHEA 477 7E4J A: F GB G: 8 78FF < A B99-6B
 E8GBHEABE GBHF 7BF 78FF 4F 4H 5HE84H 7B 6BA68CG-BA

F9J GCB < GC HMF < GC FE I 989GFVJ GCBG
 NC B9 F9J " 89G7 F-DHC B 85H9 6MDSF

BC1H9G

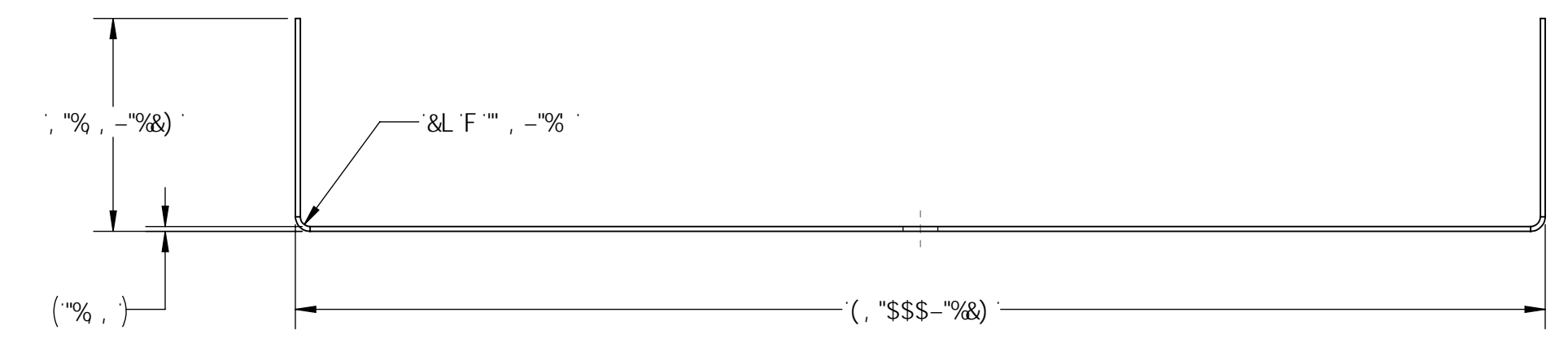
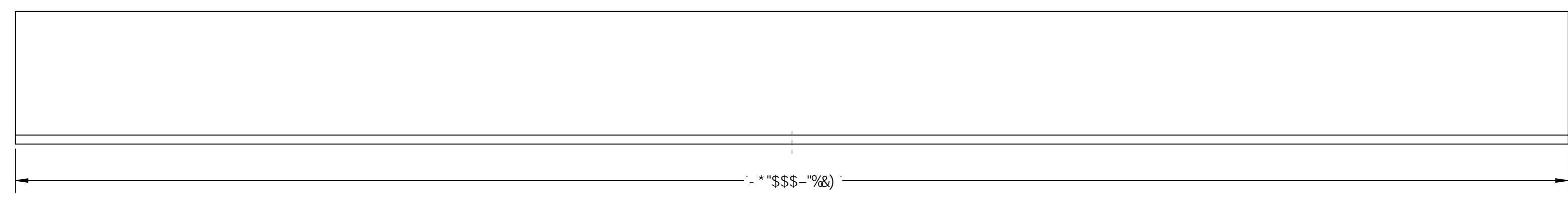
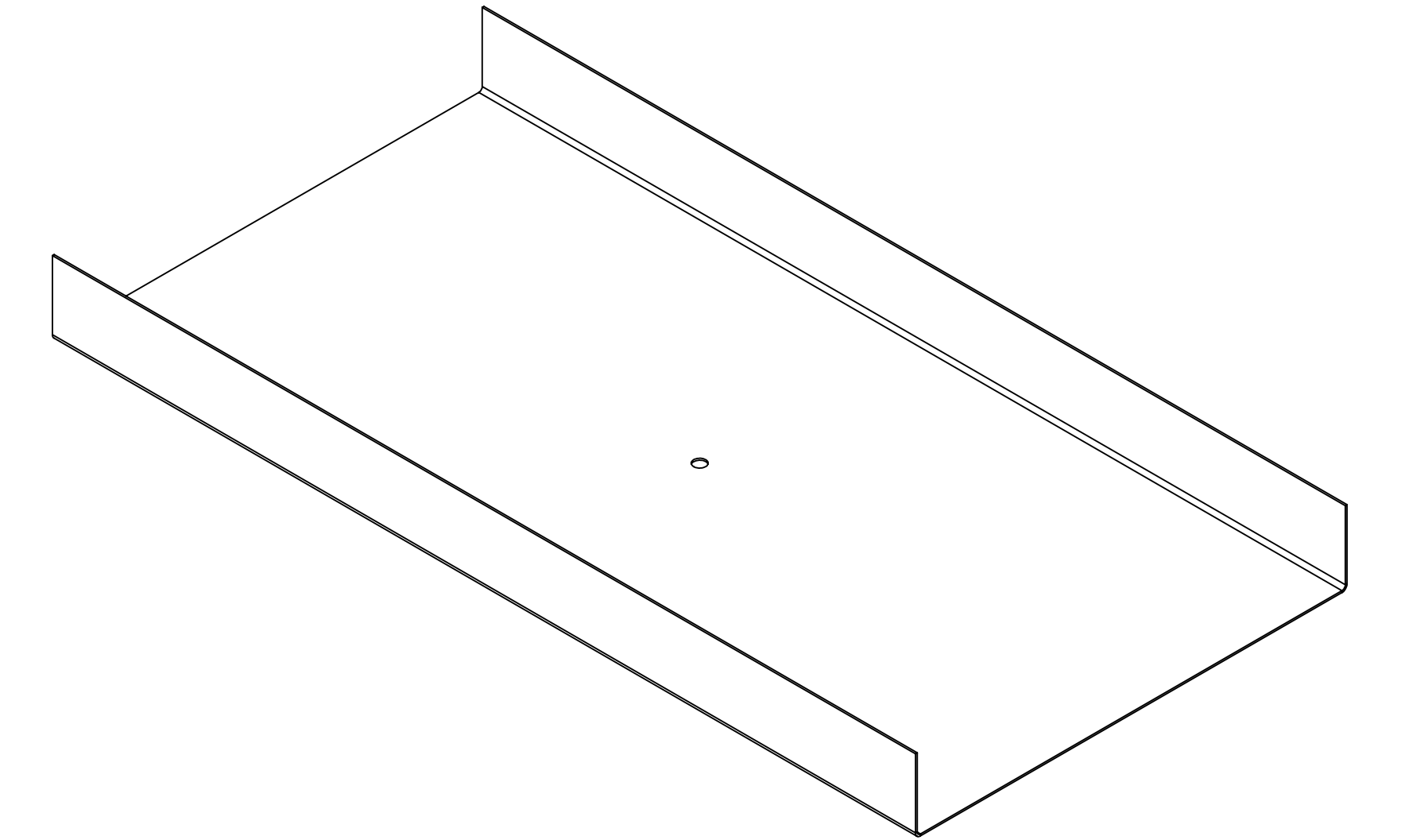
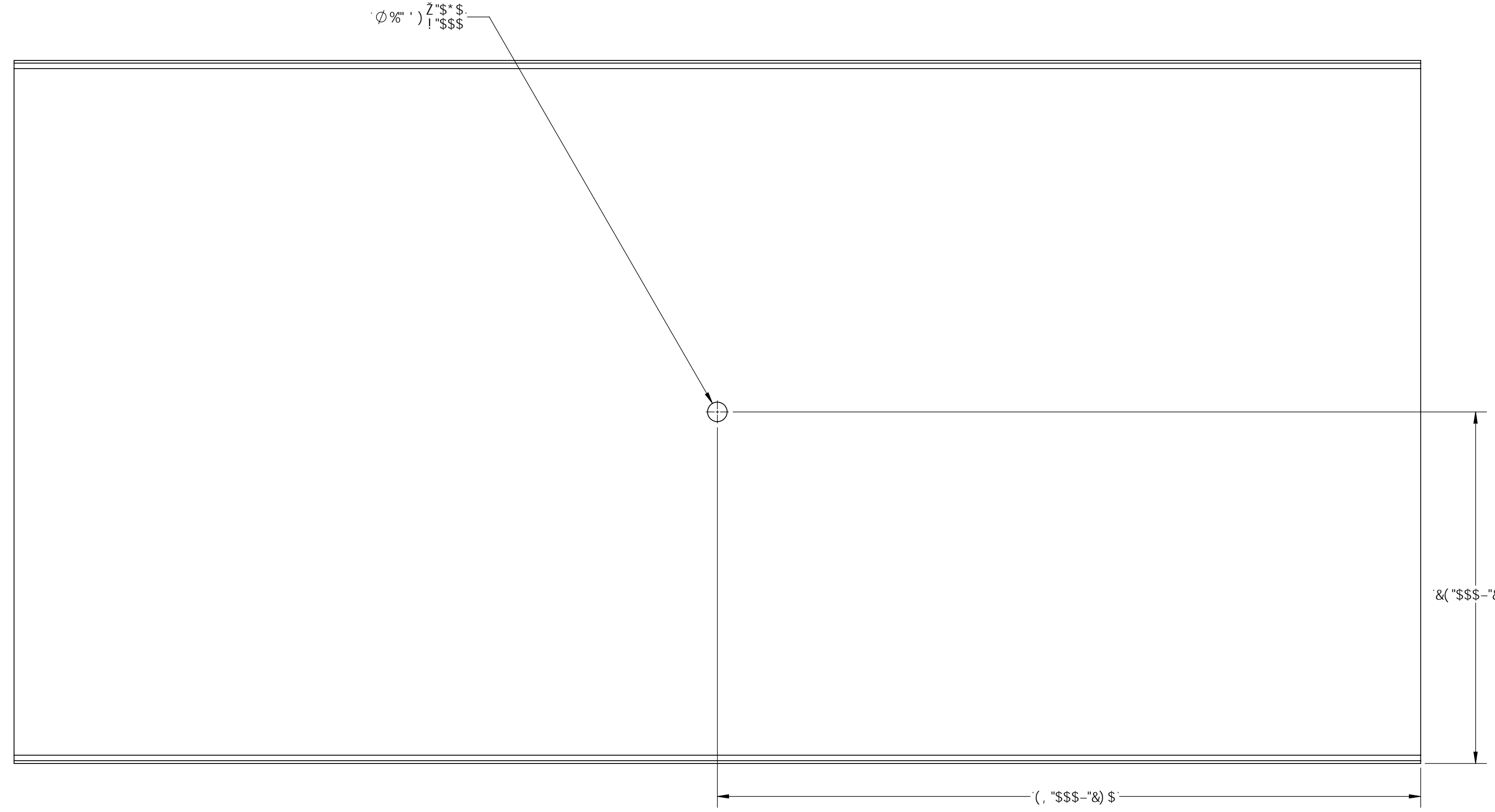


#DA	8F5K -B; 'BC"	89G7 F-DHC B	E HM
%	A C 89@(%	<C B9MK 9@@@C 58'7 9@@f) \$'\$@L	%
&	%@ - , !&\$!\$*D	@ 58'7 9@@D@H9	%
'	-(, -) 5, %	<9LBI H' #, !&('f) F589', D@H98L	%
(-\$\$((5%)+	G<7 G' #, !&('L' %)+ \$'f@5 7? 'CL-89L	%
)	-%&)%5) *\$	G<7 G' #, !&('L' %)+ \$'f@5 7? 'CL-89L	*

GB78E4A68F GB7uE4A68F	@4G8E-47' @4G8E-87		
HA78FF BG: 8EJ -F8 ABG87 F4H9 -47-64G-8A 6BA6E4-E8	-B4G GE84G! GE4-G@BAG G: 8E@	7XfZa`TaW9TLeWTg`ba`FXei`WXf FXei`WX`WX`6baVXcg`ba`Xg`WX`9TLeWTg`ba Y&S% ZBUHj:bU`FYg`URWw 7 ci bWj	
477 7@BAF-BAF -A -46: BF 7@BAF-BAF BA CH68F	9A4: '9A<	@ 58'7 9@@D58'5 GG9A 6@M : I 9@D5B'5 GG9A 6@M %@* - , !75@ F-A 9@HF'5 B8': I 9@D5B	
IK: : : : #F&f IKK: : : #F&f IKKK: : : #F&f 477 9E4GG-BAF ±58%	F4C 6B7B 598	7 C B G H 98% - , !@ 58'7 9@@D58'5 GG9A 6@M %C: #B9% % % 7E4J A! 78FF 4u! >'B9A 9FG FGE8FF " 6BAI 6 86-871 uE-9I 400" 400 >'B9A 9FG 74G8 &+ #5%#&5%	
4A: 1P4E ±1(* / 1P5 9@	7E4J A! 78FF 4u! >'B9A 9FG	@B787 A4@B " AB@B 7B @B7878 %C: #B9% % % 4FF8@57L AB" AD 4FF8@574: B 7E4J -A: AD" AD 78FF -A 98% - , !&\$!\$&	
6BA9BE@F GB*6BA9BE@B 4 4F@B L5!5# P5#F#	F4C 6B7B 598	7 C B G H @B7 64E7 98% - , !&\$!\$&	
5E84> 477 F: 4EC B7: 8F 6 4A9E848E GBHGBF 4EEAGBF 6BHCAAGF 1P5 P1P5#	74G8 &+ #5%#&5%	7 !	

7B ABC F6478 7E4J A
 AS CAP 08FHE8S 7HE 7B 78F F A
 F328E C 477 8E8E E F G 0 28F A 89968
 F < A478E GBHGF BEE8EF 4H 8HE8H 7B 68A88C8A
 E8G8A 477 7E4J A F 08 G 8 78F A 89968
 E88E88E GBH 78F 78F A 4H 8HE8H 7B 68A88C8A

BCHG

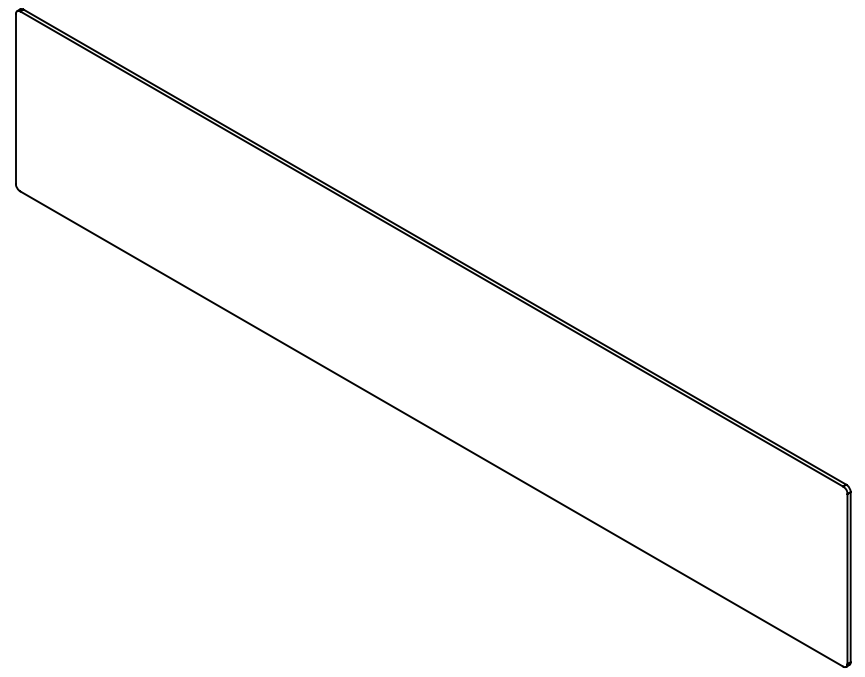


GB78E 4A88F 8B7UE 4A88F HAT8FF BG BEJ 48 ABC87 FAHP A 76468A 68AGE 4E8	5GA 5' G990 ' #8' 1H-2? 840 UE840 0E4 688A0 0' 8E8 BC B9	7XfZa TaW9TLeWTgba Fxei Vxf Fxei Vx Wk 6baVXcgba Xg Wk 9TLeWTgba Y 88% 1BUH8bu FYgUNNA 7 ci bW	NRC-CARC
477 7488AF 8AF 4 A6 8F 7488AF 8AF 8A C88GF IK ... 478F IKKX 478F 477 9E48G8AF 488%	B5H F5@ F4C 487B 7E4J A1 78E F 4A1 78E1 68A88G0 >789A 9FC 7E4J A1 78E F 4A1 >789A 9FC FGE8F 48A1 0 86871 UE 8 400 400 >789A 9FC 74GB 84898888	D5B A 5-B D85H9 : I 9@D5B 5GG9A 6@M 98%- , !7 5@CF A 9H9F 5B8 : I 9@D5B	8

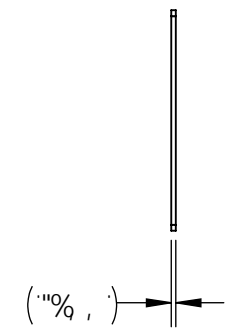
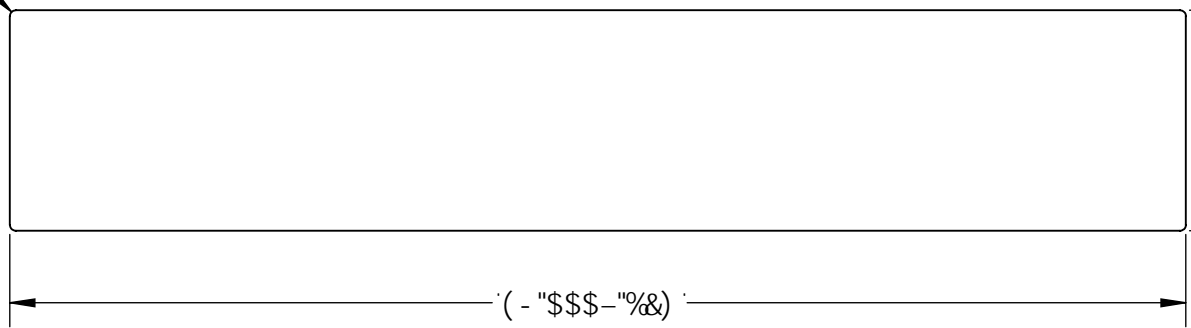
7B ABG F6478 7E4J A:
 A8 C4F @BFHEBE FHE 78 78FF-A
 E8CBEG 4?? 8EEBEF GB G: 8 78F< A B99-68
 F< A478E GBHG8F 8EE8HEF 4H 5HE84H 78 6BA68CG-BA
 E8GHEA 4?? 7E4J A: F GB G: 8 78FF< A B99-68
 E8GBHEA8E GBHF 78F 78FF-AF 4H 5HE84H 78 6BA68CG-BA

F9J GCB < GCFM# < GCFE I 989GFVJ GCBG			
NCB9	F9J"	89G7 F-DHC B	85H9
		6M#D5F	

BCHG



(L F "&) - "%

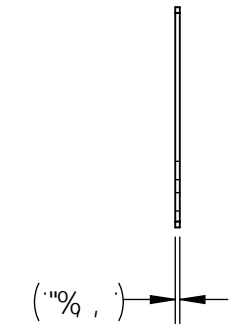
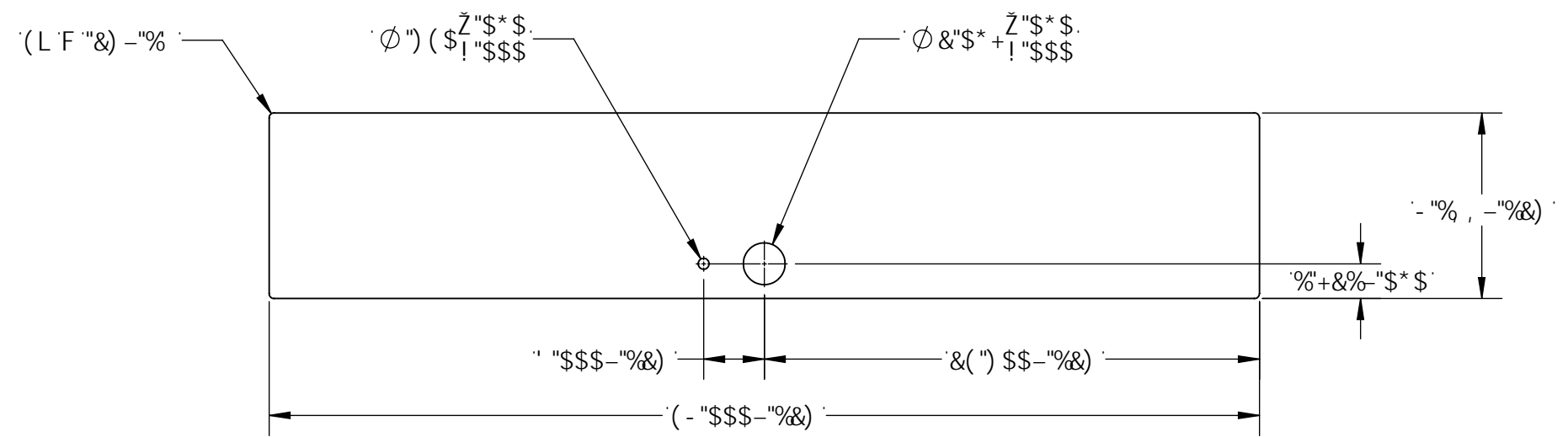
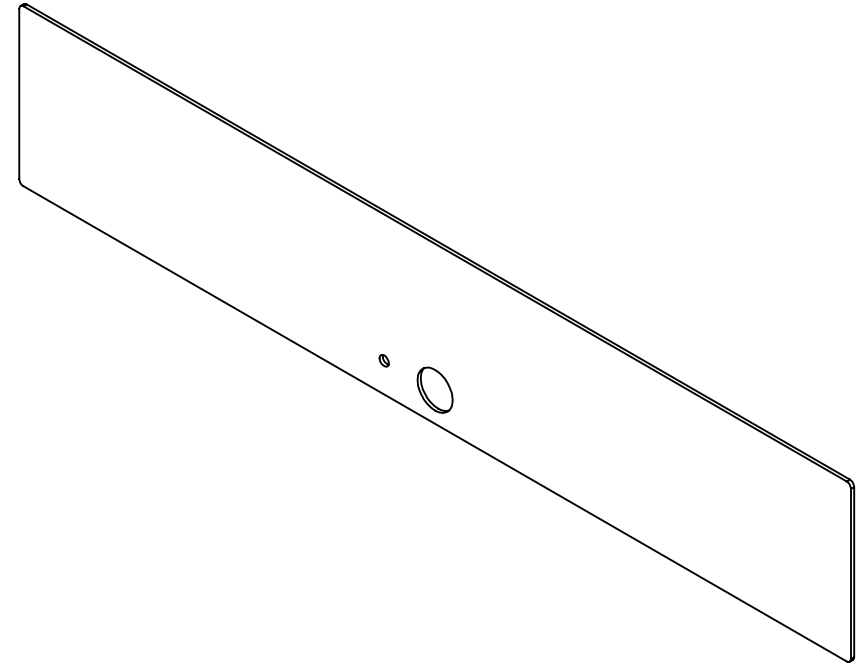


GB?8E4A68F*GB?uE4A68F HA?8FF'BG: 8EJ 48 ABG87 F4H9 A7-64G-BA 6BAGE4-E8 4?? 7@BAF-BAF A A6: 8F 7@BAF-BAF BA C#H68F !K' : : !#&# !KK' : : !#&# !KKK' : : !#&# 4?? 9E46G-BAF ±\$&% 4A: H?4E' : : !(#* !#&# 9@ 6BA9BE@F GB*6BA9BE@8 4 4F@8 L\$!\$# b%## 5E8A> 4?? F: 4EC 87: 8F 6: 4A9E8-A8E GBHG8F 4EEAG8F 6BHC4AGF !#&# b!#%#	@4G8E 4?? @4GuE-8? 5GH A 5' * GH9@ ' #%' "Hk 7? : 84G GE84G! GE4-G@8AG G: 8E@ BC B9 9A4: *9A< B5H F5@ %&) F4C 6B78 5% 78F! *6BA68CG! >"8 9A 9FG 7E4J A! 78FF-Au! >"8 9A 9FG FGE8FF ** 6BA! 6: 86>87! uE-9! 4CC! 4CC! 74G8 &+ #5%#&\$%&	BUHcbU F YgYUWV 7 ci bWj 7UbUXU 7cbgY] bUjcbU XY YWYUWV Yg 7UbUXU 7XfVzA TaW9T UeVTgba FXei WXf FXei WX WX 6baVXcgba Xg WX 9T UeVTgba ¥&\$% žBUHcbU FYgYUWV 7 ci bWj G678 *GGE8 D5 B 9B 8 D@5 H9 : I 9@D5 B 5 GG9A 6@M %* - , ! 7 5 @ C F A 9H9F 5 B 8 : I 9@D5 B @B78? A4@8 " AB@8 78 @B78?8 F: 88G 98H?8 F6478"u6: 8??8 DGL! 7 C B G H %& - , ID5 B 9B 8 D5 B 9@ %C : #8 9% %, % @B7 64E7 4FF8@57L " AB! Ab 4FF8@5?4: 8 7E4J A: Ad! Ab 78FF-A EBI! %& - , !&\$!\$% %& - , !&\$!\$&D 6 !
---	---	---

7B ABG F6478 7E4J A:
 A8 C4F @8FHEBE FHE 78 78FF-A
 E8CBEG 4?? 8EEBEF GB G: 8 78F< A B99-68
 F< A478E GBHG8F 8EE8HEF 4H 5HE84H 78 6BA68CG-BA
 E8GHEA 4?? 7E4J A: F GB G: 8 78FF< A B99-68
 E8GBHEA8E GBHF 78F 78FF-AF 4H 5HE84H 78 6BA68CG-BA

F9J GC B < GC HFM# < GC FE I 9'89GFVJ GC BG			
NC B9	F9J "	89G7 F-DHC B	85H9
			6M#D5F

BC HPG



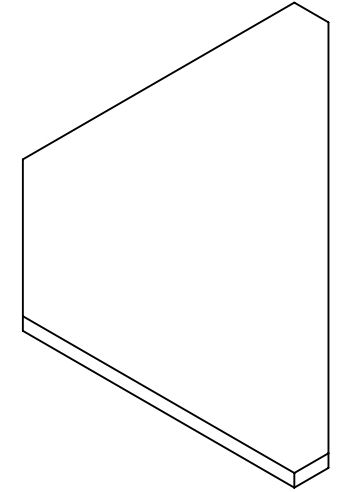
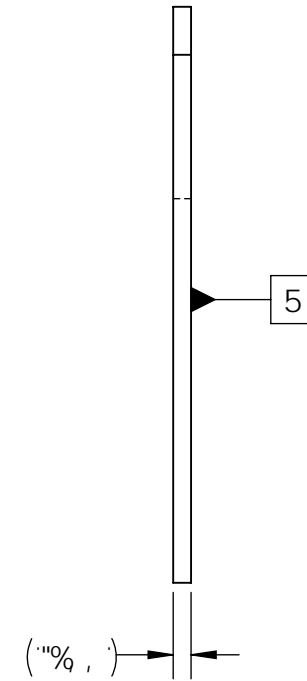
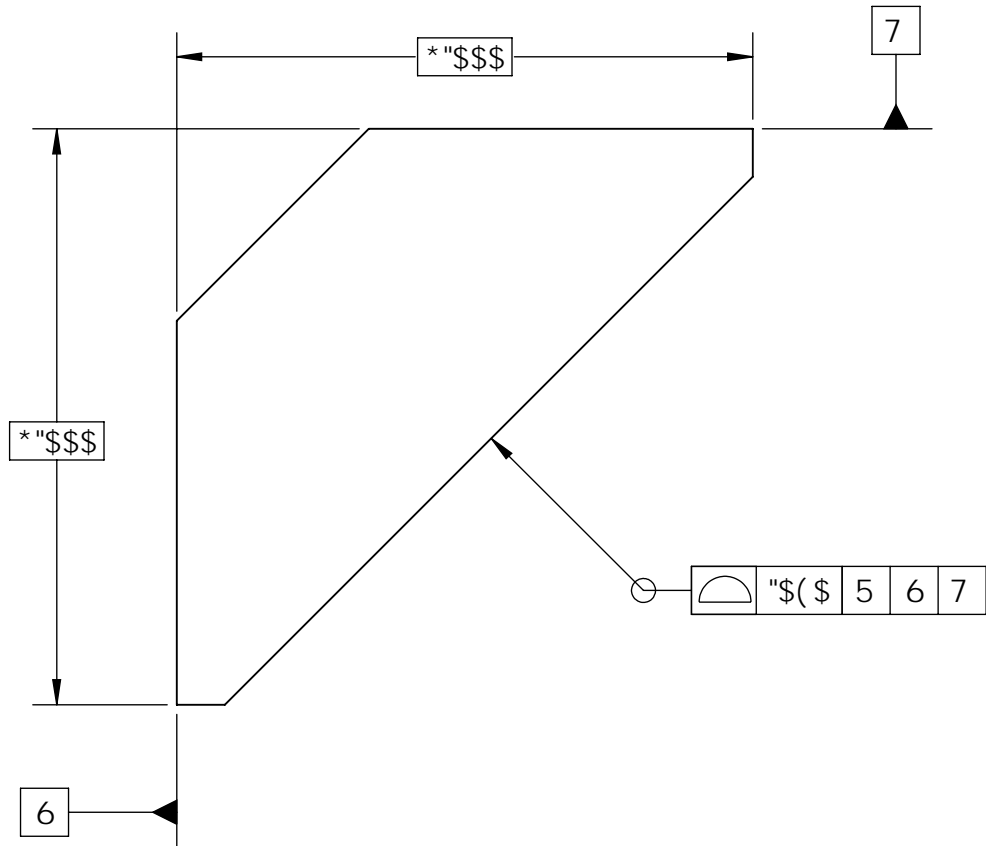
GB78E4A68F*GB?uE4A68F HA?8FF'BG: 8EJ 48 ABG87 F4H9 A7-64G-BA 6BAGE4-E8 4?? 7@BAF-BAF A A6: 8F 7@BAF-BAF BA C#H68F !K : : : !#&# !KK : : : !#&# !KKK : : : !#&# 4?? 9E46G-BAF ±\$&% 4A: H?4E : : !(#* !#&# 9@ 6BA9BE@F GB*6BA9BE@8 4 4F@8 L\$!#&# b%## 5E84> 4?? F: 4EC 87: 8F 6: 4A9E8-A8E GBHG8F 4EEAG8F 6BHC4AGF !#&# b!#%#	@4GBE 4?? @4GuE-8? 5GHA 5' * G#9@ ' #%' "Hk 7? : 84G GE84G! GE4-G@8AG G: 8E@ BC B9 9A4: *9A< B5H F5@ %&/ F4C 6B78 5% 78F! *6BA68CG! >"8 9A 9FG 7E4J A! 78FF-Au! >"8 9A 9FG FGE8FF ** 6BA! 6: 86>87! uE-9! 4CC! 4CC! 74G8 &+ #5%#&\$%	BUHcbU F YgYUWV 7 ci bW 7UbUXU 7cbgY] bUjcbU XY YWYUWV Yg 7UbUXU NRC-CNRC 7XfVzA TaW9TUEVTgba FXei WXf FXei WX WX 6baVXcgba Xg WX 9TUEVTgba ¥ &\$% žBUHcbU FYgYUWV 7 ci bW] G678 * GGE8 D5 B 9B 8 D@5 H9! 8F 5 B : I 9@D5 B 5 GG9A 6@M %* - , ! 7 5 @ C F A 9H9F 5 B 8 : I 9@D5 B @B78? A4@8 " AB@8 78 @B78?8 F: 88G 98H?8 F6478"u6: 8??8 DGL! 7 C B G H %%- , ID5 B 9B 8 D5 B 9@8F 5 B %C: #8 9% %, % @B7 64E 7 4FF8@57L AB! Ab 4FF8@5?4: 8 7E4J A: Ad! Ab 78FF-A EBI! %%- , !&\$!\$% %%- , !&\$!\$% D 6 !
--	---	---

7B ABG F6478 7E4J A:
 A8 C4F @8FHEBE FHE 78 78FF-A
 E8CBEG 4?? 8EEBEF GB G: 8 78F< A B99-68
 F< A478E GBHG8F 8EE8HEF 4H 5HE84H 78 6BA68CG-BA
 E8GHEA 4?? 7E4J A: F GB G: 8 78FF< A B99-68
 E8GBHEA8E GBHF 78F 78FF-AF 4H 5HE84H 78 6BA68CG-BA

F9J GCB < GCFM# < GCFEI 989GFVJ GCBG			
NCB9	F9J"	89G7F DHC B	85H9
			6M#D5F

BCHG

%' &8 758 85H5 G DD@98: CF K 5HF > 9H7I H8B;
 &" 8-A 9BGC BGEI 9F-98: FCA 758 AC 89@5F9 65G-7

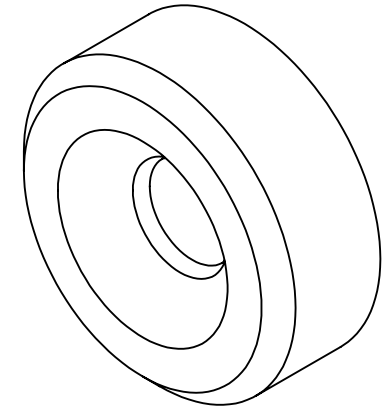
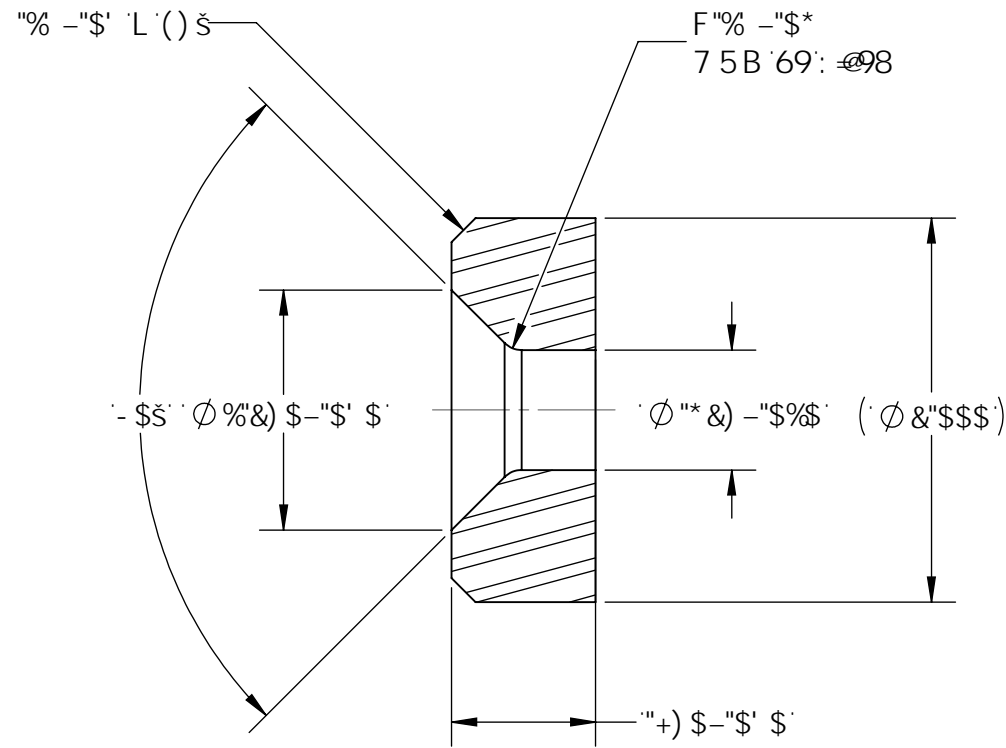
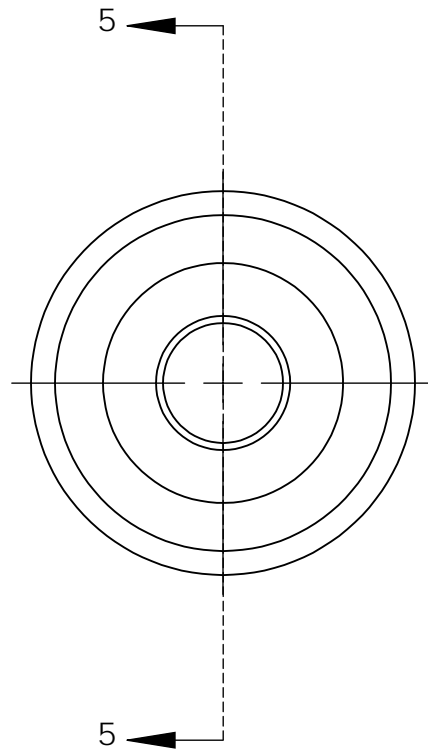


GB78E4A68F*GB?uE4A68F HA?8FF'BG: 8EJ 48 ABG87 F4H9 A7-64G-BA 6BAGE4-E8 4?? 7@BAF-BAF A A6: 8F 7@BAF-BAF BA C#H68F !K ' ' ' !#&# !KK ' ' ' !#&# !KKK ' ' ' !#&# 4?? 9E46G-BAF ±\$&% 4A: H?4E ' ' !(#* !#&# 9@ 6BA9BE@F GB*6BA9BE@8 4 4F@8 L\$!#&# b%## 5E84> 4?? F: 4EC 87: 8F 6: 4A9E8-A8E GBHG8F 4EEAG8F 6BHC4AGF !#&# b!#%#	@4GBE 4?? @4GU E-8? 5GA 5' * G#9@ ' #%' "Hk 7? : 84G GE84G*GE4-G@8AG G: 8E@ BC B9 9A4: *9A< B5H F5@ %&/ F4C 6B78 5% 78F! *6BA68CG! >"8 9A 9FG 7E4J A! 78FF-Au! >"8 9A 9FG FGE8FF ** 6BA! 6: 86>87! uE-9! 4CC! 4CC! >"8 9A 9FG 74GB &+ #5%#&\$%#	BUHcbU F YgYUWV 7 ci bW 7 UbuXU 7cbgY] BUHcbU XY YWYUWV Yg 7 UbuXU NRC-CNRC 7XfVzA TaW9TUEVTgba FXei WXf FXei WX WX 6baVXcgba Xg WX 9TUEVTgba ¥&\$% žBUHcbU FYgYUWV 7 ci bW] G678 *GGE8 >57? ; I GG9H : I 9@D5 B 5 GG9A 6@M %*% -, !75@CFA 9HF 5B8 : I 9@D5 B @B78? A4@8 " AB@8 78 @B78?8 %& -, !>57? ; I GG9H %C: #89% %& @B7 64E7 4FF8@57L " AB! "Ab 4FF8@5?4: 8 7E4J A: Ad! "Ab 78FF-A %& -, !&\$!\$% %& -, !&\$!\$(D 6 !
--	--	---

7B ABG F6478 7E4J A:
 A8 C4F @BFHEBE FHE 78 78FF-A
 E8CBEG 4?? 8EEBEF GB G: 8 78F< A B99-68
 F< A478E GBHG8F 8EE8HEF 4H 5HE84H 78 6BA68CG-BA
 E8GHEA 4?? 7E4J A: F GB G: 8 78FF< A B99-68
 E8GBHEA8E GBHF 78F 78FF-AF 4H 5HE84H 78 6BA68CG-BA

F9J GC B < GC HFM# < GC FE I 989GFVJ GC BG			
NC B9	F9J "	89G7 F DHC B	85H9
			6M#D5F

BC HPG



G97 H€ B 5!5

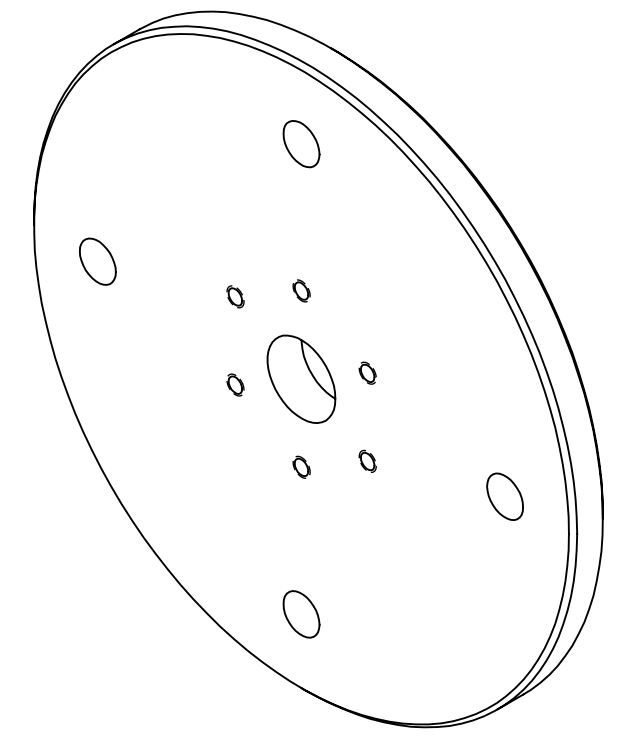
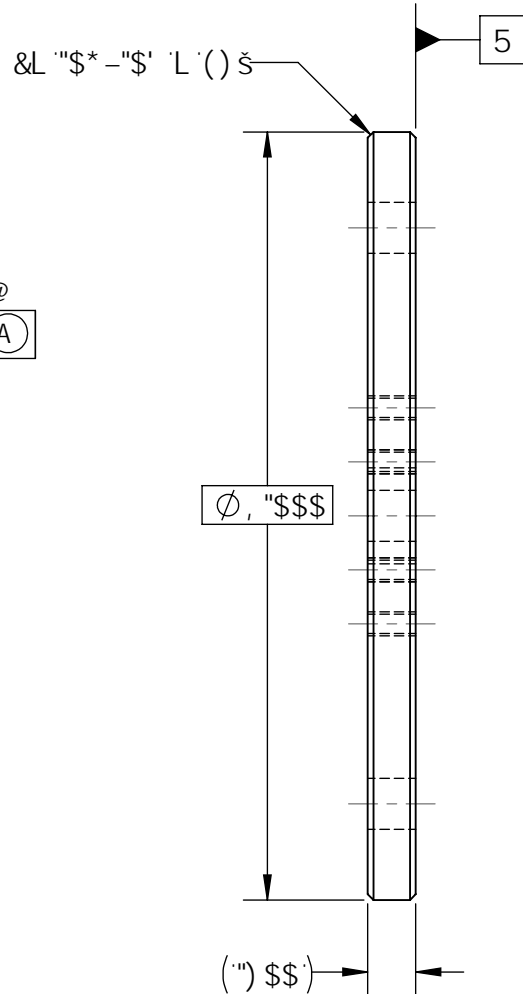
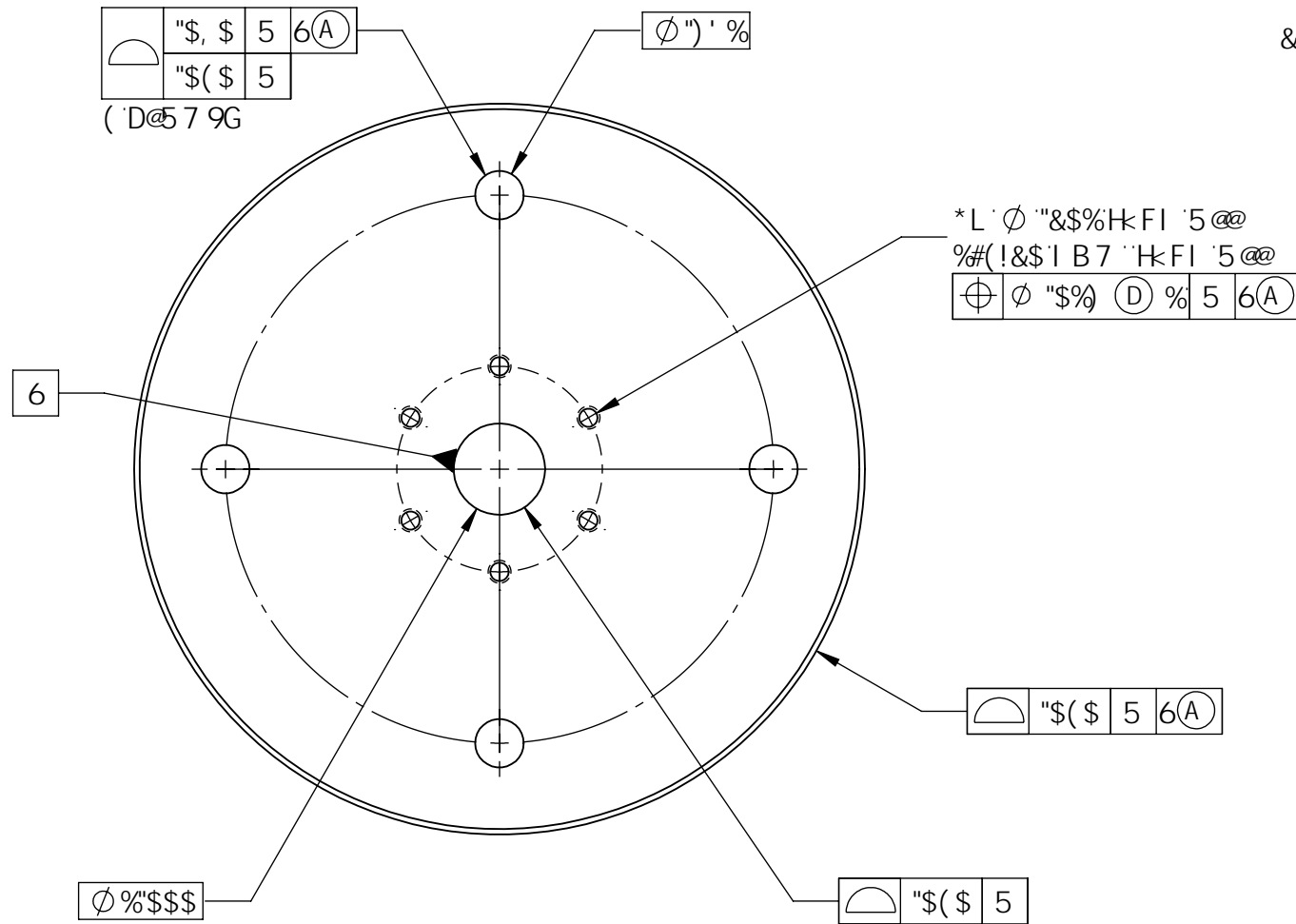
GB?8E4A68F*GB?uE4A68F	@4GBE 4?? @4GuE-8?		
HA?8FF BG: 8EJ 48 ABG87 F4H9 A7-64G-BA 6BAGE4-E8	D@5 B 7 5 F 6 C B G H99@ &"FC I B 8 65 F 84G GE84G GE4-G@8AG G: 8E@ BC B9	7XfZa TaW9TUEVTgba FXei WXf FXei WX WX 6baVXcgba Xg WX 9TUEVTgba ¥ &\$% žBUHcbU FYgUFW 7 ci bWJ G678 GGE8	
4?? 7@BAF-BAF A A6: 8F 7@BAF-BAF BA C#H68F	9A4: *9A< B5H F5@	@ 58 7 9@@@ 7 5HC F D58 : I 9@D5 B 5 GG9A 6@M %* - , ! 7 5 @ F A 9H9F 5 B 8 : I 9@D5 B	
!K : : : !#&# !KK : : : !#&# !KKK : : : !#&# 4?? 9E46G-BAF ±\$&% 4A: H?4E : : ! (#* !#&# 9@	F4C 6B78	78F! *6BA68CG! >"8 9A 9FG 7E4J A! 78FF-Au! >"8 9A 9FG	
6BA9BE@F GB*6BA9BE@8 4 4F@8 L\$!#&# b#&##	FGE8FF ** 6BA!	AFGI 67-8AG	@B78? A4@8 * AB@8 78 @B78?8
5E84 > 4?? F: 4EC 87: 8F 6: 4A9E8-A8E GBHG8F 4EEAG8F 6BHC4AGF !#&# b!#&#	6: 86>87 I uE-9! 4CC! 4CC! 74GB	7 C B G H	F: 88G 98H?8 F6478 u6: 8??8 %C: #8 9% % @B7 64E7 4FF8@57L AB! Ab 4FF8@5?4: 8 7E4J A: Ab! Ab 78FF-A %* - , !&\$!\$% D
	&+ # \$ % & \$ %		6 !

7B ABG F6478 7E4J A:
 A8 C4F @8FHEBE FHE 78 78FF-A
 E8CBEG 4?? 8EEBEF GB G: 8 78F< A B99-68
 F< A478E GBHG8F 8EE8HEF 4H 5HE84H 78 6BA68CG-BA
 E8GHEA 4?? 7E4J A: F GB G: 8 78FF< A B99-68
 E8GBHEA8E GBHF 78F 78FF-AF 4H 5HE84H 78 6BA68CG-BA

BC1HG

%! &8 7 58 85H5 G DD@98 : CF K 5HF > 9H7I H1B;
 &" 8-A 9BGCBGEI 9F-98 : FCA 758 AC89@5F965G7

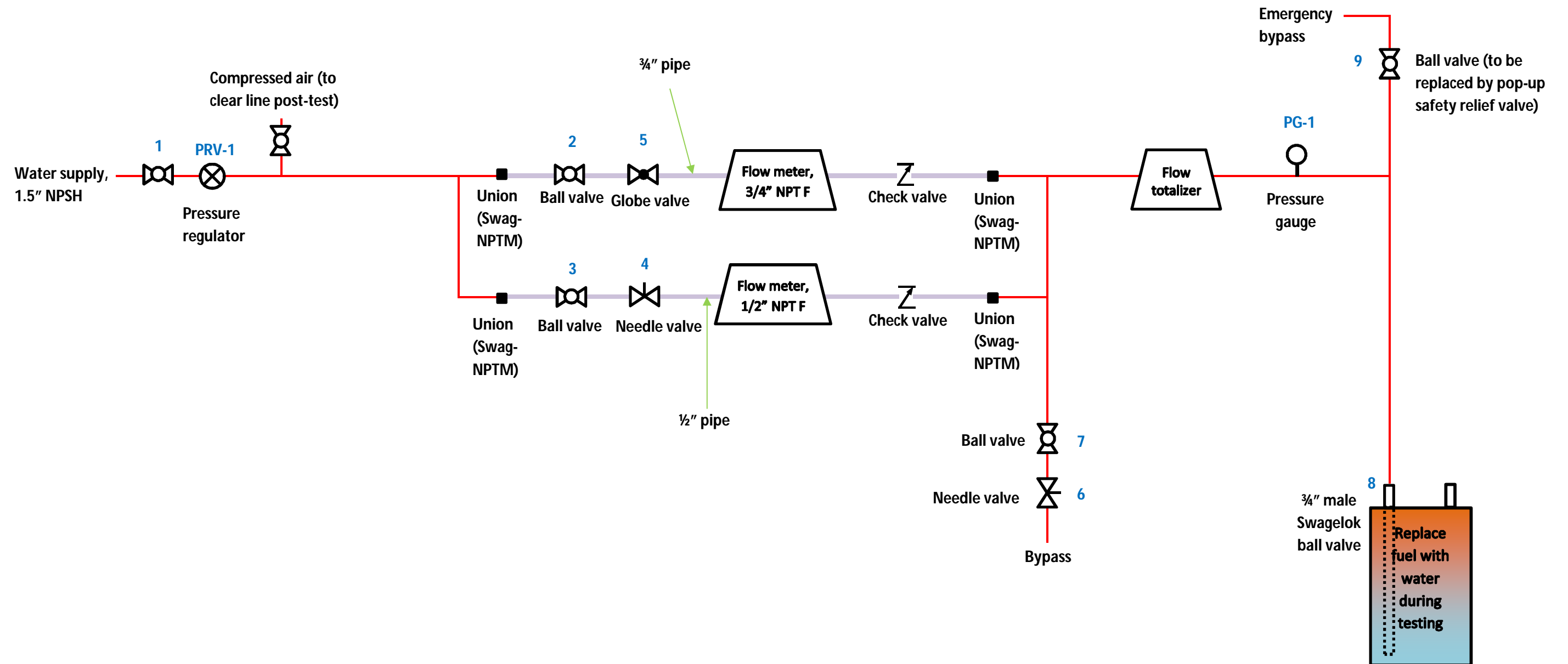
F9J GC B < GC HFM# < GC F E I 9 89GFVJ GC BG	
NC B9	F9J "
89G7 F DHC B	
85H9	6M#D5F



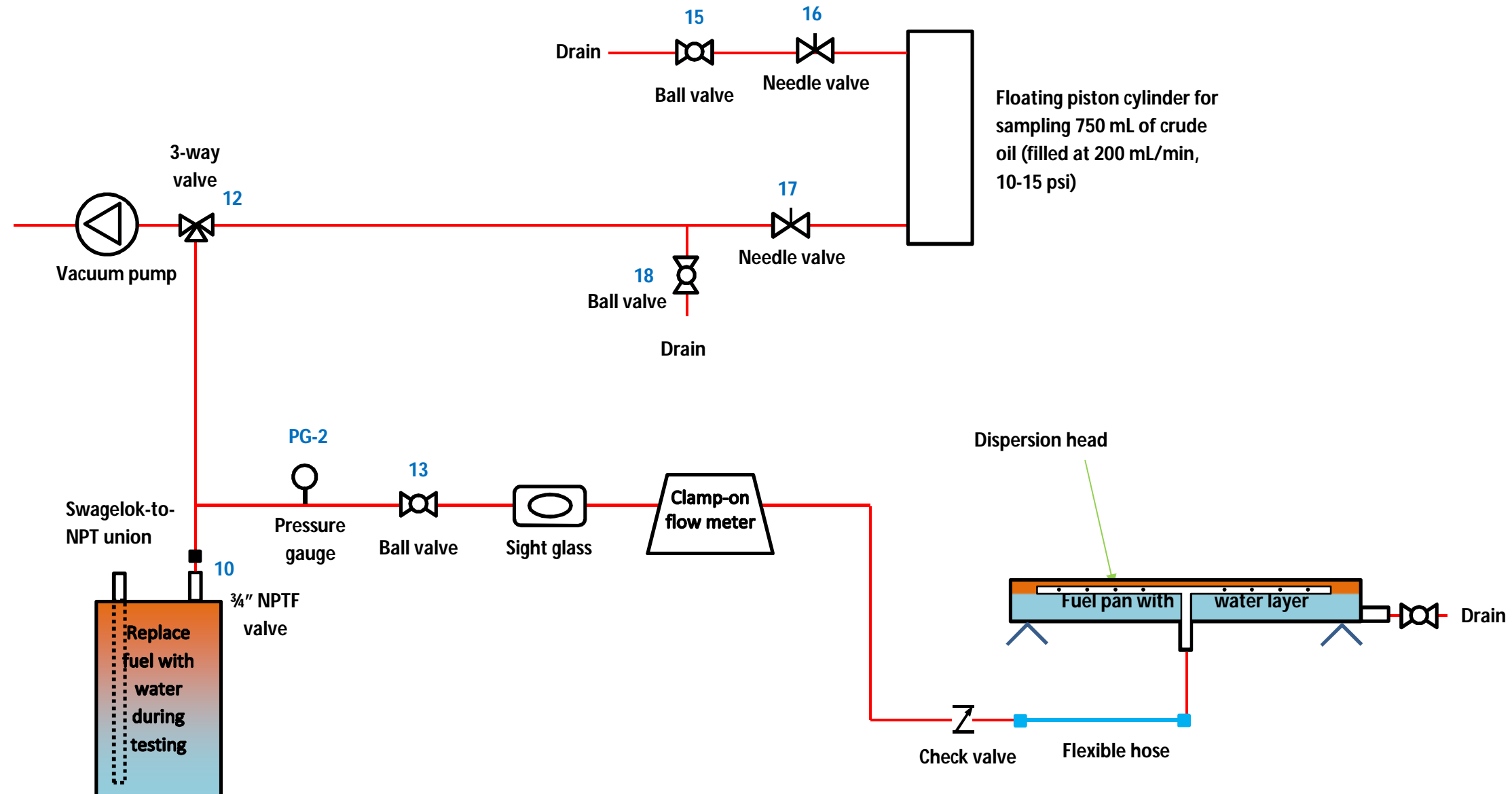
<p>GB78E4A68F GB?uE4A68F HA?8FF BG: 8EJ 48 ABG87 F4H9 A7-64G-BA 6BAGE4-E8 4?? 7@BAF-BAF A A6: 8F 7@BAF-BAF BA C#H68F !K' : : !#&# !KK : : !#&# !KKK : : !#&# 4?? 9E46G-BAF ±\$&% 4A: H?4E : : !(#* !#&# 9@ 6BA9BE@F GB*6BA9BE@8 4 4F@8 L\$!#&# b%## 5E84> 4?? F: 4EC 87: 8F 6: 4A9E8-A8E GBHG8F 4EEAG8F 6BHC4AGF !#&# b!#%#</p>	<p>@4GBE 4?? @4GU E-8? 5GA 5' * GH9@ %& "Hk 7? : 84G GE84G GE4-G@8AG G: 8E@ BC B9 9A4: *9A< B5H F5@ %&/ F4C 6B78 5% 78F! *6BA68CG! >"8 9A 9FG 7E4J A! 78FF-Au! >"8 9A 9FG FGE8FF ** 6BA! 6: 86>87 I uE-9! 4CC! 4CC! 74GB &+#\$%#&\$%</p>	<p>BUHcbU F YgYUWV 7 ci bW 7 UbuXU 7cbgY] bUHcbU XY YWYUWV Yg 7 UbuXU NRC-CNRC 7XfVa TaW9T UeVTgba FXei WXf FXei WX WX 6baVXcgba Xg WX 9T UeVTgba ¥ &\$% žBUHcbU FYgYUWV 7 ci bW] G678 * GGE8 @C 58 7 9@D@5 H9 : I 9@D5 B 5 GG9A 6@M %&* -, !75 @C F A 9H9F 5 B 8 : I 9@D5 B @B78? A4@8 * AB@8 78 @B78?8 F: 88G 98H?8 F6478 u6: 8??8 DGL! 7 C B G H %& -, !@C 58 7 9@D@5 H9 %C: #8 9% %& (@B7 64E7 4FF8@57L AB! AB 4FF8@5?4: 8 7E4J A: AB! AB 78FF-A EBI! %& -, !&\$! \$% %& -, !&\$! \$% D 6 !</p>
---	---	--

Supplement B – Crude Oil Feed System

Water Side



Fuel Side



Operational Safe Work Procedure - Crude Oil Delivery System

Step 1 of 3 - Instruction on how to drain hot water from the system

1. Check that all valves are closed
2. Start water
 - a. Start fire pump
 - b. Open main water supply valve on the building side
3. Open Valve "1"
4. Open Valve "2"
5. Fully open bypass Valve "7"
6. Open Valve "9"
7. Slowly open Valve "5" and adjust to 25 L/ min
8. Open Valve "3"
9. Slowly open Valve "4" and adjust to 4 L / min
10. Close Valve "9"
11. Close Valve "3"
12. Read pressure gauge 1 and adjust inlet pressure regulator **PRV -1** to achieve prescribed pressure.
 - a. Diesel / Heptane max pressure 15 PSI
 - b. Crude Oil max pressure 35 PSI

Operational Safe Work Procedure - Crude Oil Delivery System

Step 2 of 3 - Instruction on how to take Oil Samples

1. Close Valve **"9"**
2. Use Valve **"6"** to adjust **PG-1** pressure to 12 PSI
3. Open Valve **"8"** (Drum Inlet) and Valve **"17"**
4. Turn **ON** Vacuum pump
5. Toggle Valve **"12"** Until – 30 inches of Hg
 - a. Once completed leave the Valve **"12"** pointing towards the sample vessel.
6. Close Valve **"17"**
7. Turn **OFF** the Vacuum pump

8. Open Valve **"10"** (Drum outlet)
9. Open Valve **"18"**
10. Drain approximately 250 ml of Oil
11. Close Valve **"18"**

12. Open Valve **"17"**
13. Open Valve **"15"**
14. Slowly open Valve **"16"**
15. Collect 750 ml of water

16. Close Valve **"17"**
17. Close Valve **"16"**
18. Close Valve **"15"**
19. Close Valve **"12"** and point it to PG-2

Operational Safe Work Procedure - Crude Oil Delivery System

Step 3 of 3 – Start of the Experiment

1. Close Valve **"15"**, Open Valve **"8"** and Valve **"10"**
2. Open Valve **"13"**
3. Close Valve **"7"**
 - a. Adjust totalizer to 0
4. Open Valve **"5"** and adjust to 15 L / min
5. Request IGNITION ; Confirm Ignition
6. Fill the pan to 50 L
7. Close Valve **"2"** and " Valve **"5"**
8. Use Valve **"4"** to adjust flow on OMEGA to 6 L / min
9. If flow greater than 8 L / min
 - a. Open Valve **"2"**
 - b. Slowly Adjust Valve **"5"**

Emergency Shut Down Procedure

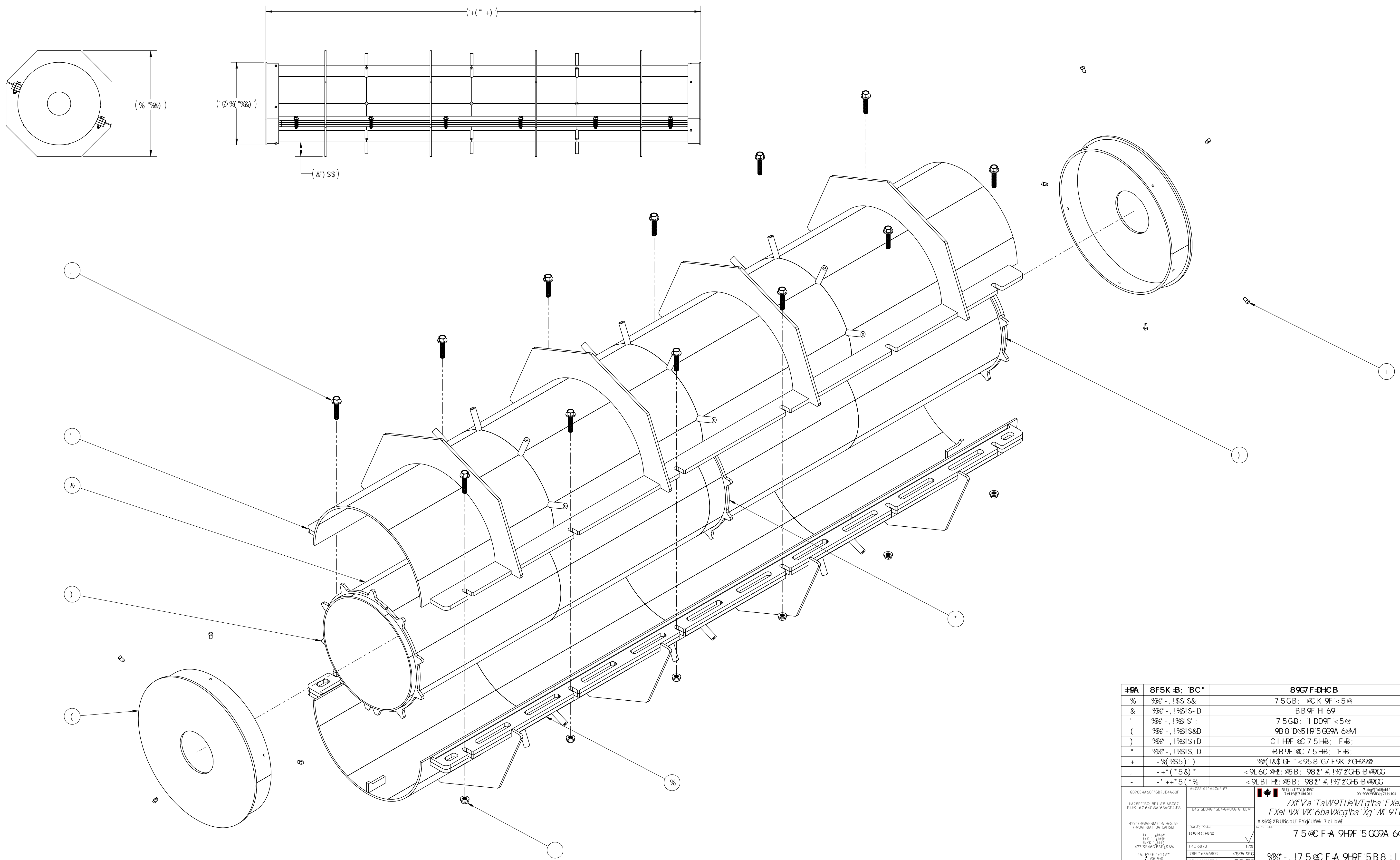
1. Close Valve **"1"**
2. Close Valve **"8"**
3. Close Valve **"10"**

Supplement C – Calorimeter Engineering Drawings

7B ABC F6478 7E41 A
 AB CAP 089888 HE 78 78F F A
 F328EC 477 8E28EF 6B C 8 78F F A 89948
 F: A478E GBH88F 8E28EF 4H 8E84H 78 68A88C8A
 E8G8A 477 7E41 A F 6B C 8 78F F A 89948
 E8G8A8E GBH 78F 78F F A 4H 8E84H 78 68A88C8A

BCHG

% D5-BHC1 HF G F: 57 9GC: H-95G9A 6@B 75@CF-A 9HF K H: HBA D@
 DMCA 5F? & \$\$ fl 6H6@7?L D5-BH 895-@B D5-BH-BGFI 7 HCBG5F9
 :C1 B8-B H-9G DD@B D8: 8C 71 A 9BHFD?& \$\$: 6@SISHBGdXz



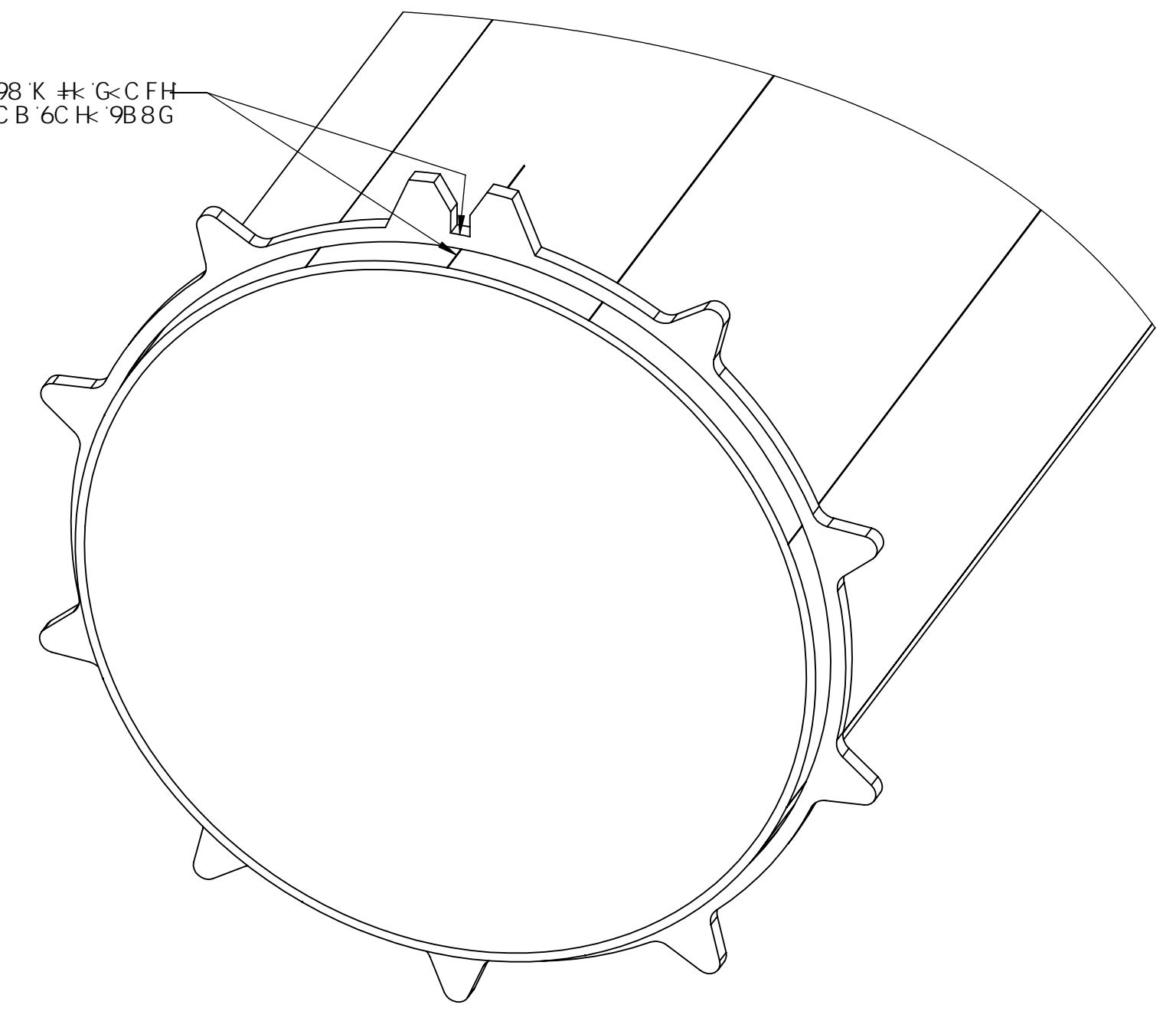
#DA	8F5K-B: BC"	89G7 F-DHCB	E HM
%	988 - , !\$\$!S:&	7 5GB: @C K 9F <5@	%
&	988 - , !\$\$!S: D	BB9F H 69	%
'	988 - , !\$\$!S' :	7 5GB: 1 DD9F <5@	%
(988 - , !\$\$!S&D	9B8 D@5H 5G9A 6@M	&
)	988 - , !\$\$!S+D	C1 HF @C 7 5HB: F B:	&
*	988 - , !\$\$!S, D	BB9F @C 7 5HB: F B:	%
+	-(%&5)'	%!(1&5 CE " <95.8 G7 F9K ZGH9@	%\$
,	-+*(5&)*	<9L6C @#: @B: 98Z' # 1% ZGH5 B @XG	%&
-	-'+*5(*%*	<9L6C @#: @B: 98Z' # 1% ZGH5 B @XG	%&

GB78E 4A68F GB7UE 4A68F H478FF BG BEJ F8 ABG87 F4HP A746G8A 68AGE 4E8	84C UE840" CE 4 K88AV 0: BEH 99BC HP % 99BC HP % 78F1 68A88C8D >789A 9FC 7E4J A1 78F F A 1 >789A 9FC FGE8F1 " @BA1 0: B8-B71 UE-8 400" 400 >789A 9FC 74GB 󪕲"	7Xf Za TaW9TLe WTgba Fxei Wxf Fxei WX WX 6baVXcgba Xg WX 9TLe WTgba Y 88% 1BUHebu FYgUNNA 7 ci bW 7 5 @CF A 9HF 5G9A 6@M 988 - , !7 5 @CF A 9HF 5B8 : 1 9@D5B	MIC-CIRC 8
---	---	---	----------------------

7B ABC F6478 7E4J A
 AB CAF 88F8E8 7HE 7B 78F F A
 F028E C 477 8E8E F 8B C 8 78F F A 89948
 F 4 A478E 88F8E8 8E8E8E F 4H 8E8AH 7B 68A88C8A
 E8G8A 477 7E4J A F 8B C 8 78F F A 89948
 E8G8A8E 88F 78F 78F A F 4H 8E8AH 7B 68A88C8A

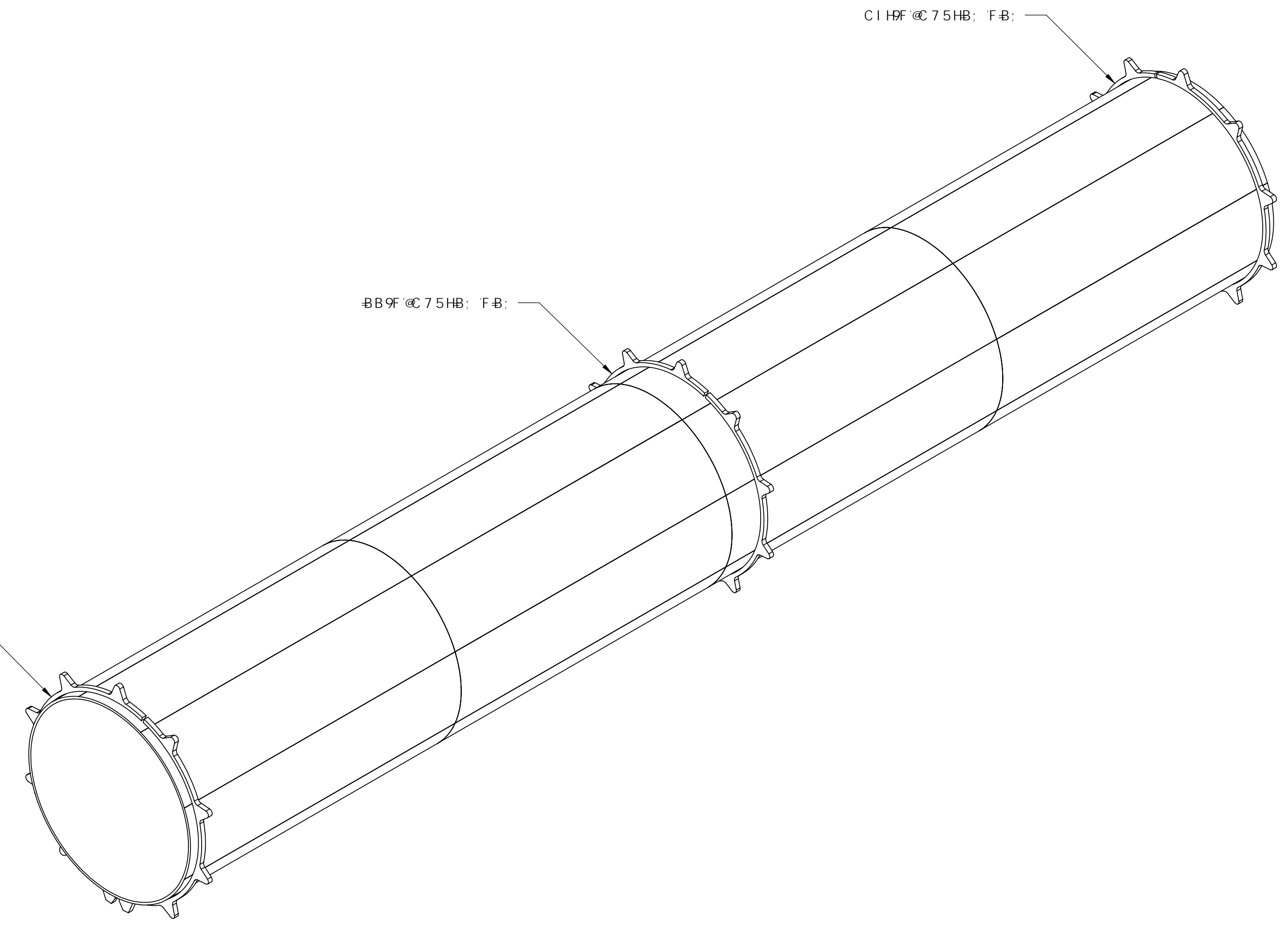
BCHG

:95H F95@: B98 K H: G:CFH
 G7 F 698 @B9CB 6CH: 9B8G



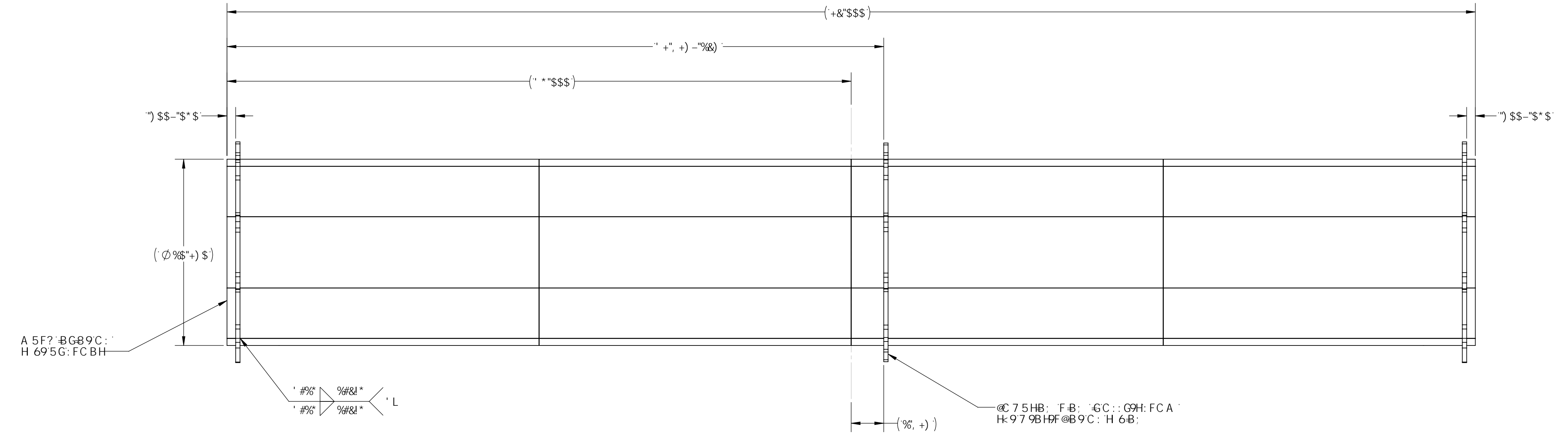
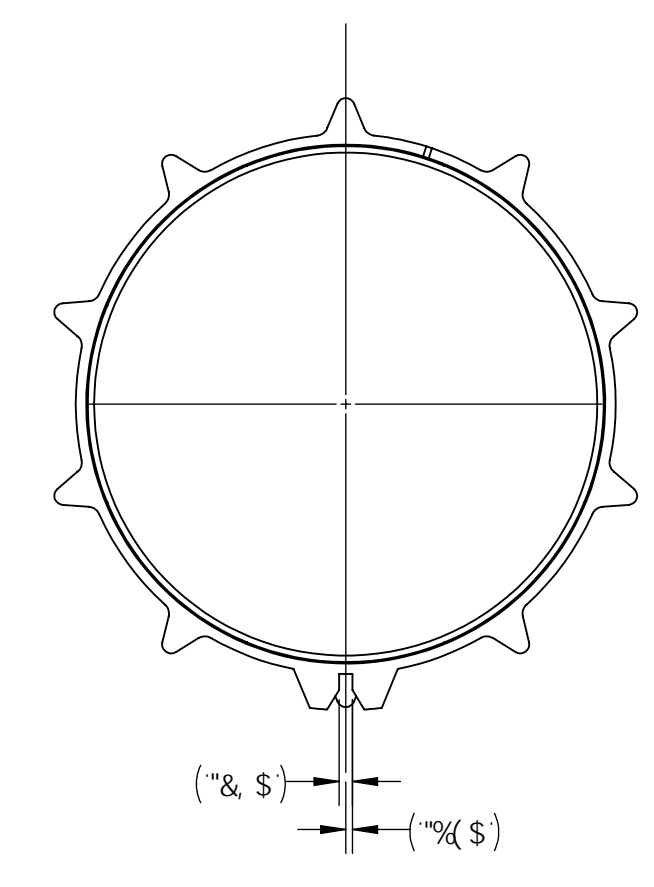
D5FH5@6CHCA J 9K C: @75HB; F-B; 5@ BA 9BH

C1HF @75HB; F-B;



BB9F @75HB; F-B;

C1HF @75HB; F-B;



A 5F? BG89C:
 H 695G: FCBH

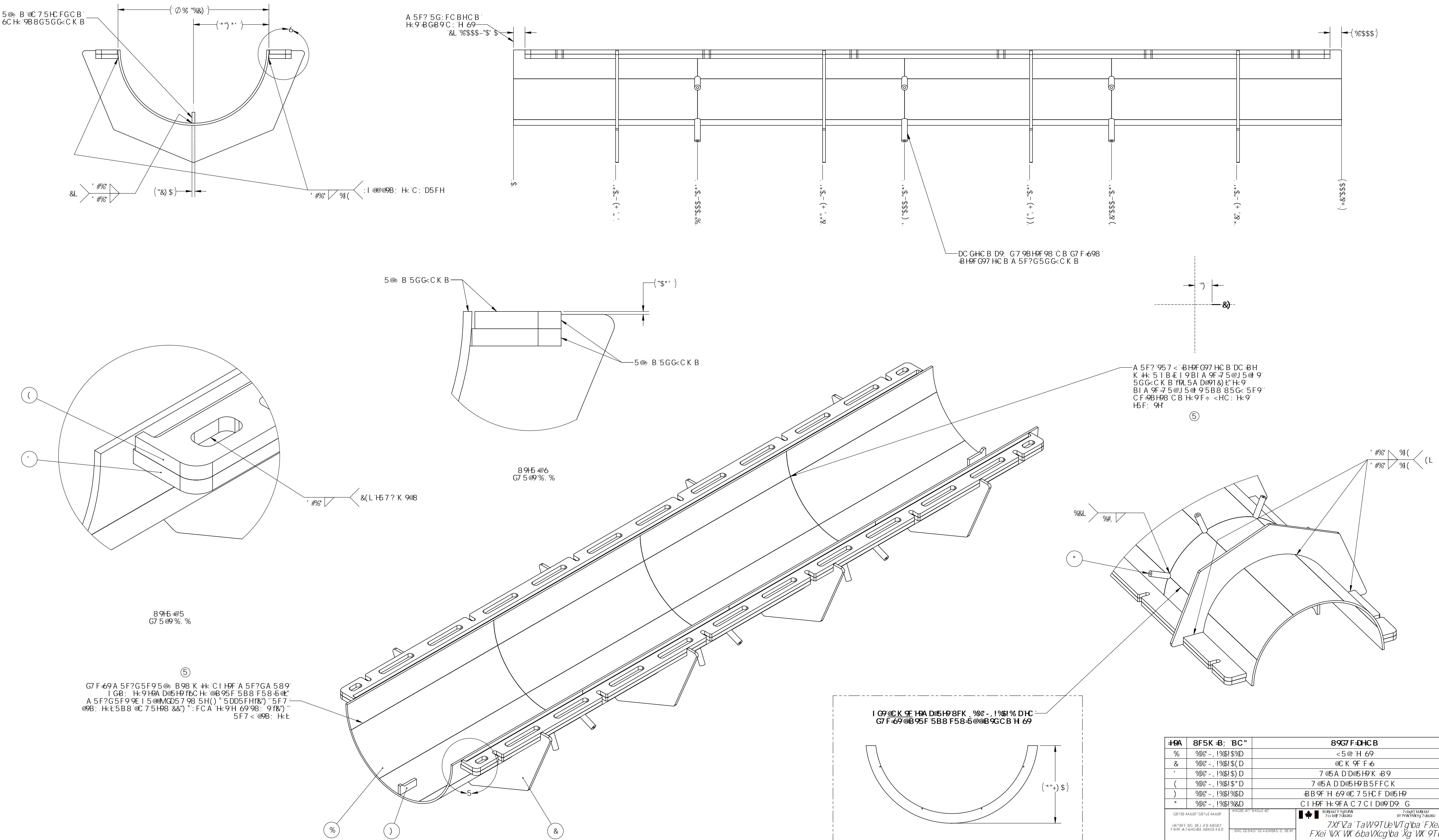
@75HB; F-B; GC:: C9H: FCA
 H: 97 9BHDF @B9C: H 6B;

<p>7XfZa TaW9TLe WTg'ba F'XeI WXf F'XeI WX WX' 6ba WXg'ba Xg WX' 9TLe WTg'ba Y 88% 1BUH8bu FYg UNN 7 ci bW</p>	
<p>7 5 @ C F A 9 H F 5 G 9 A 6 @ M</p>	
<p>F4C 6B7B</p>	<p>598</p>
<p>7CBGH</p>	<p>8</p>

7B ABC F6478 7E41 A
 AB CAP 987654 3HE 7B 789 F A
 F328E C 477 8E2EF GB C 8 789 F A 899 69
 F: A478E GB48F 8E28EF 4H 5HEBAH 7B 68A68C8A
 E89EA 477 7E41 A F GB C 8 789 F A 899 69
 E89EA477 7E41 A F GB C 8 789 F A 899 69

F0J 6GB < 0CFHMF < QCF E I 989FVJ 6C8G			
NC B9	F0J	89G7 F DHC B	85H9
7-298	5	58898 G7F 69A 5F7G5B8 BIA 69F B: CB H: 9 BB9F G F 579C: H: 9 < 5 @ H 69	% #58859%
			6M05F
			>58

BCHG



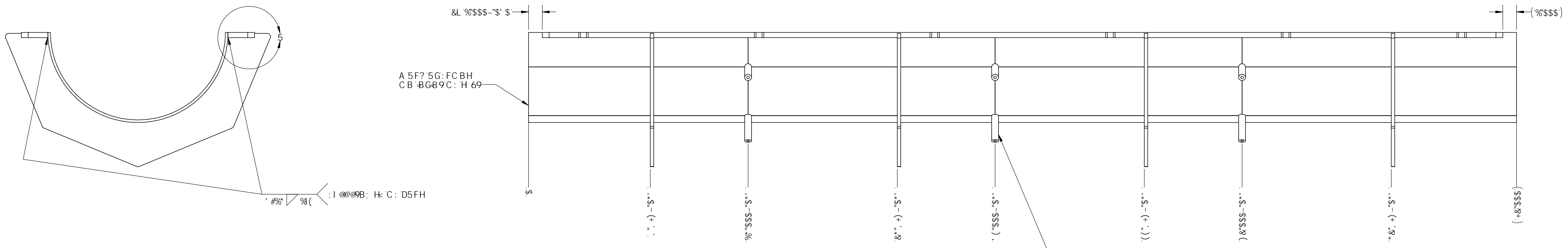
#DA	8FK B: BC"	89G7 F-DHC B	E HM
%	%8 - , 1%\$!\$D	<5 @ H 69	%
&	%8 - , 1%\$!(D	@K 9F F 6	(
*	%8 - , 1%\$!\$D	7 @A DD@H9K @9	&
(%8 - , 1%\$!\$D	7 @A DD@H9 B5FFCK	&
)	%8 - , 1%\$!\$D	BB9F H 69 @ 7 5HC F D@HP	&
*	%8 - , 1%\$!\$D	C I HF H: 9FA C 7 C I D @ D9. G	%&

7Xf Za TaW9TLe WTgba Fxei Vxf Fxei WX WX 6baVXgva Xg WX 9TLe WTgba Y 88% 1BUHbu TYgUNW 7 ci bW		75GB: @K 9F < 5 @ 75 @ FA 9HF 5B8: 1 9 @ D5B %8 - , 175 @ FA 9HF 5B8: 1 9 @ D5B	
75GB: @K 9F < 5 @ 75 @ FA 9HF 5B8: 1 9 @ D5B %8 - , 175 @ FA 9HF 5B8: 1 9 @ D5B		8	

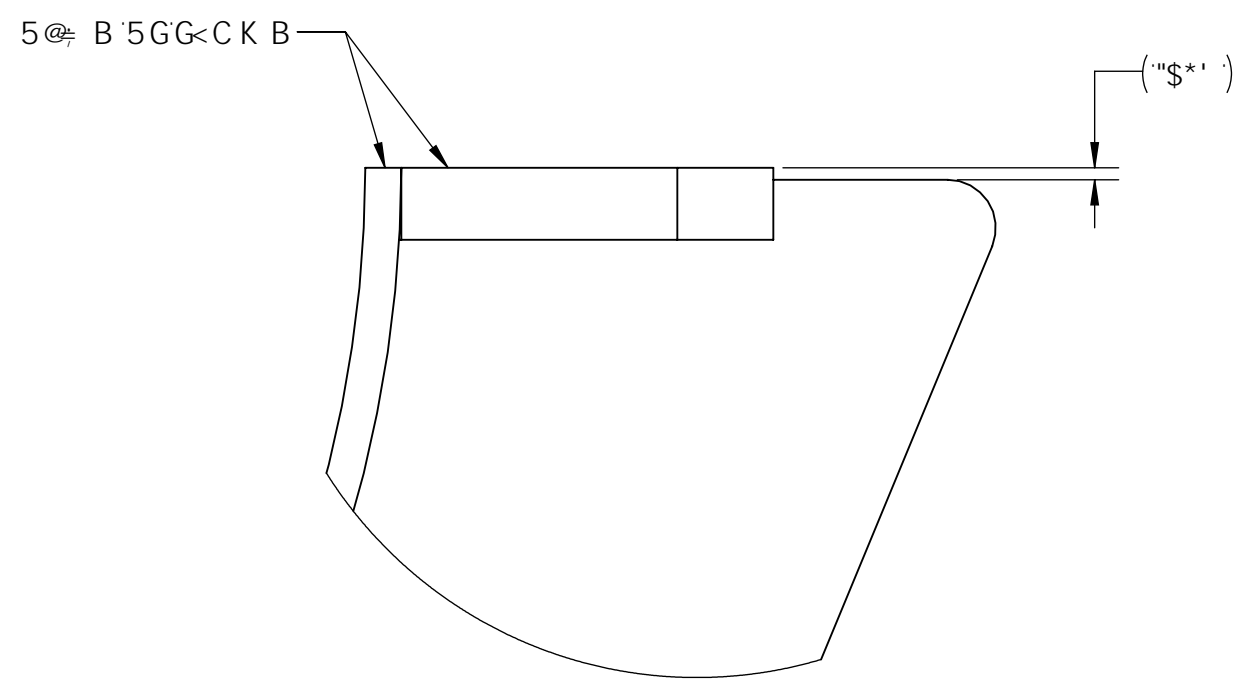
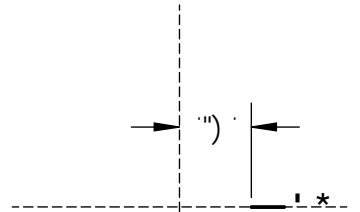
7B ABC F6478 7E4J A
 AB CAF H8H888 FHE 7B 78F F A
 F328E C 477 8E8E8 F8 C 8 78F F A 89968
 F: A478E GBH88F 8E88E8F 4H 8E88H 7B 68A88C8A
 E8G8A 477 7E4J A F 8B C 8 78F F A 89968
 E8G8A8E GBH 78F 78F A F 4H 8E88H 7B 68A88C8A

F0J 6GB < 6C FHM# < 6C F E I 989GFVJ 6C BG		89G7 F DHC B		B5H9		6M05F	
NC B9	F9J	5	58898 G7 F 69 A 5F7G5B8 B I A 69F B C B H: 9 BB9F G F: 579C: H: 9 < 5 @ H 69	% #58898			> 58

BCHG

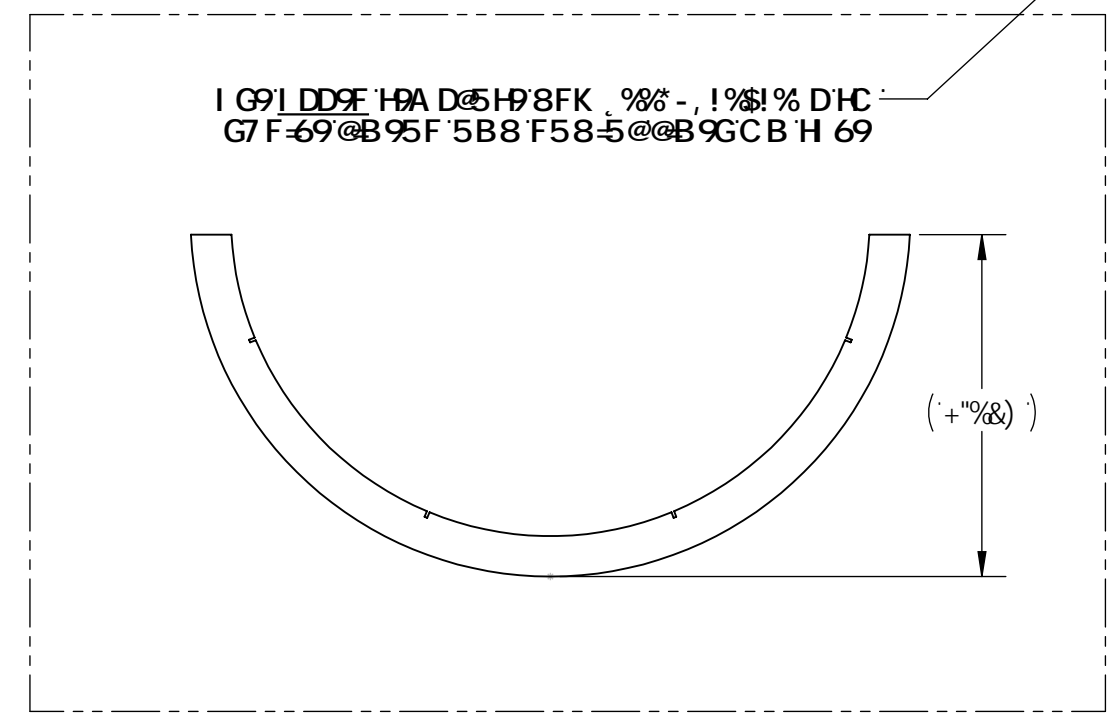


DC GHC B D9 G 7 9B H8F 98 C B G 7 F 698
 B H8F G97 HC B A 5F? G5GG<CK B



A 5F? 957 < B H8F G97 HC B DC B H
 K # 5 1 B E I 9 B I A 9 F 7 5 @ J 5 @ 9
 5 G G < C K B I 9 L 5 A D @ 7 1 1 H 9
 B I A 9 F 7 5 @ J 5 @ 9 5 B 8 8 5 G < 5 F 9
 C F 9 B I 9 8 C B H 9 F < < H C: H 9
 H 5 F: 9 H

G7 F 69 A 5 F? G5 F9 5 @ B 98 K # C I H F A 5 F? G A 5 8 9
 I GB: H: 9 H A D @ H F 6 C H: @ B 9 5 F 5 B 8 F 5 8 5 @
 A 5 F? G 5 F 9 9 E I 5 @ M G 5 7 9 8 5 H () 5 D D 5 F H 8) 5 F 7
 @ B: H: L 5 B 8 @ 7 5 H 8 &) : F C A H: 9 H 6 9 9 8: 9 F 8)
 5 F 7 < @ B: H: L



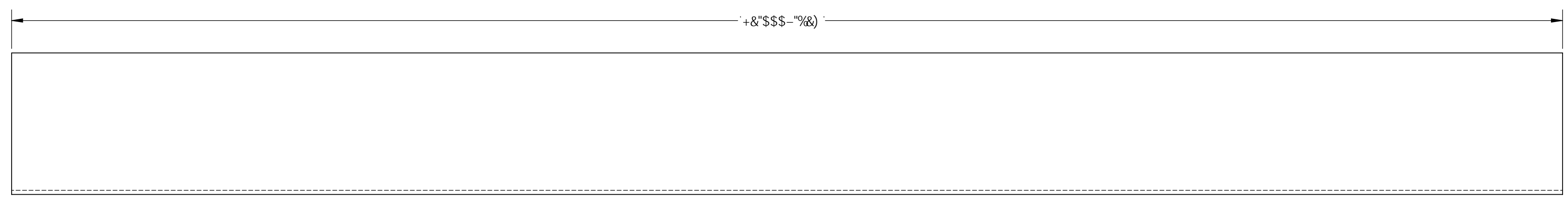
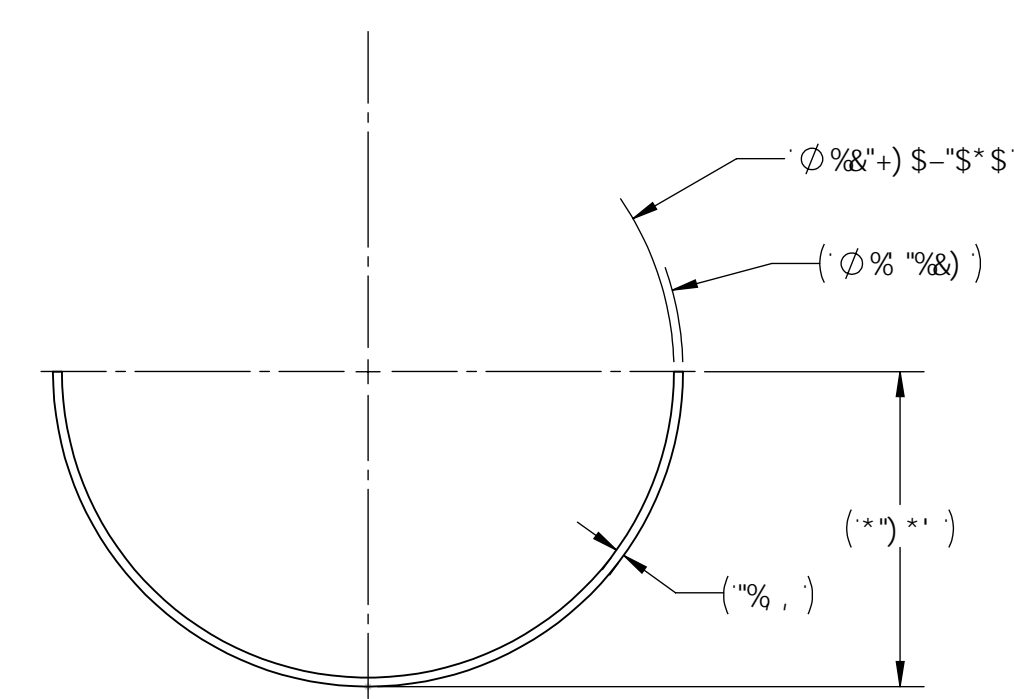
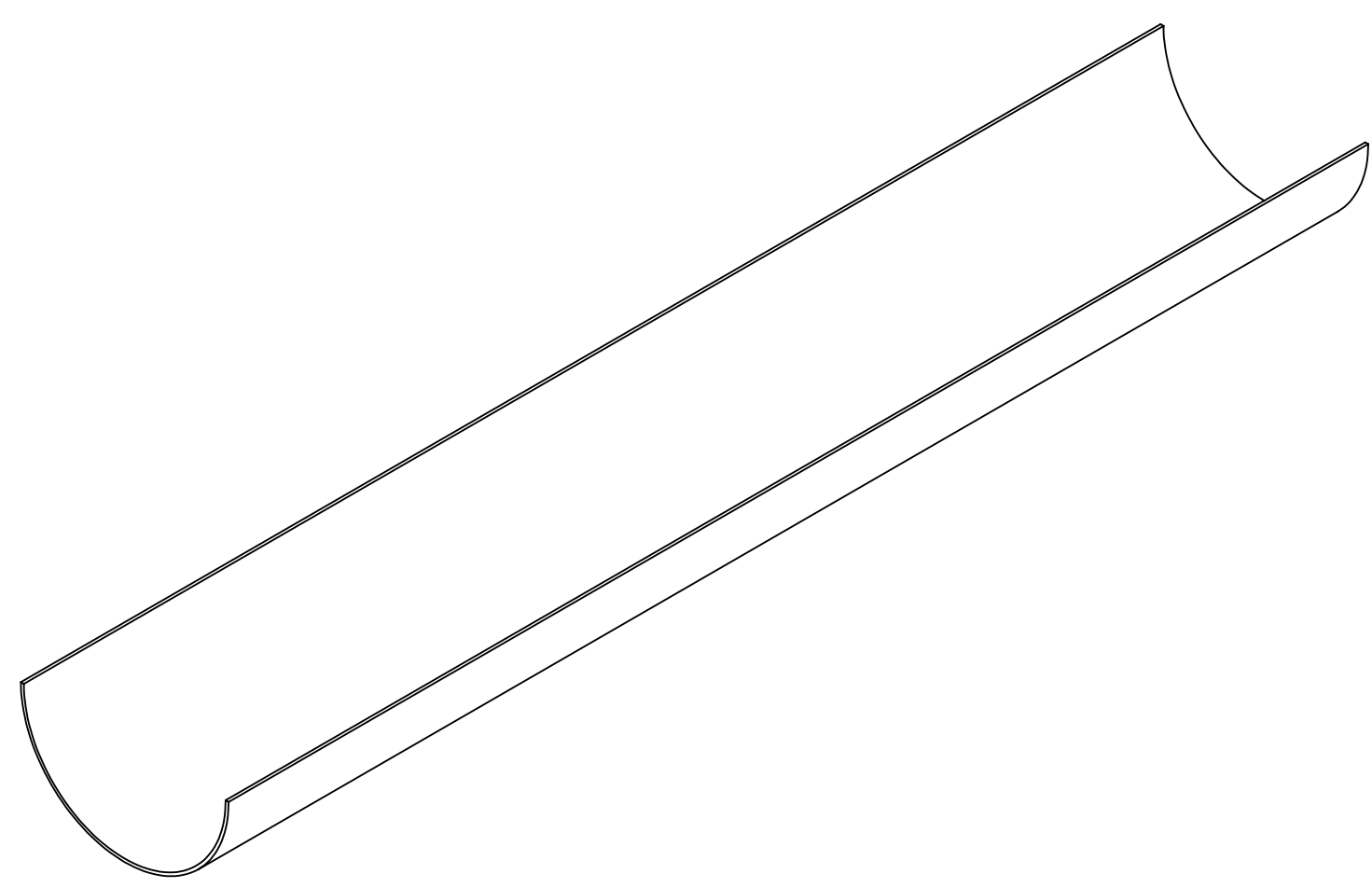
#DA	8F5K B; BC"	89G7 F DHC B	E H M
%	% % - 1 % % \$ % D	< 5 @ H 69	%
&	% % - 1 % % \$ ' D	I D D 9 F F 6	(
'	% % - 1 % % \$) D	7 @ A D D @ H K - 8 9	&
(% % - 1 % % \$ & D	C I H F H: 9 F A C 7 C I D @ D 9 G	% &

7Xf Za TaW9TLe WTgba Fxei Vxf
 Fxei WX WX' 6baVXcgba Xg WX' 9TLe WTgba
 Y 88% 1BUHebu FYgUNW 7 ci bW

75GB: 1 DD9F < 5 @
 75 @ F A 9 H F 5 B 8 : 1 9 @ D 5 B
 % % - , 1 7 5 @ F A 9 H F 5 B 8 : 1 9 @ D 5 B

GB78E 4A 68F GB7UE 4A 68F	840 UE 840 0E 4 68BAV 0: 8E8	89G7 F DHC B	7 C B G H	8
---------------------------	------------------------------	--------------	-----------	---

7B ABC F6478 7E4J A
 AS CAP 08H808 FHE 7B 78FF A
 F028EC 477 7E4J A F US G 8 78FF A 899A8
 F< A478E GBHGF BEBHEF 4H 5HEBAH 7B 6BA68CG8A
 E8GHA 477 7E4J A F US G 8 78FF A 899A8
 E8GHEA8E GBH 78F 78FF A 4H 5HEBAH 7B 6BA68CG8A



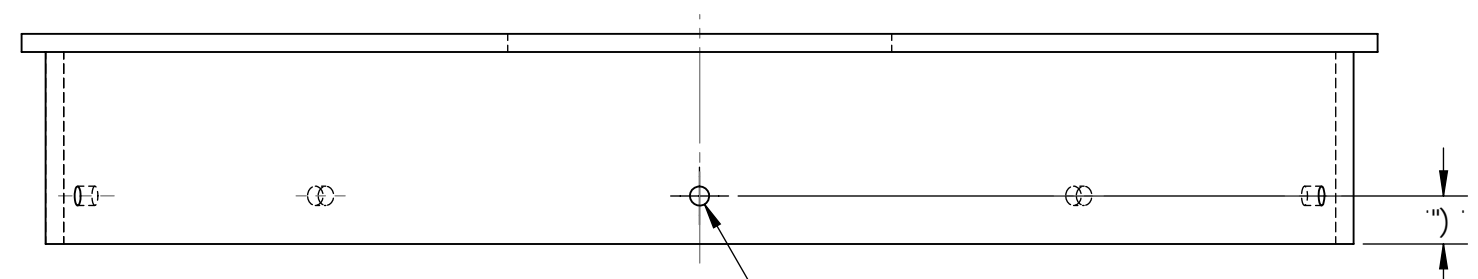
GB78E 4A68F GB7UE 4A68F HAT8FF BG BEJ EB ABC87 FAHQ A 764G8A 68AG 4E8	477 7ABAF 8AF A 46 8F 7ABAF 8AF 8A C888F IK 11FAM IKK 11F 477 9E48G 8AF 1988 4A 104E 11F 719 9A	477 9E48G 8AF 1988 719 9A 4A 104E 11F 719 9A	477 9E48G 8AF 1988 719 9A 4A 104E 11F 719 9A	477 9E48G 8AF 1988 719 9A 4A 104E 11F 719 9A	477 9E48G 8AF 1988 719 9A 4A 104E 11F 719 9A	477 9E48G 8AF 1988 719 9A 4A 104E 11F 719 9A	477 9E48G 8AF 1988 719 9A 4A 104E 11F 719 9A
---	---	---	---	---	---	---	---

7XfZa TaW9TLe WTgba Fxei Vxf
 Fxei Vx Wk 6baVXcgba Xg Wk 9TLe WTgba
 Y 88% 1BUHeBU FYgUNNA 7 ci bW

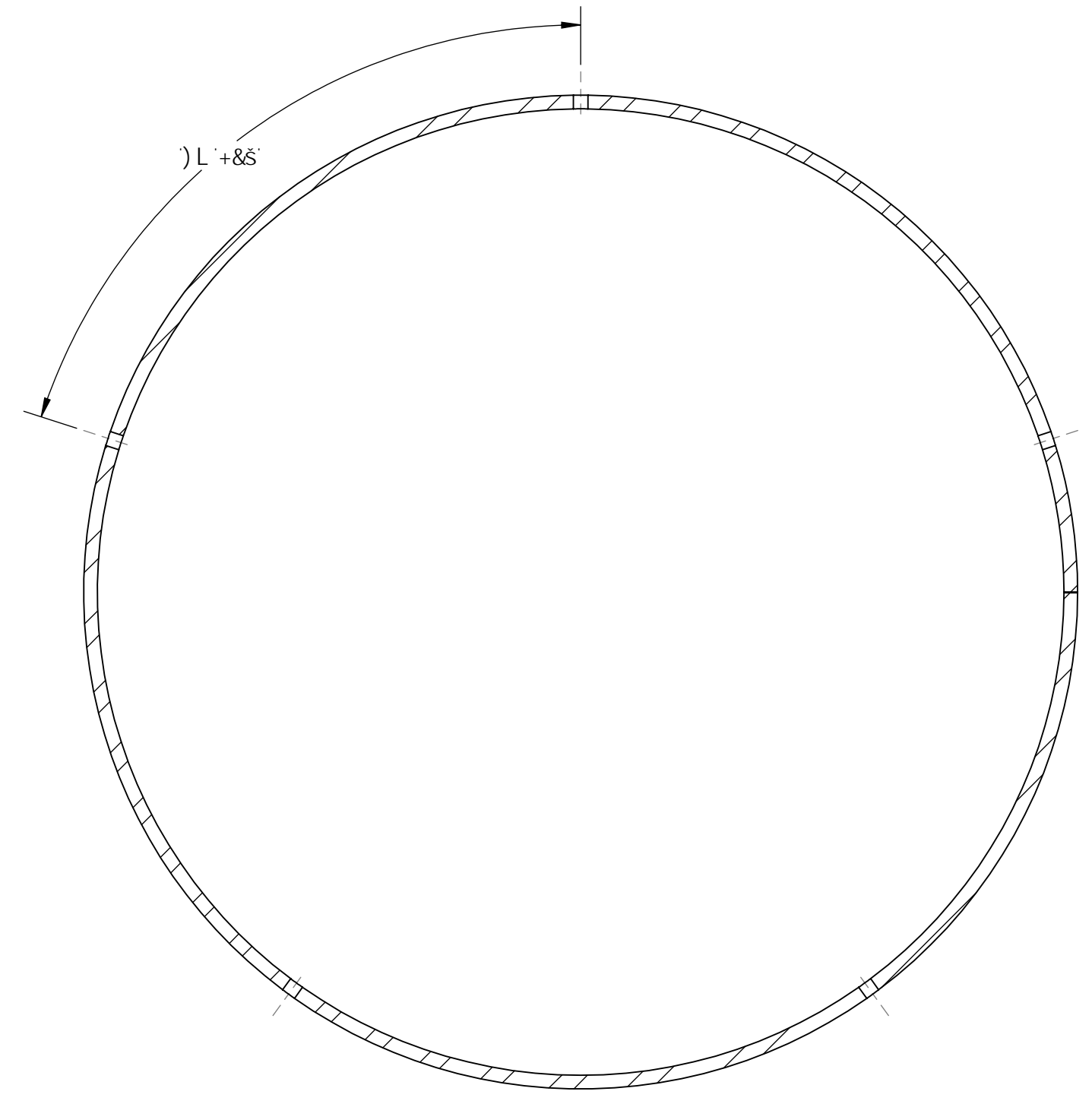
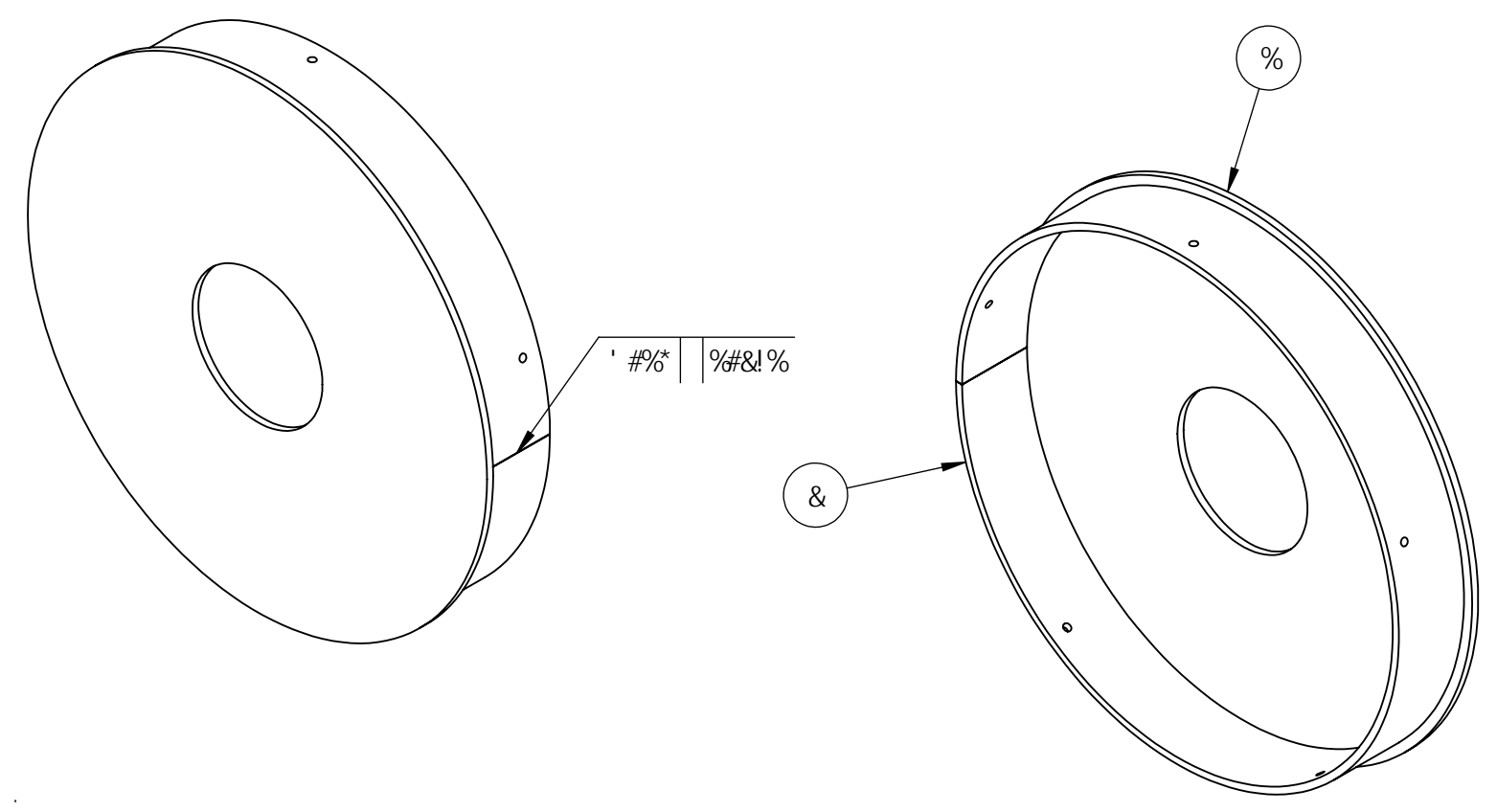
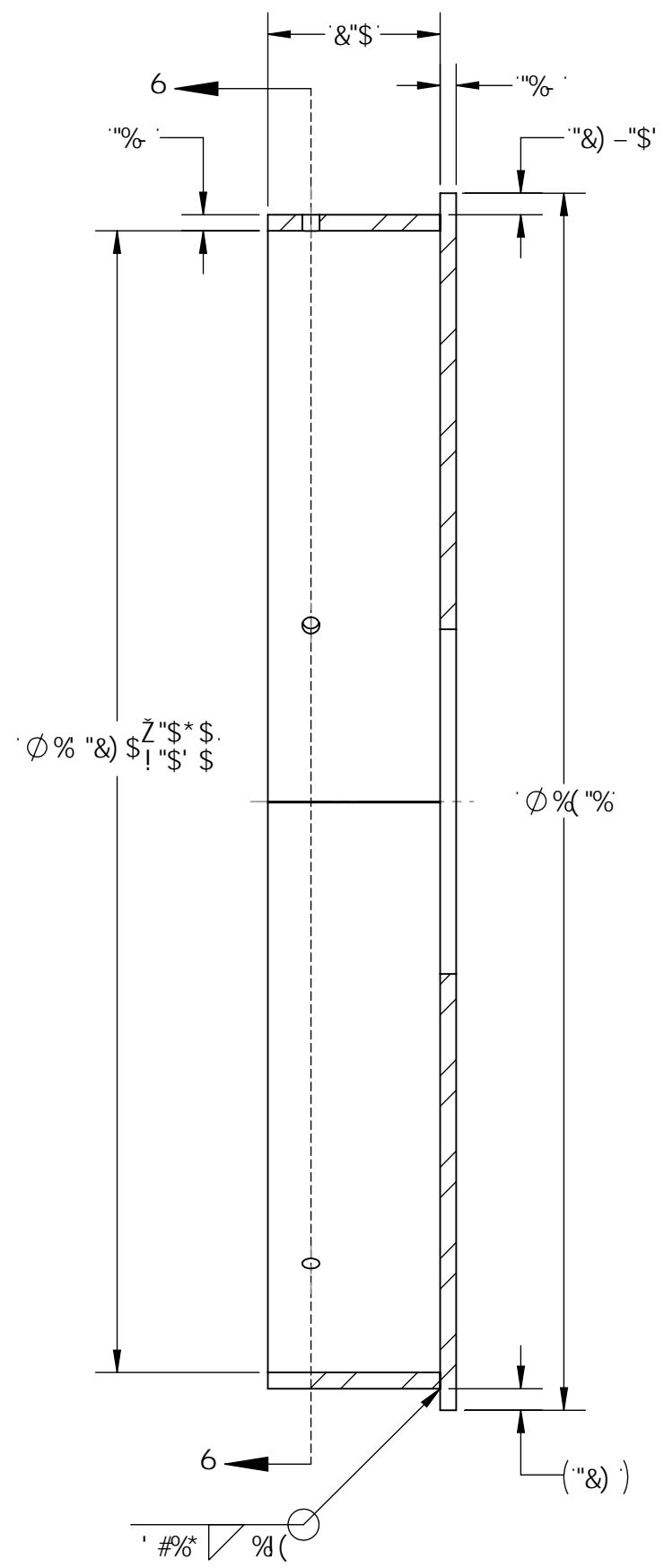
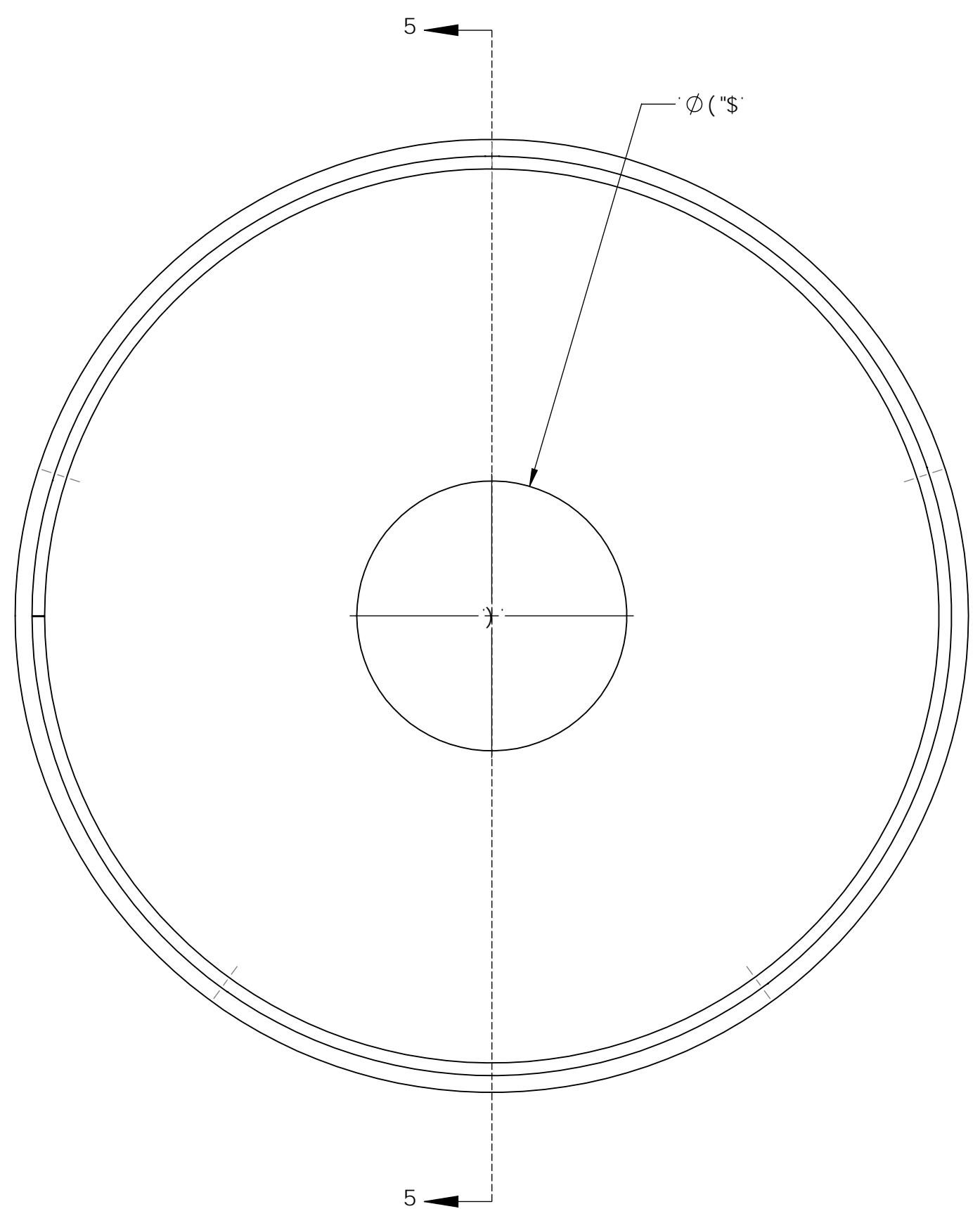
<5@ 'H 69
 75GB; '@C K 9F# DD9F '<5@
 98% -, !75@C F A 9H9F 5B8 : I 9@D5B

7B ABG F647B 7E4J A:
 A8 C4F @6FHE8E FHE 7B 78FF-A
 EBCBEG 477 BEEBEF GB G. 8 7BF < A B99-6B
 F < A478E GBHG8F BEEBHEF 4H 5HE84H 7B 6BA68CG-BA
 E8GHEA 477 7E4J A: F GB G. 8 78FF < A B99-6B
 E8GBHEABE GBHF 7BF 78FF-AF 4H 5HE84H 7B 6BA68CG-BA

F9J GC B < GC HMF < GC F E I 989GFVJ GC BG
 NC B9 F9J 89G7 F-DHC B 85H9 6MDSF



) L · Ø " & \$ % H · K · F I
 % # (! & \$! B 7 " H · K · F I



G97 HC B '616

G97 HC B '515

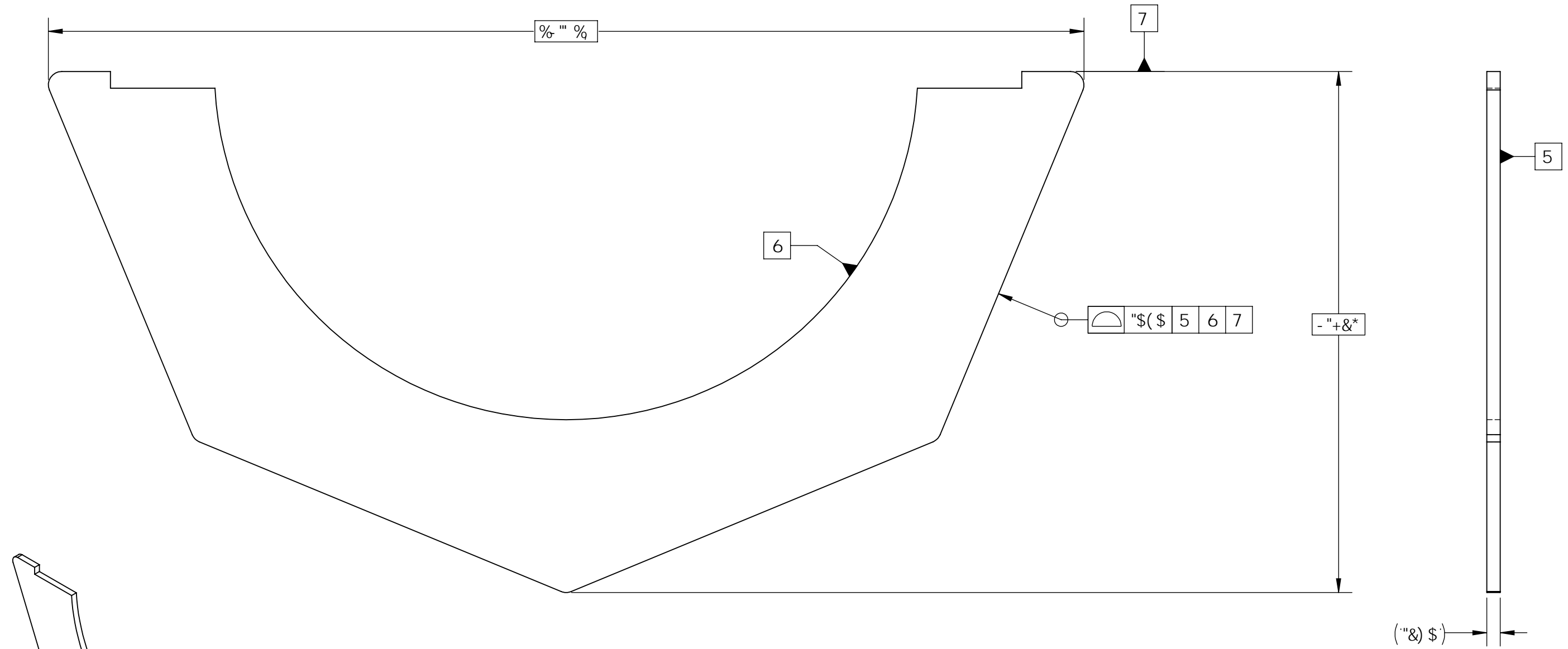
#DA	89G7 F-DHC B	A 5HF-5@	E HM
%	9B 8 'D@5 H9	' \$('GUJb Ygg GYY'	%
&	9B 8 'D@5 H9 F-B;	' \$('GUJb Ygg GYY'	%
<p>GB78E4A68F GB7uE4A68F @4G8E-47 @4G8E-87 HA78FF BG 8EJ F8 ABG87 F4H9 A7-64G-8A 6BA6E4-E8 477 7@BAF-BAF A-46 BF 7@BAF-BAF BA CFH68F IKK... 1#8# IKK... 1#8# IKKK... 1#8# 477 9E46G-BAF 158% 4A: 1P4E 1(1# 1#8# 9@ 6BA9BE@F GB*6BA9BE@B 4 AF@B L515# P#8# 5B4> 477 F-4EC B7: 8F 6 4A9E848E GBHG8F 4EEAG8F 6BHCAAGF 1#8# P1#8#</p>			
<p>7XfYzA TaW9TLeWTg'ba FXei WXf FXei WX'WX'6baVXcg'ba Xg'WX'9TLeWTg'ba Y&S% ZBUHj:bU'FYg'URW 7 ci bWj</p>			
<p>9B 8 'D@5 H9 '5 GG9A 6@M '7 5@C F-A 9HF '5 GG9A 6@M %&* -, !7 5@C F-A 9HF '5 B 8 : ! 9@D5 B</p>			
<p>7c9j] bUjbu xy rWYrWYg 7U8UxU NRC-CARC</p>			
<p>7 7 C B G H 74G8 &+ #5#65% 98% -, !9B 8 'D@5 H9 '5 GG9A 6@M 4FF8@57L ABTAD 4FF8@574: 8 98% -, !%8!5%</p>			
<p>7 7 !</p>			

7B ABG F6478 7E4J A:
 A8 C4F @BFHEBE FHE 78 78FF-A
 E8CBEG 4?? 8EEBEF GB G: 8 78F< A B99-68
 F< A478E GBHG8F 8EE8HEF 4H 5HE84H 78 6BA68CG-BA
 E8GHEA 4?? 7E4J A: F GB G: 8 78FF< A B99-68
 E8GBHEA8E GBHF 78F 78FF-AF 4H 5HE84H 78 6BA68CG-BA

BC HPG

%! &8 7 58 85H5 G DD@98 : CF K 5HF >9H7I HHB;
 &" 8-A 9BG-CBGE I 9F-98 : FCA 7 58 A C 89@5F9 65G-7

F9J GC B < GC HFM# < GC F E I 9 8 9 GFVJ GC BG			
NC B9	F9J "	8 9 G 7 F DHC B	6M#D5F



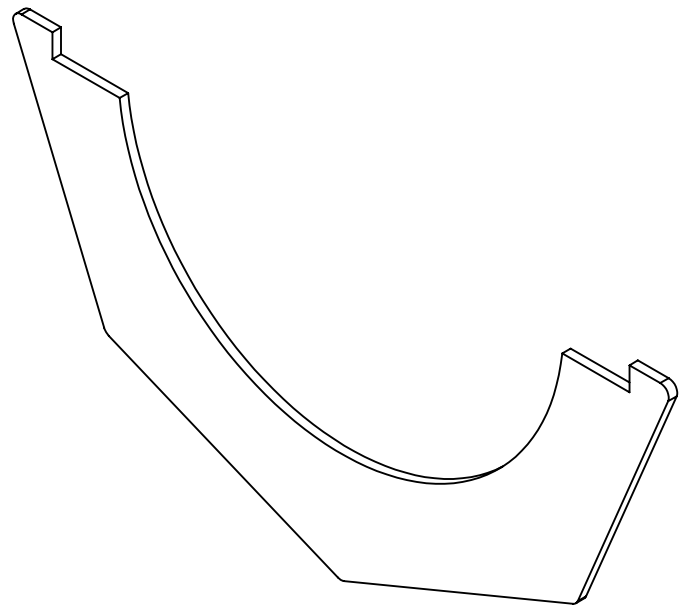
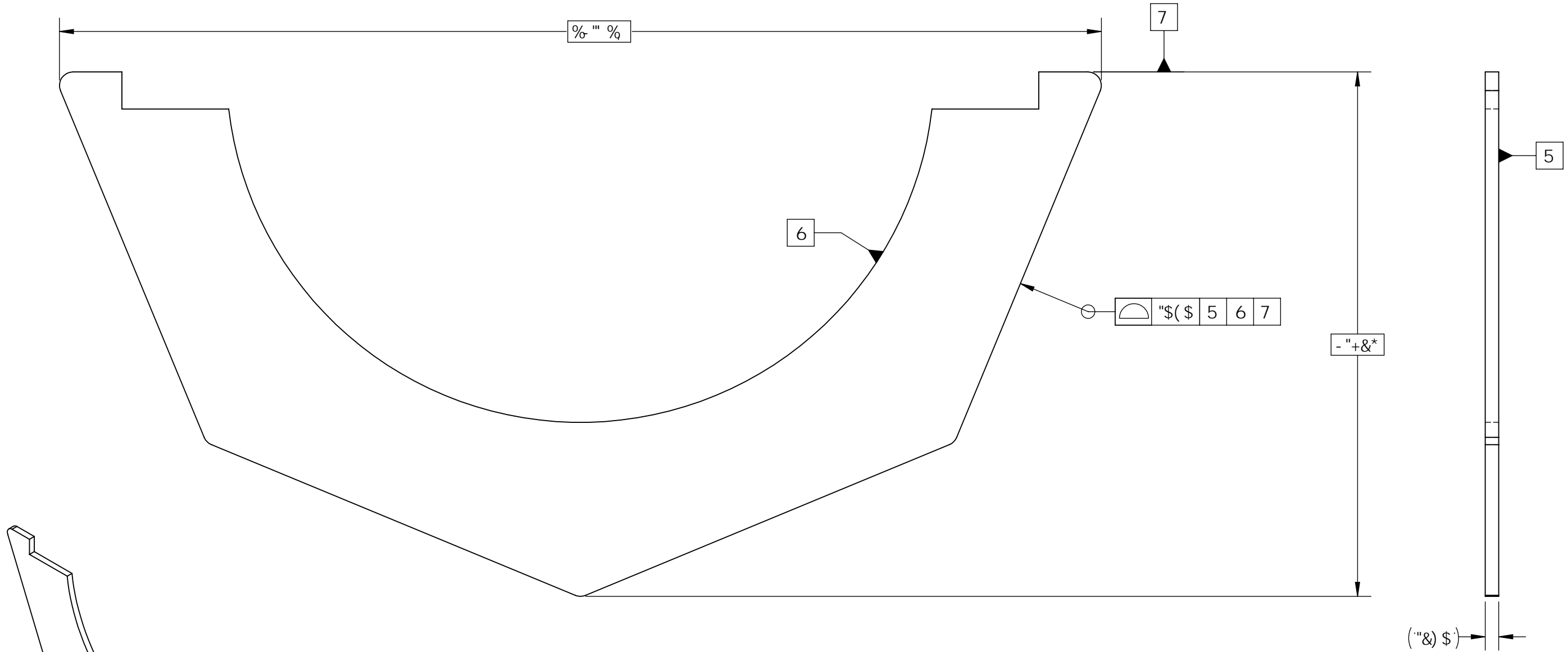
GB?8E4A68F*GB?uE4A68F HA?8FF BG: 8EJ f8 ABG87 F4H9 A7-64G-BA 6BAGE4-E8 4?? 7@BAF-BAF A A6: 8F 7@BAF-BAF BA C#H68F !K : : !#&# !KK : : !#&# !KKK : : !#&# 4?? 9E46G-BAF ±\$&#% 4A: H?4E : : !(#* !#&# 9@ 6BA9BE@F GB*6BA9BE@8 4 4F@8 L\$!#&# b%## 5E84> 4?? F: 4EC 87: 8F 6: 4A9E8-A8E GBHG8F 4EEAG8F 6BHC4AGF !#&# b!#%#	@4GBE 4?? @4GuE-8? ' \$(G5-B @CG GH9@ %#("H-?? : 84G GE84G! GE4-G@8AG G: 8E@ BC B9 9A4: *9A< B5H F5@ %&# F4C 6B78 5% 78F! *6BA68CG! >"8 9A 9FG 7E4J A! 78FF-Au! >"8 9A 9FG FGE8FF ** 6BA! 6: 86>87! uE-9! 4CC! 4CC! 74G8 &+ # \$ % & \$ %	<table border="1"> <tr> <td colspan="2"> </td> </tr> <tr> <td colspan="2"> BUHcbU F YgYUWV 7 ci bWj 7UbUXU 7cbgYj BUHcbU XY YWYUWV Yg 7UbUXU </td> </tr> <tr> <td colspan="2"> 7XfVzA TaW9TUEVTgba FXei Wxf FXei WX WX 6baVXcgba Xg WX 9TUEVTgba ¥ & \$ % ž BUHcbU FYgYUWV 7 ci bWj </td> </tr> <tr> <td colspan="2"> I DD9F F-6 7 5 GB; i DD9F < 5 @ %* - , ! 7 5 @ C F A 9 H F 5 B 8 : I 9 @ D 5 B </td> </tr> <tr> <td> AFGI 67-8AG 7 C B G H </td> <td> @B78? A4@8 " AB@8 78 @B78?8 %& - , I I DD9F F-6 %C : #8 9 % %& </td> </tr> <tr> <td> @B7 64E7 4FF8@57L " AB! " Ab 4FF8@5?4: 8 %& - , ! % \$! \$; </td> <td> F: 88G 98H?8 F6478"u6: 8??8 DGL! 7E4J A: Ab! " Ab 78FF-A %& - , ! % \$! \$ ' D 6 ! </td> </tr> </table>			BUHcbU F YgYUWV 7 ci bWj 7UbUXU 7cbgYj BUHcbU XY YWYUWV Yg 7UbUXU		7XfVzA TaW9TUEVTgba FXei Wxf FXei WX WX 6baVXcgba Xg WX 9TUEVTgba ¥ & \$ % ž BUHcbU FYgYUWV 7 ci bWj		I DD9F F-6 7 5 GB; i DD9F < 5 @ %* - , ! 7 5 @ C F A 9 H F 5 B 8 : I 9 @ D 5 B		AFGI 67-8AG 7 C B G H	@B78? A4@8 " AB@8 78 @B78?8 %& - , I I DD9F F-6 %C : #8 9 % %&	@B7 64E7 4FF8@57L " AB! " Ab 4FF8@5?4: 8 %& - , ! % \$! \$;	F: 88G 98H?8 F6478"u6: 8??8 DGL! 7E4J A: Ab! " Ab 78FF-A %& - , ! % \$! \$ ' D 6 !
BUHcbU F YgYUWV 7 ci bWj 7UbUXU 7cbgYj BUHcbU XY YWYUWV Yg 7UbUXU														
7XfVzA TaW9TUEVTgba FXei Wxf FXei WX WX 6baVXcgba Xg WX 9TUEVTgba ¥ & \$ % ž BUHcbU FYgYUWV 7 ci bWj														
I DD9F F-6 7 5 GB; i DD9F < 5 @ %* - , ! 7 5 @ C F A 9 H F 5 B 8 : I 9 @ D 5 B														
AFGI 67-8AG 7 C B G H	@B78? A4@8 " AB@8 78 @B78?8 %& - , I I DD9F F-6 %C : #8 9 % %&													
@B7 64E7 4FF8@57L " AB! " Ab 4FF8@5?4: 8 %& - , ! % \$! \$;	F: 88G 98H?8 F6478"u6: 8??8 DGL! 7E4J A: Ab! " Ab 78FF-A %& - , ! % \$! \$ ' D 6 !													

7B ABG F6478 7E4J A:
 A8 C4F @BFHEBE FHE 78 78FF-A
 E8CBEG 4?? 8EEBEF GB G: 8 78F< A B99-68
 F< A478E GBHG8F 8EE8HEF 4H 5HE84H 78 6BA68CG-BA
 E8GHEA 4?? 7E4J A: F GB G: 8 78FF< A B99-68
 E8GBHEA8E GBHF 78F 78FF-AF 4H 5HE84H 78 6BA68CG-BA

BCHPG

% &8 758 85H5 G DD@98 : CF K 5H9F >9H7I H8B;
 &" 8-A 9BGC BGEI 9F-98 : FCA 758 AC89@5F965G7

F9J GC B < GC HFM# < GC F E I 989GFVJ GC BG			
NC B9	F9J "	89G7 F DHC B	85H9
			6M#D5F



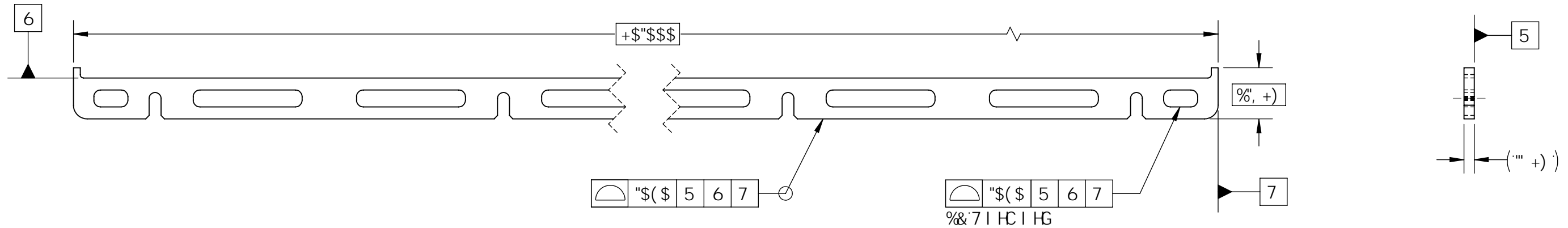
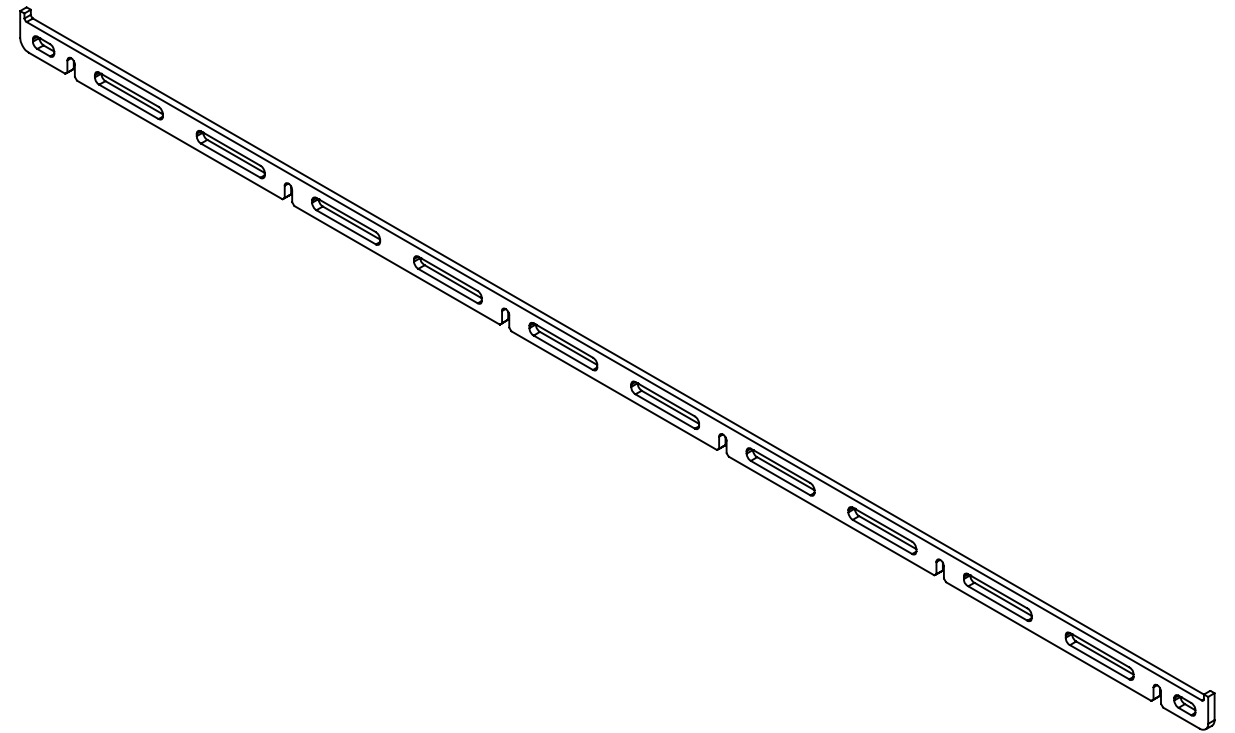
GB?8E4A68F*GB?uE4A68F HA?8FF'BG: 8EJ f8 ABG87 F4H9 A7-64G-BA 6BAGE4-E8 4?? 7@BAF-BAF A A6: 8F 7@BAF-BAF BA C#H68F !K' : : !#&# !KK' : : !#&# !KKK' : : !#&# 4?? 9E46G-BAF ±\$&% 4A: H?4E' : : !(#* !#&# 9@ 6BA9BE@F GB*6BA9BE@8 4 4F@8 L\$!#&# b%## 5E84> 4?? F: 4EC 87: 8F 6: 4A9E8-A8E GBHG8F 4EEAG8F 6BHC4AGF !#&# b!#%#	@4GBE 4?? @4GuE-8? ' \$(G5-B @CG GH9@ %#("H-?? : 84G GE84G! GE4-G@8AG G: 8E@ BC B9 9A<: *9A< B5H F5@ F4C 6B78 5% 78F! *6BA68CG! >"8 9A 9FG 7E4J A! 78FF-Au! >"8 9A 9FG FGE8FF ** 6BA! 6: 86>87! uE-Q! 4CC! 4CC! 74GB &+ #5%#&\$%	BUhcbU F YgYUWV 7 ci bW 7UbUXU 7cbgY] BUhcbU XY YWYUWV Yg 7UbUXU NRC-CNRC 7XfVzA TaW9TUEVTgba FXei WXf FXei WX WX 6baVXcgba Xg WX 9TUEVTgba ¥ &\$% žBUhcbU FYgYUWV 7 ci bW] G678 *GGE8 @C K 9F F-6 75GB; i DD9F <5@ %&* -, !75@CFA 9H9F 5B8 : i 9@D5B AFGI 67-8AG @B78? A4@8 " AB@8 78 @B78?8 F: 88G 98H?8 F6478"u6: 8??8 DGL! 7 CBGH %& -, !@C K 9F F-6 %C: #8 9% %& (@B7 64E7 4FF8@57L AB! Ab 4FF8@5?4: 8 7E4J A: Ad! Ab 78FF-A EBI! %& -, !%\$!\$& %& -, !%\$!\$(D 6 !
--	---	---

7B ABG F6478 7E4J A:
 A8 C4F @BFHEBE FHE 78 78FF-A
 E8CBEG 4?? 8EEBEF GB G: 8 78F< A B99-68
 F< A478E GBHG8F 8EE8HEF 4H 5HE84H 78 6BA68CG-BA
 E8GHEA 4?? 7E4J A: F GB G: 8 78FF< A B99-68
 E8GBHEA8E GBHF 78F 78FF-AF 4H 5HE84H 78 6BA68CG-BA

F9J GCB < GCFM# < GCFE I 989GFVJ GCBG			
NCB9	F9J"	89G7 F-DHC B	85H9
			6M#D5F

BC HG

% &8 758 85H5 G DD@98 : CF K 5HF >9H7I HHB;
 &" 8-A 9BGC BGE I 9F-98 : FCA 758 AC 89@5F965G7



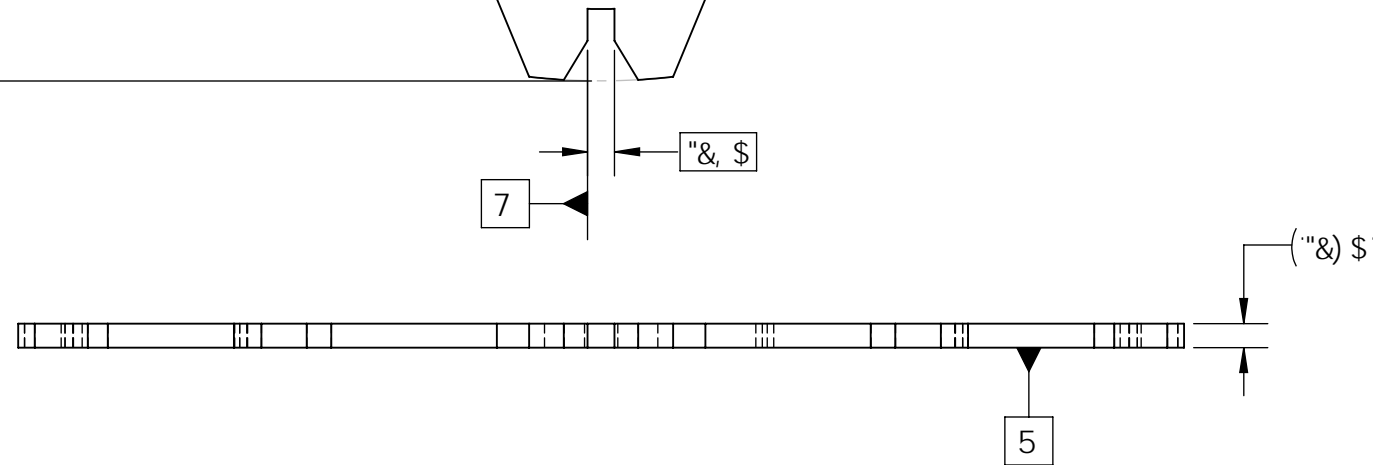
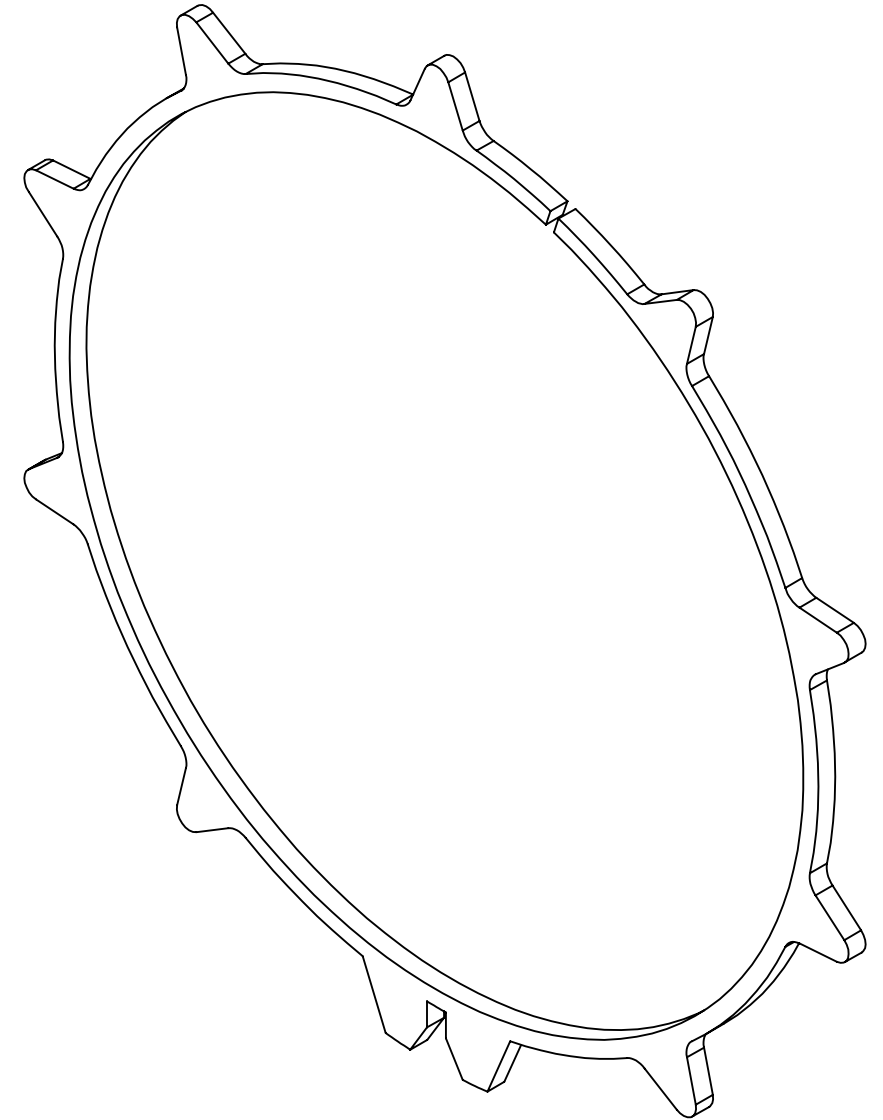
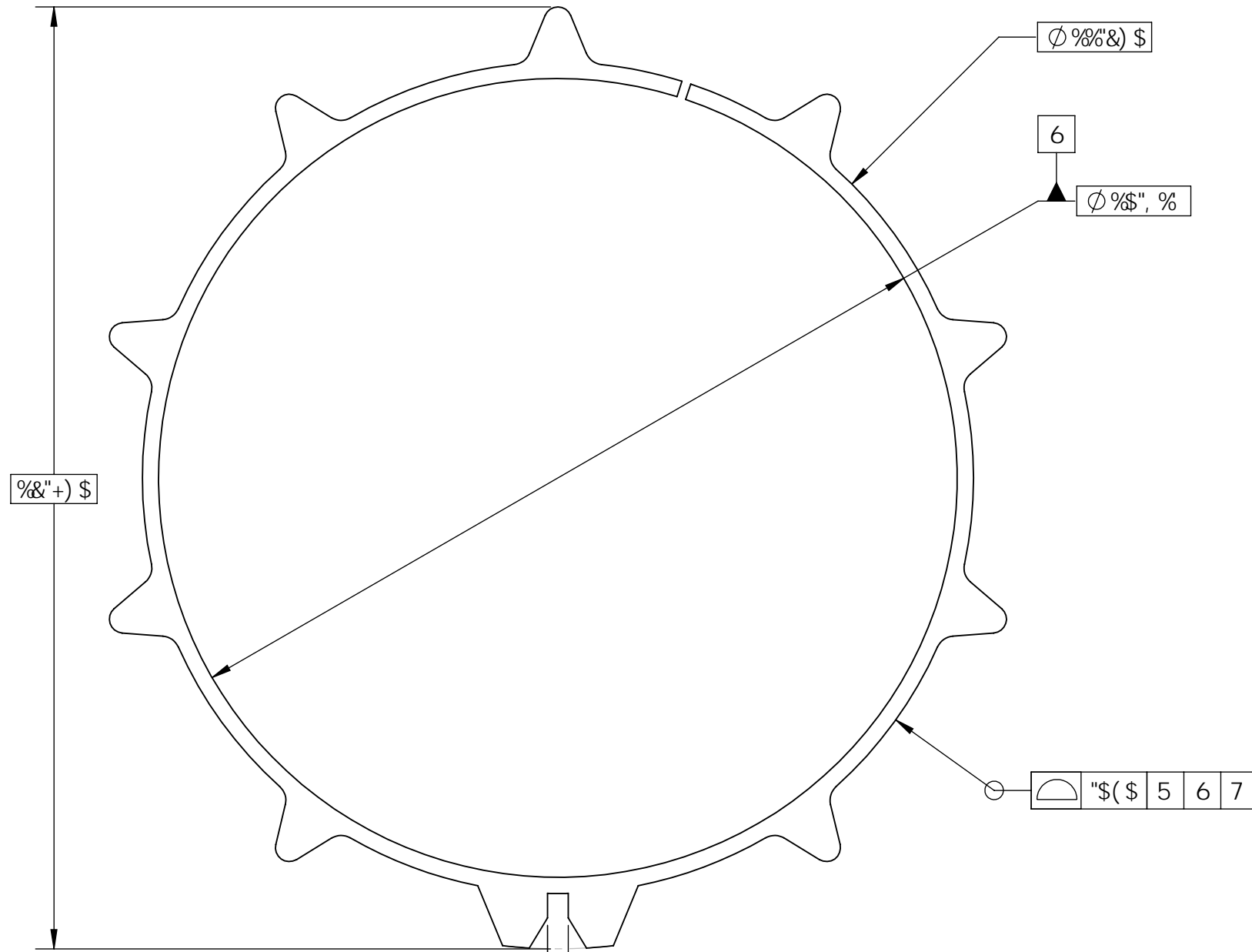
GB78E4A68F*GB?UE4A68F HA?8FF'BG: 8EJ 48 ABG87 F4H9 A7-64G-BA 6BAGE4-E8 4?? 7@BAF-BAF A A6: 8F 7@BAF-BAF BA C#H68F !K' : : !#&# !KK' : : !#&# !KKK' : : !#&# 4?? 9E46G-BAF ±\$&#% 4A: H?4E' : : !(#* !#&# 9@ 6BA9BE@F GB*6BA9BE@8 4 4F@8 L\$!#&# b%## 5E84> 4?? F: 4EC 87: 8F 6: 4A9E8-8E GBHG8F 4EEAG8F 6BHC4AGF !#&# b!#%#	@4G8E 4?? @4GUÉ-8? ' \$(G5-B @CG GH9@ ' #, "H-?? : 84G GE84G*GE4-G@8AG G: 8E@ BC B9 9A4: *9A< B5H F5@ %&# F4C 6B78 5% 78F! *6BA68CG! >"8 9A 9FG 7E4J A! 78FF-Au! >"8 9A 9FG FGE8FF ** 6BA! 6: 86>87" I uE-9! 4CC! 4CCI >"8 9A 9FG 74GB &+#\$%#&\$%#	BUHcbU F YgYUWV 7 ci bW 7 UbUXU 7cbgY] bUjcbU XY YVWYUWYg 7 UbUXU 7XfVz TaW9TUEVTgba FXei WXf FXei WX WX 6baVXcgba Xg WX 9TUEVTgba ¥&\$% žBUHcbU FYgYUWV 7 ci bWJ G678 GGE8 7 @5A D'D@5H9'B5FFCK 75GB; @CK 9F'<5@ %&* -, !75@CFA 9H9F 5B8 : I 9@D5B @B78? A4@8 " AB@8 78 @B78?8 %&# -, !7 @A DD@H9B5FFCK F: 88G 98H?8 F6478"u6: 8??8 %C: #89% %(& @B7 64E7 4FF8@57L " AB! "Ab 4FF8@5?4: 8 7E4J A: Ad! "Ab 78FF-A %&# -, !%\$!\$& %&# -, !%\$!\$*D 6 !
--	---	--

7B ABG F6478 7E4J A:
 A8 C4F @8FHEBE FHE 78 78FF-A
 E8CBEG 4?? 8EEBEF GB G: 8 78F < A B99-68
 F < A478E GBHG8F 8EE8HEF 4H 5HE84H 78 6BA68CG-BA
 E8GHEA 4?? 7E4J A: F GB G: 8 78FF < A B99-68
 E8GBHEA8E GBHF 78F 78FF-AF 4H 5HE84H 78 6BA68CG-BA

BCHHG

%' &8 7 58 85H5 G DD@98 : CF K 5H7 > 9H7I H8B;
 &" 8-A 9BGC BGEI 9F-98 : FCA 7 58 A C 89@5F9 65G-7

F9J GC B < GC HFM# < GC FE I 989GFVJ GC BG			
NCB9	F9J"	89G7 F-DHC B	85H9 6M#D5F



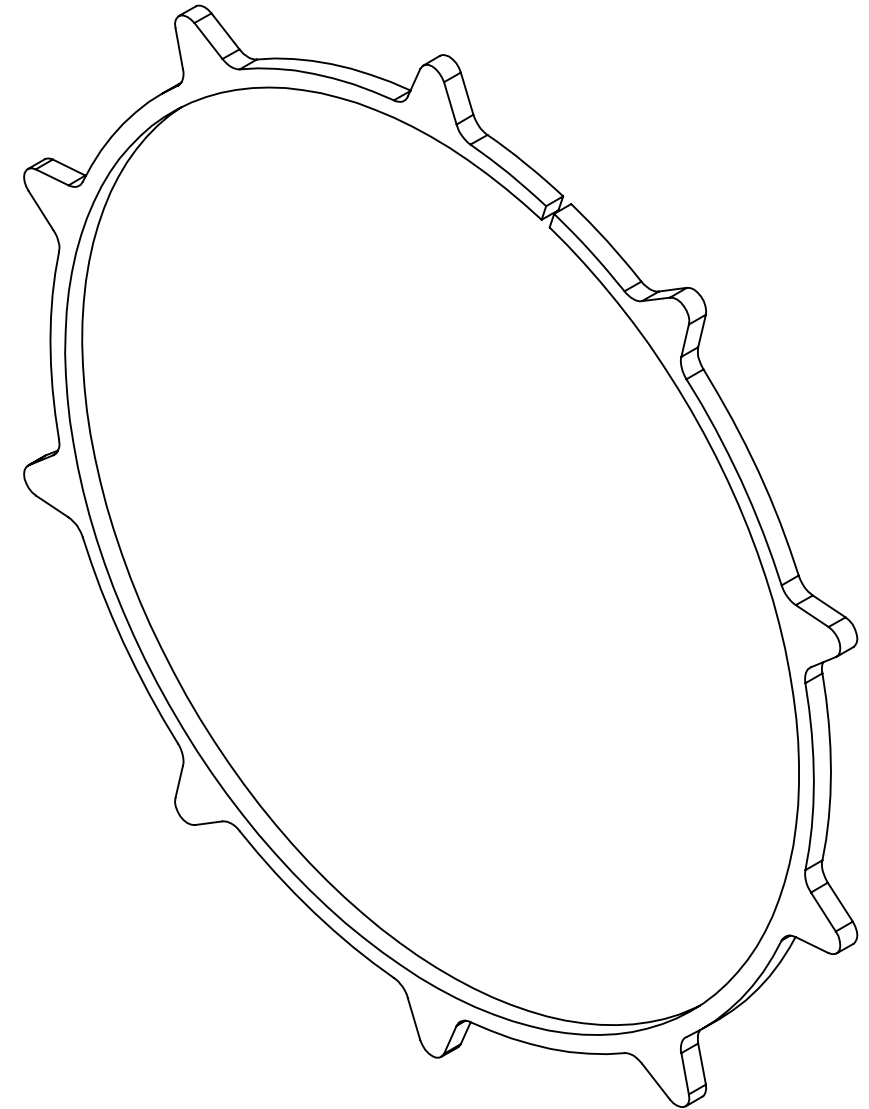
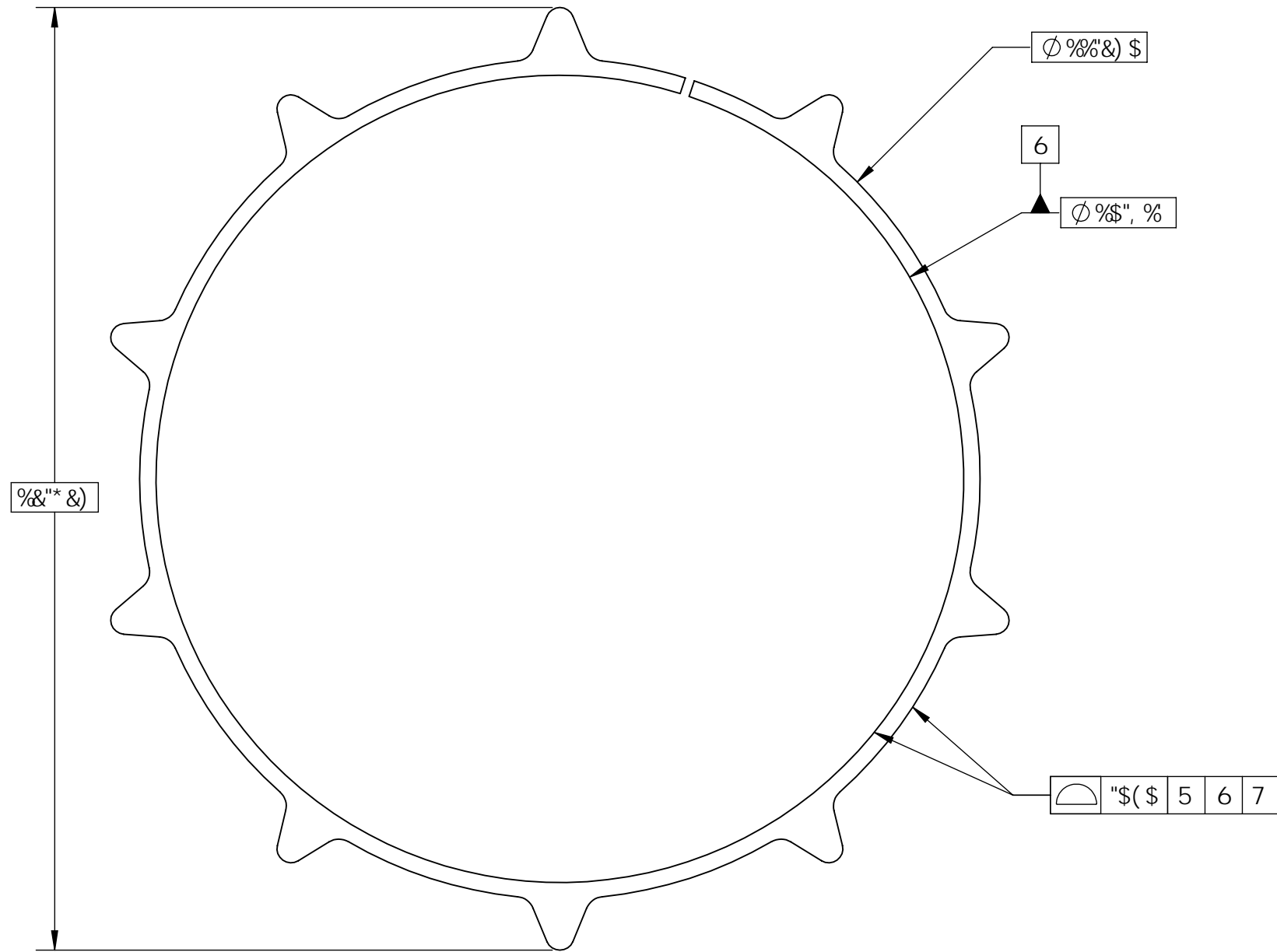
GB78E4A68F*GB7UE4A68F HA?8FF'BG: BEJ 48 ABG87 F4H9 47-64G-BA 6BAGE4-E8 4?? 7@BAF-BAF A A6: 8F 7@BAF-BAF BA C#H68F !K' : : !#&# !KK' : : !#&# !KKK' : : !#&# 4?? 9E46G-BAF ±\$&% 4A: H?4E' : !(#* !#&# 9@ 6BA9BE@F GB*6BA9BE@8 4 4F@8 L\$!#&# b%## 5E84 > 4?? F: 4EC 87: 8F 6: 4A9E8-A8E GBHG8F 4EEAG8F 6BHC4AGF !#&# b!#%#	@4GBE 4?? @4GUÉ-8? ' \$(G5-B @CG GH9@ %#("H: 7? : 84G GE84G! GE4-G@8AG G: 8E@ BC B9 9A4: *9A< B5H F5@ F4C 6B78 5% 78F! *6BA68CG! >"8 9A 9FG 7E4J A! *78FF-Au! >"8 9A 9FG FGE8FF ** 6BA! 6: 86>87! UÉ-9! 4CC! 4CC! >"8 9A 9FG 74G8 &+ #5%#&\$%#	BUHcbU F YgYUWV 7 ci bW 7 UbuXU 7 cbgY BUHcbU XY YWYUWV Yg 7 UbuXU 7XfZa TaW9TUEVTgba FXei WXf FXei WX WX 6baVXcgba Xg WX 9TUEVTgba ¥ &\$% žBUHcbU FYgYUWV 7 ci bWJ G678 *GGE8 C I H7F @C 7 5HB; F B; G 7 5 @ C F A 9 H7F 5 GG9A 6 @ M %* - , ! 7 5 @ C F A 9 H7F 5 B 8 : I 9 @ D 5 B @B78? A4@8 " AB@8 78 @B78?8 F: 88G 98H?8 F6478"u6: 8??8 DGL! 7 C B G H %* - , I C I H7F @C 7 5HB; F B; %C: #8 9% %& & @B7 64E7 4FF8@57L " AB! "Ab 4FF8@5?4: 8 7E4J A: Ad! "Ab 78FF-A EBI! %* - , !%\$!\$% %* - , !%\$!\$+D 6 !
--	---	---

7B ABG F6478 7E4J A:
 A8 C4F @BFHEBE FHE 78 78FF A
 E8CBEG 4?? 8EEBEF GB G: 8 78F < A B99 68
 F < A478E GBHG8F 8EE8HEF 4H 5HE84H 78 6BA68CG-BA
 E8GHEA 4?? 7E4J A: F GB G: 8 78FF < A B99 68
 E8GBHEA8E GBHF 78F 78FF AF 4H 5HE84H 78 6BA68CG-BA

BCHG

% 88 7 58 85H5 G DD@98 : CF K 5H7 > 9H7I HB;
 &" 8-A 9BGC BGEI 9-98 : FCA 758 AC89@5F9 65G7

F9J GCB < GCFM# < GCFEI 989GFVJ GCBG			
NCB9	F9J"	89G7 F DHC B	85H9 6M#D5F



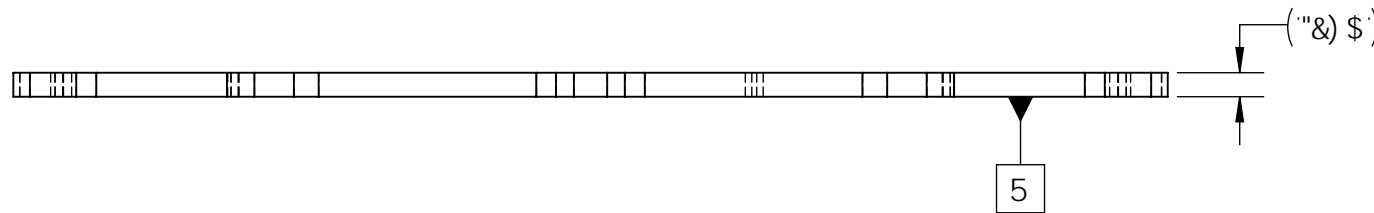
%&"* &)

∅ %&" & \$

6

∅ %\$", %

∅ (\$ 5 6 7



5

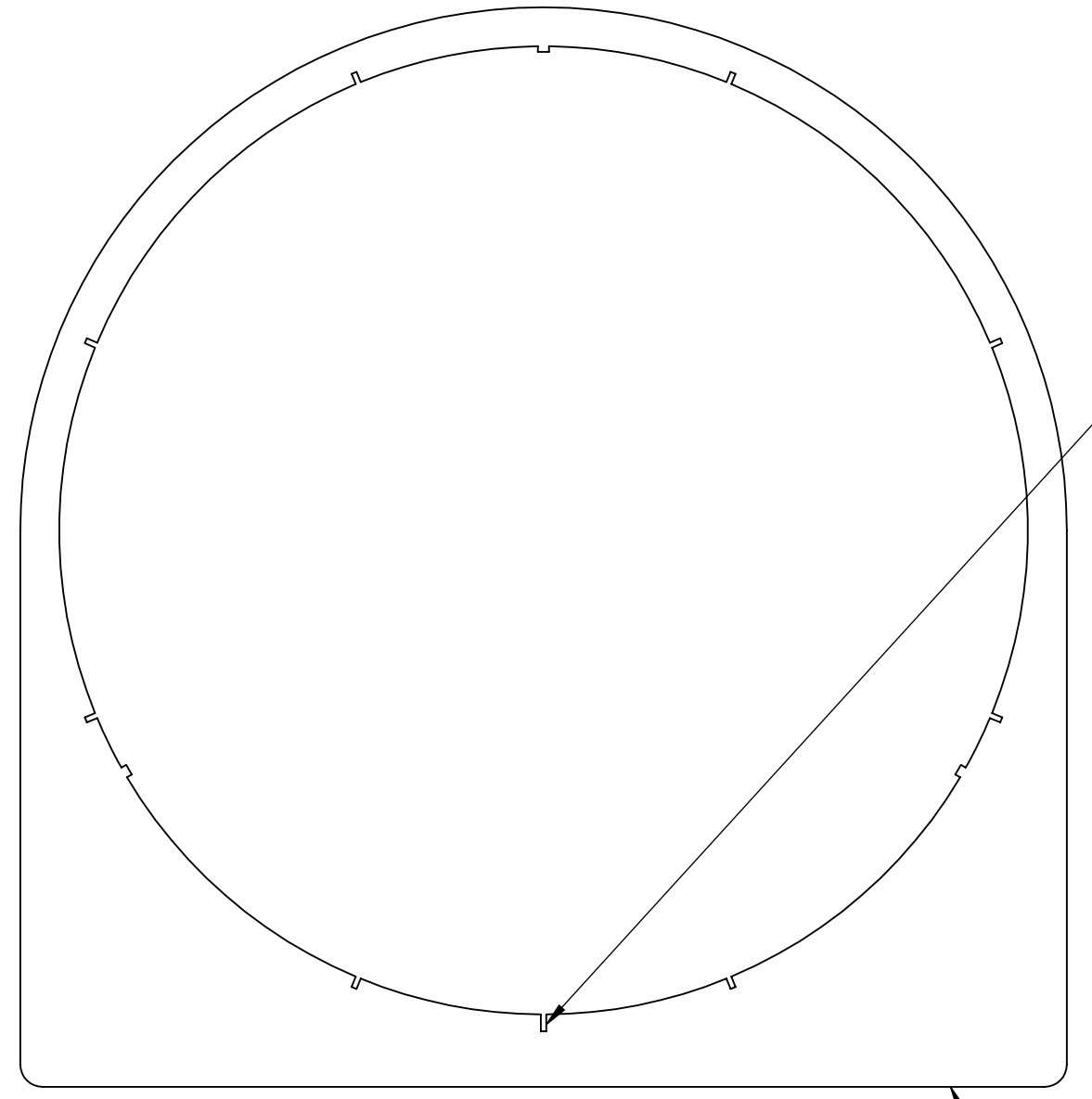
("& \$)

GB78E4A68F GB7UE4A68F	@4GBE 4?? @4GU E-8?		
HA78FF BG: BEJ 48 ABG87 F4H9 A7 64G-BA 6BAGE4-E8	' \$(G5 B @CG GH9@	BUHcbU F YgUUVW 7 ci bW 7 UbUXU 7cbgY BUHcbU XY YVWYUVW Yg 7 UbUXU	
4?? 7 @BAF-BAF A A6: 8F 7 @BAF-BAF BA C#H68F	84G GE84G GE4 G @8AG G: 8E@ BC B9	7Xf Za TaW9T Ue VTg ba FXei WXf FXei WX WX 6ba VXcg ba Xg WX 9T Ue VTg ba ¥ & \$ % ž BUHcbU FYg UUVW 7 ci bWJ G678 GGE8	
!K !#&# !KK !#&# !KK !#&# 4?? 9E46G-BAF ± \$ & % 4A: H74E ! (#* !#&# 9@	9A4: *9A < B5H F5@	BB9F @ 75HB; FB; 75 @ FA 9H9F 5GG9A 6@M %&* -, !75 @ FA 9H9F 5B8 : I 9@D5B	
6BA9BE@F GB 6BA9BE@8 4 4F@8 L \$!#&# b%##	F4C 6B78	AFGI 67 8AG	@B78? A4@8 AB@8 78 @B78?8
5E84 > 4?? F: 4EC 87: 8F 6: 4A9E8-8E GBHG8F 4EEAG8F 6BHC4AGF !#&# b!#%#	78F! 6BA68CGI 7E4J AI 78FF Au!	7 CBGH	F: 88G 98H?8 F6478 u6: 8??8 DGL!
	FGE8FF * 6BA! 6: 86 > 87 I U E 9! 4CC! 4CCI 74GB	@B7 64E7	%C: #89% %& %
			7E4J A: Ad! Ab 78FF-A EBI!
			%&* -, !%\$! \$, D 6 !

7B ABC F6478 7E4J A.
 AB CAF 98765 3HE 7B 78F F A
 F02DE C 477 9E7EF 6B C 8 78F A 89948
 F A478E GBHGF BEEBHEF 4H 9HE8AH 7B 68A68CG8A
 E8GHA 477 7E4J A. F 6B C 8 78F A 89948
 E8GBHAE 6BH 78F 78F A. 4H 9HE8AH 7B 68A68CG8A

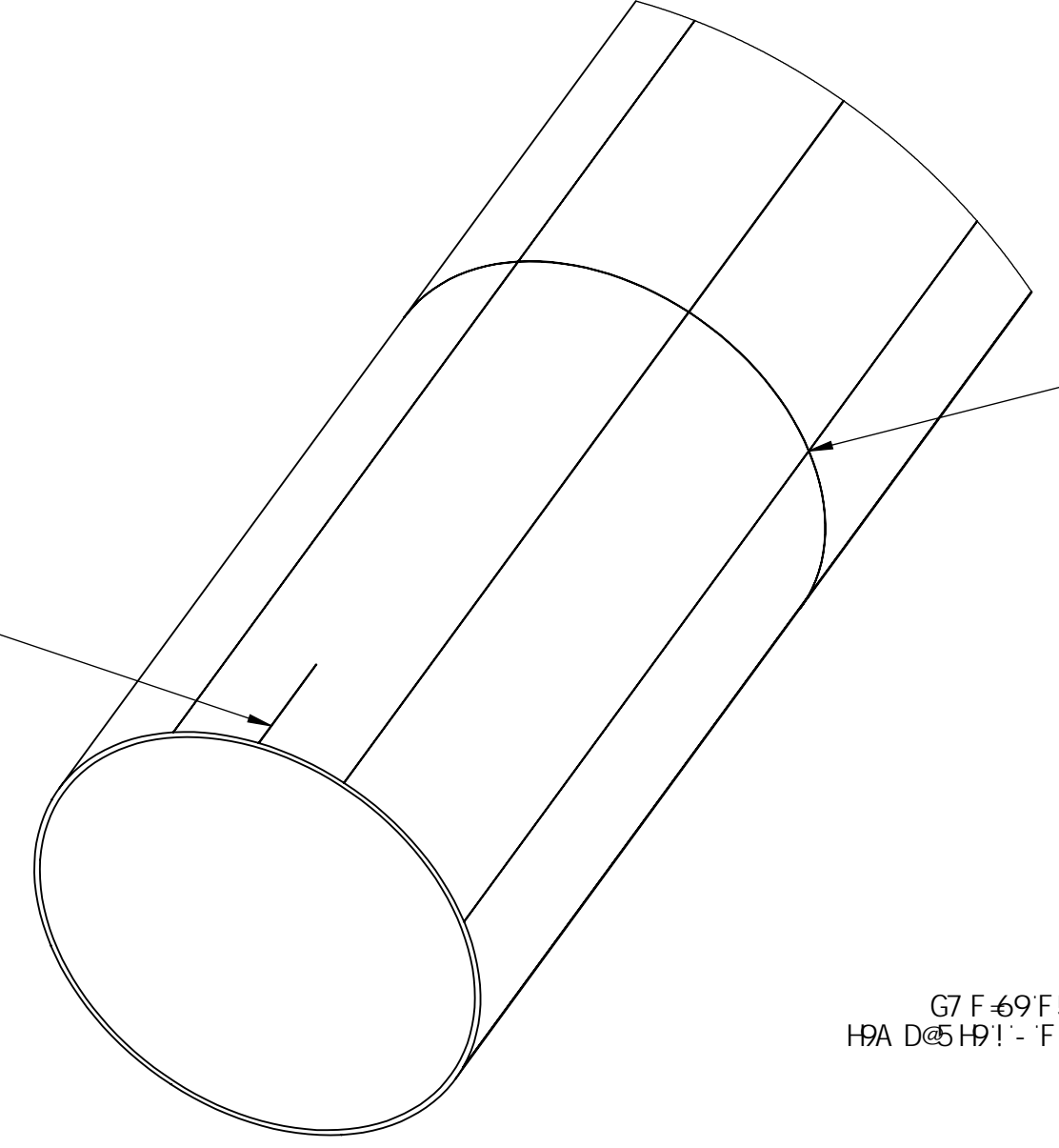
NC B9	F0J	F0J 6GB < 6CFMF < 6CF E 1 989GFVJ 6GBG	B5H9	6M05F
(5	58898 BIA 69F B: 5HG7 F 69A 5F7 BHEFG97 HC B DC 8HG	% #58859%	>58

BCHG



I 0919A D65HGFE HM&E8FK .98% - 1%81 %0DHC
 G7F-69@B95F5B8F58-5@B9GCBH 69

G7F 69G< CFH@B9: CF
 C1HF @75HB: F:B:
 5@ BA 9BH

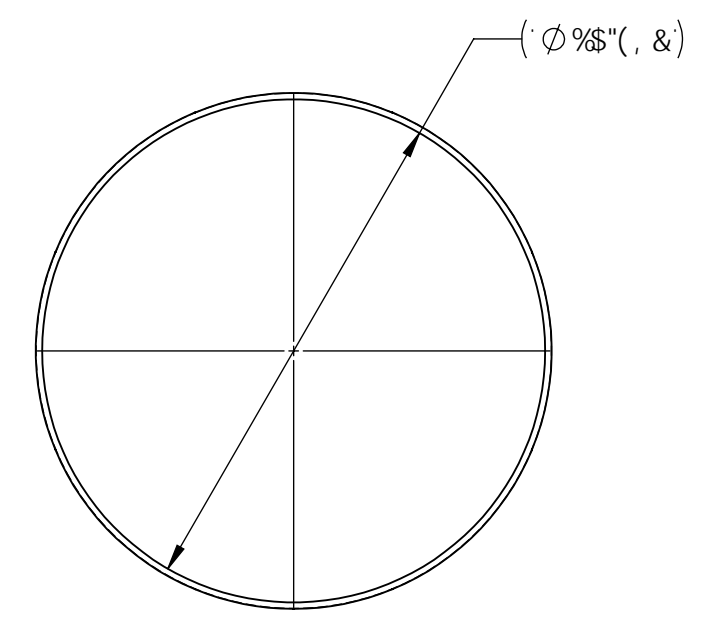
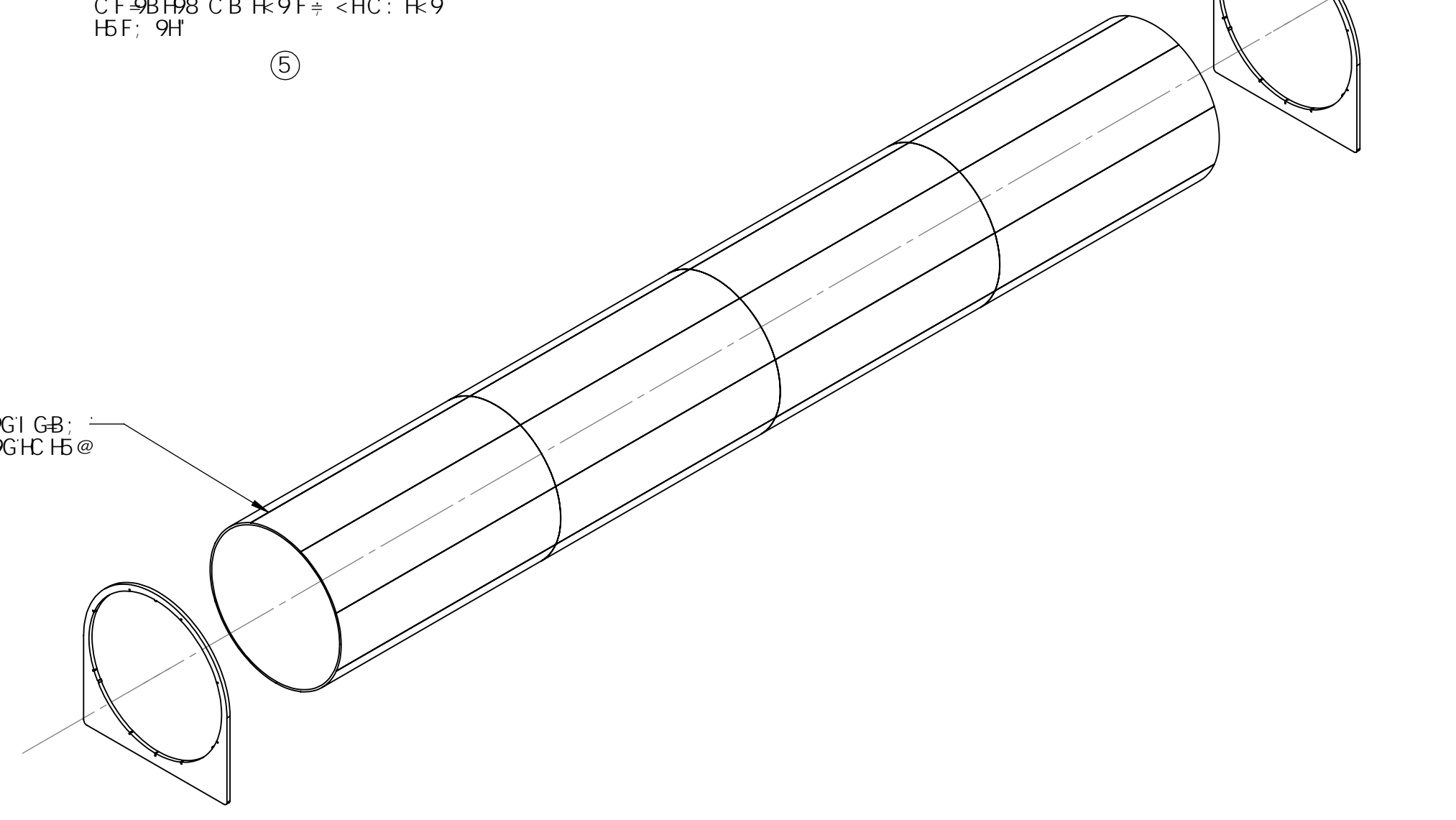


6CHCA J 9K

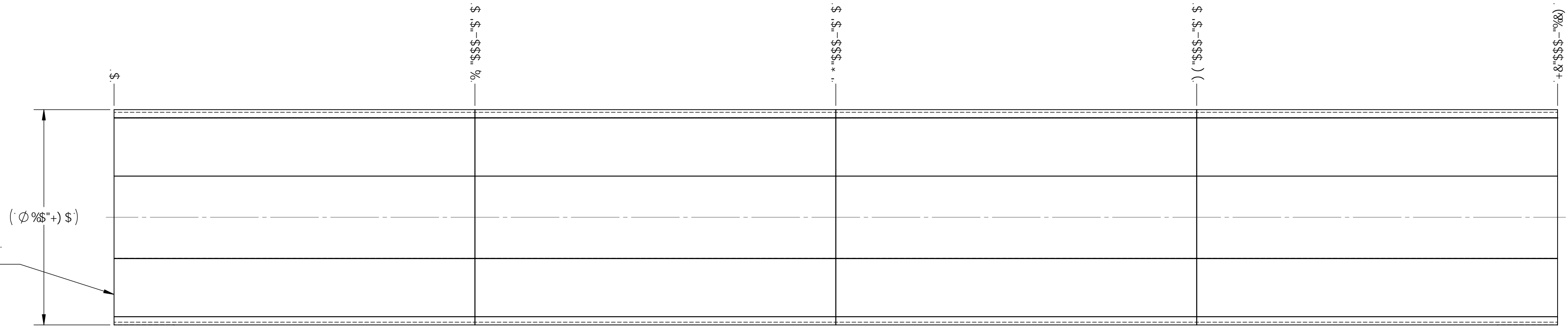
A 5F? 957 < BHEFG97 HC B DC BH
 K 4E 5 1 BE I 9BIA 9F 7 5@J 5@ 9
 5GG<C K B FPL5A D@1%L H 9
 BIA 9F 7 5@J 5@ 95B8 85G< 5F9
 CF 9BHE8 CB H 9F+ <HC: H 9
 HF: 9H

5

G7F 69F58 5@B9GI GB:
 HPA D65H9! - F58 5@B9GHC H6@



A 5F? 5G: FCBH'CB'
 H:9 4BG89C: H 69



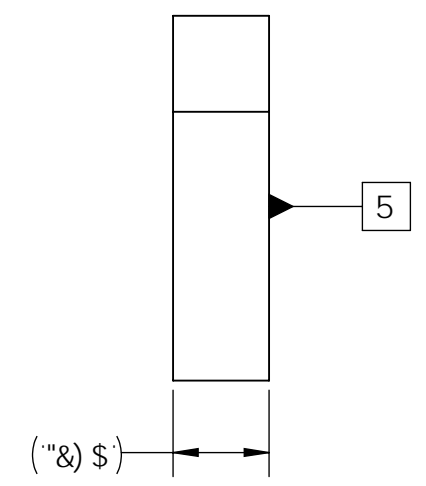
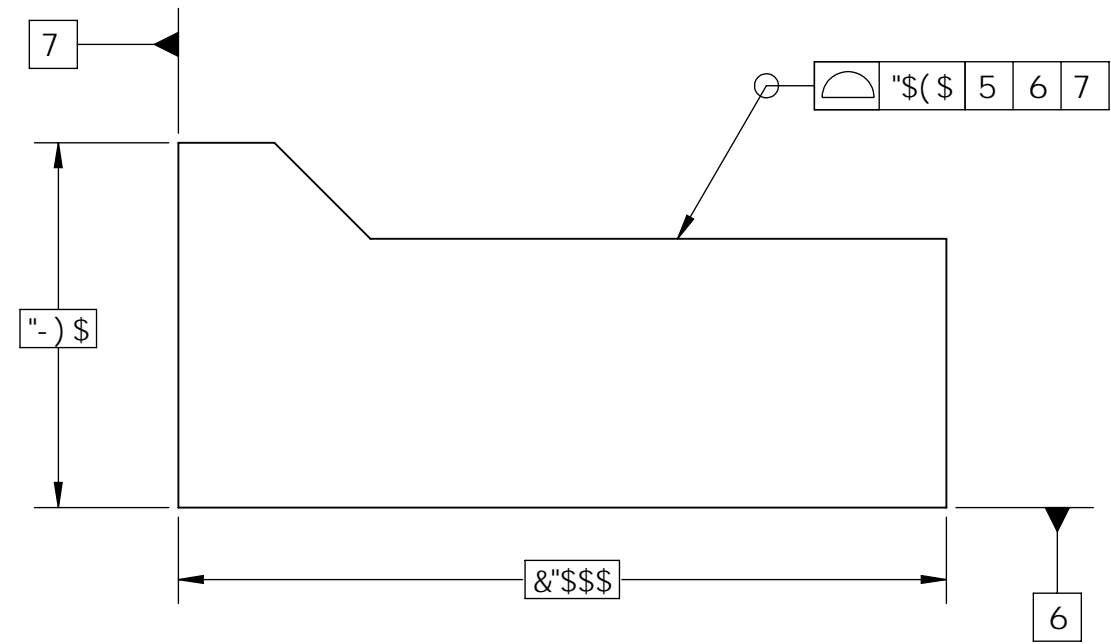
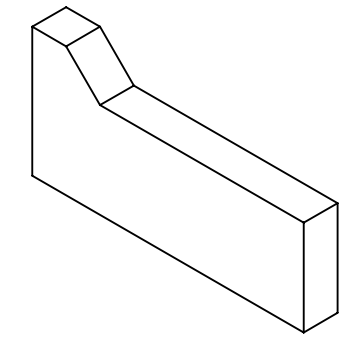
GB78E 4A68F GB7UE 4A68F HAT8FF BG BEJ EB ABG87 FAHP A7464GBA 68AGE 4E8	477 J46B4F 6AF A 46: 8F 74684 8AH 8A C8G8F IK: 1FAA IKK: 4F8 477 9E46G8AF 4586 AA 194E: 811K 7199 944	477 9E46G8AF 4586 7199 944 477 9E46G8AF 4586 7199 944	477 9E46G8AF 4586 7199 944 477 9E46G8AF 4586 7199 944	477 9E46G8AF 4586 7199 944 477 9E46G8AF 4586 7199 944
75@CF A 9HF 5G9A 6AM 98% - 175@CF A 9HF 5B8 : I 9@D5B	BB9F H 69	75@CF A 9HF 5G9A 6AM	98% - 175@CF A 9HF 5B8 : I 9@D5B	

7B ABG F6478 7E4J A:
 A8 C4F @8FHEBE FHE 78 78FF-A
 E8CBEG 4?? 8EEBEF GB G: 8 78F< A B99-68
 F< A478E GBHG8F 8EE8HEF 4H 5HE84H 78 6BA68CG-BA
 E8GHEA 4?? 7E4J A: F GB G: 8 78FF< A B99-68
 E8GBHEA8E GBHF 78F 78FF-AF 4H 5HE84H 78 6BA68CG-BA

F9J GC B < GC HFM# < GC F E I 9 8 9 GFVJ GC BG			
NC B9	F9J "	8 9G7 F DHC B	6M D5F
		85H9	

BCHG

%' &8 7 5 8 8 5 H 5 G DD@98 : CF K 5 H F > 9 H 7 I H H B ;
 &" 8 - A 9 B G C B G E I 9 F - 9 8 : F C A 7 5 8 A C 8 9 @ 5 F 9 6 5 G - 7



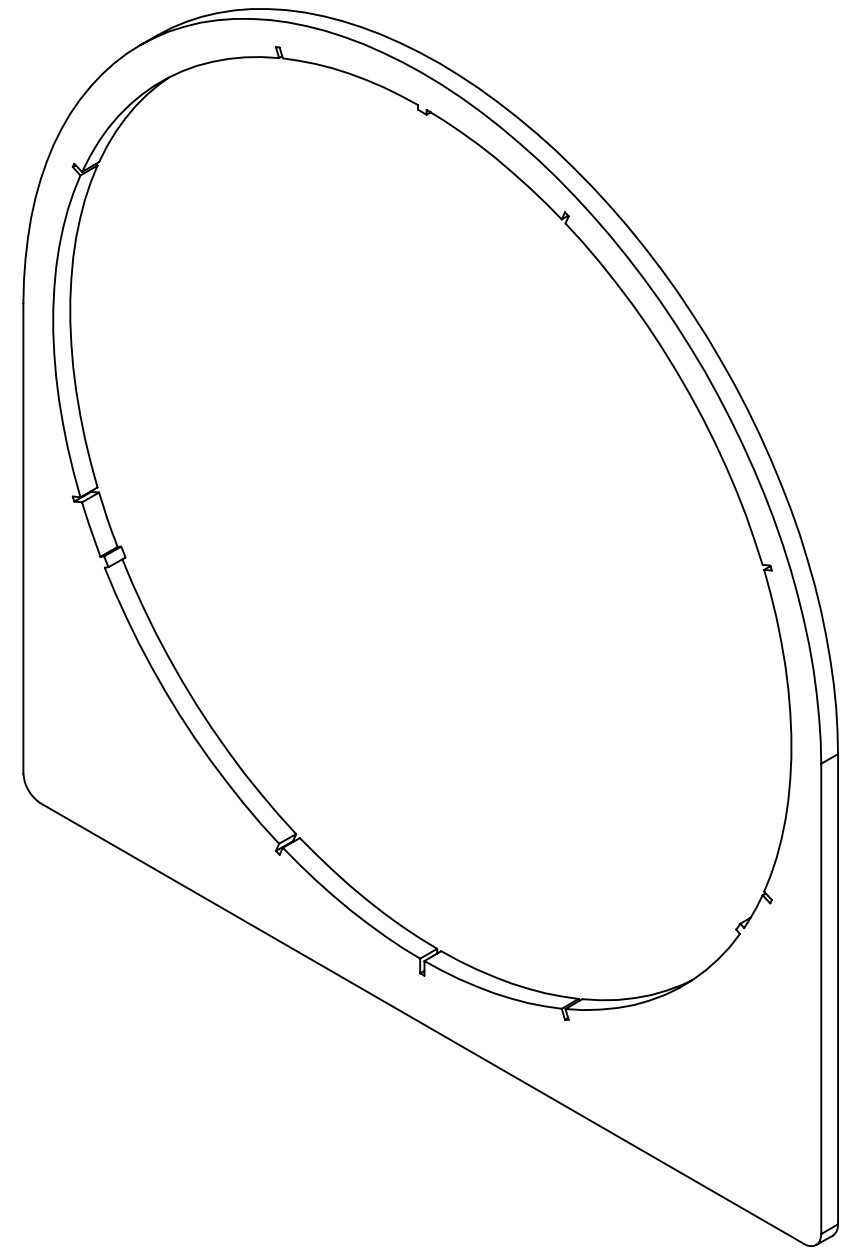
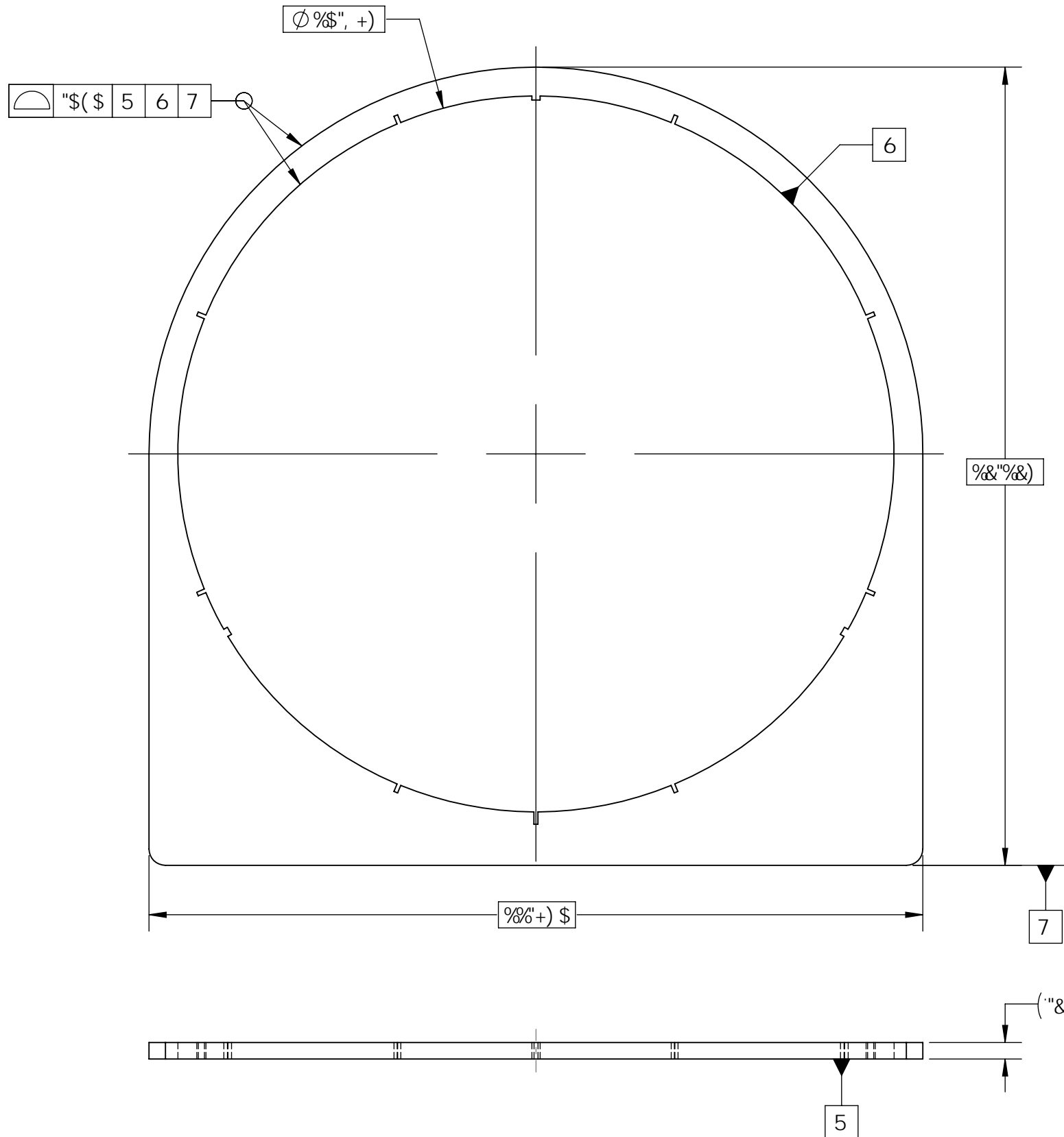
GB?8E4A68F*GB?uE4A68F HA?8FF'BG: 8EJ 48 ABG87 F4H9 A7 64G-BA 6BAGE4-E8 4?? 7@BAF-BAF A A6: 8F 7@BAF-BAF BA C#H68F !K ' ' ' ' !#&# !KK ' ' ' ' !#&# !KKK ' ' ' ' !#&# 4?? 9E46G-BAF ±\$&% 4A: H?4E ' ' ' !(#* !#&# 9@ 6BA9BE@F GB*6BA9BE@8 4 4F@8 L\$!#&# b%## 5E84> 4?? F: 4EC 87: 8F 6: 4A9E8-A8E GBHG8F 4EEAG8F 6BHC4AGF !#&# b!#%#		@4G8E 4?? @4GuE-8? ' \$(G5-B @CG GH9@ %#("H-? ? : 84G GE84G! GE4-G@8AG G: 8E@ BC B9 9A4: *9A< B5H F5@ %&/ F4C 6B78 5% 78F! *6BA68CG! >"8 9A 9FG 7E4J A! 78FF-Au! >"8 9A 9FG FGE8FF ** 6BA! 6: 86>87! uE-9! 4CC! *4CC! 74G8 &+ # \$ % & \$ %	BUHcbU F YgYUWV 7 ci bW 7 UuXU 7cbgY] bUjcbU XY YWYUWV Yg 7 UuXU NRC-CNRC 7XfVz 'TaW9T UeVTg'ba 'FXei WXf F'XeI WX'WX' 6baVXcg'ba Xg'WX' 9T UeVTg'ba ¥&\$% žBUHcbU FYgYUWV 7 ci bW] G678 *GGE8 BB9F 'H 69'@ 7 5HCF 'D@5H9 7 5GB; @CK 9F '<5@ %%* -, !75@CFA 9H9F '5B8 : I 9@D5B @B78? A4@8 " AB@8 78 @B78?8 F: 88G 98H?8 F6478"u6: 8??8 DGL! 7CBGH %%- , I-BB9F 'H 69@ 7 5HCF 'D@5H9 %C: #89% &% & @B7 64E7 4FF8@57L " AB! "Ab 4FF8@5?4: 8 7E4J A: Ad! "Ab 78FF-A EBI! %%- , !%\$!\$& %%- , !%\$!\$D 6 !
--	--	--	--

7B ABG F6478 7E4J A:
 A8 C4F @8FHEBE FHE 78 78FF-A
 E8CBEG 4?? 8EEBEF GB G: 8 78F< A B99-68
 F< A478E GBHG8F 8EE8HEF 4H 5HE84H 78 6BA68CG-BA
 E8GHEA 4?? 7E4J A: F GB G: 8 78FF< A B99-68
 E8GBHEA8E GBHF 78F 78FF-AF 4H 5HE84H 78 6BA68CG-BA

BC HPG

%! && 7 58 85H5 G DD@98: CF K 5HF > 9H7I HFB;
 &" 8-A 9BG-CBGE I 9F-98: FCA 7 58 A C 89@5F9 65G7

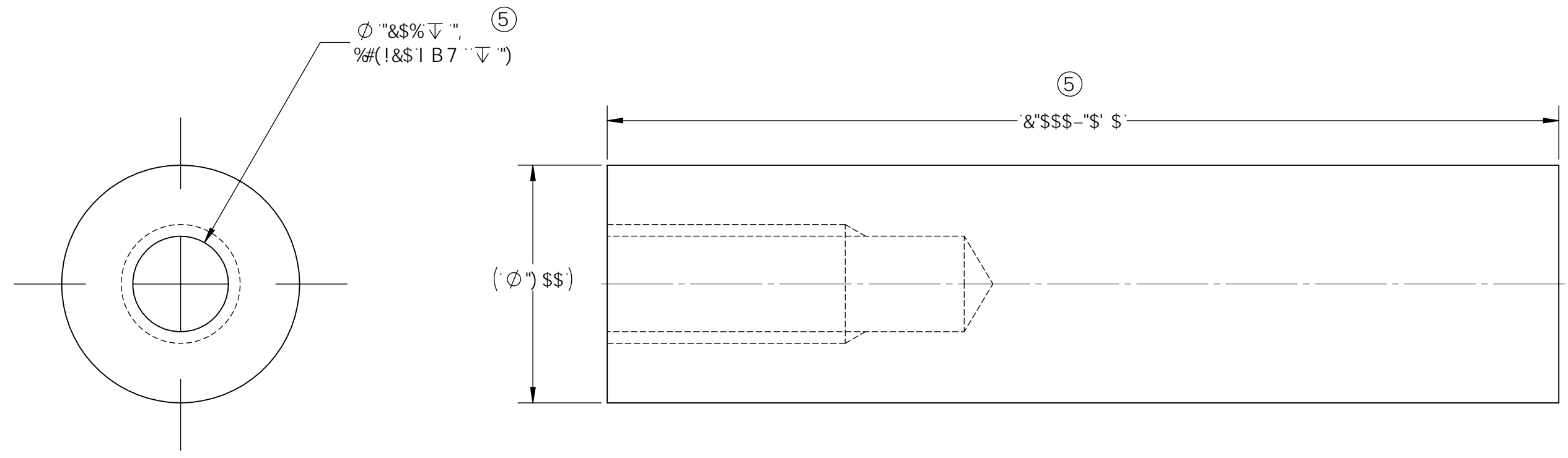
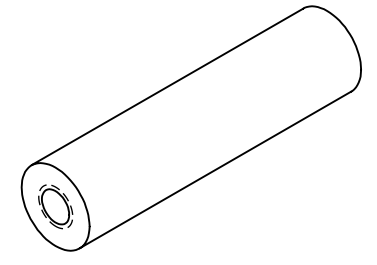
F9J GC B < GC HFM# < GC F E I 9 89GFVJ GC BG			
NC B9	F9J "	89G7 F DHC B	85H9
			6M/D5F



GB78E4A68F*GB?UE4A68F HA?8FF'BG: 8EJ F8 ABG87 F4H9 A7-64G-BA 6BAGE4-E8 4?? 7@BAF-BAF A A6: 8F 7@BAF-BAF BA C#H68F !K' : : !#&# !KK' : : !#&# !KKK' : : !#&# 4?? 9E46G-BAF ±\$&% 4A: H?4E' : : !(#* !#&# 9@ 6BA9BE@F GB*6BA9BE@8 4 4F@8 L\$!#&# b%## 5E84> 4?? F: 4EC 87: 8F 6: 4A9E8-A8E GBHG8F 4EEAG8F 6BHC4AGF !#&# b!#%#	@4GBE 4?? @4GU E-8? D@5 B 7 5F6C B G H9@ %#("H-? ? : 84G GE84G! GE4-G@8AG G: 8E@ BC B9 9A4: *9A< B5H F5@ %&/ F4C 6B78 5% 78F! *6BA68CG! >"8 9A 9FG 7E4J A! *78FF-Au! >"8 9A 9FG FGE8FF ** 6BA! 6: 86>87" I uE-9! 4CC! *4CC! 74GB &+ #5%#&\$%	BUHcbU F YgYUWV 7 ci bW 7 UbuXU 7cbgY] BUHcbU XY YWYUWV Yg 7 UbuXU NRC-CNRC 7XfZa TaW9TUEVTgba FXei WXf FXei WX WX' 6baVXcg'ba Xg WX' 9TUEVTg'ba ¥&\$% žBUHcbU FYgYUWV 7 ci bW] G678 *GGE8 Hk 9FA C 7 C I D@H9A D@5H9 %* - , !75@CFA 9HF 5B8 : I 9@D5B AFGI 67-8AG @B78? A4@8 " AB@8 78 @B78?8 F: 88G 98H?8 F6478"u6: 8?78 DGL! 7 CBGH %%- , !Hk9FA C 7 C I D@H9A D@5H9 %C: #89% %& %& @B7 64E7 4FF8@57L " AB! Ab 4FF8@574: 8 7E4J A: Ad! Ab 78FF-A EBI! %* - , !%\$!%&D 6 !
--	--	--

7B ABG F6478 7E4J A:
 A8 C4F @BFHEBE FHE 78 78FF-A
 E8CBEG 4?? 8EEBEF GB G: 8 78F< A B99-68
 F< A478E GBHG8F 8EE8HEF 4H 5HE84H 78 6BA68CG-BA
 E8GHEA 4?? 7E4J A: F GB G: 8 78FF< A B99-68
 E8GBHEA8E GBHF 78F 78FF-AF 4H 5HE84H 78 6BA68CG-BA

F9J GCB < GCFM# < GCFE I 989GFVJ GCBG				
NCB9	F9J"	89G7 F DHC B	85H9	6M/D5F
6&Z6'	5	58898 H5DD98 <C @ 8-A "&\$\$\$K 5G%\$\$\$	&+##\$#&\$%	>58



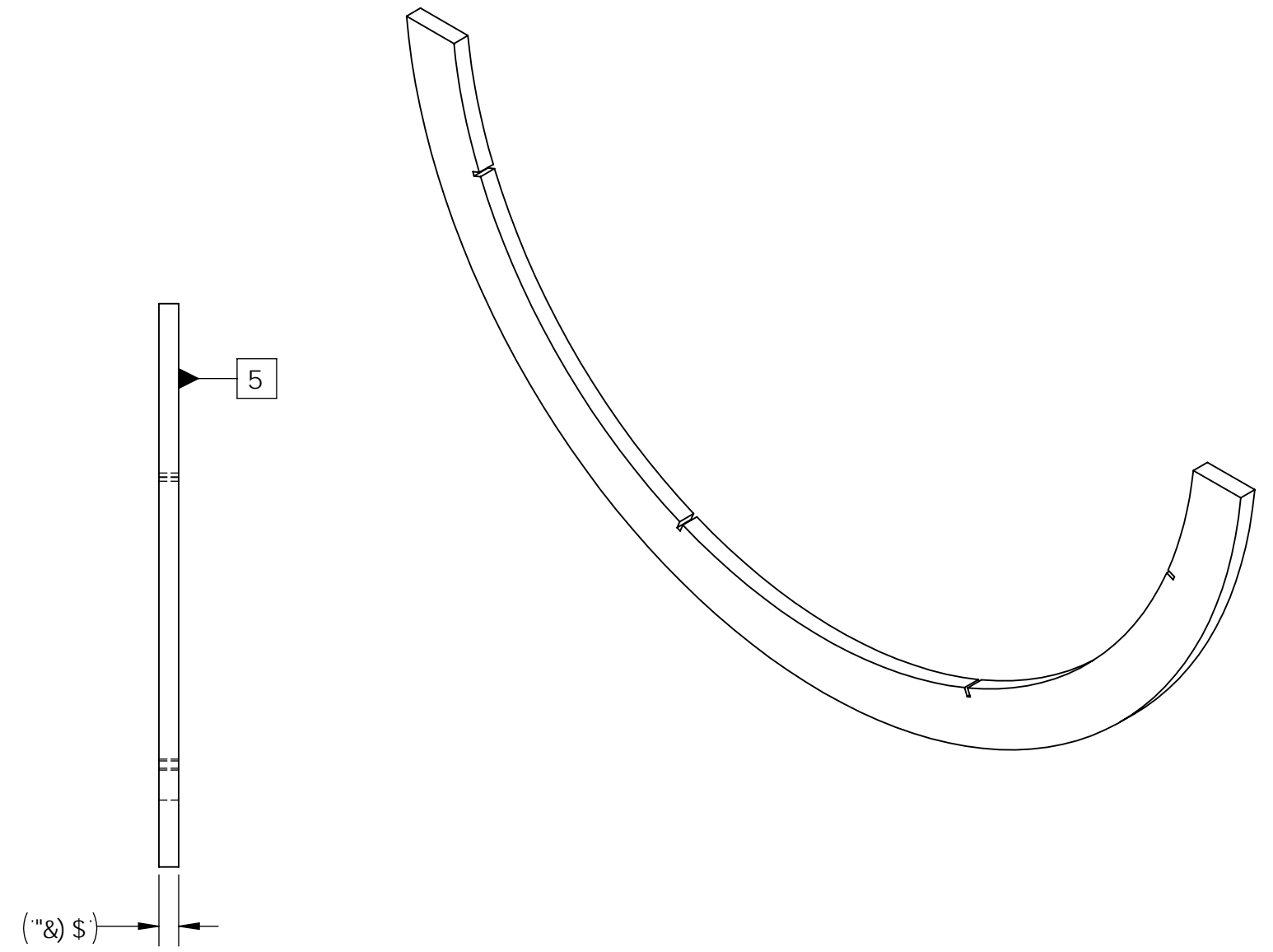
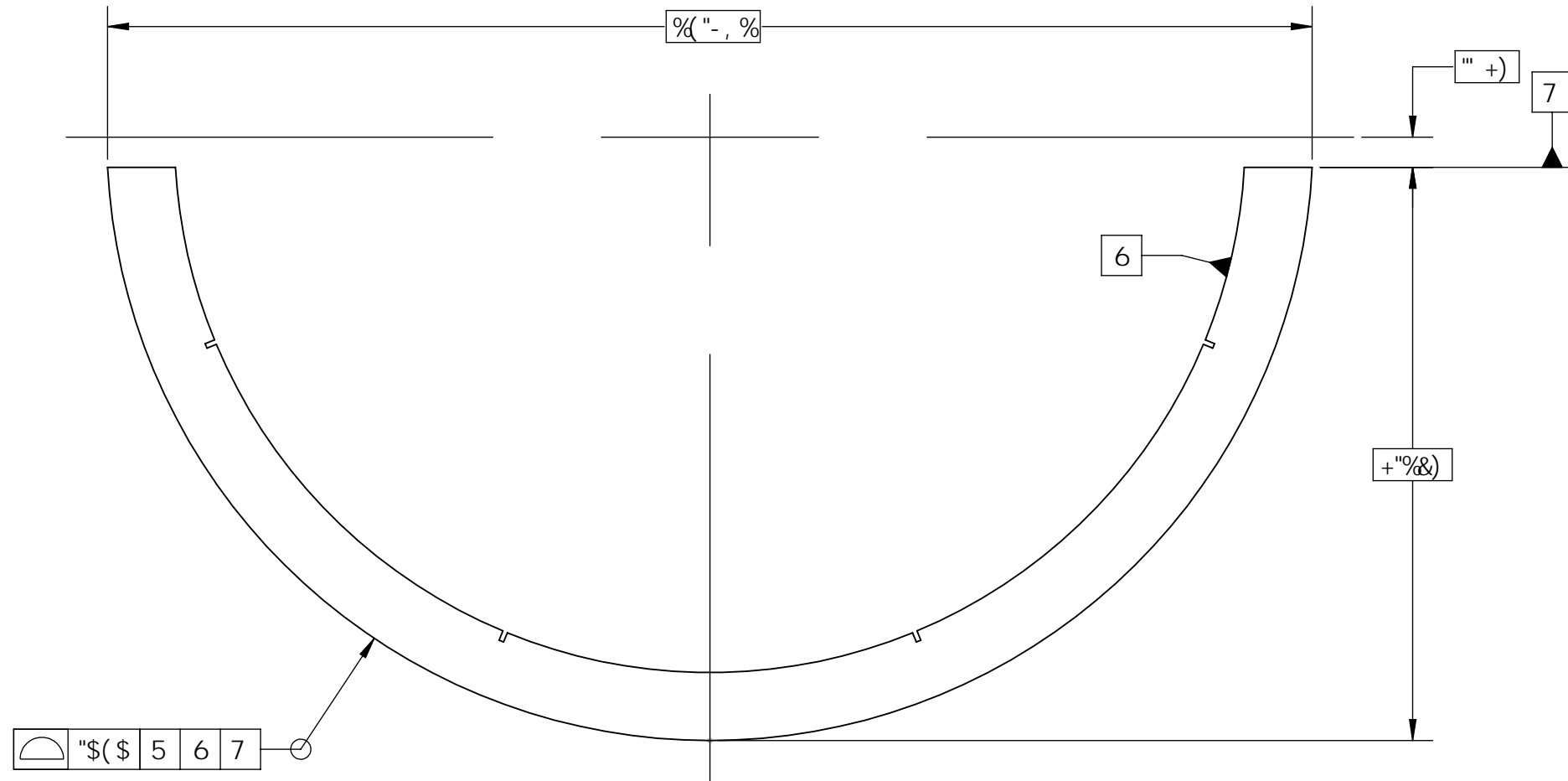
GB78E4A68F*GB?UE4A68F HA?8FF'BG: 8EJ 48 ABG87 F4H9 A7-64G-BA 6BAGE4-E8 4?? 7@BAF-BAF A A6: 8F 7@BAF-BAF BA C#H68F !K' : : !#&# !KK' : : !#&# !KKK' : : !#&# 4?? 9E46G-BAF ±\$&#% 4A: H?4E' : : !(#* !#&# 9@ 6BA9BE@F GB*6BA9BE@8 4 4F@8 L\$!#&# b%## 5E84> 4?? F: 4EC 87: 8F 6: 4A9E8-A8E GBHG8F 4EEAG8F 6BHC4AGF !#&# b!#%#	@4G8E 4?? @4GU E-8? ' \$(G-5-B @CG GH9@ %&# 8-5" FC 8 : 84G GE84G! GE4-G@8AG G: 8E@ BC B9 9A4: *9A< B5H F5@ %&# F4C 6B78 5% 78F! *6BA68CG! >"8 9A 9FG 7E4J A! 78FF-Au! >"8 9A 9FG FGE8FF ** 6BA! 6: 86>87" I uE-Q! 4CC! 4CC! 74G8 &&#&\$%	BUHcbU F YgYUWV 7 ci bW 7 UbuXU 7cbgY] bUjcbU XY YWVYUWYg 7 UbuXU NRC-CNRC 7XfVzA TaW9TUEVTgba FXei WXf FXei WX WX' 6baVXcg'ba Xg WX' 9TUEVTgba ¥ &\$% žBUHcbU FYgYUWV 7 ci bW] G678" GGE8 C I H9F Hk 9FA C 7 C I D@9D9; G 7 5GB; @C K 9F # DD9F <5@ %* - , ! 75 @ C F A 9H9F 5B8 : I 9@D5B AFGI 67-8AG @B78? A4@8 " AB@8 78 @B78?8 F: 88G 98H?8 F6478" u6: 8??8 DGL! 7 CBGH %&# - , ! C I H9F Hk 9FA C 7 C I D@9D9; G %C: #8 9% (. % &(@B7 64E7 4FF8@57L " AB! " Ab 4FF8@5?4: 8 7E4J A: Ad! " Ab 78FF-A EBI! %&# - , ! %\$! &# \$' ; %&# - , ! %\$! %&D 6 5
---	--	---

7B ABG F647B 7E4J A
 A8 C4F @8FHE8E FHE 7B 78FF A
 EBCBEG 47? BEEBEF GB G 8 7BF < A B99-6B
 F < A478E GBHGF BEEBHEF 4H 5HE84H 7B 6BA68CG-BA
 E8GHEA 47? 7E4J A: F GB G 8 78FF < A B99-6B
 E8GBHEABE GBHF 7BF 78FF A F 4H 5HE84H 7B 6BA68CG-BA

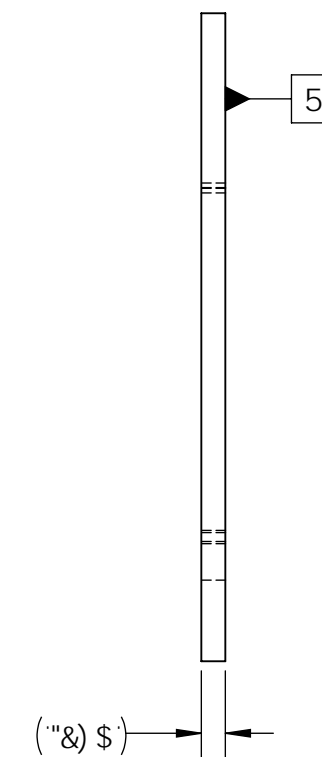
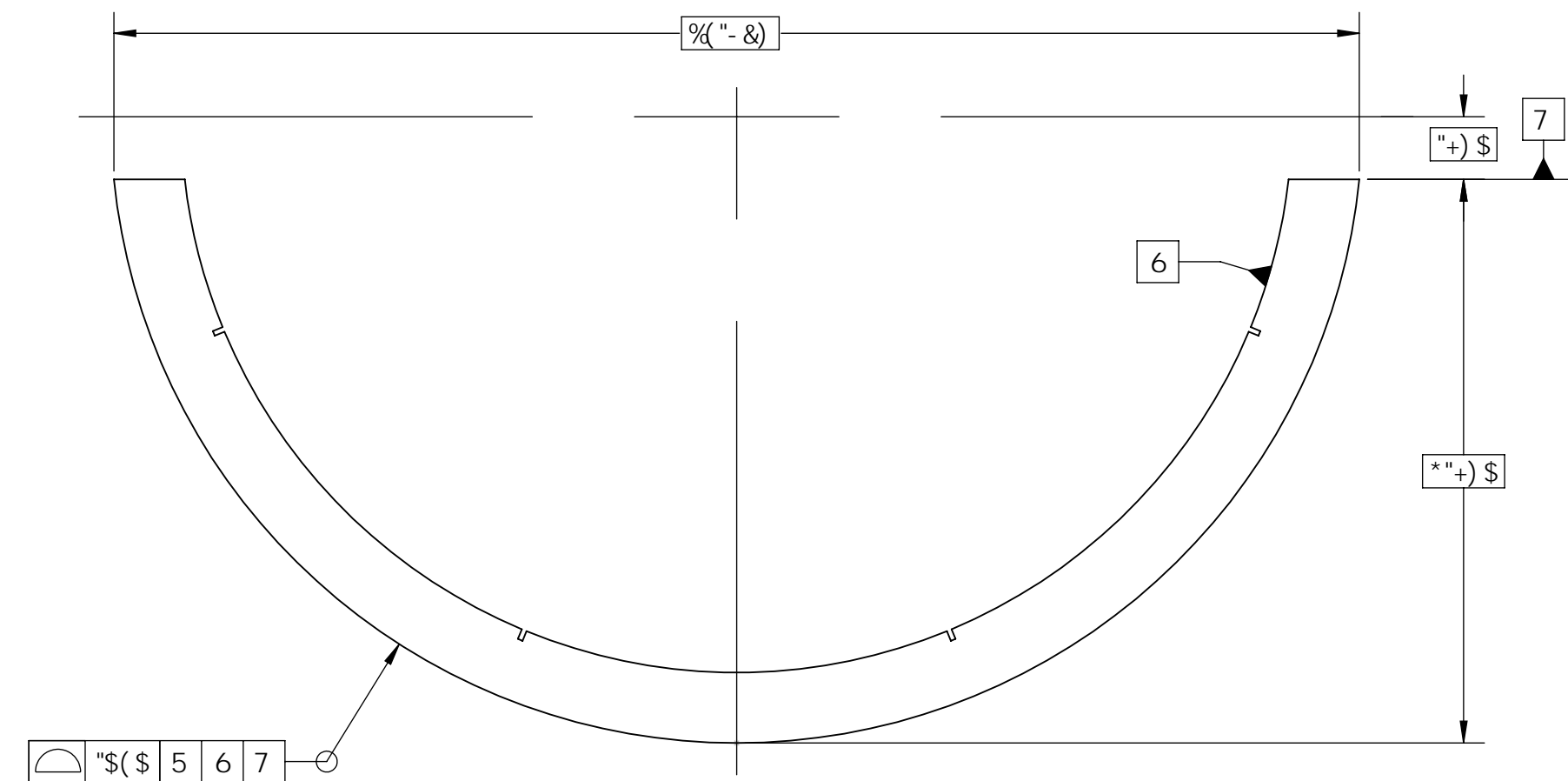
F9J GCB < GC HMF < GC FE I 989GFVJ GCBG
 NC B 9 F9J " 89G7 F-DHC B 85H9 6MD5F

BC HFG

% &8 7 5 8 8 5 H 5 G DD @ 9 8 : C F K 5 H F > 9 H 7 I H H B ;
 & " 8 A 9 B G C B G E I 9 F - 9 8 : F C A 7 5 8 A C 8 9 @ 5 F 9 6 5 G - 7
 ' " H C H 5 @ E H M & Z E H M P % C : I D D 9 F H A D 5 H 9 F E H M P % C : @ C K 9 F
 H A D 5 H 9



I DD9F H9A D5H9FE HM%&



@ C K 9 F H A D 5 H 9 F E H M P % &

GB?8E4A6BF?GB?uE4A6BF	@4GBE4? @4GDE 8?		
HA78FF BG 8EJ F8 ABG87 F4H9 A7-64G-8A 6BA6E4-E8	D5 B 7 5 F 6 C B G H9@ %(- " Hk 7?	BUHbu F YgUWV 7ci bW 7UBU 7cbg 7 UBU XY YWYVWYg 7UBU	
47? 7 @BAF-BAF A A6 BF 7 @BAF-BAF BA CH6BF	B4G GE84G GE4G @BAG C 8E @ BC B 9	7XfYzA TaW9T UeVTgba FXei VXF FXei VX WX 6baVXcgba Xg VW 9T UeVTgba Y & S % Z BUHj:bu FYg URM 7 ci bW	
IKK : : 1#8# IKK : : 1#9# IKKK : : 1## 47? 9E4GG-BAF 158%	9A4 : 9A < B5H F5@	C I H9F Hk 9FA C 7 C I D @ H9A D5H9	
4A: H24E 1(#* / 1#9 9 @	F4C 6B7B 598 78F1 *6BA68CGI > 89A 9FG 7E4J A1 78FF Aul	%* - , ! 7 5 @ F A 9 H9F 5 B 8 : I 9 @ D 5 B	
6BA9BE @F GB *6BA9BE @B 4 AF @B L S 1 9 # P 9 # #	FGE8FF " 6BAI 6 86-871 U E-9I 400 " 400 > 89A 9FG 74G8 & + # 9 # & 5 %	@F C I 67 2A G 7 C B G H @B 7 64 E 7 4FF8 @ 5 7 L A B I * A D 4FF8 @ 5 7 4 : B 7E4J A: A D 78FF A %* - , ! % 8 1 % D # % (D 7 !	

Supplement D – Statement of Work by Omnicon Consultants Inc.

September 25, 2015 (Revised December 18, 2015)

Cecilia Lam
Research Officer
National Research Council Canada
1200 Montreal Road, Building M-59
Ottawa, Ontario K1A 0R6

Subject: Crude Oil Flammability Study — Sample Collection

Cecilia

As requested we have prepared a brief proposal to coordinate the sample collection, initial properties testing and transportation of a crude oil sample to the Nation Research Council in Ottawa. The proposal outlines the proposed method for sample capture and means of containment for transportation as well as recommendations for creating a composite sample, if required.

The work has been broken down into four key milestones:

1. Scope Development, Cost Estimate and Crude Oil Recommendation.
2. Preparation for Sample Collection
3. Sample Collection.
4. Ongoing Project Support.

Our normal practice is to bill our time on an hourly basis as outlined in the appended document. We have however prepared a cost estimate based on best available information, and the quoted estimate will be adhered to providing there are no changes in the scope of work.

If you have any questions, please contact us at your convenience.

Regards,



Dave Murray
Andre Lemieux
Omnicon Consultants Inc.

Objectives

The objective of this project is the collection of a sample(s) of crude oil, representative of the condition in which it would normally be transported by rail or tank truck. This includes maintaining the light end components such as methane, ethane, propane and butane in the same concentration as they exist at the sample point.

Work Plan

Milestone 1 — Includes the development of the project scope including meetings, teleconferences, and other related activities.

Milestone 2 — Includes all activities relating to preparation for sample collection. Specific activities are outlined in Table 1.

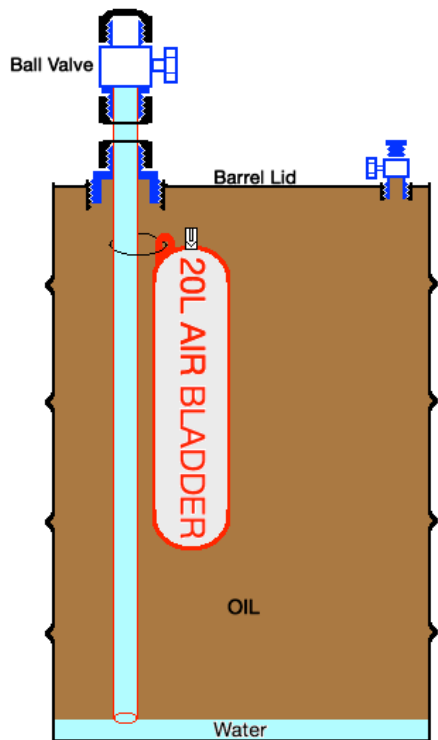
Milestone 3 — Includes all activities relating to sample collection and transportation. Specific activities are outlined in Table 1.

Milestone 4 — Includes ongoing support activities required during the project.

Sample Collection

As per discussion, sampling will be performed using a single-phase transfer protocol.

Ten (10) standard 219 L (nominal) UN Rated barrels will be outfitted as follows (See Fig 1):



- 2" threaded bung will have a stainless steel 2" NPT to 1" bushing installed.
- Stainless steel 1" NPT to 3/4" to tube adapter will be installed in the bushing.
- 3/4" Stainless steel tubing will be passed through the tube adapter and sealed. Tubing will be inserted to within 1" of the barrel floor.
- 3/4" Stainless steel ball valve will be installed on the end of the tubing.
- 3/4" bung will have a stainless steel 3/4" NPT valve installed.
- 20 L inflatable air bladder will be installed and fixed to the 3/4" stainless steel tubing to allow installation and removal.

Figure 1. Proposed Barrel Schematic

To ensure the barrel (means of containment) meets TDG requirements for ullage and to ensure the crude oil is not exposed to atmospheric air, a custom 20 L internal air bladder will act as a 10% ullage volume within the barrel. The air bladder will compress in the event of thermal expansion similar to vapor headspace typically used as ullage. This option provides an environment that is least likely to impact the properties of the crude oil and provides the suitable thermal expansion volume without risk of compromising the crude properties.

Prior to sampling operations, the internal air bladder will be filled with air at 110 kPa then the barrel will be filled completely with glycol/water (50/50). Once at the sampling location, the crude oil will be sampled through the 3/4" valve on the top of the barrel displacing water through the 3/4" tubing through transparent tubing into a secondary wastewater capture barrel. When crude is just visible in the transparent tubing sample transfer operations will be stopped and the barrel valves closed with the captured sample. A residual 1" of water will remain in the barrel. A total of approximately 960 L of crude will be captured (192L per barrel). A sub-sample of the crude oil will be taken in a sealed sample cylinder at the midpoint of sample transfer into each barrel. Wastewater will require environmental analysis to confirm disposal requirements as it has been in contact with crude oil.

Upon receipt of the barrels at the NRC, water is injected through the 3/4" valve and tubing into bottom of the barrel displacing the crude through the 3/4" valve at the top of the barrel. Standard municipal water pressure is typically 40-80 psi (275-550 kPa) and should be suitable for displacement. Alternately the water used in the sampling operations could be used to displace the oil from the barrels for use in testing.

A suitable sample collection contractor has been identified and Omnicon will supervise all sampling activities directly. NRS Oilfield Sampling Services Inc. will be used to carry out the sampling operations.

Homogeneity Between Sample Barrels

Samples taken from each barrel will be tested for composition (ASTM D8003), vapor pressure (ASTM D6377), Simulated Distillation (ASTM D7169) and density (ASTM D5002). If the comparative properties of all 10 barrels are within test method reproducibility tolerances then a sample composite will not be required since each barrel contains a sample with the same properties as the others. If the comparative properties of the barrels are not within test method reproducibility tolerances then a composite sample should be prepared as outlined below. Once homogenized, a single sample of the composite sample should be tested to confirm the sample properties prior to fire testing. Hydrogen sulfide analysis by UOP 163 will be performed on a sample taken at the mid-point in the sampling program.

Sample Composite (as required)

Depending on the variation in properties between barrels it may be necessary to combine all 10 barrels into a single composite sample for use in testing. In this instance, it is recommended that all 5 barrels be transferred into a single vessel and homogenized using a circulation pump. A suitable vessel would include potentially a 1000 L fuel bladder.

Supplement E – Summary of Results of Crude Oil Sample Homogeneity Testing

February 24, 2016

National Research Council Canada
1200 Montreal Road, Building M-59
Ottawa, Ontario K1A 0R6

Attention: Cecilia Lam, Research Officer

Subject: Crude Oil Flammability Study — Sample Homogeneity Results Summary

The following are the results from the homogeneity testing performed during sample collection on February 2nd, 2016. Ambient conditions at the time of sampling were -5°C with an average tank temperature of 9.7°C. Tank head pressure estimated at 15-18 psig.

Table 1 — Properties Testing

Test Method	ASTM D5002	ASTM D5002	ASTM D6377	UOP 163**	
Test Description	Density	Density	Vapor Pressure	H ₂ S Content	Mercaptan Content
Conditions	15°C	15°C (Onsite)	VPCR ₄ @ 37.8°C	Ambient P & T	Ambient P & T
Unit	kg/m ³	kg/m ³	(kPa)	mg/kg	mg/kg
Barrel/Sample #					
1	868.9	870.0	65.7	6.2	65.2
2	868.6	868.8	65.5	10.6	66.2
3	868.7	868.5	65.2	15.4	54
4	868.7	868.4	65.1	9.9	62.2
5	868.5	869.4	65.4	11.7	74.7
6	868.6	870.3	67.3	1.8	63.8
7	868.4	869.5	65.2	1.8	65.7
8	868.9	NA*	63.5	2.9	65.9
9	868.6	869.3	64.1	2.2	65.9
10	868.7	869.0	64.3	7.3	58.2
Min	868.4	868.4	63.5	1.8	54
Max	868.9	870.3	67.3	15.4	74.7
Average	868.7	869.2	65.1	7.0	64.2
Standard Deviation * 2.77	0.4	1.8	2.9	Not Applicable	
Test Method Reproducibility	3.6	3.6	4.3		
PASS/FAIL	OK	OK	OK		

*Sample not available for testing.

** Test method does not provide precision statement so no comparison is available for reproducibility.

Table 2 – Compositional Analysis Result Using Merged ASTM D8003 & D7169

Component Name	Sample 1	Sample 2	Sample 3	Sample 4	Sample 5	Sample 6	Sample 7	Sample 8	Sample 9	Sample 10
C1	0.009	0.009	0.010	0.010	0.010	0.010	0.010	0.010	0.010	0.009
C2	0.023	0.024	0.024	0.025	0.025	0.024	0.025	0.025	0.025	0.024
C3	0.245	0.252	0.252	0.260	0.264	0.253	0.262	0.259	0.263	0.251
iC4	0.632	0.649	0.650	0.665	0.680	0.650	0.674	0.668	0.681	0.645
nC4	1.370	1.413	1.408	1.434	1.467	1.397	1.454	1.436	1.461	1.390
neo C5	0.000	0.000	0.000	0.000	0.000	0.000	0.000	0.000	0.000	0.000
iC5	0.888	0.911	0.917	0.925	0.949	0.902	0.933	0.925	0.949	0.897
nC5	1.016	1.047	1.076	1.084	1.111	1.054	1.092	1.083	1.111	1.051
C6¹	2.169	2.220	2.226	2.234	2.280	2.162	2.230	2.229	2.302	2.173
Benzene	0.028	0.027	0.027	0.027	0.028	0.026	0.026	0.026	0.028	0.027
C7^{1,2}	3.378	3.465	3.526	3.565	3.601	3.417	3.495	3.533	3.653	3.456
C8¹	4.220	4.325	4.413	4.502	4.510	4.304	4.347	4.436	4.578	4.358
C9¹	3.277	3.352	3.429	3.517	3.516	3.409	3.349	3.454	3.544	3.409
C10¹	4.044	3.305	2.443	3.351	3.358	3.292	3.403	3.415	3.196	3.311
C11¹	2.900	2.800	2.800	2.800	2.800	2.800	2.700	2.800	2.700	2.700
C12¹	2.700	2.700	2.700	2.700	2.800	2.700	2.800	2.700	2.600	2.700
C13¹	3.000	2.900	2.900	2.900	2.900	2.900	2.900	2.900	2.800	2.900
C14¹	3.100	3.000	3.100	3.100	3.100	3.000	3.100	3.100	3.000	3.000
C15¹	2.900	2.900	2.900	2.900	2.900	2.900	2.800	2.900	2.800	2.800
C16¹	2.500	2.400	2.500	2.500	2.500	2.500	2.500	2.500	2.400	2.400
C17¹	3.200	3.200	3.100	3.200	3.200	3.100	3.200	3.200	3.000	3.100
C18¹	2.600	2.500	2.600	2.600	2.600	2.500	2.600	2.600	2.500	2.500
C19¹	2.200	2.200	2.200	2.200	2.300	2.200	2.200	2.200	2.100	2.200
C20¹	2.200	2.200	2.200	2.200	2.200	2.200	2.100	2.200	2.100	2.100
C21¹	2.200	2.100	2.200	2.200	2.100	2.200	2.200	2.100	2.100	2.200
C22¹	2.100	2.100	2.000	2.000	2.100	2.000	2.000	2.100	2.000	2.000
C23¹	2.000	1.900	2.000	2.000	2.000	2.000	2.000	2.000	1.900	1.900
C24¹	1.900	1.900	1.900	1.900	1.900	1.800	1.900	1.900	1.800	1.900
C25+³	43.200	44.200	44.500	43.200	42.800	44.300	43.700	43.300	44.400	44.600
Totals	100.000	100.000	100.000	100.000	100.000	100.000	100.000	100.000	100.000	100.000

¹ The cut point carbon interval C_{xx} - the mass percent obtained between the end of n-paraffin nC_{xx-1} and the end of n-paraffin nC_{xx}.

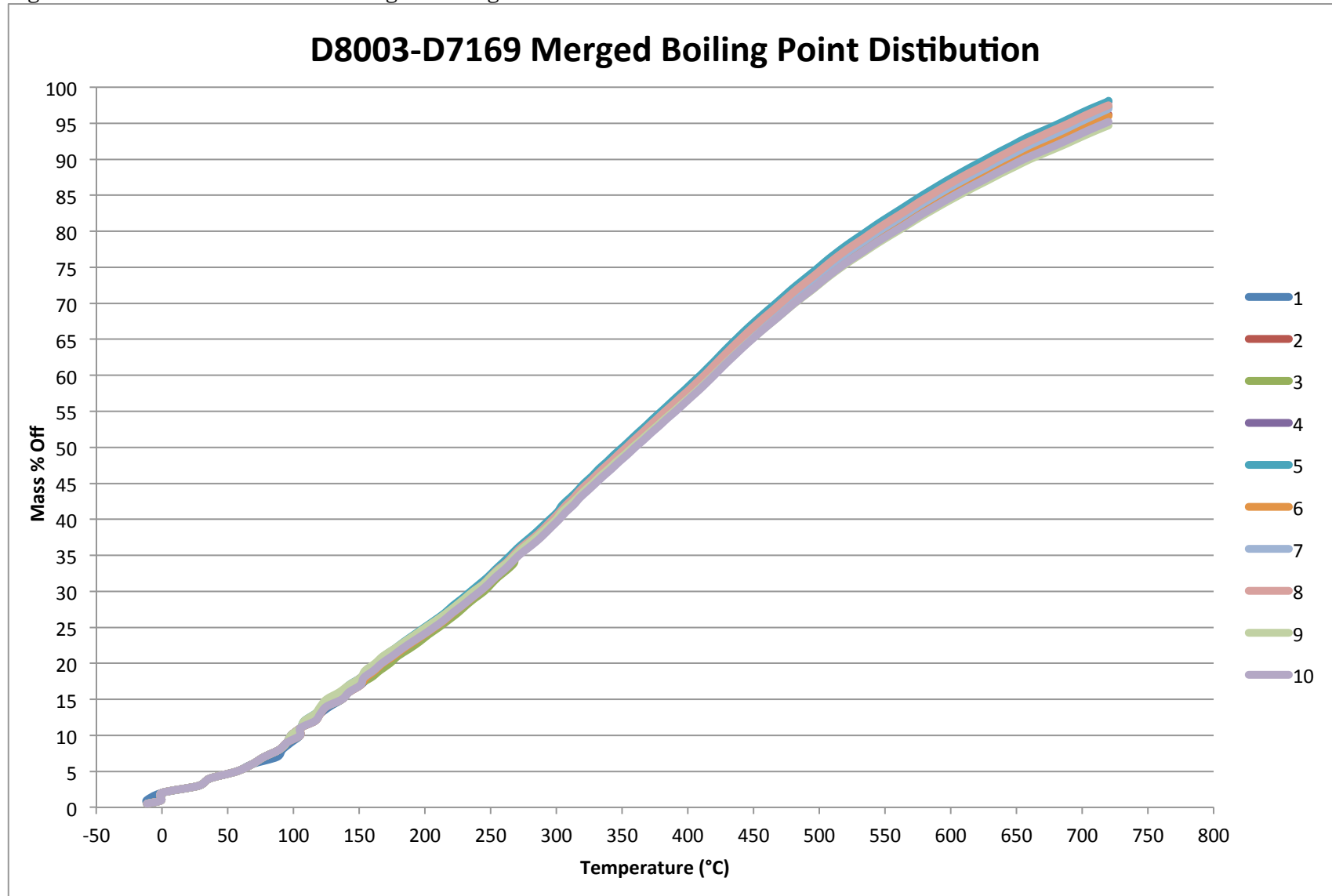
² C7 cut point carbon interval does not contain the mass percent of benzene, as this is reported as an individual component.

³ The residue of the sample not eluted without discrimination by the GC conditions. This is defined as the mass percent of material starting at the end of n-paraffin nC₂₄ and covering all the material not accounted for before the end of nC₂₄ on the chromatogram (water, inorganic solids, asphaltenes etc...).

Table 3 – Statistics for Compositional Analysis Result Using Merged ASTM D8003 & D7169

Component Name	Min	Max	Average	Standard Deviation*2.77	D8003 Method Repeatability	Pass
C1	0.009	0.010	0.010	0.001	0.03	PASS
C2	0.023	0.025	0.024	0.002	0.01	PASS
C3	0.245	0.264	0.256	0.018	0.96	PASS
iC4	0.632	0.681	0.659	0.046	0.08	PASS
nC4	1.370	1.467	1.423	0.091	0.23	PASS
neo C5	0.000	0.000	0.000	0.000	Not Applicable	
iC5	0.888	0.949	0.919	0.057		
nC5	1.016	1.111	1.073	0.084		
C6¹	2.162	2.302	2.223	0.127		
Benzene	0.026	0.028	0.027	0.002		
C7^{1,2}	3.378	3.653	3.509	0.233		
C8¹	4.220	4.578	4.399	0.303		
C9¹	3.277	3.544	3.426	0.237		
C10¹	2.443	4.044	3.312	1.064		
C11¹	2.700	2.900	2.780	0.175		
C12¹	2.600	2.800	2.710	0.157		
C13¹	2.800	3.000	2.900	0.131		
C14¹	3.000	3.100	3.060	0.143		
C15¹	2.800	2.900	2.870	0.134		
C16¹	2.400	2.500	2.470	0.134		
C17¹	3.000	3.200	3.150	0.196		
C18¹	2.500	2.600	2.560	0.143		
C19¹	2.100	2.300	2.200	0.131		
C20¹	2.100	2.200	2.170	0.134		
C21¹	2.100	2.200	2.160	0.143		
C22¹	2.000	2.100	2.040	0.143		
C23¹	1.900	2.000	1.970	0.134		
C24¹	1.800	1.900	1.880	0.117		
C25+³	42.800	44.600	43.820	1.818		

Figure 1 — ASTM D8003-D7169 Merged Boiling Point Distribution



Homogeneity Evaluation

Table 1 shows the sample source was reasonably homogeneous throughout the period required to complete the sampling operations. Both density and vapor pressure fluctuated slightly throughout however the amount of fluctuation is indistinguishable from test method precision therefore the individual samples can be considered representative of the whole volume sampled.

The wider variation in the H₂S results can be largely attributed to the ambient conditions and sample handling required to perform the test itself. This test was not considered as basis for homogeneity but for information purposes to ensure for safe handling for the NRC.

Table 3 displays the composition of each sample from C1-C25+ based on the ASTM D8003 and D7169 merged data. Table 4 contains the statistics based on Table 3 data. The compared compositions of C1 through C4 are well within the method repeatability. There is no method repeatability data available for the merged D8003-D7169 data therefore values beyond C4 are not comparable. D8003 repeatability criteria alone were used. The data provides further verification that the individual samples can be considered representative of the whole volume sampled.

Figure 4 contains the boiling point distributions (simulated distillation curves) for the 10 samples based on merged ASTM D8003 and D7169 analysis. The curves are all closely overlaid as would be expected with samples originating from the same source.

The data presented above indicates the 10 individual samples can be considered representative of the whole volume sampled.

Regards,



Dave Murray
Andre Lemieux
Omnicon Consultants Inc.